



**UNIVERSIDADE FEDERAL DO RIO GRANDE DO SUL**

Em Cotutela International com  
**Universidade de Rennes 1, França**

Título da Tese :

**Yttrium and Aluminum Catalysts and Model  
Complexes for Ring-Opening Polymerization of  
Lactide and  $\beta$ -Butyrolactone**

**Joice Sandra Klitzke**

**Porto Alegre, 28 de agosto de 2013**

## **THESIS COMMITTEE MEMBERS**

- Osvaldo de Lázaro Casagrande Jr. (Thesis Co-Director) – Full Professor at University of Rio Grande do Sul, Institute of Chemistry, Porto Alegre, Rio Grande do Sul, Brazil.
- Jean-François Carpentier (Thesis Co-Director) – Full Professor at University of Rennes 1, Rennes, Bretagne, France.
- Samuel Dagherne – Research Director at CNRS at University of Strasbourg, Alsace, France.
- Marcos Lopes Dias – Associate Professor at University of Rio de Janeiro, Rio de Janeiro, Brazil.
- Cesar Liberato Petzhold – Full Professor at University of Rio Grande do Sul, Porto Alegre, Rio Grande do Sul, Brazil.

# GENERAL INDEX

<b>THESIS COMMITTEE MEMBERS</b>	<b>I</b>
<b>GENERAL INDEX</b>	<b>II</b>
<b>FIGURE INDEX</b>	<b>V</b>
<b>SCHEME INDEX</b>	<b>XV</b>
<b>TABLE INDEX</b>	<b>XVI</b>
<b>LIST OF ABBREVIATIONS</b>	<b>XVII</b>
<b>ABSTRACT</b>	<b>XIX</b>
<b>CHAPTER 1. INTRODUCTION</b>	<b>1</b>
<b>1.1 GENERAL INTRODUCTION</b>	<b>1</b>
<b>1.2 ALIPHATIC BIODEGRADABLE POLYESTERS</b>	<b>2</b>
<b>1.2.1 Poly(lactic acid) (PLA)</b>	<b>3</b>
<b>1.2.2 Poly(3-hydroxybutyrate) (PHB)</b>	<b>5</b>
<b>1.3 MECHANISMS FOR THE RING-OPENING POLYMERIZATION (ROP)     OF CYCLIC ESTERS</b>	<b>6</b>
<b>1.3.1 Cationic Ring-Opening Polymerization</b>	<b>7</b>
<b>1.3.2 Anionic Ring-Opening Polymerization</b>	<b>7</b>
<b>1.3.3 Activated Monomer Mechanism</b>	<b>8</b>
<b>1.3.4 Organo-Catalyzed and Dual ROP Mechanism</b>	<b>9</b>
<b>1.3.5 Coordination-Insertion Ring-Opening Mechanism</b>	<b>11</b>
<b>1.3.5.1 Stereocontrol in ROP of Lactide and <math>\beta</math>-Butyrolactone</b>	<b>12</b>
<b>1.3.6 Transfer Process (Transesterification Side-Reactions)</b>	<b>16</b>
<b>1.4 CATALYSTS</b>	<b>17</b>
<b>1.4.1 Aluminum-Based Initiators for the ROP</b>	<b>17</b>
<b>1.4.1.1 Well-Defined Aluminum Complexes Featuring Ancillary             Ligands</b>	<b>18</b>
<b>1.4.1.1.1 SALEN-Based Aluminum Complexes</b>	<b>20</b>
<b>1.4.1.1.2 SALAN-Based Aluminum Complexes</b>	<b>26</b>
<b>1.4.1.1.3 Phenoxy-Imine-Based Aluminum Complexes</b>	<b>29</b>
<b>1.4.1.1.4 Phenoxy-Amine-Based Aluminum Complexes</b>	<b>33</b>
<b>1.4.1.1.5 Other Phenolate-Based Aluminum Complexes</b>	<b>34</b>
<b>1.4.1.1.6 Aluminum Complexes Supported by Fluorinated                 Ligands</b>	<b>36</b>
<b>1.4.2 Yttrium-Based Initiators for the ROP</b>	<b>37</b>

1.5 STRUCTURAL, MECHANISTIC AND COMPUTATIONAL STUDIES ON WELL-DEFINED INITIATOR FOR THE ROP OF LACTIDES AND $\beta$ -BUTYROLACTONE	48
<b>CHAPTER 2. OBJECTIVES</b>	<b>60</b>
<b>CHAPTER 3. EXPERIMENTAL</b>	<b>61</b>
3.1 GENERAL PROCEDURES	61
3.2 PRO-LIGAND SYNTHESIS	62
3.2.1 1-(methoxymethyl)-4-methyl-2-(2-phenylpropan-2-yl)benzene	62
3.2.2 One-pot Synthesis of $\{\text{ONO}^{\text{Me,Cumyl}}\}\text{H}_2$ ( <b>1c</b> )	63
3.3 COMPLEXES SYNTHESIS	64
3.3.1 $\{\text{ONO}^{\text{SiPh}_3}\}\text{AlMe}$ ( <b>2a</b> )	64
3.3.2 $\{\text{ONO}^{\text{SiMe}_2\text{tBu}}\}\text{AlMe}$ ( <b>2b</b> )	65
3.3.3 $\{\text{ONO}^{\text{SiPh}_3}\}\text{Al}^i\text{Bu}$ ( <b>2c</b> )	65
3.3.4 $\{\text{ONO}^{\text{Me,Cumyl}}\}\text{AlMe}$ ( <b>2d</b> )	66
3.3.5 $\{\text{ONO}^{\text{SiPh}_3}\}\text{AlO}^i\text{Pr}$ ( <b>3a</b> )	66
3.3.6 $\{\text{ONO}^{\text{SiPh}_3}\}\text{Al}(i\text{Pr}(S)\text{-lactate})$ ( <b>4a</b> )	67
3.3.7 $\{\text{ONO}^{\text{SiMe}_2\text{tBu}}\}\text{Al}(i\text{Pr}(S)\text{-lactate})$ ( <b>4b</b> )	67
3.3.8 $\{\text{ONO}^{\text{Me,Cumyl}}\}\text{Al}(i\text{Pr}(S)\text{-lactate})$ ( <b>4d</b> )	68
3.3.9 $\{\text{ONO}^{\text{SiPh}_3}\}\text{Al}((R)\text{-OCH}(\text{CH}_3)\text{CH}_2\text{COOMe})$ ( <b>5a</b> )	69
3.3.10 $\{\text{ONO}^{\text{Me,Cumyl}}\}\text{Al}((R)\text{-OCH}(\text{CH}_3)\text{CH}_2\text{COOMe})$ ( <b>5d</b> )	70
3.3.11 $\{\text{ONO}^{\text{SiPh}_3}\}\text{Al}((rac)\text{-OCH}(\text{CF}_3)\text{CH}_2\text{COOEt})$ ( <b>6a</b> )	70
3.3.12 $\{\text{ONO}^{\text{Me,Cumyl}}\}\text{Al}((rac)\text{-OCH}(\text{CF}_3)\text{CH}_2\text{COOEt})$ ( <b>6d</b> )	71
3.3.13 Propagating species formed from 4a and L-LA ( <b>7a</b> )	72
3.3.14 First insertion product from 5a and L-LA ( <b>8a</b> )	73
3.3.15 $\{\text{ONO}^{\text{Me,Cumyl}}\}\text{Y}[\text{N}(\text{SiHMe}_2)_2](\text{THF})(\text{Et}_2\text{O})$ ( <b>9</b> )	73
3.3.16 $\{\text{ONO}^{\text{Me,Cumyl}}\}\text{Y}((R)\text{-OCH}(\text{CH}_3)\text{CH}_2\text{COOMe})$ ( <b>10</b> )	75
3.3.17 $\{\text{ONO}^{\text{Me,Cumyl}}\}\text{Y}((S,S)\text{-OCH}(\text{CH}_3)\text{CO}_2\text{CH}(\text{CH}_3)\text{CO}_2\text{Me})$ ( <b>11</b> )	75
3.4 REACTIVITY TOWARD LACTIDES AND <i>rac</i> - $\beta$ -BUTYROLACTONE	76
3.4.1 Typical Procedure for <i>rac</i> -Lactide Polymerization.	76
3.4.2 Typical Procedure for <i>rac</i> -Lactide Polymerization in Presence of ROH (R = Bn; <i>i</i> Pr).	77
3.4.3 Typical Procedure for <i>rac</i> - $\beta$ -Butyrolactone Polymerization.	77
3.5 POLYMER CHARACTERIZATION.	77
3.5.1 Size Exclusion Chromatography (SEC).	77

3.5.2 Nuclear Magnetic Resonance (NMR)	78
<b>CHAPTER 4. RESULTS AND DISCUSSION</b>	<b>79</b>
<b>4.1 DISCRETE LACTATE AND <math>\beta</math>-ALKOXY-BUTYRATE ALUMINUM BIS(NAPHTHOLATE)-PYRIDINE COMPLEXES</b>	<b>79</b>
4.1.1 Preparation of alkyl $\{\text{ONO}^{\text{SiR}_3}\}\text{AlR}'$ complexes ( $\text{R}' = \text{Me}$ , $\text{SiR}_3 = \text{SiPh}_3$ , <b>2a</b> ; $\text{SiMe}_2t\text{Bu}$ , <b>2b</b> ; $\text{R}' = i\text{Bu}$ , $\text{SiR}_3 = \text{SiPh}_3$ , <b>2c</b> ).	80
4.1.2 Preparation of $\{\text{ONO}^{\text{SiR}_3}\}\text{AlOR}$ complexes ( $\text{R} = i\text{Pr}$ , <b>3a</b> ; ( <i>S</i> )- $\text{CH}(\text{Me})\text{CO}_2i\text{Pr}$ , <b>4a</b> , <b>4b</b> ; ( <i>R</i> )- $\text{CH}(\text{Me})\text{CH}_2\text{CO}_2\text{Me}$ , <b>5a</b> ; ( <i>rac</i> )- $\text{CH}(\text{CF}_3)\text{CH}_2\text{CO}_2\text{Et}$ , <b>6a</b> ).	82
4.1.3 Studies on the ring-opening polymerization of <i>rac</i> -lactide with aluminum bis(naphtholate)pyridine complexes.	93
4.1.4 Reactivity studies and mechanistic considerations on ring-opening polymerization of D-, L- and <i>rac</i> -lactide.	99
4.1.4.1 Studies of the reactivity of Al(III)-(isopropyl ( <i>S</i> )-lactate) complexes <b>4a</b> and <b>4b</b> .	99
4.1.4.2 Studies of the reactivity of Al(III)-(methyl ( <i>R</i> )- $\beta$ -alkoxybutyrate) complex <b>5a</b> .	109
<b>4.2 WELL-DEFINED Al- AND Y- COMPLEXES BEARING A TRIDENTATE CUMYL ORTHO-SUBSTITUTED BIS(PHENOLATE)PYRIDINE LIGAND.</b>	<b>114</b>
4.2.1 Preparation of the new pro-ligand $\{\text{ONO}^{\text{Me,Cumyl}}\}\text{H}_2$ ( <b>1c</b> ).	114
4.2.2 Preparation of $\{\text{ONO}^{\text{Me,Cumyl}}\}\text{AlOR}$ complexes ( $\text{R} = \text{Me}$ , <b>2d</b> ; ( <i>S</i> )- $\text{CH}(\text{Me})\text{CO}_2i\text{Pr}$ , <b>4d</b> ; ( <i>R</i> )- $\text{CH}(\text{Me})\text{CH}_2\text{CO}_2\text{Me}$ , <b>5d</b> ; ( <i>rac</i> )- $\text{CH}(\text{CF}_3)\text{CH}_2\text{CO}_2\text{Et}$ , <b>6d</b> ).	116
4.2.3 Studies of the reactivity of Al(III)-(isopropyl ( <i>S</i> )-lactate) complex <b>4d</b> toward L- and <i>rac</i> -Lactides.	121
4.2.4 Preparation of $\{\text{ONO}^{\text{Me,Cumyl}}\}\text{YR}$ complexes ( $\text{R} = \text{N}(\text{SiHMe}_2)_2(\text{THF})(\text{Et}_2\text{O})$ , <b>9</b> ; O( <i>R</i> )- $\text{CH}(\text{Me})\text{CH}_2\text{CO}_2\text{Me}$ , <b>10</b> ; ( <i>S,S</i> )- $\text{OCH}(\text{CH}_3)\text{CO}_2\text{CH}(\text{CH}_3)\text{CO}_2\text{Me}$ , <b>11</b>	123
4.2.5 Studies on the ring-opening polymerization of <i>rac</i> -lactide and <i>rac</i> - $\beta$ -butyrolactone with Yttrium pyridine-Bis(phenolate) complexes.	130
<b>CHAPTER 5. CONCLUSIONS</b>	<b>138</b>
<b>CHAPTER 6. REFERENCES AND NOTES</b>	<b>140</b>
<b>CHAPTER 7. ANNEXES</b>	<b>150</b>

## FIGURE INDEX

<b>Figure 1</b>	Stereoisomers of lactide.	<b>4</b>
<b>Figure 2</b>	Homonuclear decoupled $^1\text{H}$ NMR spectra (methine region) of PLA generated from (A) [(Cyclooctane-1,5-diyl)bis[(4 <i>S</i> ,7 <i>R</i> )-7,8,8-trimethyl-4,5,6,7-tetrahydro-4,7-methano-2 <i>H</i> -indazol-2-yl]borato]CaN(SiMe <sub>3</sub> ) <sub>2</sub> ·2THF and (B) SALAN Ligand-AlMe/PhCH <sub>2</sub> OH ( <i>P<sub>m</sub></i> ) 0.79 and (C) SALAN Ligand-AlMe/PhCH <sub>2</sub> OH ( <i>P<sub>r</sub></i> ) 0.96.	<b>14</b>
<b>Figure 3</b>	Carbonyl region of the $^{13}\text{C}\{^1\text{H}\}$ NMR spectra (125 MHz, CDCl <sub>3</sub> , 40 °C) of PHBs prepared by ROP of <i>rac</i> -BBL. Key: (A) with Y[N(SiHMe <sub>2</sub> ) <sub>3</sub> ](THF) <sub>2</sub> ( <i>P<sub>r</sub></i> ) 0.64; (B) with complex [(L)Y(N-(SiHMe <sub>2</sub> ) <sub>2</sub> )(THF)], L = 3,5-dicumyl-aminoalkoxybis(phenolate) ( <i>P<sub>r</sub></i> ) 0.88; (C) with complex [(L')Y(N-(SiHMe <sub>2</sub> ) <sub>2</sub> )(THF)] L' = 5-methyl-3-triphenyl-aminoalkoxybis(phenolate) ( <i>P<sub>r</sub></i> ) 0.94.	<b>15</b>
<b>Figure 4</b>	Examples of Single-Site Metal (pre)Catalysts for the ROP of Cyclic Esters	<b>17</b>
<b>Figure 5</b>	Equilibrium between the tetramer and trimer of Al(O <i>i</i> Pr) <sub>3</sub> . Only aluminium atoms (grey) and oxygen atoms (white) are shown for clarity.	<b>18</b>
<b>Figure 6</b>	Aluminum Complexes ( <b>1</b> ) Bearing Porphyrins Reported by Inoue <i>et al.</i>	<b>19</b>
<b>Figure 7</b>	Aluminum Complexes ( <b>3-5</b> ) Featuring SALEN Ligands	<b>21</b>
<b>Figure 8</b>	Salen-Aluminum Complexes ( <b>6-7</b> ) for Isoselective Lactide ROP	<b>22</b>
<b>Figure 9</b>	Salen-Aluminum Complexes ( <b>8-10</b> ) for Isoselective Lactide ROP	<b>23</b>
<b>Figure 10</b>	Nomura's Salen-Aluminum Complex ( <b>11</b> )	<b>24</b>
<b>Figure 11</b>	Aluminum Complexes ( <b>12</b> ) Supported by SALEN Ligands Developed by Lin <i>et al.</i>	<b>24</b>
<b>Figure 12</b>	Aluminum Complexes ( <b>13</b> ) and ( <b>14</b> ).	<b>25</b>
<b>Figure 13</b>	Aluminum Complexes ( <b>15</b> ) Featuring SALAN Ligands.	<b>26</b>
<b>Figure 14</b>	Aluminum Complexes ( <b>16</b> ) Supported by SALAN Type Ligands.	<b>27</b>
<b>Figure 15</b>	Aluminum-Homopiperazine Complexes ( <b>17</b> ).	<b>28</b>
<b>Figure 16</b>	Phenoxy-Imine Aluminum Complexes Developed by Pappalardo <i>et al.</i> ( <b>18a-c</b> ) and Nomura <i>et al.</i> ( <b>18b, 18c, d-i</b> ) and Carpentier <i>et al.</i> ( <b>19</b> ).	<b>30</b>
<b>Figure 17</b>	Dinuclear Aluminum Complexes Supported by Amino- ( <b>20</b> ) or Imino-Phenolate ( <b>21</b> ) Ligands.	<b>31</b>
<b>Figure 18</b>	Ethyl- ( <b>22-24</b> ), Isopropoxide- ( <b>25</b> ) and Methyl-Aluminum ( <b>26</b> ) Complexes Supported by Tridentate Schiff-Base Ligands.	<b>32</b>
<b>Figure 19</b>	Tetradentate Amino-Phenolate Aluminum Complexes ( <b>27</b> ) Reported by Gibson <i>et al.</i>	<b>33</b>
<b>Figure 20</b>	Aluminum Methyl Complexes Reported by Lamberti <i>et al.</i> ( <b>28</b> ) and Ma <i>et al.</i> ( <b>29</b> and <b>30</b> ).	<b>34</b>

<b>Figure 21</b>	Dinuclear Aluminum Complexes (31-34) Featuring Biphenolate Ligands	<b>35</b>
<b>Figure 22</b>	Aluminum Complexes (35) and (36).	<b>36</b>
<b>Figure 23</b>	Aluminum Complexes Supported by Fluorinated Amino- (37) and Imino-Alkoxy (38, 39, 41, 41'), and $\beta$ -Diketonate (40) Ligands.	<b>37</b>
<b>Figure 24</b>	Yttrium Initiators (42-46) Bearing <i>N,N</i> -Donor Ligands.	<b>39</b>
<b>Figure 25</b>	Tris(Alkoxy-Phosphonate) Yttrium Complexes (50).	<b>41</b>
<b>Figure 26</b>	Yttrium Initiators (51-52) Supported by <i>N,O,O,O</i> - and <i>N,N,O,O</i> -Donor Ligands.	<b>42</b>
<b>Figure 27</b>	Yttrium Initiators (53) Bearing Bis(Naphtholate) Ligands	<b>44</b>
<b>Figure 28</b>	Yttrium Initiators (54-56) Bearing <i>N,N,S,S</i> - and <i>N,N,O,O</i> -Donor Ligands	<b>45</b>
<b>Figure 29</b>	Yttrium Complexes (57) Supported by 1, $\omega$ -Dithiaalkanediyl-Bridged Bis(Phenolate) Ligands.	<b>45</b>
<b>Figure 30</b>	SALEN-Like Yttrium Complexes (58-61).	<b>47</b>
<b>Figure 31</b>	Rare Examples of Metal Complexes (65-69) and (72) Fully Characterized in Solid State and in Solution.	<b>52</b>
<b>Figure 32</b>	Aluminum Lactidate and Dilactate Complexes (73-74).	<b>53</b>
<b>Figure 33</b>	Complex (75) and Monomer Involved.	<b>56</b>
<b>Figure 34</b>	Free Energy Profile for the Initiation Step of the ROP of $\beta$ -Butyrolactone Catalyzed by the Yttrium Complex (75).	<b>58</b>
<b>Figure 35</b>	Numbering scheme of 1,1-bis(naphtholate)-1',1'pyridine ligand (left) and 1,1-bis(phenolate)-1',1'pyridine ligand (right).	<b>64</b>
<b>Figure 36</b>	Molecular structure of $\{\text{ONO}^{\text{SiPh}_3}\}\text{AlMe}$ ( <b>2a</b> , $\text{C}_7\text{H}_8$ ) (all solvents molecules and hydrogen atoms are omitted for clarity; thermal ellipsoids drawn at 50% probability). Selected bond distances ( $\text{\AA}$ ) and angles (deg): Al(1)–O(51), 1.7445(14); Al(1)–O(11), 1.7588(14); Al(1)–N(2), 1.9394(15); Al(1)–C(1), 1.922(2); O(51)–Al(1)–O(11), 110.18(7); O(51)–Al(1)–C(1), 115.85(9); O(11)–Al(1)–C(1), 119.39(9); C(1)–Al(1)–N(2), 117.05(9); O(51)–Al(1)–N(2), 95.95(6); O(11)–Al(1)–N(2), 94.15(7).	<b>81</b>
<b>Figure 37</b>	$^1\text{H}$ NMR spectrum (300 MHz, $\text{C}_6\text{D}_6$ , 298 K) of the crude product of the 1:1 reaction between $\{\text{ONO}^{\text{SiPh}_3}\}\text{H}_2$ and $(i\text{PrO})\text{AlMe}_2$ (toluene, 80 $^\circ\text{C}$ , 4 days).	<b>84</b>
<b>Figure 38</b>	$^1\text{H}$ - $^1\text{H}$ NOESY NMR spectrum (toluene- $d_8$ at 25 $^\circ\text{C}$ , 400 MHz) of the $\{\text{ONO}^{\text{SiPh}_3}\}\text{Al}((S)\text{-OCH}(\text{CH}_3)\text{CO}_2i\text{Pr})$ ( <b>4a</b> ).	<b>86</b>
<b>Figure 39</b>	Variable Temperature $^1\text{H}$ NMR spectra (500 MHz, toluene- $d_8$ ) of $\{\text{ONO}^{\text{SiPh}_3}\}\text{Al}((S)\text{-OCH}(\text{Me})\text{CO}_2i\text{Pr})$ ( <b>4a</b> ); bottom, 298 K; middle, 353 K; top, 373 K (* stands for residual solvent resonances).	<b>88</b>
<b>Figure 40</b>	Molecular structure of $\{\text{ONO}^{\text{SiPh}_3}\}\text{Al}((S)\text{-OCH}(\text{Me})\text{CO}_2i\text{Pr})$ ( <b>4a</b> ) (thermal ellipsoids drawn at 50 % probability level; all solvents molecules and hydrogen atoms, except that of the isopropyl moiety of	<b>90</b>

the isopropyl (*S*)-lactate group, are omitted for clarity). Selected bond distances (Å) and angles (deg): Al–O(74), 1.745(6); Al–O(11), 1.761(6); Al–O(51), 1.777(6); Al–O(71), 2.018(5); Al–N, 2.018(6); N–Al–O(71), 176.9(3); O(51)–Al–O(11), 114.9(3); O(51)–Al–O(74), 123.3(4); O(11)–Al–O(74), 121.2(4); O(74)–Al–O(71), 84.1(3); O(11)–Al–O(71), 89.0(2); O(51)–Al–O(71), 89.7(2); O(74)–Al–N, 93.1(3); O(11)–Al–N, 91.5(3); O(51)–Al–N, 92.9(3).

- Figure 41** ORTEP drawing of  $\{\text{ONO}^{\text{SiPh}_3}\}\text{Al}((R)\text{-OCH}(\text{Me})\text{CH}_2\text{CO}_2\text{Me})$  (**5a**) (thermal ellipsoids drawn at 50 % probability level; all solvents molecules and hydrogen atoms, except that of the methoxy moiety of the (*R*)- $\beta$ -alkoxy-butyrate group, are omitted for clarity). Selected bond distances (Å) and angles (deg): Al–O(74), 1.729(2); Al–O(51), 1.779(2); Al–O(11), 1.780(2); Al–O(71), 1.993(2); Al–N, 2.023(3); O(74)–Al–O(51), 121.83(12); O(74)–Al–O(11), 122.35(12); O(51)–Al–O(11), 115.77(11); O(71)–Al–N, 175.62(11); O(51)–Al–O(71), 86.37(10); O(74)–Al–O(71), 92.90(11); O(11)–Al–O(71), 88.15(10); O(74)–Al–N, 91.15(11); O(51)–Al–N, 90.08(11); O(11)–Al–N, 91.09(11). **91**
- Figure 42** ORTEP drawing of  $\{\text{ONO}^{\text{SiPh}_3}\}\text{Al}((rac)\text{-OCH}(\text{CF}_3)\text{CH}_2\text{CO}_2\text{Et})$  (**6a**) (thermal ellipsoids drawn at 30 % probability level; all solvents molecules and hydrogen atoms, except that of the ethyl of the (*rac*)- $\beta$ -alkoxy-trifluorobutyrate group, are omitted for clarity). Selected bond distances (Å) and angles (deg): Al–O(74), 1.755(2); Al–O(11), 1.767(2); Al–O(51), 1.777(2); Al–O(71), 2.030(2); Al–N, 2.017(2); O(74)–Al–O(11), 120.62(12); O(74)–Al–O(51), 120.86(12); O(11)–Al–O(51), 118.23(11); O(74)–Al–N, 92.14(10); O(11)–Al–N, 91.86(10); O(51)–Al–N, 91.28(10); O(74)–Al–O(71), 91.20(10); O(11)–Al–O(71), 87.82(10); O(51)–Al–O(71), 85.63(10); N–Al–O(71), 176.29(10). **92**
- Figure 43**  $^1\text{H}$  NMR spectrum (500 MHz,  $\text{CDCl}_3$ , 298 K) of a polylactide produced from the  $\{\text{ONO}^{\text{SiPh}_3}\}\text{AlMe}$  (**2a**)/*i*PrOH (1:1) system (Table 3, entry 16). **97**
- Figure 44**  $^1\text{H}$  NMR spectrum (500 MHz,  $\text{CD}_2\text{Cl}_2$ , 298 K) of a polylactide generated from the  $\{\text{ONO}^{\text{SiPh}_3}\}\text{AlMe}$  (**2a**)/BnOH (1:1) system (Table 3, entry 9). **97**
- Figure 45** Details of the methine (left) and methyl (right) regions of the  $^1\text{H}$  NMR spectra (500 MHz, toluene- $d_8$ , 298 K) of (a) (*S*)-**4a**, and mixtures of (*S*)-**4a** with (b) 1.1 equiv. of *rac*-LA, (c) 1.8 equiv. of L-LA, (d) 1.1 equiv. of D-LA, and (e) of *rac*-LA alone (\*stands for residual hexane resonances). **100**
- Figure 46** Details of the  $^1\text{H}$  NMR spectra (500 MHz, toluene- $d_8$ , 298 K) (a) (*S*)-**4b**, (b) a 1:1.1 (*S*)-**4b**/*rac*-LA reaction mixture after 30 min at 25 °C, and (d) *rac*-LA. **101**
- Figure 47** Details of the  $^1\text{H}$  NMR spectra (500 MHz,  $\text{CD}_2\text{Cl}_2$ , 298 K) of (a) (*S*)-**4a**, (b) a 1:1.2 (*S*)-**4a**/*rac*-LA mixture, and (c) *rac*-LA. **102**
- Figure 48** Details of the  $^1\text{H}$  NMR spectra (500 MHz, THF- $d_8$ , 298 K) (a) (*S*)-**4a**, **103**



	(b) a 1:1.7 mixture of ( <i>S</i> )- <b>4a</b> and <i>rac</i> -LA, and (c) <i>rac</i> -LA.	
<b>Figure 49</b>	Details of the low-field aliphatic region of the <sup>1</sup> H NMR spectra (500 MHz, CD <sub>2</sub> Cl <sub>2</sub> , 298 K) of a 1:6.26 mixture of ( <i>S</i> )- <b>4a</b> and L-LA kept at 25 °C. The bottom spectrum is that of pure ( <i>S</i> )- <b>4a</b> .	<b>104</b>
<b>Figure 50</b>	Details of the high-field aliphatic region of the <sup>1</sup> H NMR spectrum (500 MHz, CD <sub>2</sub> Cl <sub>2</sub> , 298 K) of a 1:6.26 mixture of <b>4a</b> and L-LA kept at 25 °C. The bottom spectrum is that of pure <b>4a</b> .	<b>105</b>
<b>Figure 51</b>	Detail of the aliphatic region of the <sup>1</sup> H NMR spectrum (500 MHz, CD <sub>2</sub> Cl <sub>2</sub> , 298 K) of a 1:6.26 <b>4a</b> /L-LA mixture after 503 h at 25 °C (66% conversion of L-LA).	<b>106</b>
<b>Figure 52</b>	Detail of the aliphatic region of the <sup>1</sup> H NMR spectrum (500 MHz, toluene- <i>d</i> <sub>8</sub> , 298 K) of the reaction mixture <b>4a</b> /L-LA (1:6 equiv.) after 17 h at 80 °C (88% conversion of L-LA) (*stands for residual solvent resonances).	<b>106</b>
<b>Figure 53</b>	Plot of L-LA conversion vs. time for the reaction mixture of <b>4a</b> /L-LA (1:6.26) in CD <sub>2</sub> Cl <sub>2</sub> at 25 °C, [LA] <sub>0</sub> = 0.3932 mol.L <sup>-1</sup> .	<b>107</b>
<b>Figure 54</b>	Semi-logarithmic plot of L-LA conversion vs. time initiated by complex ( <i>S</i> )- <b>4a</b> (25 °C, CD <sub>2</sub> Cl <sub>2</sub> , [LA] <sub>0</sub> = 0.3932 mol.L <sup>-1</sup> ).	<b>108</b>
<b>Figure 55</b>	Plot of L-LA conversion vs. time for the reaction mixture of <b>4a</b> /L-LA (1:5) at 80 °C in toluene- <i>d</i> <sub>8</sub> , [LA] <sub>0</sub> = 0.269 mol.L <sup>-1</sup> .	<b>109</b>
<b>Figure 56</b>	Semi-logarithmic plot of L-LA conversion vs time initiated by complex ( <i>S</i> )- <b>4a</b> (80 °C, toluene- <i>d</i> <sub>8</sub> , [LA] <sub>0</sub> = 0.269 mol.L <sup>-1</sup> ).	<b>109</b>
<b>Figure 57</b>	<sup>1</sup> H NMR monitoring (500 MHz, CD <sub>2</sub> Cl <sub>2</sub> , 298 K) of the reaction of a 1:1.35 mixture of ( <i>R</i> )- <b>5a</b> and L-LA in CD <sub>2</sub> Cl <sub>2</sub> at 25 °C (* stands for residual solvent resonances). The bottom spectrum is that of pure ( <i>R</i> )- <b>5a</b> .	<b>111</b>
<b>Figure 58</b>	<sup>1</sup> H NMR spectrum (500 MHz, CD <sub>2</sub> Cl <sub>2</sub> , 298 K) of the 1:1.35 reaction of a mixture of ( <i>R</i> )- <b>5a</b> and L-LA after 23 h at 25 °C (* stands for residual solvent resonances).	<b>112</b>
<b>Figure 59</b>	<sup>1</sup> H NMR spectra (500 MHz, CD <sub>2</sub> Cl <sub>2</sub> , 298 K) of the 1:1.35 reaction of a mixture of ( <i>R</i> )- <b>5a</b> and L-LA after (bottom) 23 h and (top) 21 days at 25 °C (* stands for residual solvent resonances).	<b>113</b>
<b>Figure 60</b>	Molecular structure of pro-ligand {ONO <sup>Me,Cumyl</sup> }H <sub>2</sub> (all hydrogens atoms, except those of hydroxyl groups, are omitted for clarity; thermal ellipsoids drawn at 50 % probability). Selected bond distances (Å) and angles (deg): H(O(1))-N = 1.919; H(O(2))-N = 1.985; ∠Py-Ph(1) = 23.55; ∠Py-Ph(2) = 23.21.	<b>116</b>
<b>Figure 61</b>	ORTEP drawing of {ONO <sup>Me,Cumyl</sup> }Al(( <i>R</i> )-OCH(Me)CH <sub>2</sub> CO <sub>2</sub> Me) ( <b>5d</b> ) (thermal ellipsoids drawn at 50 % probability level; all solvents molecules and hydrogen atoms are omitted for clarity. Selected bond distances (Å) and angles (deg): (on the left): Al-O(74) = 1.745(2); Al-O(51) = 1.757(2); Al-O(11) = 1.762(2); Al-O(71) = 2.006(2); Al-N = 2.017(2); O(74)-Al-O(51) = 118.16(12); O(74)-Al-O(11) = 118.18(11); O(51)-Al-O(11) = 122.96(11); O(71)-Al-N = 171.00(11);	<b>120</b>

O(51)–Al–O(71) = 84.58(10); O(74)–Al–O(71) = 93.40(10); O(11)–Al–O(71) = 84.05(10); O(74)–Al–N = 95.44(10); O(51)–Al–N = 92.72(10); O(11)–Al–N = 90.26(10). (on the right): Al(2)–O(9) = 1.743(2); Al(2)–O(8) = 1.757(2); Al(2)–O(7) = 1.771(2); Al(2)–N(2) = 1.996(3); Al(2)–O(10) = 2.057(2); O(9)–Al(2)–O(8) = 120.76(12); O(9)–Al(2)–O(7) = 119.58(11); O(8)–Al(2)–O(7) = 119.06(11); O(9)–Al(2)–N(2) = 92.25(10); O(8)–Al(2)–N(2) = 92.62(11); O(7)–Al(2)–N(2) = 92.83(11); O(9)–Al(2)–O(10) = 91.27(10); O(8)–Al(2)–O(10) = 85.07(10); O(7)–Al(2)–O(10) = 85.95(10); N(2)–Al(2)–O(10) = 176.44(10).

- Figure 62** Detail of the aliphatic region of the  $^1\text{H}$  NMR spectrum (500 MHz, toluene- $d_8$ , 298 K) of; bottom, (*S*)-**4d**, and mixtures of (*S*)-**4d** with; middle, 1 equiv. of *rac*-LA and; top, of *rac*-LA (\*stands for residual solvent resonances). **122**
- Figure 63** Detail of the aromatic region of the  $^1\text{H}$  NMR spectrum (500 MHz, toluene- $d_8$ , 298 K) of the reaction mixture; bottom, (*S*)-**4d**, and mixtures of (*S*)-**4d** with; top, 1 equiv. of *rac*-LA. **122**
- Figure 64** Details of the aliphatic region of the VT- $^1\text{H}$  NMR spectra (500 MHz, toluene- $d_8$ , 298–363 K) of  $\{\text{ONO}^{\text{Me,Cumyl}}\}\text{Y}[\text{N}(\text{SiHMe}_2)_2](\text{THF})(\text{Et}_2\text{O})$  (**9**); bottom, 298 K; middle, 333 and 353 K; top, 363 K. (A)  $\text{C}_2$ -symmetric species. (B and C) Decomposition products (\*refers to residual solvent resonances). **124**
- Figure 65** ORTEP drawing of  $\{\text{ONO}^{\text{Me,Cumyl}}\}\text{Y}[\text{N}(\text{SiHMe}_2)_2](\text{THF})(\text{Et}_2\text{O})$  (**9**) (thermal ellipsoids drawn at 50% probability level; all hydrogen atoms are omitted for clarity). Selected bond distances (Å) and angles (deg): Y(1)–O(11) = 2.1427(19); Y(1)–O(51) = 2.144(2); Y(1)–O(61) = 2.366(2); Y(1)–O(71) = 2.358(2); Y(1)–N(2) = 2.615(2); Y(1)–N(3) = 2.268(3); Y(1)–Si(1) = 3.4276(10); Y(1)–Si(2) = 3.4158(11); N(2)–Y(1)–N(3) = 176.57(9); O(11)–Y(1)–O(51) = 153.77(7); O(71)–Y(1)–O(61) = 162.75(9); O(11)–Y(1)–N(2) = 76.32(7); O(11)–Y(1)–N(3) = 106.16(8); O(11)–Y(1)–O(61) = 90.60(8); O(11)–Y(1)–O(71) = 85.44(8); O(51)–Y(1)–N(2) = 77.76(7); O(51)–Y(1)–N(3) = 99.91(9); O(51)–Y(1)–O(61) = 88.43(8); O(51)–Y(1)–O(71) = 87.77(8); O(71)–Y(1)–N(2) = 83.58(8); O(71)–Y(1)–N(3) = 98.90(9); O(61)–Y(1)–N(2) = 79.17(7); O(61)–Y(1)–N(3) = 98.33(9); Si(2)–N(3)–Y(1) = 118.58(14); Si(1)–N(3)–Y(1) = 118.78(14) = Si(2)–N(3)–Si(1) = 122.63(16). **126**
- Figure 66**  $^1\text{H}$  NMR spectrum (500 MHz,  $\text{CDCl}_3$ , 298 K) of a PLA produced from  $\{\text{ONO}^{\text{Me,Cumyl}}\}\text{Y}((R)\text{-OCH}(\text{CH}_3)\text{CH}_2\text{COOMe})$  (**10**) (Table **10**, entry 10). **133**
- Figure 67**  $^1\text{H}$ - $^1\text{H}$  COSY NMR spectrum (500 MHz,  $\text{CDCl}_3$ , 298 K) of a PLA produced from  $\{\text{ONO}^{\text{Me,Cumyl}}\}\text{Y}((R)\text{-OCH}(\text{CH}_3)\text{CH}_2\text{COOMe})$  (**10**) (Table **10**, entry 10). **134**
- Figure 68** Carbonyl (A) and Methylene (B) regions of the  $^{13}\text{C}\{^1\text{H}\}$  NMR spectrum (100 MHz,  $\text{CDCl}_3$ , 298 K) of a PHB produced from  $\{\text{ONO}^{\text{Me,Cumyl}}\}\text{Y}((R)\text{-OCH}(\text{CH}_3)\text{CH}_2\text{COOMe})$  (**10**) (Table **10**, entry **136**

	21).	
<b>Figure 69</b>	$^1\text{H}$ NMR spectrum (500 MHz, $\text{CDCl}_3$ , 298 K) of a PHB produced from $\{\text{ONO}^{\text{Me,Cumyl}}\}\text{Y}((R)\text{-OCH}(\text{CH}_3)\text{CH}_2\text{COOMe})$ ( <b>10</b> ) (Table 10, entry 21).	<b>137</b>
<b>Figure 70</b>	$^1\text{H}$ - $^1\text{H}$ COSY NMR spectrum (500 MHz, $\text{CDCl}_3$ , 298 K) of a PHB produced from $\{\text{ONO}^{\text{Me,Cumyl}}\}\text{Y}((R)\text{-OCH}(\text{CH}_3)\text{CH}_2\text{COOMe})$ ( <b>10</b> ) (Table 10, entry 21).	<b>137</b>
<b>Figure 1A</b>	$^1\text{H}$ NMR spectrum (300 MHz, $\text{CDCl}_3$ , 298 K) of 1-(methoxymethyl)-4-methyl-2-(2-phenylpropan-2-yl)benzene.	<b>151</b>
<b>Figure 2A</b>	$^1\text{H}$ NMR spectrum (500 MHz, $\text{CDCl}_3$ , 298 K) of $\{\text{ONO}^{\text{Me,Cumyl}}\}\text{H}_2$ ( <b>1c</b> ).	<b>152</b>
<b>Figure 3A</b>	$^{13}\text{C}\{^1\text{H}\}$ NMR spectrum (125 MHz, $\text{CDCl}_3$ , 298 K) of $\{\text{ONO}^{\text{Me,Cumyl}}\}\text{H}_2$ ( <b>1c</b> ) (stands for residual solvent resonances).	<b>153</b>
<b>Figure 4A</b>	$^1\text{H}$ NMR spectrum (500 MHz, $\text{C}_6\text{D}_6$ , 298 K) of $\{\text{ONO}^{\text{SiPh}_3}\}\text{AlMe}$ ( <b>2a</b> ) (*stands for residual solvent resonances).	<b>154</b>
<b>Figure 5A</b>	Aromatic selected region of $^{13}\text{C}\{^1\text{H}\}$ NMR spectrum (125 MHz, $\text{C}_6\text{D}_6$ , 298 K) of $\{\text{ONO}^{\text{SiPh}_3}\}\text{AlMe}$ ( <b>2a</b> ).	<b>155</b>
<b>Figure 6A</b>	$^1\text{H}$ NMR spectrum (500 MHz, $\text{C}_6\text{D}_6$ , 298 K) of $\{\text{ONO}^{\text{SiMe}_2\text{tBu}}\}\text{AlMe}$ ( <b>2b</b> ) (*stands for residual toluene resonance).	<b>156</b>
<b>Figure 7A</b>	$^{13}\text{C}\{^1\text{H}\}$ NMR spectrum (125 MHz, $\text{C}_6\text{D}_6$ , 298 K) of $\{\text{ONO}^{\text{SiMe}_2\text{tBu}}\}\text{AlMe}$ ( <b>2b</b> ).	<b>157</b>
<b>Figure 8A</b>	$^1\text{H}$ NMR spectrum (500 MHz, $\text{C}_6\text{D}_6$ , 298 K) of $\{\text{ONO}^{\text{SiPh}_3}\}\text{Al}i\text{Bu}$ ( <b>2c</b> ) (*stands for residual toluene resonance).	<b>158</b>
<b>Figure 9A</b>	$^{13}\text{C}\{^1\text{H}\}$ NMR spectrum (125 MHz, $\text{C}_6\text{D}_6$ , 298 K) of $\{\text{ONO}^{\text{SiPh}_3}\}\text{Al}i\text{Bu}$ ( <b>2c</b> ) (*stands for residual hexane resonances).	<b>159</b>
<b>Figure 10A</b>	$^1\text{H}$ NMR spectrum (500 MHz, $\text{CD}_2\text{Cl}_2$ , 298 K) of $\{\text{ONO}^{\text{Me,Cumyl}}\}\text{AlMe}$ ( <b>2d</b> ) (*stands for residual solvent resonances).	<b>160</b>
<b>Figure 11A</b>	$^{13}\text{C}\{^1\text{H}\}$ NMR spectrum (125 MHz, $\text{CD}_2\text{Cl}_2$ , 298 K) of $\{\text{ONO}^{\text{Me,Cumyl}}\}\text{AlMe}$ ( <b>2d</b> ).	<b>161</b>
<b>Figure 12A</b>	<b>Figure 12A.</b> $^1\text{H}$ NMR spectrum (500 MHz, toluene- $d_8$ , 298 K) of $\{\text{ONO}^{\text{SiPh}_3}\}\text{AlO}i\text{Pr}$ ( <b>3a</b> ) (*stands for residual toluene resonance and methane release).	<b>162</b>
<b>Figure 13A</b>	$^{13}\text{C}\{^1\text{H}\}$ NMR spectrum (125 MHz, toluene- $d_8$ , 298 K) of $\{\text{ONO}^{\text{SiPh}_3}\}\text{AlO}i\text{Pr}$ ( <b>3a</b> ).	<b>163</b>
<b>Figure 14A</b>	$^1\text{H}$ NMR spectrum (500 MHz, toluene- $d_8$ , 298 K) of $\{\text{ONO}^{\text{SiPh}_3}\}\text{Al}(i\text{Pr}(S)\text{-lactate})$ ( <b>4a</b> ) (*stands for residual toluene resonance and methane release).	<b>164</b>
<b>Figure 15A</b>	$^{13}\text{C}\{^1\text{H}\}$ NMR spectrum (125 MHz, toluene- $d_8$ , 298 K) of $\{\text{ONO}^{\text{SiPh}_3}\}\text{Al}(i\text{Pr}(S)\text{-lactate})$ ( <b>4a</b> ).	<b>165</b>
<b>Figure 16A</b>	$^1\text{H}$ NMR spectrum (500 MHz, toluene- $d_8$ , 298 K) of $\{\text{ONO}^{\text{SiMe}_2\text{tBu}}\}\text{Al}(i\text{Pr}(S)\text{-lactate})$ ( <b>4b</b> ) (*stands for residual toluene and silicon grease resonances).	<b>166</b>
<b>Figure 17A</b>	$^{13}\text{C}\{^1\text{H}\}$ NMR spectrum (125 MHz, toluene- $d_8$ , 298 K) of	<b>167</b>

	$\{\text{ONO}^{\text{SiMe}_2\text{tBu}}\}\text{Al}(i\text{Pr}(S)\text{-lactate})$ ( <b>4b</b> ).	
<b>Figure 18A</b>	$^1\text{H}$ NMR spectrum (500 MHz, toluene- $d_8$ , 298 K) of $\{\text{ONO}^{\text{Me,Cumyl}}\}\text{Al}(i\text{Pr}(S)\text{-lactate})$ ( <b>4d</b> ) (*stands for residual solvent resonances).	<b>168</b>
<b>Figure 19A</b>	$^{13}\text{C}\{^1\text{H}\}$ NMR spectrum (125 MHz, toluene- $d_8$ , 298 K) of $\{\text{ONO}^{\text{Me,Cumyl}}\}\text{Al}(i\text{Pr}(S)\text{-lactate})$ ( <b>4d</b> ).	<b>169</b>
<b>Figure 20A</b>	$^1\text{H}-^1\text{H}$ NOESY NMR spectrum (400 MHz, toluene- $d_8$ , 298 K) of $\{\text{ONO}^{\text{Me,Cumyl}}\}\text{Al}(i\text{Pr}(S)\text{-lactate})$ ( <b>4d</b> ).	<b>170</b>
<b>Figure 21A</b>	$^1\text{H}$ NMR spectrum (500 MHz, $\text{CD}_2\text{Cl}_2$ , 298 K) of $\{\text{ONO}^{\text{SiPh}_3}\}\text{Al}((R)\text{-OCH}(\text{CH}_3)\text{CH}_2\text{COOMe})$ ( <b>5a</b> ) (*stands for residual solvent resonances).	<b>171</b>
<b>Figure 22A</b>	$^{13}\text{C}\{^1\text{H}\}$ NMR spectrum (125 MHz, $\text{CD}_2\text{Cl}_2$ , 298 K) of $\{\text{ONO}^{\text{SiPh}_3}\}\text{Al}((R)\text{-OCH}(\text{CH}_3)\text{CH}_2\text{COOMe})$ ( <b>5a</b> ).	<b>172</b>
<b>Figure 23A</b>	$^1\text{H}$ NMR spectrum (500 MHz, $\text{CD}_2\text{Cl}_2$ , 298 K) of $\{\text{ONO}^{\text{Me,Cumyl}}\}\text{Al}((R)\text{-OCH}(\text{CH}_3)\text{CH}_2\text{COOMe})$ ( <b>5d</b> ). (*stands for residual solvent resonances). (P.S: we can notice the release of the ligand. We didn't succeed to purify this complex to use it in polymerization).	<b>173</b>
<b>Figure 24A</b>	$^1\text{H}$ NMR spectrum (500 MHz, $\text{CD}_2\text{Cl}_2$ , 298 K) of $\{\text{ONO}^{\text{SiPh}_3}\}\text{Al}((rac)\text{-OCH}(\text{CF}_3)\text{CH}_2\text{COOEt})$ ( <b>6a</b> ) (*stands for residual solvent resonances).	<b>174</b>
<b>Figure 25A</b>	$^{13}\text{C}\{^1\text{H}\}$ NMR spectrum (125 MHz, $\text{CD}_2\text{Cl}_2$ , 298 K) of $\{\text{ONO}^{\text{SiPh}_3}\}\text{Al}((rac)\text{-OCH}(\text{CF}_3)\text{CH}_2\text{COOEt})$ ( <b>6a</b> ).	<b>175</b>
<b>Figure 26A</b>	$^{19}\text{F}\{^1\text{H}\}$ NMR spectrum (185 MHz, $\text{CD}_2\text{Cl}_2$ , 298 K) of $\{\text{ONO}^{\text{SiPh}_3}\}\text{Al}((rac)\text{-OCH}(\text{CF}_3)\text{CH}_2\text{COOEt})$ ( <b>6a</b> ).	<b>176</b>
<b>Figure 27A</b>	$^1\text{H}$ NMR spectrum (500 MHz, $\text{CD}_2\text{Cl}_2$ , 298 K) of $\{\text{ONO}^{\text{SiPh}_3}\}\text{Al}((rac)\text{-OCH}(\text{CF}_3)\text{CH}_2\text{COOEt})$ ( <b>6d</b> ) (*stands for residual solvent resonances).	<b>177</b>
<b>Figure 28A</b>	$^{13}\text{C}\{^1\text{H}\}$ NMR spectrum (125 MHz, $\text{CD}_2\text{Cl}_2$ , 298 K) of $\{\text{ONO}^{\text{Me,Cumyl}}\}\text{Al}((rac)\text{-OCH}(\text{CF}_3)\text{CH}_2\text{COOEt})$ ( <b>6d</b> ) (*stands for residual solvent resonances).	<b>178</b>
<b>Figure 29A</b>	$^{19}\text{F}\{^1\text{H}\}$ NMR spectrum (185 MHz, $\text{CD}_2\text{Cl}_2$ , 298 K) of $\{\text{ONO}^{\text{Me,Cumyl}}\}\text{Al}((rac)\text{-OCH}(\text{CF}_3)\text{CH}_2\text{COOEt})$ ( <b>6d</b> ).	<b>179</b>
<b>Figure 30A</b>	$^1\text{H}-^1\text{H}$ NOESY NMR spectrum (400 MHz, $\text{CD}_2\text{Cl}_2$ , 298 K) of $\{\text{ONO}^{\text{Me,Cumyl}}\}\text{Al}((rac)\text{-OCH}(\text{CF}_3)\text{CH}_2\text{COOEt})$ ( <b>6d</b> ).	<b>180</b>
<b>Figure 31A</b>	$^1\text{H}$ NMR spectrum (500 MHz, toluene- $d_8$ , 298 K) of the 1:5 reaction of a mixture of ( <i>S</i> )- <b>4a</b> and L-LA after 18 h at 80 °C in toluene- $d_8$ (*stands for residual toluene resonance).	<b>181</b>
<b>Figure 32A</b>	$^{13}\text{C}\{^1\text{H}\}$ NMR spectrum (125 MHz, toluene- $d_8$ , 298 K) of the 1:5 reaction of a mixture of ( <i>S</i> )- <b>4a</b> and L-LA after 18 h at 80 °C.	<b>182</b>
<b>Figure 33A</b>	Details of the upfield region [COO, CO, C-N and $\text{C}^4$ ] of the $^{13}\text{C}\{^1\text{H}\}$ NMR spectrum (125 MHz, toluene- $d_8$ , 298 K) of the 1:5 reaction of a mixture of ( <i>S</i> )- <b>4a</b> and L-LA after 18 h at 80 °C in toluene- $d_8$ .	<b>183</b>
<b>Figure 34A</b>	$^1\text{H}-^1\text{H}$ COSY NMR spectrum (500 MHz, toluene- $d_8$ , 298 K) of the 1:5 reaction of a mixture of ( <i>S</i> )- <b>4a</b> and L-LA after 18 h at 80 °C in toluene- $d_8$ (*stands for residual toluene resonance).	<b>184</b>

<b>Figure 35A</b>	$^1\text{H}$ - $^1\text{H}$ HMQC NMR spectrum (500 MHz, toluene- $d_8$ , 298 K) of the 1:5 reaction of a mixture of ( <i>S</i> )- <b>4a</b> and L-LA after 18 h at 80 °C in toluene- $d_8$ (*stands for residual toluene resonance).	<b>185</b>
<b>Figure 36A</b>	$^1\text{H}$ - $^1\text{H}$ HMQC NMR spectrum (500 MHz, toluene- $d_8$ , 298 K) of the 1:5 reaction of a mixture of ( <i>S</i> )- <b>4a</b> and L-LA after 18 h at 80 °C in toluene- $d_8$ .	<b>186</b>
<b>Figure 37A</b>	$^1\text{H}$ - $^1\text{H}$ HMBC NMR spectrum (500 MHz, toluene- $d_8$ , 298 K) of the 1:5 reaction of a mixture of ( <i>S</i> )- <b>4a</b> and L-LA after 18 h at 80 °C in toluene- $d_8$ .	<b>187</b>
<b>Figure 38A</b>	$^1\text{H}$ NMR spectrum (500 MHz, $\text{CD}_2\text{Cl}_2$ , 298 K) of the 1:1.35 reaction of a mixture of ( <i>R</i> )- <b>5a</b> and L-LA after 23 h at 25 °C in $\text{CD}_2\text{Cl}_2$ . (*stands for residual solvent resonance).	<b>188</b>
<b>Figure 39A</b>	$^{13}\text{C}\{^1\text{H}\}$ NMR spectrum (125 MHz, $\text{CD}_2\text{Cl}_2$ , 298 K) of the 1:1.35 reaction of a mixture of ( <i>R</i> )- <b>5a</b> and L-LA after 23 h at 25 °C in $\text{CD}_2\text{Cl}_2$ .	<b>189</b>
<b>Figure 40A</b>	Details of the upfield region [COO, CO, C-N and $\text{C}^4$ ] of the $^{13}\text{C}\{^1\text{H}\}$ NMR spectrum (125 MHz, $\text{CD}_2\text{Cl}_2$ , 298 K) of the 1:1.35 reaction of a mixture of ( <i>R</i> )- <b>5a</b> and L-LA after 23 h at 25 °C in $\text{CD}_2\text{Cl}_2$ .	<b>190</b>
<b>Figure 41A</b>	$^1\text{H}$ - $^1\text{H}$ COSY NMR spectrum (500 MHz, $\text{CD}_2\text{Cl}_2$ , 298 K) of the 1:1.35 reaction of a mixture of ( <i>R</i> )- <b>5a</b> and L-LA after 23 h at 25 °C in $\text{CD}_2\text{Cl}_2$ .	<b>191</b>
<b>Figure 42A</b>	$^1\text{H}$ - $^1\text{H}$ HMQC NMR spectrum (500 MHz, $\text{CD}_2\text{Cl}_2$ , 298 K) of the 1:1.35 reaction of a mixture of ( <i>R</i> )- <b>5a</b> and L-LA after 23 h at 25 °C in $\text{CD}_2\text{Cl}_2$ .	<b>192</b>
<b>Figure 43A</b>	$^1\text{H}$ - $^1\text{H}$ HMBC NMR spectrum (500 MHz, $\text{CD}_2\text{Cl}_2$ , 298 K) of the 1:1.35 reaction of a mixture of ( <i>R</i> )- <b>5a</b> and L-LA after 23 h at 25 °C in $\text{CD}_2\text{Cl}_2$ .	<b>193</b>
<b>Figure 44A</b>	$^1\text{H}$ - $^1\text{H}$ HMBC NMR spectrum (500 MHz, $\text{CD}_2\text{Cl}_2$ , 298 K) of the 1:1.35 reaction of a mixture of ( <i>R</i> )- <b>5a</b> and L-LA after 23 h at 25 °C in $\text{CD}_2\text{Cl}_2$ .	<b>194</b>
<b>Figure 45A</b>	$^1\text{H}$ NMR spectrum (500 MHz, toluene- $d_8$ , 298 K) of $\{\text{ONO}^{\text{Me,Cumyl}}\}\text{Y}[\text{N}(\text{SiHMe}_2)_2](\text{THF})(\text{Et}_2\text{O})(\mathbf{9})$ .	<b>195</b>
<b>Figure 46A</b>	$^1\text{H}$ NMR spectrum (500 MHz, Pyridine- $d_5$ , 298 K) of $\{\text{ONO}^{\text{Me,Cumyl}}\}\text{Y}[\text{N}(\text{SiHMe}_2)_2](\text{THF})(\text{Et}_2\text{O})(\mathbf{9})$ (*stands for residual solvent resonance).	<b>196</b>
<b>Figure 47A</b>	$^{13}\text{C}\{^1\text{H}\}$ NMR spectrum (500 MHz, Pyridine- $d_5$ , 298 K) of $\{\text{ONO}^{\text{Me,Cumyl}}\}\text{Y}[\text{N}(\text{SiHMe}_2)_2](\text{THF})(\text{Et}_2\text{O})(\mathbf{9})$ .	<b>197</b>
<b>Figure 48A</b>	$^1\text{H}$ NMR spectrum (500 MHz, toluene- $d_8$ , 258 K) of $\{\text{ONO}^{\text{Me,Cumyl}}\}\text{Y}((R)\text{-OCH}(\text{CH}_3)\text{CH}_2\text{COOMe})(\mathbf{10})$ .	<b>198</b>
<b>Figure 49A</b>	$^{13}\text{C}\{^1\text{H}\}$ NMR (100 MHz, toluene- $d_8$ , 258 K) of $\{\text{ONO}^{\text{Me,Cumyl}}\}\text{Y}((R)\text{-OCH}(\text{CH}_3)\text{CH}_2\text{COOMe})(\mathbf{10})$ .	<b>199</b>
<b>Figure 50A</b>	$^1\text{H}$ - $^1\text{H}$ NOESY spectrum (400 MHz, toluene- $d_8$ , 258 K) of $\{\text{ONO}^{\text{Me,Cumyl}}\}\text{Y}((R)\text{-OCH}(\text{CH}_3)\text{CH}_2\text{CO}_2\text{Me})(\mathbf{10})$ .	<b>200</b>
<b>Figure 51A</b>	$^1\text{H}$ NMR spectrum (500 MHz, THF- $d_8$ , 298 K) of $\{\text{ONO}^{\text{Me,Cumyl}}\}\text{Y}((S,S)\text{-OCH}(\text{CH}_3)\text{OCH}(\text{CH}_3)\text{COOMe})(\text{THF})(\mathbf{11})$ (*stands for residual solvent resonance).	<b>201</b>
<b>Figure 52A</b>	$^{13}\text{C}$ - $^1\text{H}$ HMQC NMR spectrum (500 MHz, THF- $d_8$ , 298 K) of	<b>202</b>

- $\{\text{ONO}^{\text{Me,Cumyl}}\}\text{Y}((S,S)\text{-OCH}(\text{CH}_3)\text{OCH}(\text{CH}_3)\text{COOMe})(\text{THF})(\mathbf{11})$ .
- Figure 53A**  $^{13}\text{C}$ - $^1\text{H}$  HMBC NMR spectrum (500 MHz, THF- $d_8$ , 298 K) of  $\{\text{ONO}^{\text{Me,Cumyl}}\}\text{Y}((S,S)\text{-OCH}(\text{CH}_3)\text{OCH}(\text{CH}_3)\text{COOMe})(\text{THF})(\mathbf{11})$ . **203**
- Figure 54A** Selected region of  $^{13}\text{C}$ - $^1\text{H}$  HMBC NMR spectrum (500 MHz, THF- $d_8$ , 298 K) of  $\{\text{ONO}^{\text{Me,Cumyl}}\}\text{Y}((S,S)\text{-OCH}(\text{CH}_3)\text{OCH}(\text{CH}_3)\text{COOMe})(\text{THF})(\mathbf{11})$ . **204**

## SCHEME INDEX

<b>Scheme 1</b>	General scheme for (a) the ring-opening polymerization of cyclic esters and (b) ROP of <i>rac</i> -lactide using a metal-alkoxide species.	<b>2</b>
<b>Scheme 2</b>	Synthetic pathway to the preparation of lactide and PLA.	<b>4</b>
<b>Scheme 3</b>	Different types of polylactides.	<b>5</b>
<b>Scheme 4</b>	PHB microstructures.	<b>6</b>
<b>Scheme 5</b>	Proposed pathway for the cationic ROP of lactide (R = H, Me or growing polymer chain, Tf = CF <sub>3</sub> SO <sub>2</sub> ).	<b>7</b>
<b>Scheme 6</b>	Anionic mechanism of the ROP of lactide.	<b>8</b>
<b>Scheme 7</b>	General activated monomer mechanism for the ROP of lactide. The charge is purely formal.	<b>9</b>
<b>Scheme 8</b>	Ring-opening of a cyclic ester by nucleophilic attack of a guanidine in presence of alcohol.	<b>10</b>
<b>Scheme 9</b>	Dual organic/organometallic approach.	<b>10</b>
<b>Scheme 10</b>	General representation of the coordination-insertion mechanism for the ROP of lactide.	<b>12</b>
<b>Scheme 11</b>	Representation of intra- and inter- molecular transesterification side-reactions.	<b>16</b>
<b>Scheme 12</b>	Structure and Synthesis of the Neutral and Cationic Aluminum Complexes ( <b>2a-c</b> ) Featuring Tridentate Diamidoamino Ligands.	<b>20</b>
<b>Scheme 13</b>	Kinetic Resolution of <i>rac</i> -Lactide with ( <i>R</i> )-(SALBinapht)Al(OCH <sub>3</sub> ) Described by Spassky <i>et al.</i>	<b>22</b>
<b>Scheme 14</b>	Yttrium Initiators ( <b>47-49</b> ) Supported by <i>N,O,P</i> - and <i>N,O,O,O</i> -Donor Ligands.	<b>40</b>
<b>Scheme 15</b>	Yttrium Piperazine-Bis(Phenolate) Complexes ( <b>62-64</b> ).	<b>48</b>
<b>Scheme 16</b>	The Reaction of <b>70</b> and One Equivalent of LLA at Ambient Temperature Affords Complex <b>71</b> .	<b>52</b>
<b>Scheme 17</b>	Free energy changes along the reaction for the first insertion of a monomer unit.	<b>55</b>
<b>Scheme 18</b>	Schematic Representation of the First Step of the ROP Mechanism of ( <i>R</i> )- $\beta$ -Butyrolactone by an Y-Salan Alkoxide Initiator ( <b>75</b> ) Computed at the DFT level. Bond Lengths are Given in Angstroms.	<b>57</b>
<b>Scheme 19</b>	Preparation of Aluminum Complexes ( <b>2-6</b> ) Featuring Bis(Naphtholate)-Pyridine Ligands.	<b>79</b>
<b>Scheme 20</b>	Preparation of Al-Methyl ( <b>2a</b> ) and Al-Isopropoxide ( <b>3a</b> ) Complexes.	<b>83</b>
<b>Scheme 21</b>	Ring-Opening Polymerization of <i>rac</i> -LA Initiated by Complexes <b>2-5</b> .	<b>94</b>
<b>Scheme 22</b>	General Scheme for the Reactions between Al-Isopropyl ( <i>S</i> ) Lactate Complexes ( <b>4a-b</b> ) and L-LA.	<b>99</b>

<b>Scheme 23</b>	Reaction between 1 equiv of Al-(methyl ( <i>R</i> )- $\beta$ -alkoxy-butyrates) ( <b>5a</b> ) and 1.35 equiv of L-LA giving the product of the first insertion of the LA molecule ( <b>8a</b> ).	<b>110</b>
<b>Scheme 24</b>	Preparation of Pro-Ligand $\{\text{ONO}^{\text{Me,Cumyl}}\}_2\text{H}_2$ ( <b>1c</b> ).	<b>115</b>
<b>Scheme 25</b>	Synthesis of Aluminum Complexes ( <b>2-6</b> ) Supported by the $\{\text{ONO}^{\text{Me,Cumyl}}\}_2^{2-}$ Ligand.	<b>117</b>
<b>Scheme 26</b>	Synthetic Route for Y-Amido Complex ( <b>9</b> ).	<b>123</b>
<b>Scheme 27</b>	Synthesis of Yttrium Complexes Supported by the $\{\text{ONO}^{\text{Me,Cumyl}}\}_2^{2-}$ Ligand ( <b>1c</b> ).	<b>127</b>
<b>Scheme 28</b>	Model geometries computed to assess possible C–H $\cdots$ $\pi$ interactions in <b>5d</b> and <b>10</b> .	<b>129</b>
<b>Scheme 29</b>	Ring-Opening Polymerization of <i>rac</i> -LA Initiated by Complexes <b>9-10</b> .	<b>131</b>
<b>Scheme 30</b>	Ring-Opening Polymerization of <i>rac</i> - $\beta$ -BL Initiated by Complexes <b>9-10</b> .	<b>131</b>



## TABLE INDEX

<b>Table 1</b>	Standard Thermodynamic Parameters of Polymerization of Common Five- and Six-Membered Cyclic Monomers.	<b>2</b>
<b>Table 2</b>	Heteroselectivity during the ROP of <i>rac</i> -LA using [OSSO]Y complexes.	<b>45</b>
<b>Table 3</b>	Comparison of the $^{13}\text{C}\{^1\text{H}\}$ NMR chemical shifts (ppm) for carbonyl groups in aluminum-{alkoxy ester} complexes <b>4a</b> , <b>4b</b> , <b>5a</b> and <b>6a</b> , and the corresponding hydroxy-ester reagent.	<b>87</b>
<b>Table 4</b>	Selected bond lengths (Å) around the Al center for compounds <b>2a</b> , <b>4a</b> , <b>5a</b> and <b>6a</b> , and close contacts (Å) for compounds <b>4a</b> , <b>5a</b> and <b>6a</b> .	<b>93</b>
<b>Table 5</b>	ROP of <i>rac</i> -lactide promoted by $\{\text{ONO}^{\text{SiR}^3}\}\text{AlR}$ complexes.	<b>95</b>
<b>Table 6</b>	Methine region of $^1\text{H}$ NMR and $^1\text{H}$ homo-decoupled NMR spectra of different PLAs.	<b>98</b>
<b>Table 7</b>	Reactions between D-, L- and <i>rac</i> -Lactide Monomers and Complexes ( <i>S</i> )- <b>4a</b> and ( <i>S</i> )- <b>4b</b> .	<b>99</b>
<b>Table 8</b>	Kinetic monitoring ( $^1\text{H}$ NMR) of the reaction of <b>4a</b> /L-LA (1:6.26) mixture in $\text{CD}_2\text{Cl}_2$ at 25 °C.	<b>107</b>
<b>Table 9</b>	Kinetic monitoring ( $^1\text{H}$ NMR) of the reaction of <b>4a</b> /L-LA (1:5) mixture in toluene- $d_8$ at 80 °C.	<b>108</b>
<b>Table 10</b>	ROP of <i>rac</i> -Lactide and <i>rac</i> - $\beta$ -butyrolactone Initiated by Complexes <b>9</b> and <b>10<sup>a</sup></b> .	<b>131</b>
<b>Table 11</b>	Methine region of $^1\text{H}$ NMR and $^1\text{H}$ homo-decoupled NMR spectra of different PLAs.	<b>135</b>
<b>Table 1A</b>	Summary of crystal and refinement data for compounds <b>2a</b> , <b>5a</b> , <b>6a</b> , <b>5d</b> , <b>1c</b> and <b>9</b> .	<b>150</b>

## LIST OF ABBREVIATIONS

(R)-SALBinapht	R-(-)-2,2'-[1,1'-binaphthyl-2,2'-diylbis(nitrilomethyldiylidene)]diphenol
BBL	$\beta$ -butyrolactone
BL	Butyrolactone
Bn	Benzyl
Box	Deprotonated chiral and nonchiral 2,2'-methylene[bis(oxazoline)]
br	Broad signal (NMR)
COSY	Correlation Spectroscopy
d	Doublet (NMR)
DFT	Density Functional Theory
Et	Ethyl
GPC	Gel Permeation Chromatography
HMBC	Heteronuclear Multiple Bond Correlation
HMQC	Heteronuclear Multiple Quantum Correlation
I	Initiator
<i>i</i> Pr	Iso-propyl
J	Coupling Constant (NMR)
LA	Lactide
m	Multiplet (NMR)
M	Monomer
MALDI-TOF-MS	Matrix assisted laser desorption ionization time-of-flight mass spectrometry
Me	Methyl
$M_n$	Number-average molecular mass
$M_{n,calc}$	Theoretic number-average molecular mass
$M_{n,exp}$	Experimental number-average molecular mass
MOM	Methoxymethyl ether (Protecting group)
$M_w$	Weight-average molecular mass
NMR	Nuclear Magnetic Resonance
NOESY	Nuclear Overhauser Effect Spectroscopy
OR	Alkoxide group
PDI	Polydispersity index ( $M_w/M_n$ )
PDLA	Enantiopure poly(D-lactide)
PET	Poly(ethylene terephthalate)

Ph	Phenyl
PHA	Poly(hydroxyalkanoate)
PHB	Poly(hydroxybutyrate)
PLA	Poly(lactide)
PLLA	Enantiopure poly(L-lactide)
$P_m$	Probability of meso linkage
$P_r$	Probability of racemic linkage
PS	Polystyrene
R	Alkyl group
<i>rac</i> -	Racemic
ROP	Ring-Opening Polymerization
SEC	Size Exclusion Chromatography
<i>t</i> Bu	Tert-butyl
$T_g$	Glass Transition
THF	Tetrahydrofurane
$T_m$	Melting Temperature
TOF	Turnover frequency
TON	Turnover number
$\delta$	Chemical shift (NMR)

## ABSTRACT

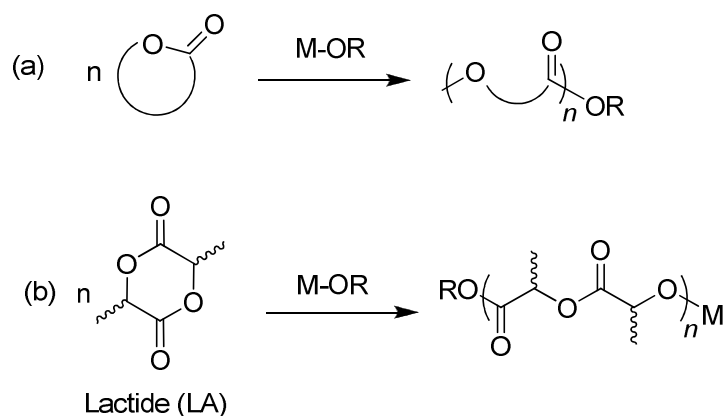
A series of new Al(III) complexes bearing silyl *ortho*-substituted 2,6-bis(naphtholate)-pyridine tridentate ligands ( $\{\text{ONO}^{\text{SiR}_3}\}^{2-}$ ,  $\text{SiR}_3 = \text{SiPh}_3, \text{SiMe}_2\text{tBu}$ ) and two monomeric Y(III) complexes bearing a new cumyl *ortho*-substituted 2,6-bis(phenolate)-pyridine tridentate ligand  $\{\text{ONO}^{\text{Me,Cumyl}}\}^{2-}$  have been prepared and structurally characterized in solution and in the solid-state. Preliminary studies on the catalytic performances of the compounds in the ROP of racemic lactide and  $\beta$ -butyrolactone are described. Also, details of the reactions of chiral Al-lactate and  $\beta$ -alkoxy ester complexes which are close models/mimics of the first intermediates and active species involved in the initiation and propagation steps of the ROP of lactides and  $\beta$ -lactones with stoichiometric amounts of lactide.

# 1. INTRODUCTION

## 1.1 GENERAL INTRODUCTION

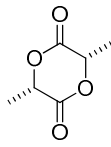
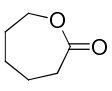
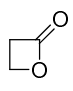
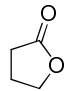
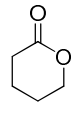
Synthetic petrochemical-based polymers have had a tremendous industrial impact since the 1940s. Despite the numerous advantages of these materials, two major drawbacks remain to be solved, namely, the use of nonrenewable resources in their production and the ultimate fate of these large-scale commodity polymers. Due to their unique properties, biodegradable polymers have been considered as alternative environmentally friendly polymers. The possibility to prepare some of these materials from renewable resources has proven to be of increasing importance and has opened commercial perspectives for a range of applications (e.g. packaging materials and biomedical systems).<sup>1</sup> Among the variety of biodegradable polymers known, aliphatic polyesters are an attractive class of thermoplastics, especially those derived from lactic acid (PLA).<sup>2</sup>

The ring-opening polymerization (ROP) of lactones and related monomers, in which the relief of ring-strain is the driving force for polymerization (Scheme 1), is the most efficient method to prepare aliphatic polyester materials. Some thermodynamic data for common five- and six-membered monomers are given in Table 1. In all the examples given, the entropic contribution into free energy is positive, like in the majority of polymerizations, and thus the monomer-polymer conversion is possible if the negative enthalpic contribution can outweigh the entropic factor.<sup>3</sup> This ROP chain-growth process proceeds with significantly better control in terms of molecular-weight and polydispersity ( $M_w/M_n$ ) than step-growth processes, that is, the polycondensation of diacid/diol comonomers or hydroxy-acid monomers.<sup>4,5</sup>



**Scheme 1.** General scheme for (a) the ring-opening polymerization of cyclic esters and (b) ROP of *rac*-lactide using a metal-alkoxide species.

**Table I.** Standard Thermodynamic Parameters of Polymerization of Common Five- and Six-Membered Cyclic Monomers.<sup>3,6,7</sup>

					
	L-Lactide	ε-Caprolactone	β-Propiolactone	γ-Butyrolactone	δ-Valerolactone
$\Delta H^\circ/(\text{kJ}\cdot\text{mol}^{-1})$	-22.9	-28.8	-82.3	5.1	-27.4
$\Delta S^\circ/(\text{J}\cdot\text{mol}^{-1}\cdot\text{K}^{-1})$	-25.0 <sup>b</sup>	-53.9 <sup>a</sup>	-74 <sup>a</sup>	-29.9 <sup>a</sup>	-65.0 <sup>a</sup>

<sup>a</sup> [Monomer] = 10 M, conducted in liquid monomer

<sup>b</sup> [Monomer] = 1 M, conducted in solution

## 1.2 ALIPHATIC BIODEGRADABLE POLYESTERS

As to synthetic biodegradable polymers, aliphatic polyesters are representatives. Nowadays, aliphatic polyesters, such as poly(lactide) and polyhydroxybutyrate, are commercially produced and their output continue to increase.

### 1.2.1 Poly(lactic acid) (PLA)

Poly(lactic acid) (PLA) is a thermoplastic material with rigidity and clarity similar to polystyrene (PS) or poly(ethylene terephthalate) (PET). End uses of PLA are in rigid packaging, flexible film packaging, cold drink cups, cutlery, apparel and staple fiber, bottles, injection molded products, extrusion coating, and so on.<sup>8</sup> PLA is bio-based, resorbable, and biodegradable under industrial composting conditions.<sup>9</sup>

PLA cannot be considered as a new polymer. As early as in 1845, PLA was synthesized by Théophile-Jules Pelouze by the condensation of lactic acid. In 1932, Wallace Hume Carothers et al. developed a method to polymerize lactide to produce PLA that was later patented by DuPont in 1954. Although PLA existed for several decades, its use was limited to biomedical applications (e.g., biocompatible sutures, implants, biologically active controlled release devices) due to its high cost. The low molecular weight PLA polymers obtained also hampered their wide-ranging applications. The breakthrough occurred in the early 1990s when Cargill Inc. succeeded in polymerizing lactide on large-scale ring-opening reactions using a Sn(II)-based catalyst (Scheme 2).<sup>2,10</sup> In 1997, Cargill Dow LLC, a joint venture between Cargill Inc. and the The Dow Chemical Company, was formed to begin truly commercially significant production of PLA resins under the trade name NatureWorks<sup>TM</sup>. This is a major landmark in PLA's history because it signifies the beginning of a large-scale use of this bio-based polymer, transforming PLA from a specialty material to a commodity thermoplastic.<sup>10</sup>

Since lactide is prepared from lactic acid, it can be found in two diastereomeric forms: *meso*-lactide and D,L-lactide, the 50:50 mixture of which is also called *rac*-lactide (Figure 1).

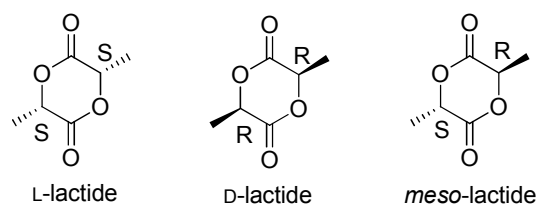
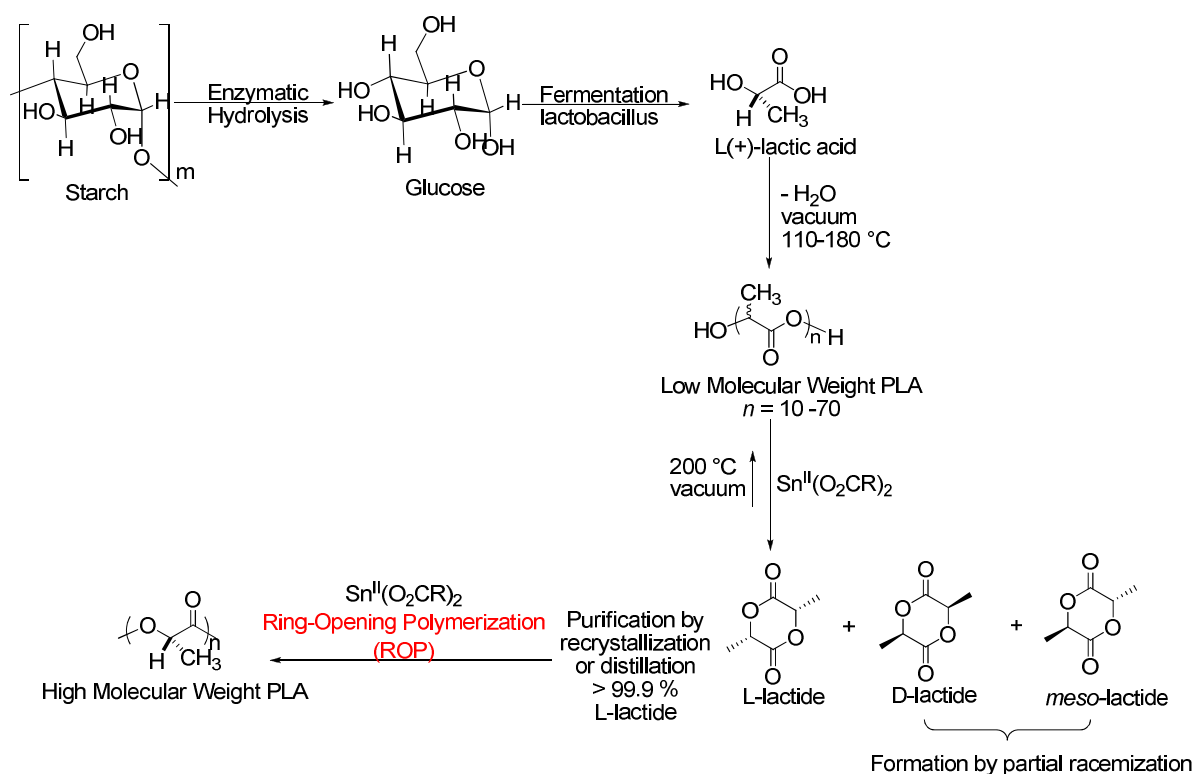


**Figure 1.** Stereoisomers of lactide.

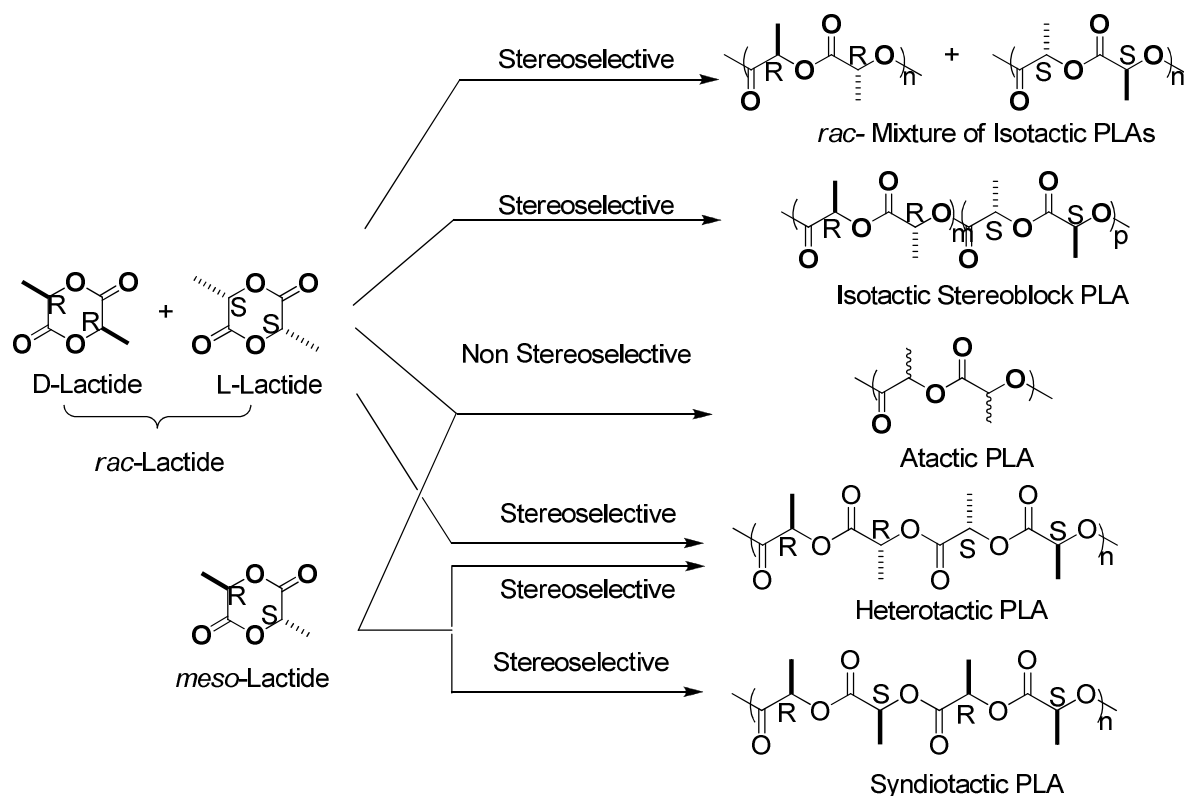
Purification of lactic acid produced by industrial bacterial fermentation is of decisive importance because crude lactic acid contains many impurities such as acids, alcohols, esters, metals, and traces of sugar and nutrients. The lactide monomer for PLA production is obtained from catalytic depolymerization of short PLA chains under reduced pressure.<sup>11</sup> This prepolymer is produced by dehydration and polycondensation of lactic acid under vacuum at high temperature. After purification, lactide is used for the production of PLA and lactide copolymers by ROP, which is conducted in bulk at temperatures above the melting point of the lactides and below temperatures that cause degradation of the formed PLA.



**Scheme 2.** Synthetic pathway to the preparation of lactide and PLA.<sup>12</sup>



The physical –notably the thermo-mechanical– properties of a polymeric material critically depend on many factors, one of which is stereochemistry. Polylactides can exhibit different microstructures depending both on the monomer involved and on the course of the polymerization reaction (Scheme 3).<sup>2,13,14</sup>



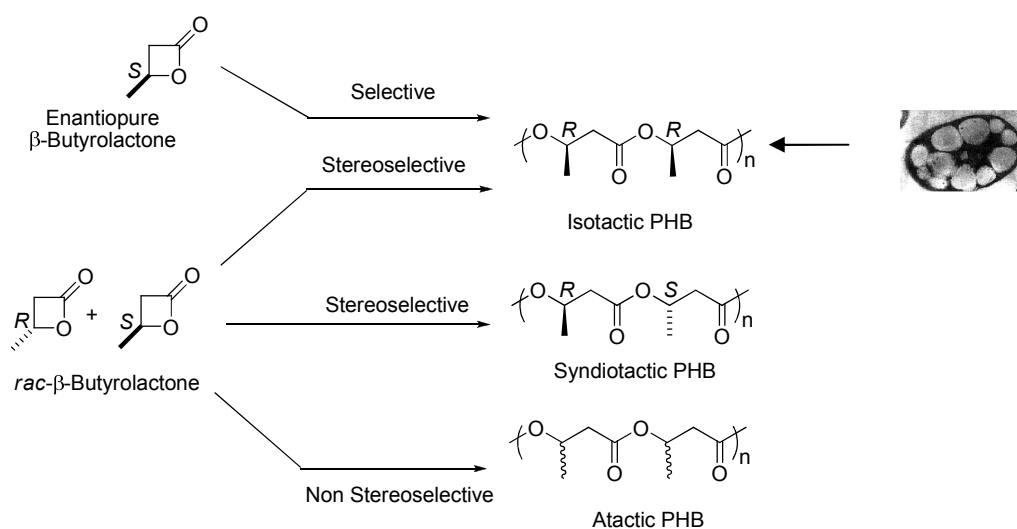
**Scheme 3.** Different types of polylactides.

### 1.2.2 Poly(3-hydroxybutyrate) (PHB)

Isotactic poly(3-hydroxybutyrate) (iPHB) is a natural polyester whose current notoriety is due to its inherent biodegradability.<sup>15</sup> iPHB is naturally produced from acetyl-CoA by bacteria. Growing on glucose, the bacterium *Ralstonia eutropha* can amass up to 85% of its dry weight in PHB, which makes this microorganism a miniature bioplastic factory.<sup>16</sup> This bacterial production yields perfectly isotactic, highly crystalline thermoplastic material ( $T_m = 180\text{ }^\circ\text{C}$ ), where the chiral center in each repeat unit has a *R* absolute configuration. In

1999, Monsanto has developed genetic modification of plants to make them produce larger quantities of PHB in an attempt to industrialize the production of this polymer material.<sup>16</sup>

Synthetic analogues of natural-origin PHB can be prepared more conveniently by the ring-opening polymerization of  $\beta$ -butyrolactone (BL – produced from 3-hydroxybutyric acid obtained via fermentation of sugars) using metal-based catalysts/initiators (Scheme 4). The ROP of specifically substituted  $\beta$ -lactone rings for the preparation of poly( $\beta$ -esters) allows for modulation of the polymer chain stereochemistry. In addition, ROP allows for the introduction of a range of pendant group structural types.<sup>17,18</sup>



**Scheme 4.** PHB microstructures.

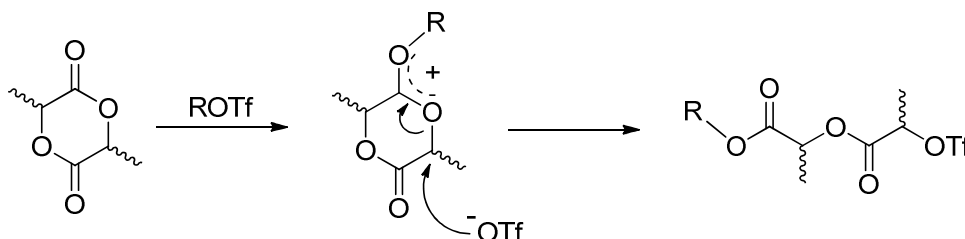
### 1.3 MECHANISMS FOR THE RING-OPENING POLYMERIZATION (ROP) OF CYCLIC ESTERS

As explained above, polylactones and polylactides of high molecular weight can be produced by the ROP of the corresponding cyclic monomers. The ring-opening reaction can be performed either as a bulk polymerization, or in solution, emulsion, or dispersion.<sup>19</sup> A catalyst and/or initiator is necessary to start the polymerization. With the most efficient ones, under rather mild conditions, high-molecular weight aliphatic polyesters of low polydispersity can be prepared in short periods of time. Depending on the catalyst/initiator, the

polymerization proceeds according to different mechanisms: cationic, anionic, by activated monomer, by coordination- insertion and by dual approaches.

### 1.3.1 Cationic Ring-Opening Polymerization

The ability of trifluoromethanesulfonic acid (HOTf) and methyl trifluoromethanesulfonate (MeOTf) to promote the cationic ROP of lactide was demonstrated by Kricheldorf *et al.*<sup>20</sup> in the late 1980s. According to <sup>1</sup>H NMR, polymers with methyl ester end groups were obtained with MeOTf as initiator. The authors proposed that the chain growth proceeds *via* alkyl-oxygen bond cleavage and involves ring-opened trifluoromethanesulfonates as intermediates (Scheme 5). The cationic polymerization is difficult to control and often only low-molecular weight polymers are formed.<sup>21</sup> Further extensions of this acid-catalyzed ROP of lactide have been developed recently by Bourissou *et al.*

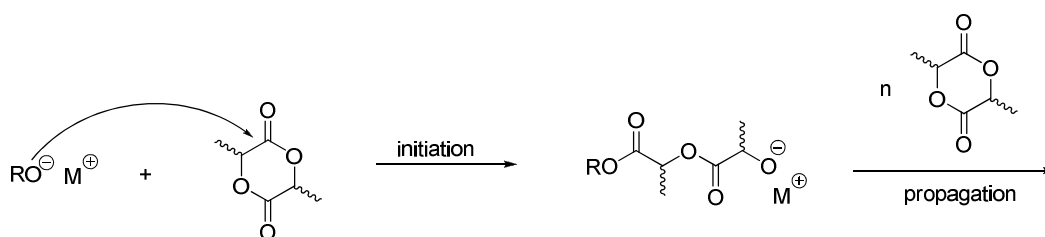


**Scheme 5.** Proposed pathway for the cationic ROP of lactide (R = H, Me or growing polymer chain, Tf = CF<sub>3</sub>SO<sub>2</sub>).

### 1.3.2 Anionic Ring-Opening Polymerization

The mechanism of anionic polymerization of lactide was studied by Kasperczyk<sup>22,23</sup> with lithium *tert*-butoxide and butyllithium as initiators to afford heterotactically-enriched PLA ( $P_r = 0.90$  at room temperature and 0.94 at  $-20$  °C). Anionic ROP of cyclic ester monomers takes place by the nucleophilic attack of a negatively charged initiator on the carbonyl carbon or on the carbon atom adjacent to the acyl oxygen, resulting in a linear

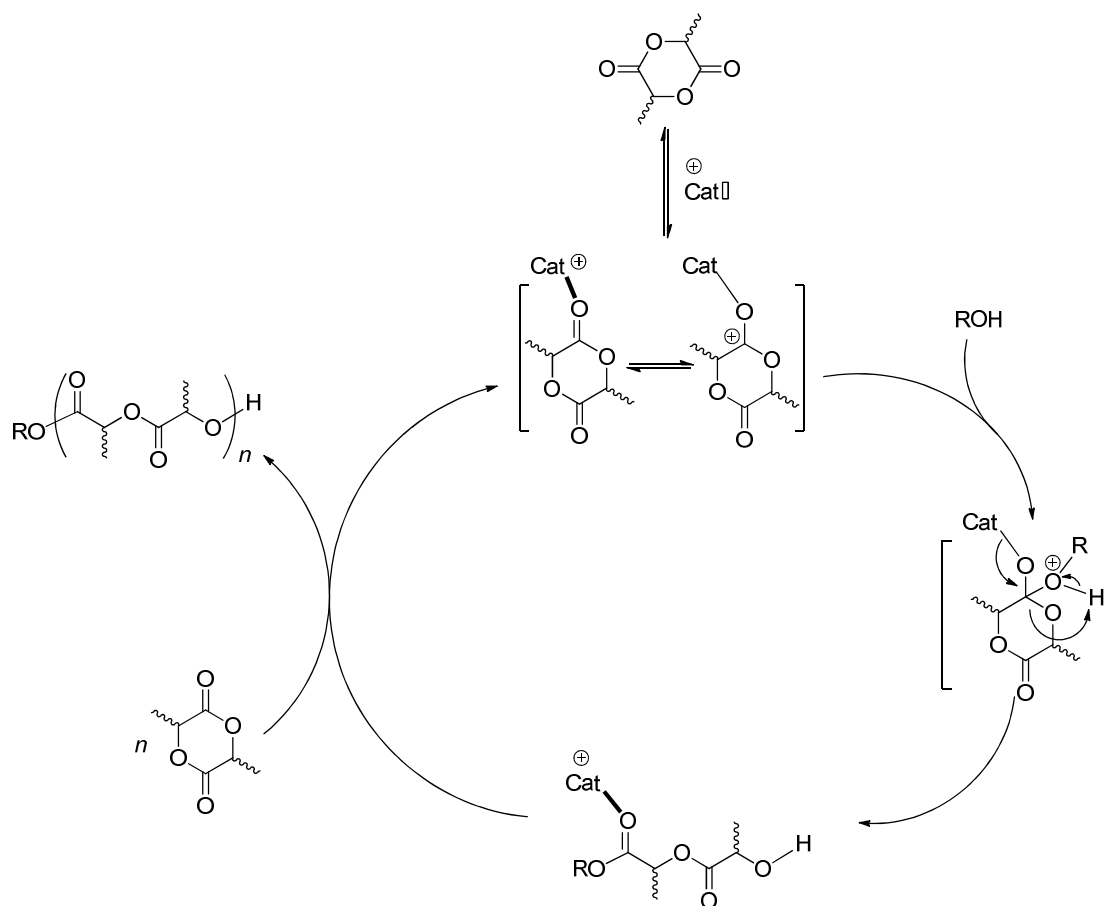
polyester (Scheme 6). The propagating species is negatively charged and is counter-balanced with a positive ion. Depending on the nature of the ionic propagating chain-end and the solvent, the reacting complex varies from completely ionic to almost covalent. One of the best controlled methods leading to high molecular weight polymers is anionic polymerization carried out in a polar solvent. The anionic ring-opening of four-membered rings ( $\beta$ -lactones) occurs through alkyl-oxygen or acyl-oxygen cleavage giving a carboxylate or alkoxide.<sup>24</sup> A problem associated with the anionic ROP is the extensive back-biting, and in some cases only polyesters of low molecular weight are achieved.<sup>25</sup>



**Scheme 6.** Anionic mechanism of the ROP of lactide.

### 1.3.3 Activated Monomer Mechanism

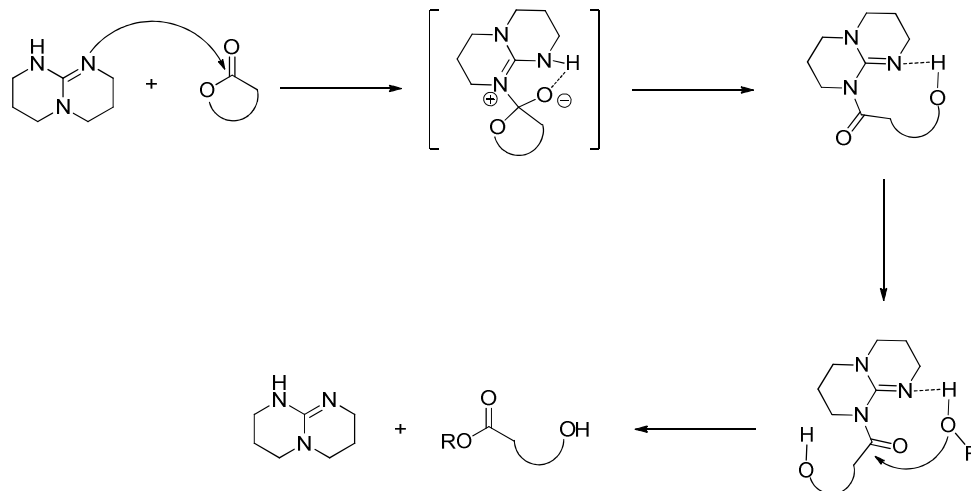
The activated monomer mechanism operates under conditions where a Lewis acid (typically, triflate or acetylacetonate salts of Al, Sn, Zn, Ln), organic molecules (*e.g.* amines) or enzymes (lipase) are induced in the polymerization reaction. First, the carbonyl group of the cyclic ester is activated by coordination onto the Lewis acid; then an external nucleophile (typically an alcohol or an amine) attacks the activated carbonyl group to initiate the polymerization *via* cleavage of the acyl-oxygen bond and formation of a propagating  $\alpha,\omega$ -hydroxyester (Scheme 7).<sup>26</sup>



**Scheme 7.** General activated monomer mechanism for the ROP of lactide. The charge is purely formal.

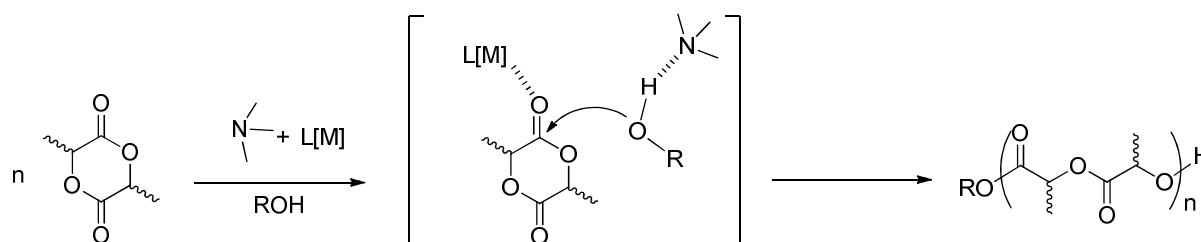
### 1.3.4 Organo-Catalyzed and Dual ROP Mechanisms

A combination of the anionic and the activated-monomer mechanisms can be performed using a Lewis acid and a Lewis base catalysts simultaneously, where both the monomer and the nucleophile are activated. Organocatalysts, such as guanidines<sup>27,28</sup> (Scheme 8) or amino-thioureas,<sup>29</sup> can promote the ROP of cyclic esters *via* such a mechanism.



**Scheme 8.** Ring-opening of a cyclic ester by nucleophilic attack of a guanidine in presence of alcohol.

A new dual approach was also developed using a Lewis acidic metal complex with an alcohol initiator and an organic base.<sup>30</sup> While the carbonyl group of the monomer is activated through coordination on the Lewis acidic metal center, the Lewis base (generally a tertiary amine such as triethylamine) activates the alcohol which acts as an external nucleophile and attacks the carbonyl group of the activated monomer (Scheme 9). This approach has the advantage to fuse the intrinsic high activity of the electrophilic metal center, its potential ability to induce stereoselectivity in the monomer enchainment, and a better tolerance to functional groups provided by the organic catalyst.

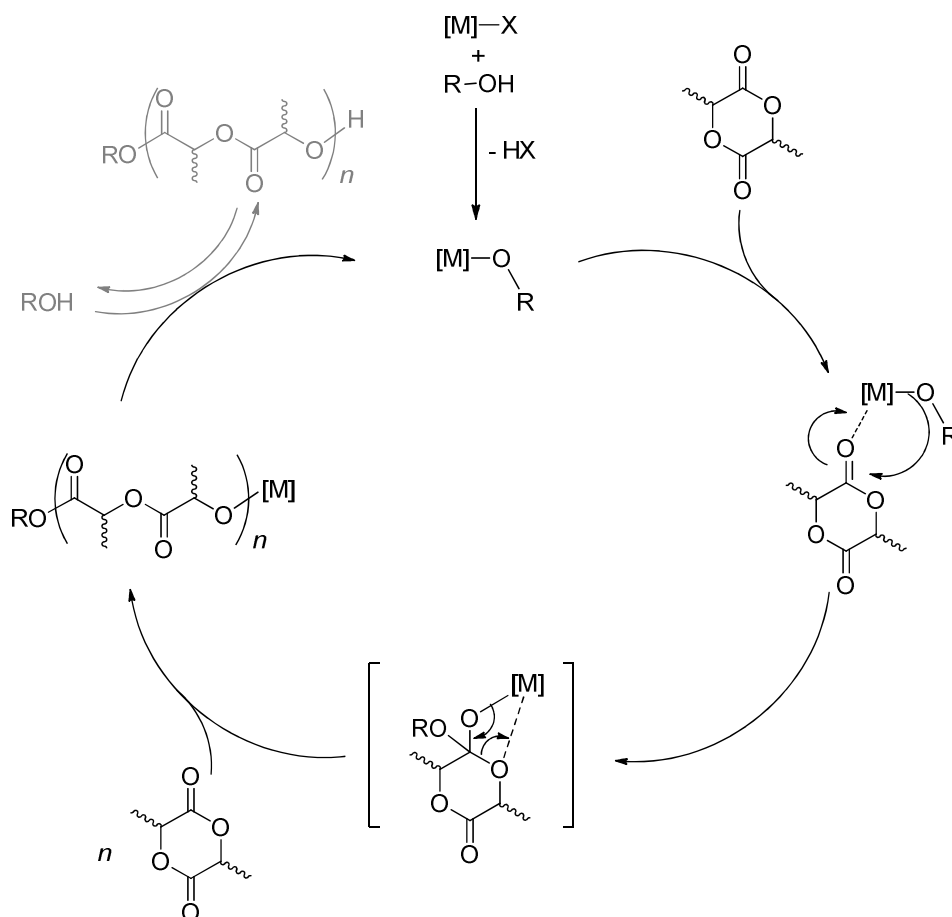


**Scheme 9.** Dual organic/organometallic approach.

### 1.3.5 Coordination-Insertion Ring-Opening Polymerization

The pseudo-anionic ROP mediated by metal complexes, typically a metal-alkoxide species (preformed or in situ generated) is often referred to as coordination-insertion ROP, since the propagation is thought to proceed by coordination of the monomer to the active species, followed by insertion of the monomer into the metal-oxygen bond (of the initiator or propagating species). This coordination-insertion mechanism for the ROP of cyclic esters was first formulated in 1971 by Dittrich and Schulz.<sup>31</sup> The first experimental proof for such a mechanism in the  $\text{Al}(\text{O}i\text{-Pr})_3$ -initiated polymerization of lactide was independently reported in the late 1980s by Kricheldorf<sup>32</sup> and Teysié.<sup>33</sup> The four steps involved in the coordination-insertion mechanism are depicted in Scheme 10: (i) coordination of the monomer to the Lewis-acidic metal center, (ii) the monomer inserts into the metal-alkoxide bonds via nucleophilic addition, (iii) ring-opening occurs via acyl-oxygen cleavage and (iv) continuous insertion of monomers.

The growing polymer chain remains attached to the metal through an alkoxide bond during propagation. The reaction, which is living under optimal conditions, is terminated by hydrolysis in the workup, forming an hydroxy end-group. The coordination-insertion type of polymerization has been thoroughly investigated since it indeed yields well-defined polyesters through “controlled-living” polymerization.



**Scheme 10.** General representation of the coordination-insertion mechanism for the ROP of lactide.

### 1.3.5.1 Stereocontrol in ROP of lactide and $\beta$ -butyrolactone

The mechanical properties of PLA and PHB rely on the stereochemistry of insertion of monomer into the polymer chain, and the process can –in principle– be controlled by the catalyst and reaction conditions used. Therefore, PLAs with desired microstructures (isotactic, heterotactic and syndiotactic) can be derived from the *rac*- and *meso*-lactide, and PHBs (isotactic and syndiotactic) can be derived from *rac*- $\beta$ -butyrolactone depending on the stereoselectivity of the metal catalysts in the course of the polymerization. Fundamentally, two different mechanisms can be distinguished: (1) a chain-end control, which essentially depends on stereochemistry of the monomer inserted in the growing polymer chain; *e.g.* if the



stereogenic center in the last unit inserted favors a *meso*-enchainment, isotactic PLA is obtained from *rac*-LA and heterotactic PLA will be obtained by using *meso*-LA. However, if the stereogenic center in the last unit favors a *racemic*-enchainment, heterotactic PLA will be obtained from *rac*-LA and syndiotactic PLA from *meso*-LA; and (2) an enantiomorphic site control, which depends on chirality of the catalyst, *e.g.* in the lactide polymerization following an enantiomorphic-site control mechanism, only isotactic (racemate or stereoblock) or syndiotactic PLA can be obtained from *rac*- or *meso*-LA, respectively.

The stereosequence distribution in PLA samples is usually determined by NMR spectroscopy. Generally, the stereosequences of the afforded PLAs are assigned from the homonuclear decoupled  $^1\text{H}$  NMR and  $^{13}\text{C}$  NMR spectra as described independently by Coates<sup>34,35</sup> and Hillmyer.<sup>36</sup>

According to Bernoullian statistics, PLA derived from *rac*-LA and *meso*-LA possesses five tetrad sequences in relative ratios, in which the propagating chain end shows a propensity for *racemic* [r-dyad] and *meso* [m-dyad] connectivity of the monomer units. Determination of the stereochemical microstructures of PLA is achieved through inspection of the methine region of homonuclear decoupled  $^1\text{H}$  NMR spectra of the polymers. Thus, although atactic PLA exhibits five resonances in its homodecoupled  $^1\text{H}$  NMR spectrum, perfectly heterotactic PLA shows only *rmr* (or *sis*) and *mrm* (or *isi*) tetrads (Figure 2). The degree of stereoregularity of PLA is quantified by coefficients  $P_m$  and  $P_r$  associated with the probability of racemic (r) or meso (m) linkages between monomer units, respectively ( $P_m = 1 - P_r$ ). For instance, for determining the isotacticity of PLAs, the  $P_m$  values are calculated from (area of *mmm* tetrad)/(total area in the methine proton region) obtained from homodecoupled  $^1\text{H}$  NMR spectra of the resulting PLA. Isotacticity of PLAs can also be determined from the following relations between  $P_m$  and intensity of the tetrads:  $[mmm] = P_m^2 + (1 - P_m)P_m/2$ ;  $[mmr] = [rmm] = (1 - P_m)P_m/2$ ;  $[rmr] = (1 - P_m)^2/2$ ; and  $[mrm] = [(1 - P_m)^2 + P_m(1 - P_m)]/2$ .<sup>35</sup>

Differences in tacticity alter the polymer melting ( $T_m$ ) and glass transition ( $T_g$ ) temperatures such that enantiopure poly(L-lactide) (PLLA) possesses  $T_g \approx 50$  °C and  $T_m = 180$  °C; and a 50:50 mixture of PLLA and poly(D-lactide) (PDLA) displays a comparable  $T_g$  to PLLA but a significantly increased  $T_m$  (ca. 230 °C). This increased melting transition is attributed to a stereocomplex microstructure.<sup>37</sup> This makes isotactic PLAs (stereoblock, stereocomplex) the most attractive targets forms of PLAs.

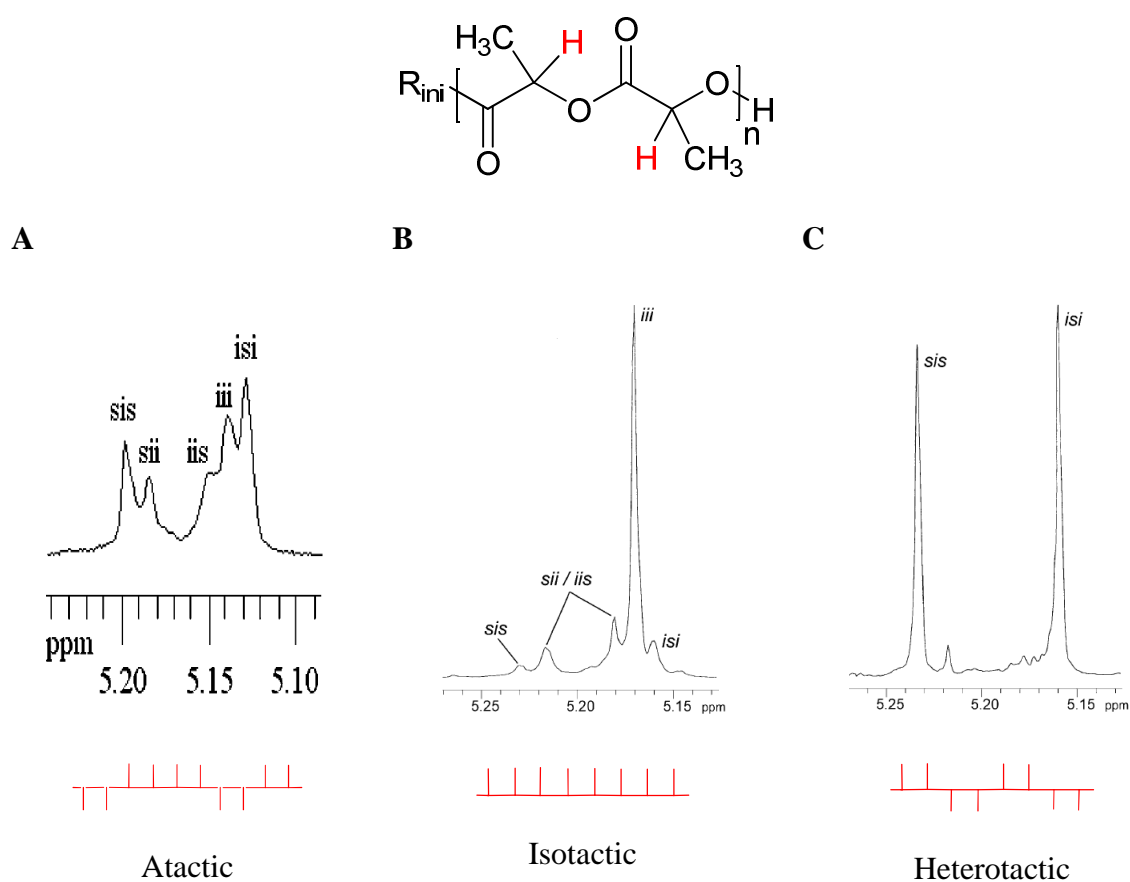


**Figure 2.** Homonuclear decoupled  $^1\text{H}$  NMR spectra (methine region) of PLA generated from (A) [(Cyclooctane-1,5-diyl)bis[(4*S*,7*R*)-7,8,8-trimethyl-4,5,6,7-tetrahydro-4,7-methano-2*H*-indazol-2-yl]borato]CaN(SiMe<sub>3</sub>)<sub>2</sub>.2THF<sup>38</sup> and (B) SALAN Ligand-AlMe/PhCH<sub>2</sub>OH ( $P_m$ ) 0.79 and (C) SALAN Ligand-AlMe/PhCH<sub>2</sub>OH ( $P_r$ ) 0.96.<sup>39</sup>

The stereochemical sequence distribution in PHB samples is usually determined by  $^{13}\text{C}$  NMR spectroscopy at a diad and triad level. A quantitative analysis of the stereochemical sequence distribution of various PHB tactic forms can be carried out by observation of the respective carbonyl and methylene signals intensities using the NMR parameters described by Gross *et al.*<sup>40</sup> In 2009, Carpentier *et al.*<sup>41</sup> prepared a range of PHBs with a syndiotacticity degree ranging from  $P_r = 0.80$ – $0.94$  in which a detailed microstructural analysis of these polymers allowed a quite complete assignment of  $^{13}\text{C}\{^1\text{H}\}$  NMR spectra (Figure 3).

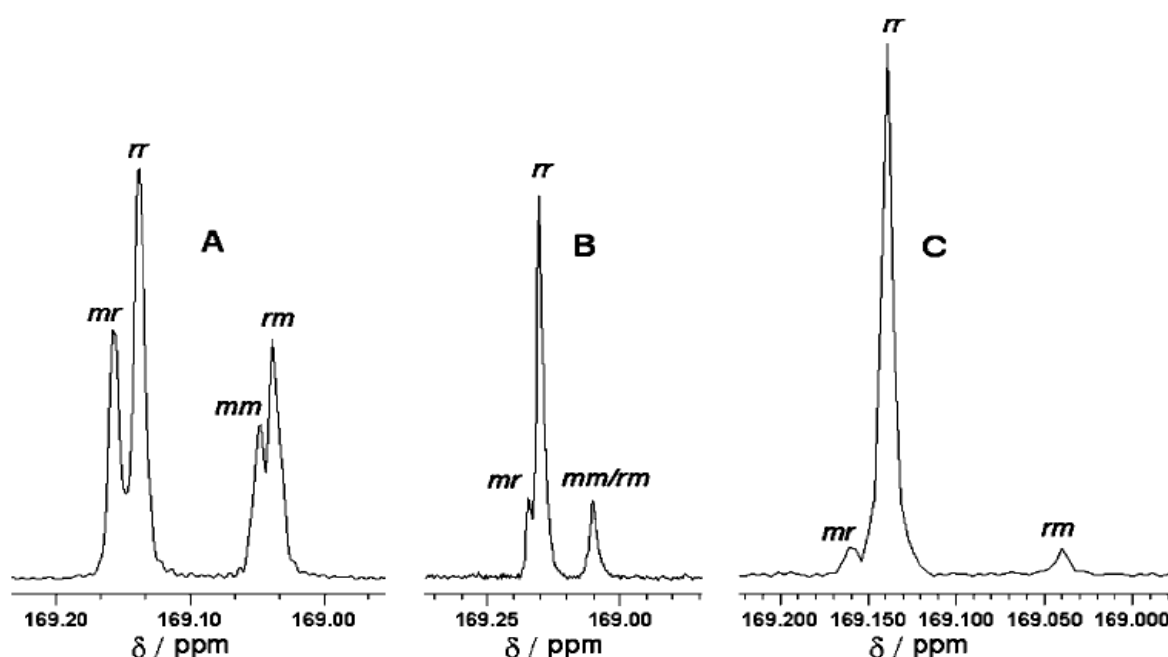
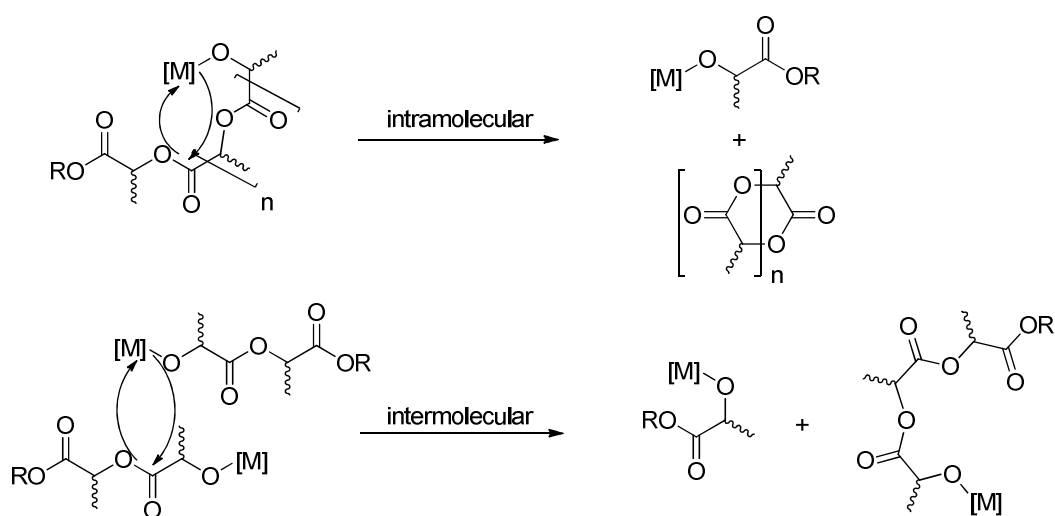


**Figure 3.** Carbonyl region of the  $^{13}\text{C}\{^1\text{H}\}$  NMR spectra (125 MHz,  $\text{CDCl}_3$ , 40 °C) of PHBs prepared by ROP of *rac*-BBL. Key: (A) with  $\text{Y}[\text{N}(\text{SiHMe}_2)_3](\text{THF})_2$  ( $P_r$ ) 0.64); (B) with complex  $[(\text{L})\text{Y}(\text{N}(\text{SiHMe}_2)_2)(\text{THF})]$ , L = 3,5-dicumyl-aminoalkoxybis(phenolate) ( $P_r$ ) 0.88); (C) with complex  $[(\text{L}')\text{Y}(\text{N}(\text{SiHMe}_2)_2)(\text{THF})]$  L' = 5-methyl-3-triphenyl-aminoalkoxybis(phenolate) ( $P_r$ ) 0.94).<sup>41</sup>

### 1.3.6 Transfer process (Transesterification Side-Reactions).

In addition to transfer reactions with intentionally added transfer agents such as alcohol molecules (“immortal” polymerizations),<sup>42</sup> there exist two main types of chain

transfer reactions in growing polyester chains: namely, intramolecular or back-biting (leading to formation of cyclics) and intermolecular transfers (conserving the activities of both chains), as shown in Scheme 11. Intramolecular chain transfer relies upon a unimolecular backbiting reaction, releasing a fragment of a macromolecule in the form of a cycle and leaving a shorter but still active macromolecule. The cyclic macromolecule can further react with growing species in the propagation step. One of the first papers discussing the ring-chain equilibrium was published in 1950 by Jacobson and Stockmayer,<sup>43</sup> concluding that only a small weight fraction of cyclic macromolecules is present in a polymerization conducted in bulk, whereas it rapidly increases upon dilution due to a gain in entropy. As far as intermolecular chain transfer is concerned, two growing macromolecules cross-react without losing the activity of the chain end-groups.



**Scheme 11.** Representation of intra- and inter- molecular transesterification side-reactions.

These transesterification side-reactions result in broader molecular-weight distributions. The extent of these undesirable transfer reactions was found to strongly depend on the metallic initiator.<sup>2</sup>

## 1.4 CATALYSTS

A large variety of organometallic/coordination compounds has been studied as initiators/catalysts in order to achieve effective polymer synthesis.<sup>2,13</sup> In addition, many reactions catalyzed by metal complexes are highly specific and, by careful selection of metal and ligands, reactions can be generated to form a desired polymer structure.<sup>2,13</sup> Figure 4 summarizes some examples of highly active and specific single-site metal catalysts to promote ROP in a good controlled manner. These single-site complexes have a general formula  $L_nMR$ , where M is a central metal atom surrounded by an ancillary ligand  $L_n$ . The ancillary ligands in the complexes were proven to play an important role in preventing side reactions, like transesterification, which lead to uncontrolled molecular weight, broad molecular weight distributions and formation of macrocycles or oligomers. R is the initiating group (alkoxide, amide, alkyl...), which nucleophilicity affects the polymerization activity of the complexes; alkoxides, which are similar to the propagating species, are the best initiating groups.

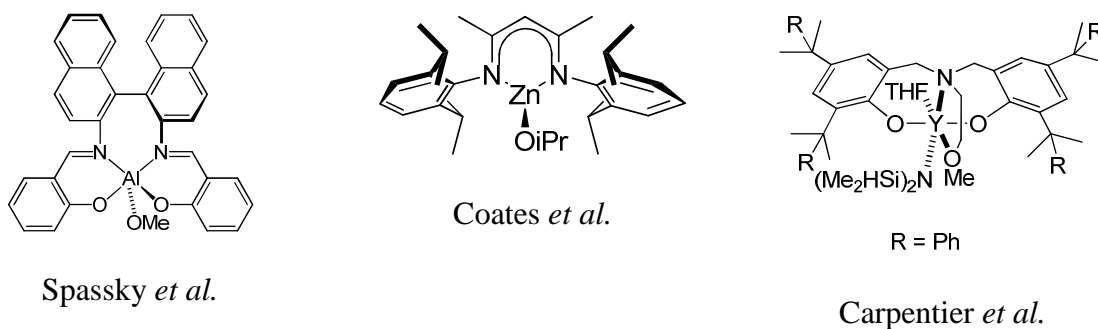


**Figure 4.** Examples of Single-Site Metal (pre)Catalysts for the ROP of Cyclic Esters.<sup>35,44,45</sup>

### 1.4.1 Aluminum-Based Initiators for the ROP

Due to their high Lewis acidity and low toxicity, aluminum compounds, especially Al-alkoxides and -aryloxides, are well-suited initiators for the ROP of cyclic esters such as lactides and lactones.<sup>46,47,48</sup> The archetypal example, namely  $Al(O^iPr)_3$ , has been largely used

for mechanistic studies. However, it has been revealed to be significantly less active than  $\text{Sn}(\text{Oct})_2$  (in bulk at 125-180 °C, reaction times of several days are usually required and molecular weights are generally lower than  $10^5$  Da). Moreover, an induction period of a few minutes is observed when applying  $\text{Al}(\text{O}^i\text{Pr})_3$  as initiator in lactide polymerization. This feature was attributed to the presence of an equilibrium between the tetramer ( $\text{A}_4$ ) and the trimer ( $\text{A}_3$ ) (Figure 5), of which  $\text{A}_3$  was demonstrated to be more reactive than  $\text{A}_4$ .<sup>49</sup>

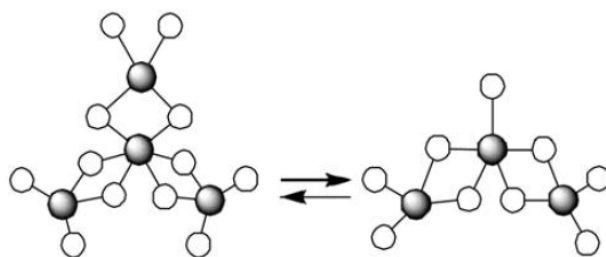


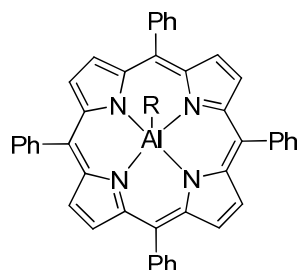
**Figure 5.** Equilibrium between the tetramer and trimer of  $\text{Al}(\text{O}^i\text{Pr})_3$ . Only aluminium atoms (grey) and oxygen atoms (white) are shown for clarity.<sup>49</sup>

Although aluminum-alkoxides were proven to be efficient catalyst/initiators for the ROP of cyclic esters, control of molecular weight is sometimes complicated by the clustered form of the active species. Molecular weight distributions are usually broadened when more than one growing chain is connected to one metallic center. For these reasons, well-defined single-site catalysts have been designed and exploited in cyclic esters polymerization. Hereafter, we present a brief selection of well-defined aluminum initiators for the ROP of lactides and butyrolactone.

#### 1.4.1.1 Well-Defined Aluminum Complexes Featuring Ancillary Ligands

Aluminum-porphyrin alkoxides (Figure 6) were demonstrated by Inoue *et al.*<sup>50</sup> to give PLAs with expected molecular weights and narrow PDIs ( $< 1.25$ ) at 100 °C. Notably, one equivalent of lactide inserted the Al–OR bond of complex **1b**, demonstrating that the polymerization proceeds by acyl–oxygen bond cleavage, as evidenced by the  $^1\text{H}$  NMR data.

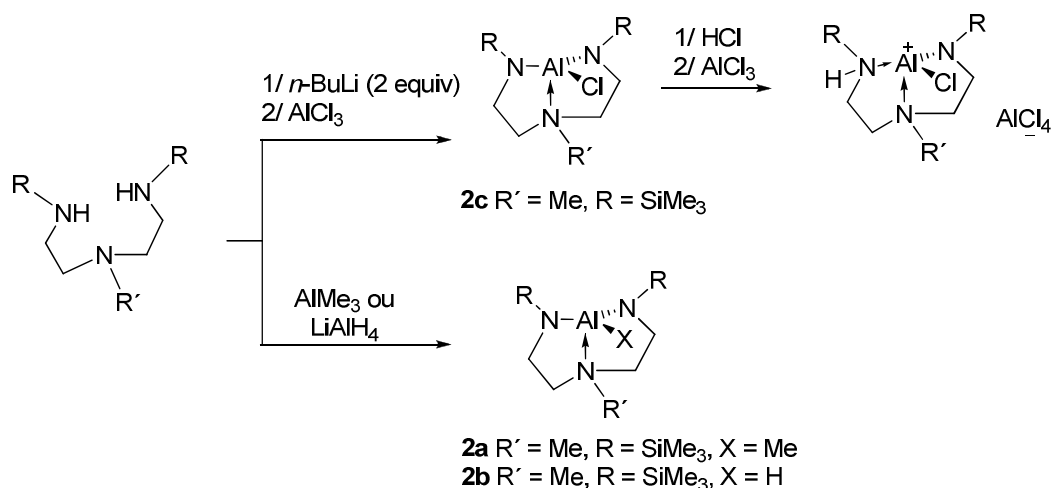
Studies of kinetics on related systems revealed that the polymerization follows a second order rate law with respect to the concentration of Al complex, suggesting that the propagation involves two aluminum porphyrins, one as a nucleophilic species involved in chain growth and the other as a Lewis acidic monomer activator.



**1 a:** R = (OCH<sub>2</sub>CH<sub>2</sub>)<sub>n</sub>Cl  
**b:** R = OMe

**Figure 6.** Aluminum Complexes (**1**) Bearing Porphyrins Reported by Inoue *et al.*<sup>50</sup>

Bertrand *et al.*<sup>51</sup> reported a series of neutral and cationic aluminum complexes involving triamine ligands, in which complexes **2a-c** (Scheme 12) exist under monomeric forms as revealed by X-ray structural studies. Due to the formation of a rather rigid bicyclic core, the tridentate ligand enforced an approximately trigonal monopyramidal coordination geometry around the aluminum, the empty axial coordination site playing the role of the reactive site during polymerization. In all of complexes, only the methyl and hydrido-aluminum derivatives **2a-c** were able to initiate the polymerization of *rac*-lactide in benzene at 80 °C, forming PLAs with PDIs of 1.79 and 1.61, respectively. The hydrido-complex **2b** was about twice as active as the methyl-aluminum derivative **2a**.



**Scheme 12.** Structure and Synthesis of the Neutral and Cationic Aluminum Complexes (**2a-c**) Featuring Tridentate Diamidoamino Ligands.<sup>51</sup>

#### 1.4.1.1.1 SALEN- Based Aluminum Complexes

Chelating ligands combining *N*- and *O*-donors have also been involved in the design of well-defined complexes for lactide ROP. Inspired by the work of Inoue and coworkers, several groups have investigated aluminum complexes featuring SALEN ligands as structural analogues of porphyrins. These Schiff-base ligands are readily available by condensation of substituted salicylaldehyde derivatives and diamines. Corresponding aluminum-alkyl complexes are synthesized by treatment of the pro-ligands with trialkyl-aluminum precursors. Aluminum-alkoxides are generally obtained either by alcoholysis of aluminum-alkyl complexes with the desired alcohol or by ligand exchange with trisalkoxy-aluminum precursors.

Spassky *et al.*<sup>52</sup> reported achiral salen-Al complexes **3a-c** active in ROP of *rac*-LA and *rac*-BBL (Figure 7). Compared with the parent methoxide **3a**, higher polymerization rates and less transesterification reactions were observed for complex **3c** featuring chlorine atoms in the *para* position of the phenol ring.<sup>53</sup> These variations have been correlated to an enhancement of the aluminum electrophilicity and an increase of the polarization of the



initiating/propagating Al–X bond. The occurrence of inter- and intramolecular side-reactions could be decreased when bulky groups were introduced at the *ortho* position of the phenolate rings (complexes **4c-e** and **5c-e**).

All of the complexes (Figure 7) were found to be active for the ROP of lactones, without any induction period, high conversions typically being obtained after a few days at 70 °C in toluene for monomer-to-initiator ratios around 100. The resulting PLAs featured ester chain-ends corresponding to the alkoxide moiety (as indicated by <sup>1</sup>H NMR spectroscopy and/or MALDI-ToF mass spectroscopy), suggesting a coordination-insertion mechanism via cleavage of one acyl–oxygen bond of lactide.<sup>53</sup>

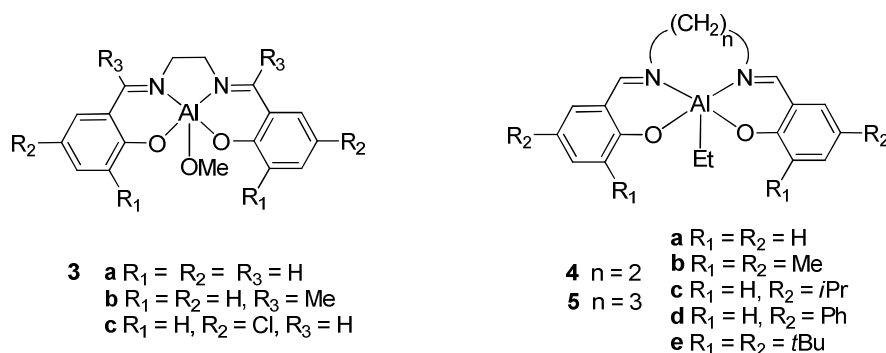


**Figure 7.** Aluminum Complexes **3-5** Featuring SALEN Ligands.<sup>52,53</sup>

In 1996, Spassky *et al.*<sup>44</sup> disclosed a most important breakthrough in the field of stereoselective ROP of *rac*-lactide. They discovered a remarkable stereocontrol of an enantiomerically pure Al complex (**R**)-**6a** leading to a tapered stereoblock PLA microstructure with high melting point ( $T_m = 187$  °C) (Figure 8). Structurally analogous *racemic* salen-Al complex **7** resulted in highly isotactic PLA.<sup>44b</sup>

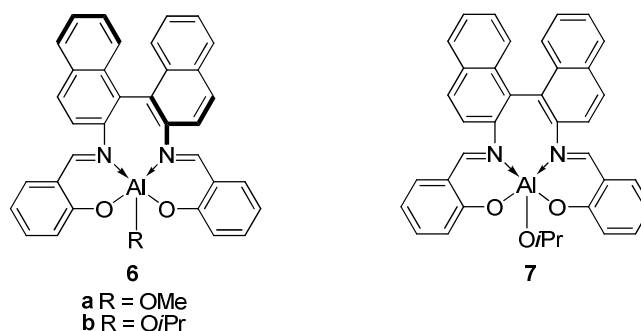
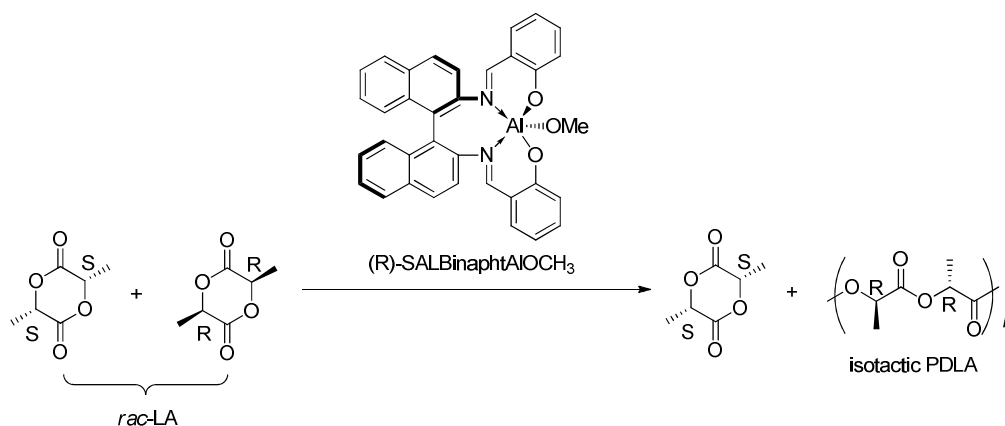


**Figure 8.** Salen-Aluminum Complexes (**6-7**) for Isoselective Lactide ROP.<sup>44</sup>

At low conversion (<40%), they demonstrated that the chiral aluminum-methoxide complex (*R*)-(SALBinapt)Al(OCH<sub>3</sub>) preferentially induces ROP of D-lactide ( $k_D/k_L=20$ ) to give optically active isotactic PDLA (88% *ee*) through an enantiomeric site-control mechanism (Scheme 13).



**Scheme 13.** Kinetic resolution of *rac*-lactide with (*R*)-(SALBinapt)Al(OCH<sub>3</sub>) described by Spassky *et al.*<sup>44a</sup>

In comparison with Spassky's catalyst, Feijen's enantiopure chiral complex (***R,R***-**8**) (Figure 9) exhibited an excellent reverse stereocontrol by preferential polymerization of L-lactide over D-lactide monomer ( $k_L/k_D = 14$ ) that resulted in PLA with enhanced thermal stability and a high  $P_m$  (0.92).<sup>54</sup>

Many *achiral* Schiff base aluminum alkyls were also proven to be efficient stereoselective catalysts for lactide ROP in the presence of an alcohol as co-initiator. Nomura *et al.*<sup>55</sup> reported on the stereoselective polymerization of *rac*-LA by in situ formed aluminum-

alkoxides from the achiral Schiff base aluminum ethyls **9a-b** with bulky *tert*-butyl groups at the *ortho* and *para* positions of the phenolate group. In the presence of benzyl alcohol as a co-initiator, complexes **9a-b** catalyzed ROP of *rac*-LA via a chain-end-control mechanism. Complex **9b** with a propylene diimine bridge furnished PLA materials with a high isotacticity ( $P_m = 0.91$ ). Complex **9b** is also able to polymerize *rac*- $\beta$ -butyrolactone with an excellent control, but yielding only atactic PHB.<sup>56</sup> In 2003, Chen *et al.*<sup>57</sup> reported a structurally similar achiral Al-Salen complex **10**/2-propanol as a catalyst/initiator system in *rac*-LA polymerization offering isotactic selectivity ( $P_m = 0.90$ ). Thermal analysis revealed that this stereoblock PLA has a  $T_m$  of 201 °C. Kinetic data indicated that the *rac*-LA ROP using the **10**/2-propanol system is first-order in monomer concentration.

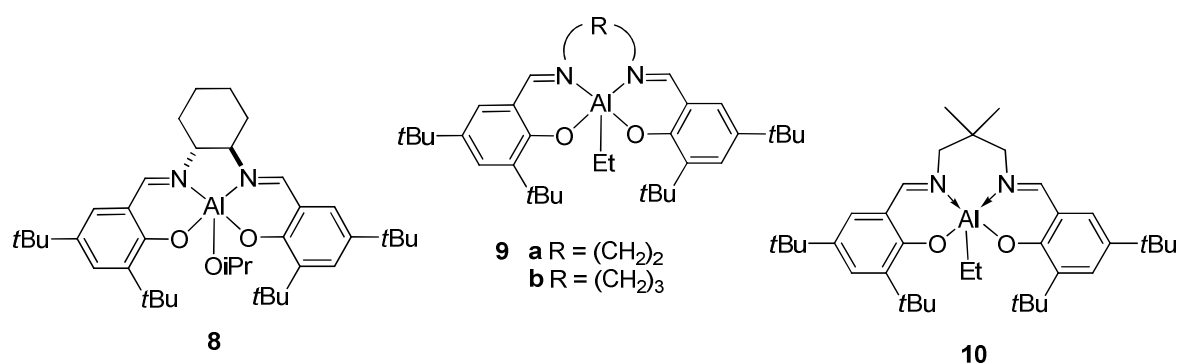


**Figure 9.** Salen-Aluminum Complexes (**8-10**) for Isoselective Lactide ROP.<sup>54-57</sup>

In 2007, Nomura *et al.*<sup>58</sup> have reported on a Schiff base aluminum complex (**11**, Figure 10) with flexible but bulky <sup>t</sup>BuMe<sub>2</sub>Si substituents at the *ortho* position of the phenolate groups. This catalyst induced stereoblock PLA formation from *rac*-LA with a  $P_m$  value of 0.98 and a  $T_m$  of 210 °C. Up to now, this is the highest isotactic stereoblock PLA material which has been prepared using an achiral catalyst/initiator system in *rac*-LA polymerization.

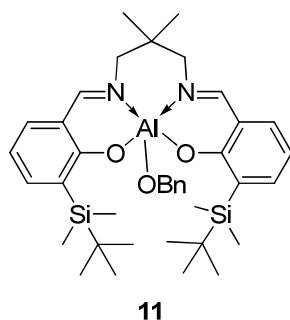


**Figure 10.** Nomura's Salen-Aluminum Complex (**11**).<sup>58</sup>

In 2011, Lin *et al.*<sup>59</sup> disclosed a series of SALEN-type ligands with sterically bulky cumyl groups in the *ortho* and *para* positions of the phenolate group to investigate the influence of the ligand on the stereochemistry of the polymerization process (Figure 11). ROP of *rac*-LA was performed using aluminum-alkoxide (**12b**) and aluminum-methyl (**12a**) complexes in the presence of benzyl alcohol. Complex **12b** displays high stereoselectivity toward *rac*-LA ( $P_m = 0.94\text{--}0.97$ ), where the highest melting point reached 205 °C. These aluminum complexes can prevent transesterification effectively, as evidenced by MALDI-ToF-MS studies. The kinetics was also investigated and revealed a first-order dependence for both the monomer and the catalyst.

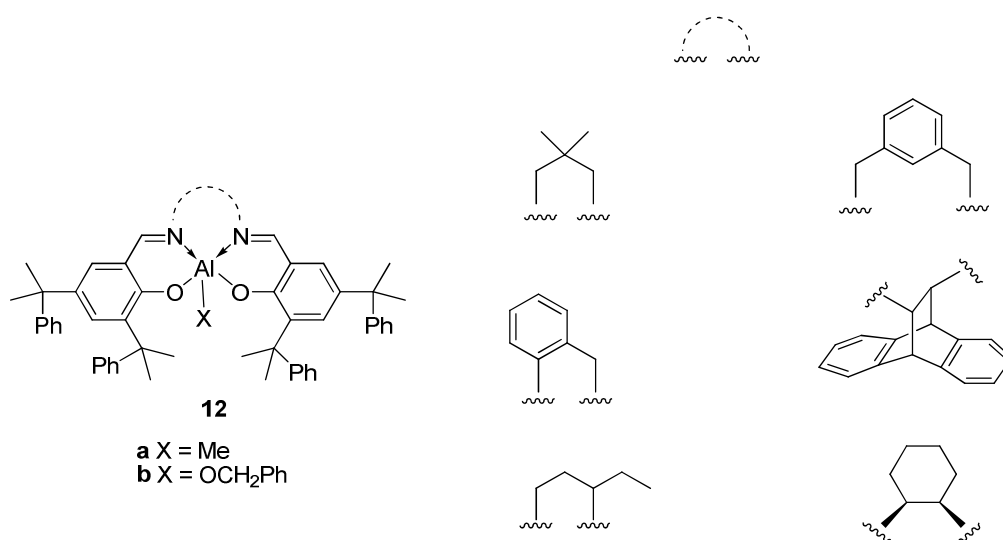


**Figure 11.** Aluminum Complexes (**12**) Supported by SALEN Ligands Developed by Lin *et al.*<sup>59</sup>

Chen *et al.*<sup>60</sup> documented the synthesis of a series of tetradentate enolic Schiff base aluminum ethyl complexes and their application as catalysts in *rac*-LA polymerization. Systematic research revealed that modifications on the auxiliary ligand exerted a dramatic influence on their catalytic performance, including activity and stereoselectivity. Lengthening the ethylene diimine bridge to a propylene diimine bridge and the presence of electron-withdrawing substituents at the 5-position in the diketone skeleton both resulted in a remarkable enhancement of stereoselectivity and polymerization rate. In the presence of 2-propanol as an initiator, complex **13** (Figure 12) polymerized *rac*-LA to form isotactic enriched PLA materials ( $P_m = 0.78$ ).<sup>60b</sup>

Recently, Jones *et al.*<sup>61</sup> have reported aluminum-SALALEN based complexes **14** (Figure 12) active for the ROP of *rac*-LA in presence of one equiv of benzyl alcohol, with the ligand influencing the stereoselectivity of the polymerization. The complexes have  $C_1$  symmetry in the solid state. It must be noted that upon complexation, the tertiary amine becomes chiral, and due to the chelation of the ligand, the metal center is also chiral, giving potentially a pair of diastereomers. In addition, when the *ortho* substituent was changed from a Me to a *t*Bu, a sharp decrease in the  $P_r$  was observed ( $P_r = 0.75$  for **14c** to  $P_r = 0.40$  for **14a**).

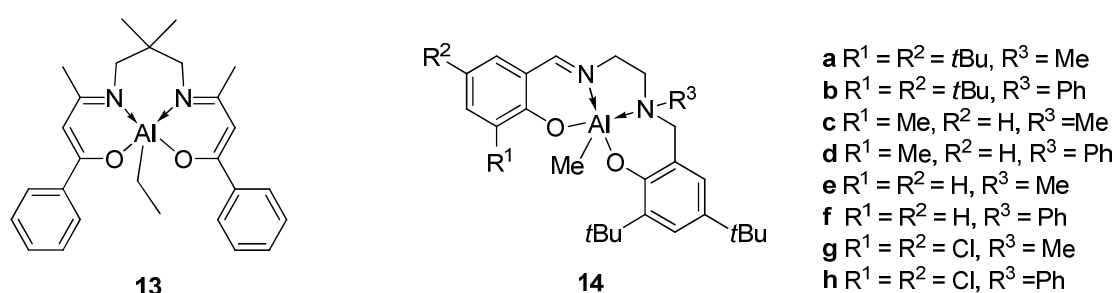


**Figure 12.** Aluminum Complexes (**13**)<sup>60</sup> and (**14**).<sup>61</sup>

#### 1.4.1.1.2 SALAN- Based Aluminum Complexes

In 2004, Gibson *et al.*<sup>39</sup> prepared achiral tetradentate *N,N'*-disubstituted bis(amino-phenoxy) (SALAN) aluminum-methyl complexes **15** (Figure 13). The free ligands were

obtained by reductive amination and subsequently treated with trimethylaluminum to give the desired complexes **15**. The corresponding alkoxide initiators for the ROP of lactide were generated by *in situ* alcoholysis of **15** using benzyl alcohol. These complexes catalyzed *rac*-LA polymerizations in a well-controlled and living manner, affording highly isotactic PLA materials with a  $P_m$  value of 0.79 by using **15e**, and highly heterotactic PLA with a  $P_r$  value of 0.96 by using **15h**. High monomer conversions were generally reached after about 1 day at 70 °C in toluene solution for an initial monomer concentration of 0.83 mol.L<sup>-1</sup> and a monomer-to-initiator ratio of 100. The highest activities were observed with complexes **15a** and **15e**, and considerably lower activities were observed with **15c** (only 66% conversion after 1464 h) and **15g** (77% conversion after 120 h). So far, this is the first time that aluminum complexes have been found to furnish a highly heterotactic PLA, and the first time that a dramatic switch in tacticity of the resulting PLA has been observed upon changing the substituent pattern at the *ortho* and *para* positions of the phenol group in the complexes. Preliminary kinetic data indicated that the *rac*-LA polymerizations catalyzed by these complexes were both first-order in monomer and catalyst.

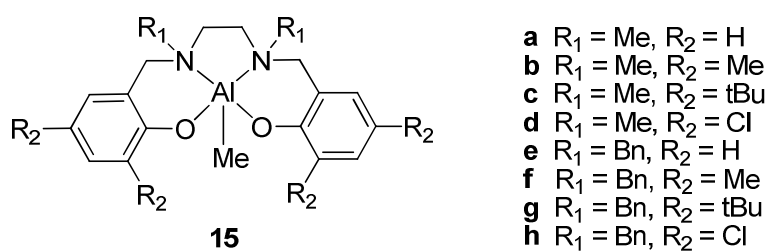


**Figure 13.** Aluminum Complexes (**15**) Featuring SALAN Ligands.<sup>39</sup>

The ability of complex **15h** to mediate the ROP of *rac*-β-BL was examined. The possibility to control the polymerization under a variety of polymerization conditions yielding atactic PHB was demonstrated. Narrow PDIs (<1.05) were observed at temperatures ranging from 25 to 120 °C and an increase of the [M]/[Al] ratio gave PHB with the corresponding

increased molecular weight. High conversions (>90%) were obtained after 2 h in toluene at 120 °C for a monomer-to-initiator ratio of 100.<sup>56</sup>

In 2009, Feijen *et al.*<sup>62</sup> evaluated the polymerization abilities in the ROP of *rac*- and *meso*- lactide of a series of ethyl-aluminum complexes bearing tetradentate bis(phenoxy-amine) (SALAN-type) ligands (Figure 14). Enantiopure pro-ligands afforded diastereoisomeric mixtures of aluminum complexes (**16 a-c**): i) one diastereoisomer featured a five-coordinated aluminum center with a *cis*-(O,O) and *cis*-(Me,Me) ligand geometry and ii) the other one featured an intermediate geometry between a *cis*-(O,O), *trans*-(Me,Me) and a *trans*-(O,O), *trans*-(Me,Me). Systems combining Al-complexes **16a-f** with 2-propanol offered moderate stereoselectivity ( $P_m = 0.66$  and  $0.62$  for **16a, d**, respectively;  $P_r = 0.55$  and  $0.57$  for **16c, f**, respectively). The Al-complex **16b**/2-propanol system afforded slightly heterotactic PLAs ( $P_r = 0.64$ ). The heterotacticity of ROP increased to 0.73 with **16e**/2-propanol. Furthermore, studies of kinetics revealed first-order dependency on both *rac*-LA and **16d**, as well as a kinetic resolution by **16a** in favor of L-LA ( $k_{SS}/k_{RR} = 10.1$ ).

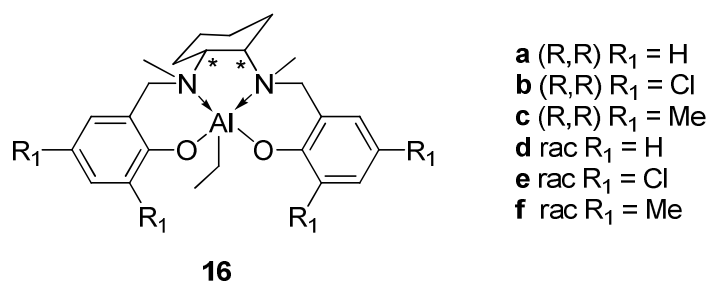


**Figure 14.** Aluminum Complexes (**16**) Supported by SALAN Type Ligands.<sup>62</sup>

One class of SALAN ligands are those utilizing a piperazine or homopiperazine backbone. In this context, Jones *et al.*<sup>63</sup> documented recently a series of aluminum-homopiperazine alkoxide complexes **17** (Figure 15) and their application in *rac*-LA ROP under melt conditions (130 °C). High conversions (>80%) were obtained after 2 h for a monomer-to-initiator ratio of 300 with complexes **17a-d**. On the other hand, complex **17e** achieved only 56% conversion under the same polymerization conditions. This is perhaps

related to the reduced steric demand of this ligand facilitating multiple chain attachment to each metal center. In all cases, atactic PLA was produced.

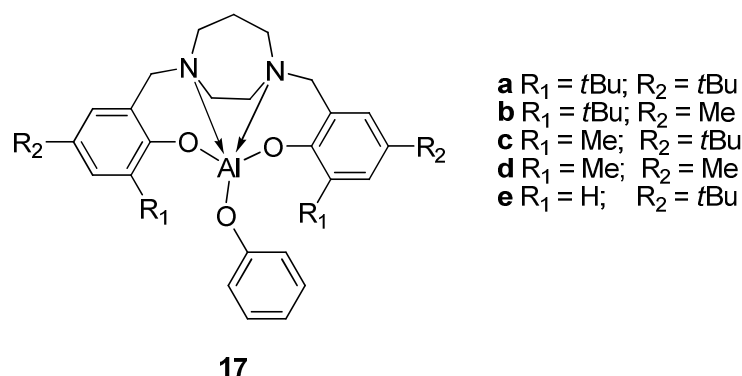


**Figure 15.** Aluminum-Homopiperazine Complexes (**17**).<sup>63</sup>

#### 1.4.1.1.3 Phenoxy-Imine-Based Aluminum Complexes

Independently, Nomura *et al.*<sup>64</sup> and Pappalardo *et al.*<sup>65</sup> reported the synthesis of alkyl-aluminum complexes bearing phenoxy-imine (“half-SALEN”) ligands by a protonolysis reaction between trimethylaluminum and the corresponding phenol-imine pro-ligand (Figure 16). Compounds **18a-h** behave as single-site initiators, giving rise to controlled polymerization, disclosing monomodal curves and narrow molecular weight distributions (PDI < 1.3). It appeared that the nature of the imino-substituent strongly affects the catalytic activity. In both studies, the highest activity was obtained with the C<sub>6</sub>F<sub>5</sub> imino moiety (**18c**) whereas the lowest one was shown by the complexes bearing more sterically crowded adamantyl (**18f**) and *t*Bu (**18d**) substituents. However, high conversions (> 80 %) of *rac*-LA were reached only after 3 days of reaction in toluene at 70 °C, in the presence of 1 equiv of MeOH. A small dependence of the microstructure on the nature of the salicylaldiminato ligand can be observed: slightly prevailing isotactic poly lactides ( $P_m = 0.6$ ) were obtained with compounds **18a** and **18c**, while an atactic polymer was obtained with **18b**.



Carpentier *et al.*<sup>66</sup> reported a series of dialkylaluminum complexes stabilized by a phenoxy-imine ligand  $\{\text{ON}^{\text{R}}\}^-$  platform, with variable R-imino substituents and functionalized by a bulky *ortho*-SiPh<sub>3</sub> in the phenoxy moiety (Figure 16). All dimethyl{phenoxy-imine}aluminum complexes **19** proved to be active in the ROP of *rac*-LA at 100 °C for period of time ranging from 2 to 20 h at [lactide]/[catalyst/initiator]/[<sup>*i*</sup>PrOH] ratio of 100/1/1 in a controlled fashion. All the PLAs formed showed unimodal and narrow molecular distributions ( $M_w/M_n = 1.10\text{--}1.24$ ). Interestingly, dimethylaluminum complexes having benzyl-type imino substituents enabled the achievement of significant isotacticity ( $P_m$  up to 0.80), and the stereocontrol within this series followed grossly the bulkiness of the aryl moiety: 3,4,5-trimethoxyphenyl (**19k**,  $P_m = 0.80$ ) > mesityl (**19g**,  $P_m = 0.76$ ) > phenyl (**19e**,  $P_m = 0.63\text{--}0.73$ ). Based on kinetic studies, a coordination-insertion mechanism was proposed for these aluminum catalysts, in contrast to the corresponding indium derivatives which were thought to operate via an activated monomer mechanism.

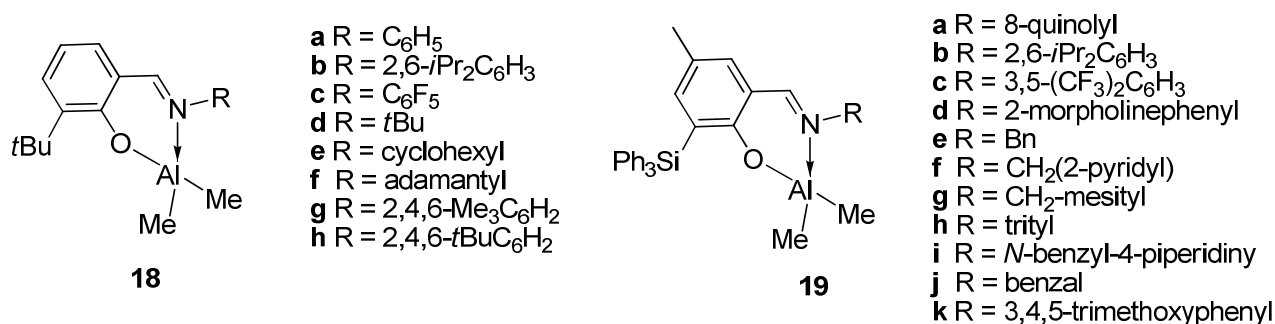


**Figure 16.** Phenoxy-Imine Aluminum Complexes Developed by Pappalardo *et al.*<sup>65</sup> (**18a-c**) and Nomura *et al.* (**18b**, **18c**, **d-i**)<sup>64</sup> and Carpentier *et al.* (**19**).<sup>66</sup>

Recently, Wang *et al.*<sup>67</sup> reported mono- and dinuclear aluminum complexes supported by amino- and imino-phenolate ligands (Figure 17). In the presence of BnOH, complexes **20** and **21** are efficient pre-catalysts for the ROP of *rac*-LA which leads to polymers with good molecular weight control and narrow molecular distribution ( $1.09 < M_w/M_n < 1.27$ ). The system **21a**/BnOH displayed the highest activity while **21b**/BnOH

showed the lowest activity (93% conversion after 16 h vs 79% conversion after 24 h, respectively, at lactide:catalyst:BnOH = 100:1:2). The high activity of complex **21a** was proposed to be related to the steric hindrance of the aryl groups on the nitrogen atoms. Furthermore, the catalytic activities of the dinuclear aluminum complexes **21a-b** and **21e** were higher than those of the corresponding mononuclear aluminum complexes reported previously by Nomura<sup>64</sup> (after 24 h, for [monomer]/[Al]/BnOH of 100:1:1, 23% conversion was obtained with **18b** and for [monomer]/[Al]BnOH of 200:1:2, 75% conversion was obtained with **21a**). The higher activity of the dinuclear complexes was proposed to arise from a cooperative effect: in the catalytic process, one aluminum atom would serve as the Lewis acid, and an alkoxy group bound to the second aluminum center would attack the carbonyl group of the incoming lactide. But other factors such as the effect of substituents on 2-position of the aromatic rings cannot be ruled out. Kinetic studies indicated that the polymerization proceeds with first-order dependence on monomer concentration.

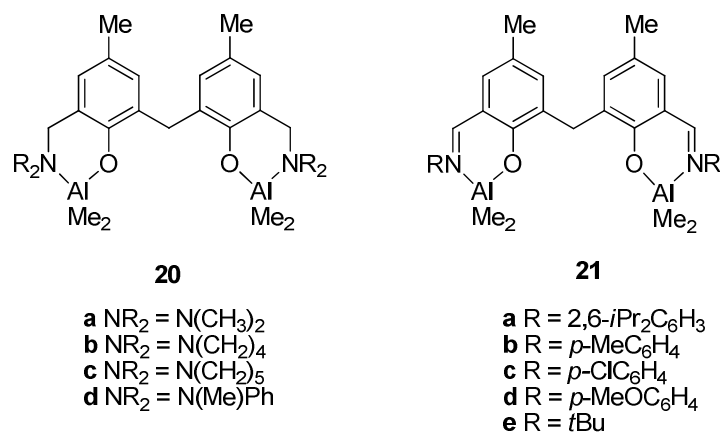


**Figure 17.** Dinuclear Aluminum Complexes Supported by Amino- (**20**) or Imino-Phenolate (**21**) Ligands.<sup>67</sup>

In 2010, Darensbourg *et al.*<sup>68</sup> prepared a series of aluminum ethyl complexes from AlEt<sub>3</sub> and *NON*-tridentate Schiff base ligands derived from chiral and achiral amino-alcohols and amino-acids (**22**, **23** and **24**, Figure **18**). Some of these metal complexes were dimeric and exhibited two isomeric structures, one with the initiators on the two aluminum centers *cis* to

one another and the other with the *trans* arrangement. Complexes **22**, **23** and **24** were found to be active in the *rac*-lactide ROP in toluene at 70 °C with good control over the polymerization process, producing isotactic PLAs ( $P_m = 0.82$ ). The most active **23c** also catalyzed the ROP of  $\beta$ -butyrolactone (89% conversion of 160 equiv after 15 h at 70 °C), affording only atactic polymers, yet in a *living* manner. Indeed, in all cases, the polymerizations proceeded in a well-controlled fashion, as indicated by the narrow molecular-weight distributions (PDI < 1.18) and the linear correlations between  $M_n$  and conversion. Kinetic parameters were investigated, and each polymerization was found to be first order with respect to monomer concentration.

In 2011, Matsubara *et al.*<sup>69</sup> reported a series of aluminum alkoxides bearing nonchiral or chiral tridentate Schiff bases, “half-SALEN” ligands. Controlled stereoselective ROP of *rac*-LA using these complexes was achieved. In particular, complex **25** (Figure 18) afforded a stereoblock copolymer of PDLLA ( $P_m$  up to 0.92).

In 2012, Carpentier *et al.*<sup>70</sup> described dimethyl-aluminum complexes derived from imino-phenol pro-ligands {ONO}H and {ONN}H. These complexes were evaluated in the ROP of *rac*-lactide. Complex **26** (Figure 18) in the presence of 1 equiv. of benzyl alcohol as co-initiator polymerized *rac*-lactide in THF or toluene solution; for an initial monomer concentration of 2 mol.L<sup>-1</sup> and a lactide-to-initiator ratio of 100, 79% conversion was obtained after 14 hours at 60 and 70 °C, respectively. Only atactic polymers were obtained though.

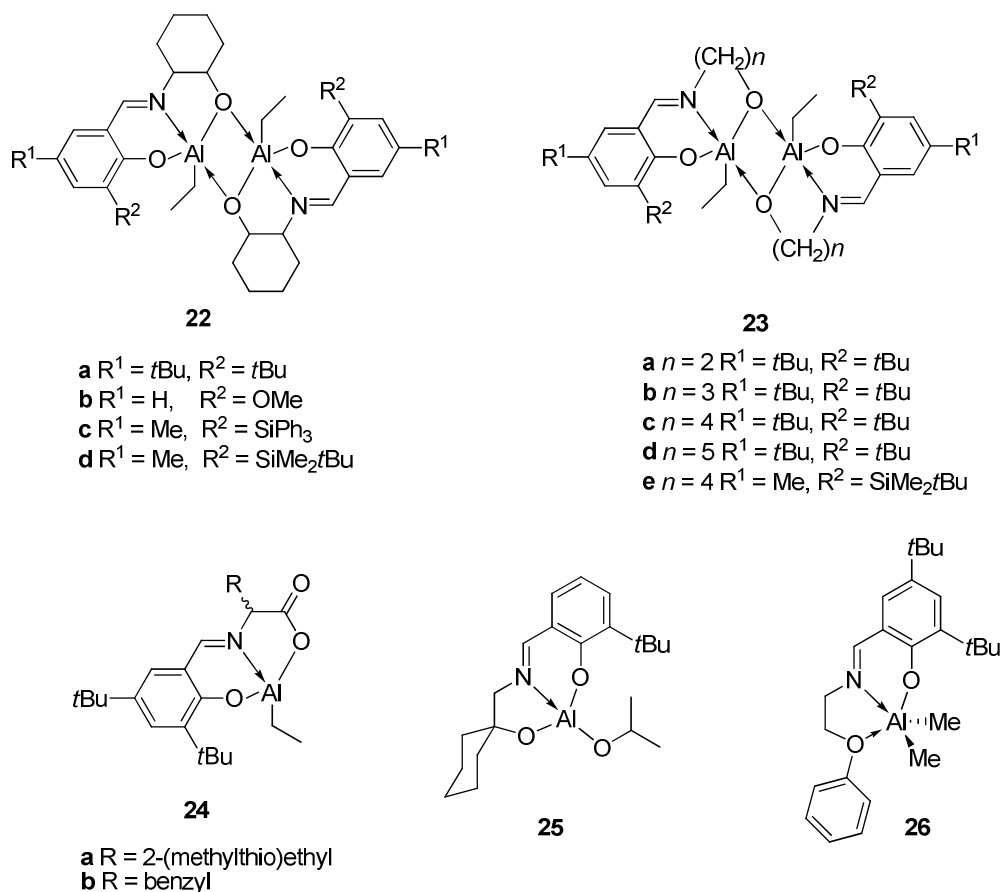


**Figure 18.** Ethyl- (**22-24**), Isopropoxide- (**25**) and Methyl-Aluminum (**26**) Complexes Supported by Tridentate Schiff-Base Ligands.<sup>68-70</sup>

#### 1.4.1.1.4 Phenoxy-amine- Based Aluminum Complexes

A family of aluminum methyl complexes supported by tetradentate amino-phenolate ligands have been prepared by Gibson *et al.*<sup>71</sup> and exploited for the ROP of *rac*-LA. It was found that, again, the catalytic behavior of complexes **27** (Figure 19) is highly dependent on the substituents at the *ortho* and *para* positions of the phenolate group. Complexes **27a** and **27b** with methyl and isopropyl *ortho/para* substituents, respectively, furnished isotactic-biased ( $P_m = 0.73$  and  $0.65$ , respectively) PLA materials. However, complex **27d** with *tert*-butyl substituents at the *ortho* and *para* positions of the phenolate group led to a slight

heterotactic polymerization of *rac*-LA ( $P_r = 0.57$ ). Complex **27c** with chlorine *ortho/para* substituents gave an atactic material from *rac*-LA.

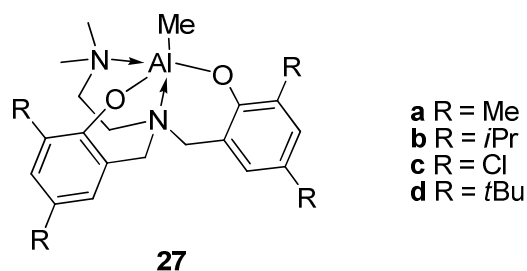


**Figure 19.** Tetradentate Amino-phenolate Aluminum Complexes (**27**) reported by Gibson *et al.*<sup>71</sup>

In 2012, Lamberti *et al.*<sup>72</sup> reported a series of aluminum-methyl complexes bearing bidentate phenoxy-thioether ligands (Figure 20), which combine a hard phenoxide donor with a soft sulfur donor. The *rac*-LA polymerizations promoted by complexes **28** in toluene solution at 80°C proceed in living fashion, leading to polymers with monomodal and narrow molecular weight distributions ( $M_w/M_n = 1.12$ – $1.16$ ); immortal polymerizations were achieved upon addition of an excess of methanol, as a chain transfer agent. The <sup>1</sup>H NMR spectra of PLAs showed an atactic microstructure.

Recently, Ma *et al.*<sup>73</sup> documented a series of aluminum complexes bearing bidentate phenoxy-amine ligands. The aluminum methyl complexes (**29** and **30**) (Figure 20) polymerize *rac*-LA in toluene at 90 °C giving rise also to atactic polymers. While the mono-ligand complexes, especially **29b** with cumyl substituents, initiated relatively slow polymerizations, much faster polymerizations were found for the bis-ligand catalyst **30** with chloro substituents on the phenoxy moiety (94% conversion in 240 h vs. 48 h, respectively; initial monomer concentration of 1 mol.L<sup>-1</sup> and monomer-to-initiator ratio = 100.)

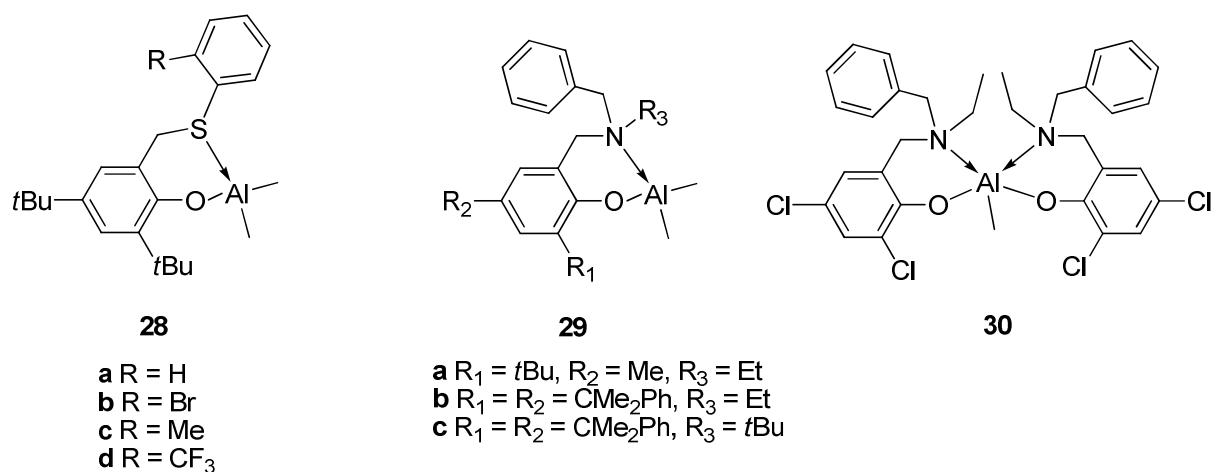


**Figure 20.** Aluminum Methyl Complexes reported by Lamberti *et al.* (**28**)<sup>72</sup> and Ma *et al.* (**29** and **30**).<sup>73</sup>

#### 1.4.1.1.5 Other Phenolate- Aluminum Based Complexes

Biphenolates and methylene-biphenolates have been evaluated as ancillary ligands for aluminum (Figure 21). The chloride complex **31** was obtained from AlEt<sub>2</sub>Cl and the biphenol pro-ligand, while the alkoxides **32** and **33** were obtained by successive reaction from methylene-biphenol with AlMe<sub>3</sub> and the appropriate alcohol.<sup>74</sup> Aluminum chloride **31** was found to be inactive in lactide ROP. The polymerization occurred very slowly with the aluminum dimer **32**, even at 80 °C, suggesting that such bridging alkoxides are poor initiators. Dimer **33** was found to be slightly more active, able to polymerize 20-50 equiv of lactide in refluxing toluene after a few days. The polymer displayed narrow molecular weight distributions ( $1.06 < M_w/M_n < 1.11$ ). Treatment of biphenol pro-ligand with 2 equiv of AlMe<sub>3</sub> followed by addition of 2,4-dimethylpentan-3-ol afforded the dinuclear aluminum complex **34**.<sup>75</sup> This latter complex showed low activity in lactide polymerization (40% conversion after 40 h at 80 °C), delivering polymers with somewhat broadened polydispersities ( $1.22 < M_w/M_n < 1.40$ ).

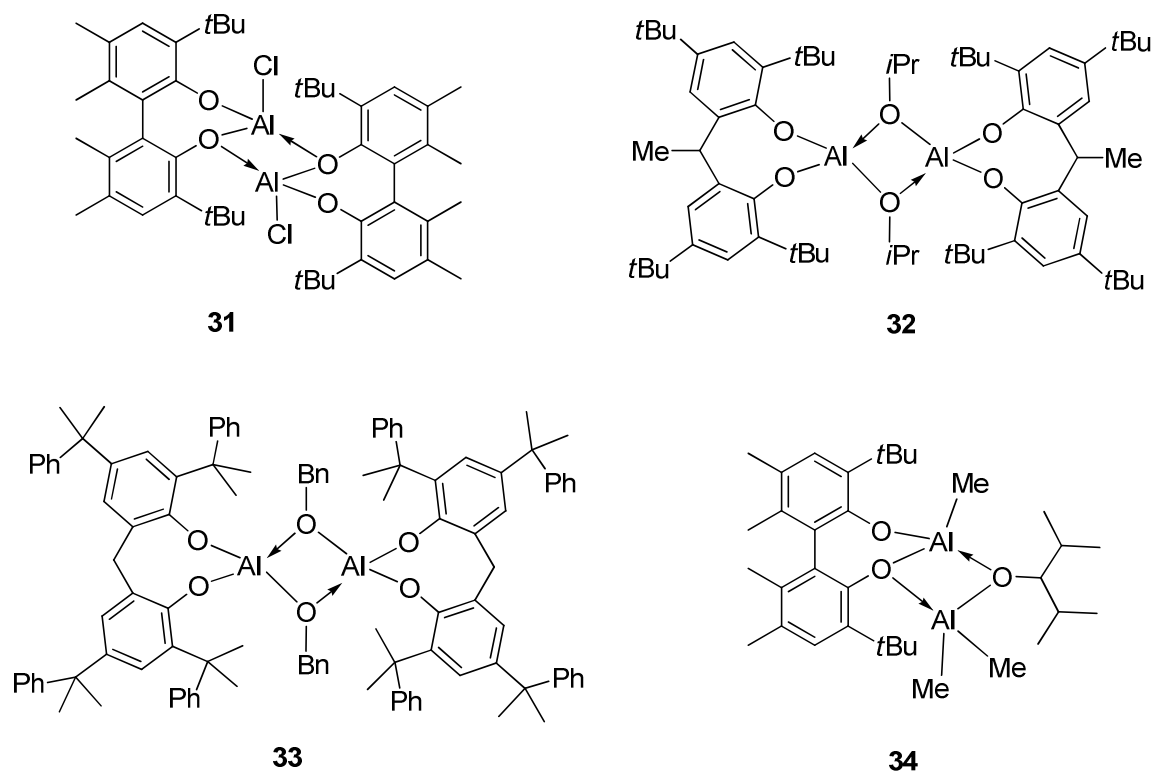


**Figure 21.** Dinuclear Aluminum Complexes (**31–34**) Featuring Biphenolate Ligands.<sup>74,75</sup>

Thiophenolate ligands have also been used for the preparation of aluminum complexes **35**, which were found to adopt monomeric structures in the solid state due to the chelating ortho methoxy group (Figure 22).<sup>76</sup> Only complex **35a** initiates lactide ROP, and for a low monomer-to-initiator ratio of 20, high conversions were achieved only after about 1 day in refluxing xylene for an initial monomer concentration of  $0.5 \text{ mol.L}^{-1}$ . Interestingly yet, the thiophenolate initiates the polymerization, as deduced from  $^1\text{H}$  NMR end-group analysis.

In 2005, Okuda *et al.*<sup>77</sup> reported aluminum complexes containing a dianionic OSSO-type ligand which in the presence of isopropanol act as efficient initiators for the *living* polymerization of *rac*-LA (PDI = 1.03 – 1.06) (Complexes **36**, Figure 22). The ligand structure influenced the tacticity of the obtained polymer, with complex **36c** giving slightly heterotactic polylactides ( $P_r = 0.65$ ) and complex **36a-b** giving atactic polymers ( $P_r = 0.5$ ).

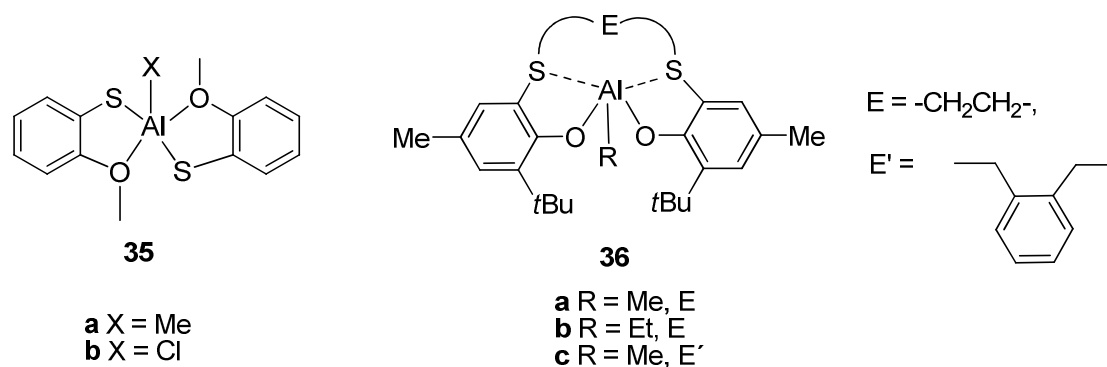


**Figure 22.** Aluminum Complexes (**35**)<sup>76</sup> and (**36**).<sup>77</sup>

#### 1.4.1.1.6 Aluminum Complexes Supported by Fluorinated Ligands

Carpentier *et al.*<sup>78</sup> prepared various aluminum complexes incorporating “fluorinated” alkoxy ligands (Figure 23) and showed that they promote efficiently ROP of cyclic esters, eventually affording polymers with controlled architectures. The nature of the ligand backbone and substituents allowed fine tuning of the intrinsic Lewis acidity of the metal center in these complexes, imparted by the strong electron-withdrawing effect of the  $\alpha$ -CF<sub>3</sub> groups at the alkoxide moieties. Interestingly, some of these fluorinated systems based on tetradentate Salen-type scaffolds such as **38** and **39** featured significant stereocontrol abilities in the ROP of *rac*-LA, producing PLAs with highly isotactic-enriched stereoblock microstructures ( $P_m$  up to 0.87).<sup>78b,c</sup>



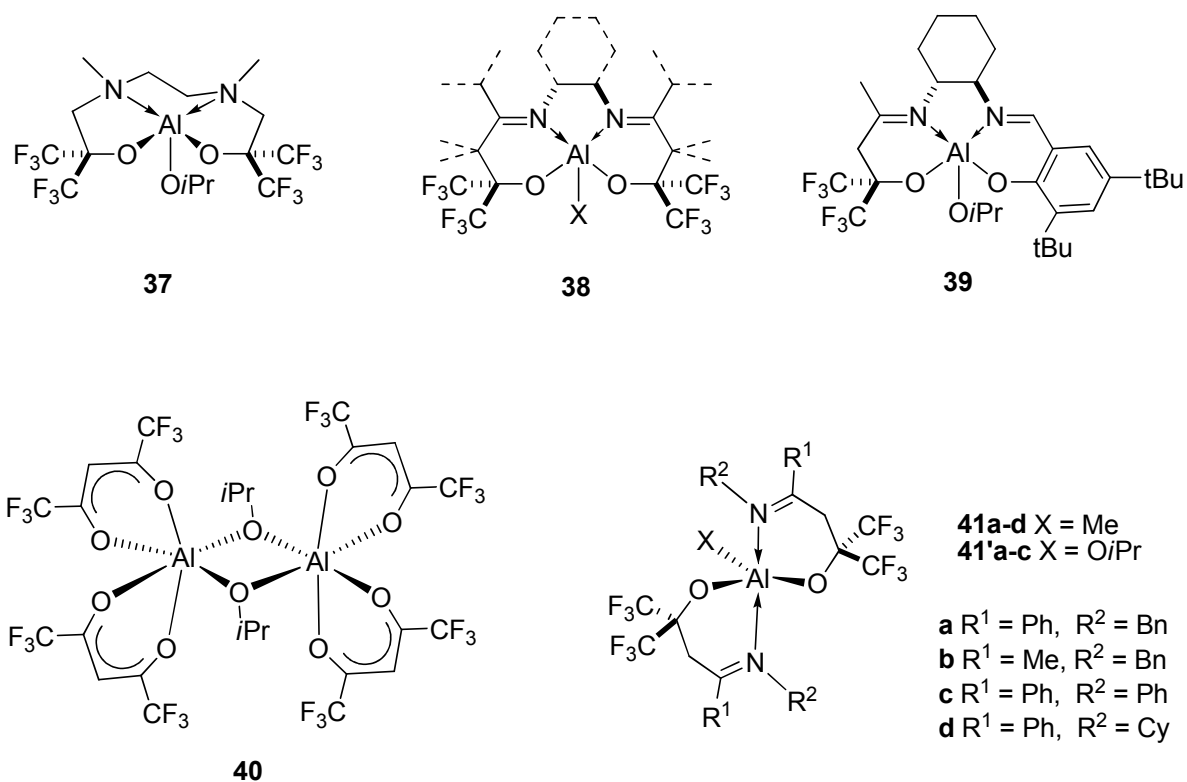


**Figure 23.** Aluminum complexes supported by fluorinated amino- (**37**) and imino-alkoxy (**38**, **39**, **41**, **41'**), and  $\beta$ -diketonate (**40**) ligands.<sup>78</sup>

#### 1.4.2. Yttrium-Based Initiators for the ROP

Lanthanide-based catalysts, despite finding a lot of application in polymerization of olefins and polar monomers, can be rather problematic due to the lability of some ligand types and the versatility of their coordination chemistry in the +3 oxidation state.<sup>79</sup> This makes the controlled synthesis of “*single-site*” Ln(+3) complexes a quite ambitious goal.

Rare-earth metal complexes have attracted considerable attention as initiators for the ROP of cyclic esters, and promising results were reported in many cases.<sup>14,17</sup> With adequate ancillaries, usually very bulky multidentate ligands, installed on the active lanthanide center, high levels of stereocontrol can be achieved in the ROP of chiral monomers. Particularly, yttrium complexes have been successfully used for the synthesis of stereocontrolled materials.

McLain *et al.*<sup>80</sup> were the first to demonstrate the high potential of an homoleptic yttrium complex ( $\text{Y}(\text{OCH}_2\text{CH}_2\text{NMe}_2)_3$ ) as an active ROP catalyst for the preparation of PLA from *rac*-LA in a controlled manner.

Spassky *et al.*<sup>81</sup> were also pioneered, in 1994, by employing an homoleptic yttrium 2-methoxyethoxide complex, described as  $\text{Y}(\text{OCH}_2\text{CH}_2\text{OCH}_3)_3$ , that proved to be highly active, with the ROP proceeding readily at room temperature. Although no stereocontrol was observed in this reaction, this salient discovery opened the way to the use of related Group 3 metal complexes for the ROP of cyclic esters, especially *meso*- and *rac*-LA.

Subsequently, Carpentier *et al.*<sup>82</sup> reported a series of bis[bis(oxazolinato)]yttrium complexes (**42-43a-c**) (Figure 24) of general type  $[\text{Box}]_2\text{Y}[\text{N}(\text{SiHMe}_2)_2]$  (Box = deprotonated chiral and nonchiral 2,2'-methylene[bis(oxazoline)] ligands) prepared by amine elimination protocols. The produced PLAs and PHBs have narrow polydispersities ( $M_w/M_n = 1.08\text{--}1.44$ ) and controlled number-average molecular weight ( $M_n$  up to  $182000 \text{ g}\cdot\text{mol}^{-1}$ ). In particular, for complex **42**, >95% conversions in 5 minutes were obtained at 20 °C in THF solution for a  $[\text{LA}]_0/[\text{I}]_0$  of 2000 ratio. However, whether chiral or nonchiral Box ligands are used, the polymers showed an atactic microstructure.

Carpentier in collaboration with Trifonov's group disclosed a series of bis(guanidinate) yttrium alkoxide complexes (**44**) (Figure 24).<sup>83</sup> These complexes are active catalysts/initiators for the controlled-living ROP of lactones, with TON up to 240 within a few hours at 20 °C in the case of *rac*-BL. They afford polyesters (PLAs, PHBs) with relatively narrow molecular weight distributions and molecular weights in a good agreement with the calculated ones. It is worth noting that complex **44** afforded highly syndiotactic PHBs ( $P_r$  up to 0.84) while in the case of *rac*-LA ROP no stereoselectivity was observed. This constitutes a rather unique example where better performance are observed with beta-lactones as compared to lactides.

In 2009, Yao *et al.*<sup>84</sup> prepared a series of mono(amidinate) yttrium metal bis(alkyl) complexes (**45a-c**) with different amidinate ligands (Figure 24). The activity of the mono(amidinate) yttrium bis(alkyl) complexes (**45a-c**) revealed the efficiency of these initiators in the production of high molecular weight PLAs with moderate polydispersities (<1.32). More recently, the yttrium amide complex **46**<sup>85</sup> has been found as a highly active initiator for L-LA polymerization in toluene at 50 °C; the conversion could reach up to 93% in 2 min when the molar ratio of [LA]<sub>0</sub>/[Y]<sub>0</sub> was up to 10,000 affording materials with unimodal molecular distributions. This represents one of the most active rare-earth metal-based catalyst for lactide polymerization, although such comparisons should always be taken with care due to different reaction conditions between authors (i.e., monomer and solvent purity, etc). Complex **46** is also active for *rac*-LA ROP to produce polymers with a moderate level of heterotacticity (*P<sub>r</sub>* up to 0.76).

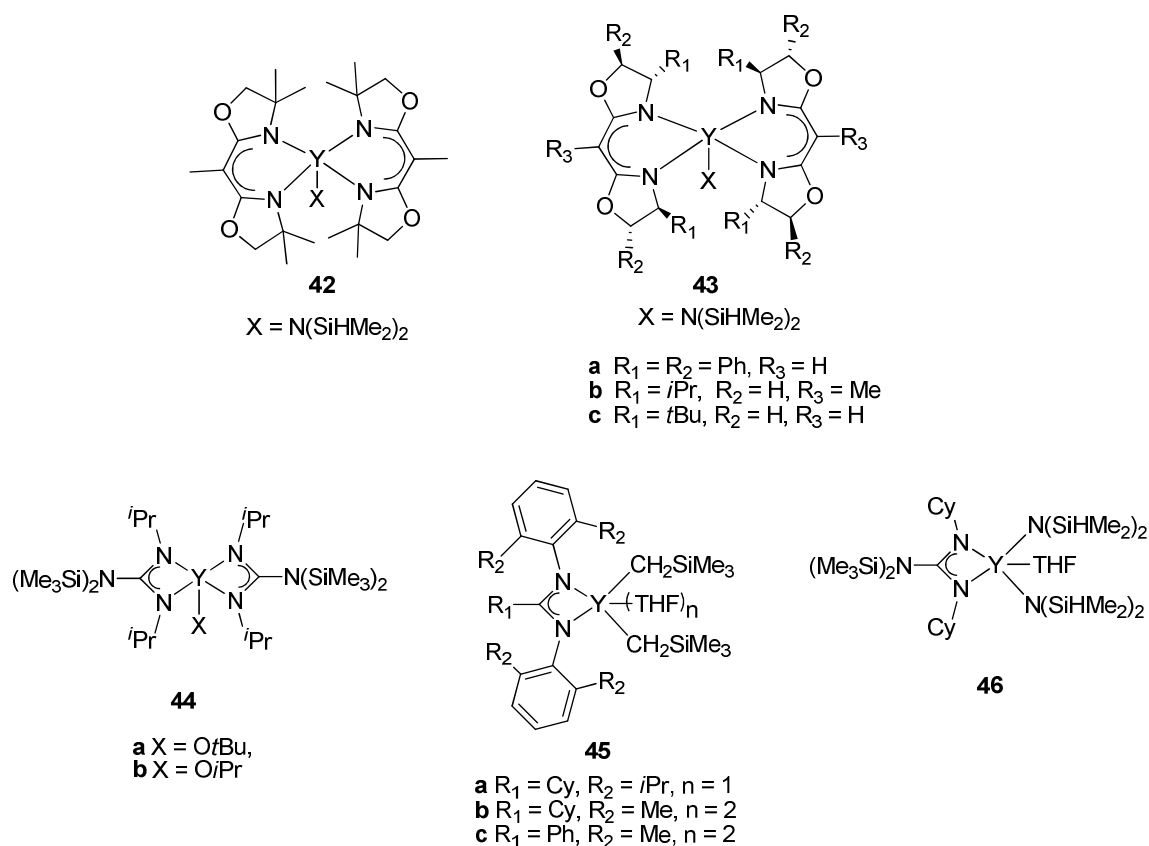
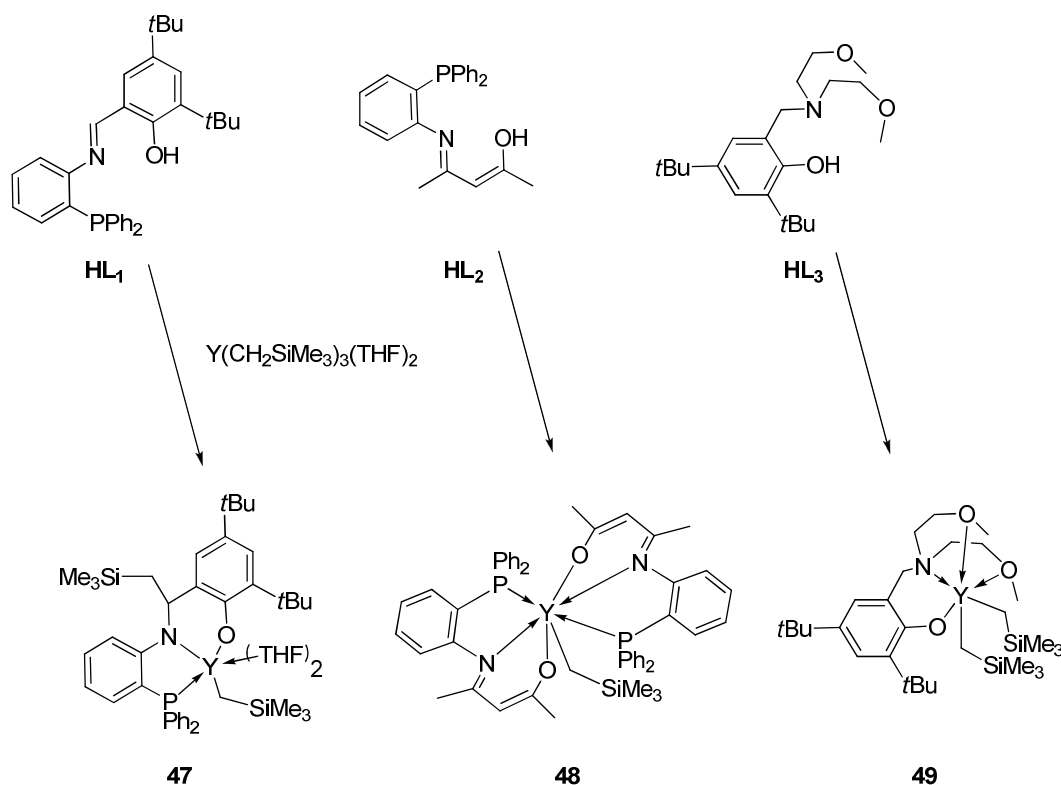


**Figure 24.** Yttrium Initiators (**42-46**) Bearing *N,N*-Donor Ligands.<sup>82-85</sup>

The swift reaction of yttrium organometallic precursor like tris(alkyl)  $Y(CH_2SiMe_3)_3(THF)_2$  with *N,O,P*-donor multidentate ligands (HL1 and HL2, Scheme 14) driven by alkane elimination, afforded the alkyl complexes **47** and **48**. In this method, HL1 was deprotonated by the metal alkyl whereas the imino C=N group was reduced by intramolecular alkylation, generating THF-solvated mono-alkyl complex **47**.<sup>86</sup> The mono(alkyl) complex **47** led to complete conversions of L-LA within 2 h at 20 °C, whereas only 1 h was needed using complex **48** as initiator under similar experimental conditions. This was attributed to the coordination of THF molecules in complex **47**. Complex **49** (Scheme 14) proved less reactive in L-LA polymerization. It might be attributed to the coordination of methoxy moieties, which play a similar role as THF in complex **47**. In all cases, the molecular weight of the resulting PLA increased with the monomer-to-catalyst ratio while the molecular weight distribution showed no change, indicating a controlled polymerization.



**Scheme 14.** Yttrium Initiators (**47-49**) Supported by *N,O,P*- and *N,O,O,O*-Donor Ligands.<sup>86</sup>

In 2008, Arnold *et al.*<sup>87</sup> described a chiral alcohol which formed homochiral  $C_3$ -symmetric yttrium complexes (**50**, Figure 25) and which showed high isoselectivity in the polymerization of *rac*-LA ( $P_m = 0.81$ ). Complete conversion was achieved in 10 min at  $-18$  °C for a monomer-to-initiator of 200.

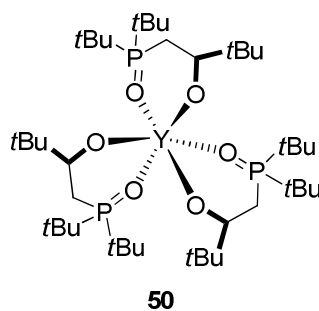


**Figure 25.** Tris(alkoxy-phosphonate) Yttrium Complexes (**50**).<sup>87</sup>

Carpentier *et al.*<sup>88</sup> discovered that yttrium amido complexes supported by an amine bis(phenolate) ligand have good syndio/heteroselectivity in the polymerization of chiral racemic lactones. The amido and alkoxide complexes **51** (Figure 26) have been used as initiators for the ROP) of *rac*-LA and *rac*- BBL to provide heterotactic-enriched PLAs and syndiotactic-enriched PHBs, respectively, by means of a chain-end control mechanism. Most of these polymerizations proceeded in a controlled fashion, giving polymers with narrow polydispersities and experimental molecular weights in good agreement with calculated values. For the polymerization of *rac*-LA, the heterotactic stereocontrol appears to be governed essentially, if not only, by steric considerations. Higher heterotacticities were achieved with complexes that possess bulkier *ortho* substituents installed on the phenolate rings, independently of their electronic nature;  $R^1 = \text{Cl}$  ( $P_r = 0.56$ );  $\text{CMe}_3$  ( $P_r = 0.80$ );  $\text{CMe}_2\text{Ph}$  ( $P_r = 0.90$ );  $\text{CMe}_2(4\text{CF}_3\text{-Ph})$  ( $P_r = 0.93\text{--}0.94$ );  $\text{CMe}_2t\text{Bu}$  ( $P_r = 0.94\text{--}0.95$ );  $\text{CPh}_3$  ( $P_r = 0.95\text{--}0.96$ ). On the other hand, for the polymerization of *rac*-BBL, electronic interactions appear to be involved in the syndiotactic stereocontrol, as higher syndiotacticities were obtained only with ligands bearing a phenyl group in the *ortho* substituents;  $R^1 = \text{Cl}$  ( $P_r = 0.42\text{--}0.45$ );  $\text{CMe}_2t\text{Bu}$  ( $P_r = 0.62\text{--}0.70$ );  $\text{CMe}_3$  ( $P_r = 0.80$ );  $\text{CMe}_2(4\text{CF}_3\text{-Ph})$  ( $P_r = 0.82\text{--}0.84$ );  $\text{CMe}_2\text{Ph}$  ( $P_r$

= 0.89);  $\text{CPh}_3$  ( $P_r = 0.94$ ). DFT computations on model intermediates confirmed a stabilizing  $\text{C-H}\cdots\pi$  interaction between a methylene  $\text{C-H}$  of the ring-opened BBL unit and the  $\pi$  system of one of the *ortho*-aryl substituents of the  $\text{ONOO}^{\text{R}1}$  ligand; by contrast, for model intermediates in the ROP of LA, no such  $\text{C-H}\cdots\pi$  interaction involving the methyl group of lactate was observed.<sup>89</sup>

Cui *et al.*<sup>90</sup> also reported a series of THF-solvated yttrium (mono)alkyl complexes supported by *ONNO*-tetradentate diamine bis(phenolate) ligands. Notably, complexes **52a-b** (Figure 26) displayed modest activity but high stereoselectivity in the polymerization of *rac*-LA to give highly heterotactic PLA materials with  $P_r$  values ranging from 0.95 to 0.99. An active oligomer connected to complex **52a** prepared from *rac*-LA was characterized by  $^1\text{H}$  NMR. The spectrum of the active oligomer demonstrated that the ligand and the pendent nitrogen atom remain coordinated to the metal ion, and the geometry around the central metal in complex **52a** did not collapse but retained its structure in solution upon monomer coordination and insertion. The spatially steric environment in the resulting propagating sites will favor the incorporation of a configurationally opposite enantiomer to lower the transition state energy.

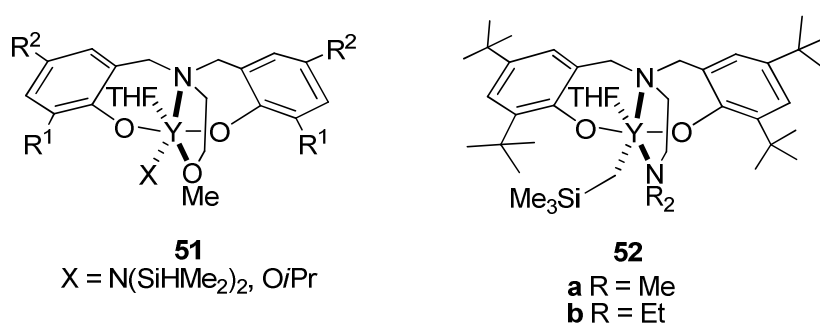


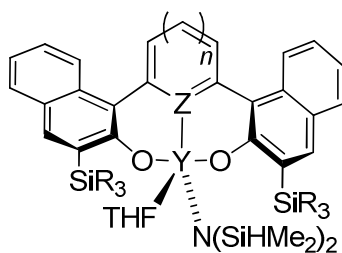
**Figure 26.** Yttrium Initiators (**51-52**) Supported by *N,O,O,O*- and *N,N,O,O*-Donor Ligands.<sup>88-</sup>

90

In 2009, Carpentier *et al.*<sup>91</sup> prepared another series of yttrium complexes (**53**) (Figure 27) based on sterically demanding silyl *ortho*-substituted tridentate 2,6-bis(naphtholate)-pyridine and 2,5-bis(naphtholate)-thiophene ligands. Such  $\{\text{OZO}^{\text{SiR}3}\}^{2-}$  ligands may confer

various symmetries at the metal center by the non-coplanar orientation of the rigid flat central heterocyclic donor and adjacent naphtholate groups, due to steric repulsion imposed between these moieties. Single-crystal X-ray diffraction and NMR studies showed that these amido complexes (**53**) all adopt  $C_s$ -symmetric structures in which the naphtholate rings twist in the same direction from the plane of the pyridine or thiophene linker. Compounds **53a-c** are *single-site* initiators for the ROP of *rac*-LA at 20 °C, affording PLAs with relatively narrow polydispersities and molecular weights in good agreement with calculated values. Atactic polymers are formed in toluene but, when carried out in THF, the polymerizations afforded heterotactic-enriched PLAs ( $P_r$  up to 0.93); the same solvent-dependence of stereoselectivity was observed in ROP of *rac*-LA with amino-alkoxy-bis(phenolate).<sup>45,88,89</sup> Interestingly, the complex **53b** having *o*-SiMe<sub>2</sub>*t*Bu substituents on the naphtholate rings was found inactive toward the ROP of *rac*-BL, while compounds **53a** and **53c** based on *o*-SiPh<sub>3</sub> substituted ligands converted *rac*-BL at 20-50°C with time-of-flight (TOF) up to 720 h<sup>-1</sup>. Syndiotactic-enriched PHBs, with  $P_r$  up to 0.87, were formed when using toluene as the solvent, whereas atactic polymers were obtained in THF; *i.e.*, the opposite trend than that observed for the ROP of *rac*-LA (*vide supra*) but a trend consistent with our previous observations in the ROP of *rac*-BBL using tetradentate bis(phenolate)-Y systems.<sup>45,88,89</sup>

The degree of stereocontrol in those polymerizations of *rac*-LA and *rac*-BBL is affected by the central linker in the ligand framework (pyridine, thiophene). For instance, complex **53c** afforded PLAs and PHBs with  $P_r = 0.5-0.68$  and  $0.52-0.67$ , respectively) while complex **53a** based on 2,6-pyridine afforded PLAs and PHBs with  $P_r = 0.5-0.9$  and  $0.76-0.87$ , respectively).



**53**

- a** Z = N, n = 1 SiR<sub>3</sub> = SiPh<sub>3</sub>  
**b** Z = N, n = 1 SiR<sub>3</sub> = SiMe<sub>2</sub>tBu  
**c** Z = S, n = 0 SiR<sub>3</sub> = SiPh<sub>3</sub>

**Figure 27.** Yttrium Initiators (**53**) Bearing Bis(naphtholate) Ligands.<sup>91</sup>

Williams *et al.*<sup>92</sup> reported a series of bis(thiophosphinic amido) yttrium complexes **54** (Figure 28), which are attractive due to their high rates and enhanced control in the ROP of L-LA polymerization activity; 94% conversion in 6 min at 25 °C for a monomer-to-initiator ratio of 100 was reached. The phosphorous substituents greatly influenced the rate of the reaction, and that the rate followed the order isopropyl > phenyl > ethoxy. In 2011, the same group prepared a series of bis(phosphinic)diamido yttrium amide, alkoxide and aryloxide initiators (**55** and **56**) (Figure 28) for use in *rac*-LA ROP. The alkoxide complexes **55** are all dimeric both in solid state and in solution, as are the amide complexes **55** substituted with isopropyl groups on the phosphorous atoms. Increasing the steric hindrance of the phosphorous substituents (*tert*-butyl), enabled isolation of mononuclear yttrium amide complexes **56** with either 2,2-dimethylpropylene or ethylene diamido ligand backbones. The alkoxide complexes **55** are the most efficient initiators among this series, showing very high rates and good polymerization control, behavior consistent with rapid rates of initiation (complete conversions in THF at 25 °C were obtained in 1 min for  $[rac\text{-LA}]_0/[Y]_0 = 400$ ). Moreover, for the series of complexes with *tert*-butyl substituents on the phosphorous atoms, it appeared that the ethylene diamido ligand fragment leads to greater rates. It was proposed that the shorter ethylene diamido linker leaves the yttrium atom more exposed than for complexes with C-3 backbone diamido group, resulting in an increase in polymerization



activity for the former. Furthermore, the mononuclear complex **56** in which the longer 2,2-dimethylpropylene ligand diamido backbone is present, showed higher heteroselectivity in the polymerization of *rac*-LA ( $P_r = 0.85$ ); however, this effect is reduced on changing the diamido backbone group to ethylene ( $P_r = 0.61$ ).<sup>93</sup>

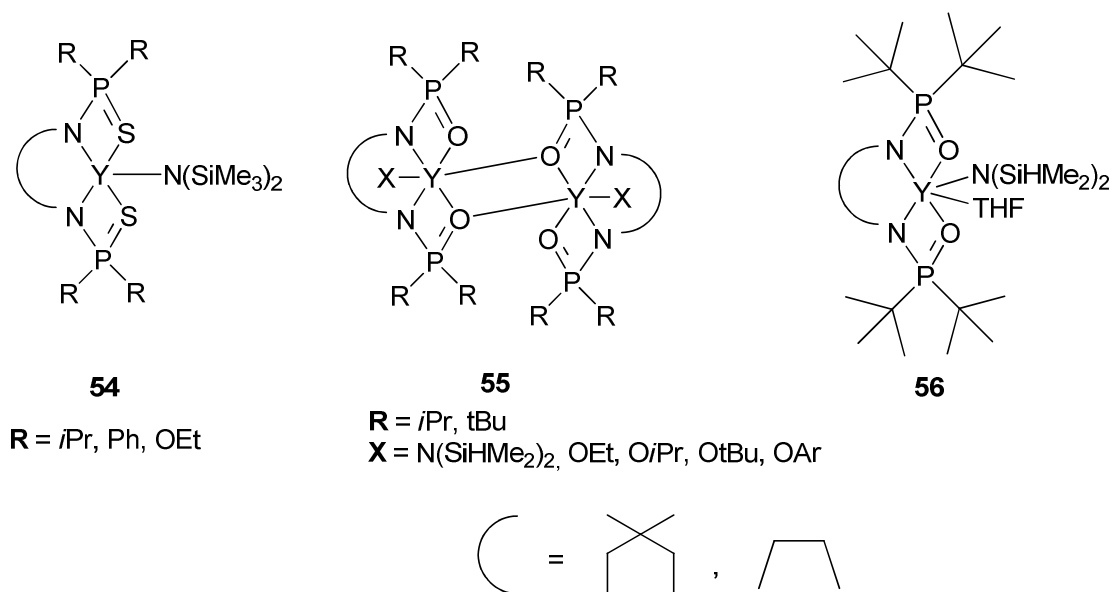


**Figure 28.** Yttrium Initiators (**54-56**) Bearing *N,N,S,S*- and *N,N,O,O*-Donor Ligands.<sup>92,93</sup>

Similar results were first documented by Okuda *et al.*<sup>94</sup> in which they observed that the heterotactic selectivity of yttrium complexes **57** (Figure 29) is apparently enhanced when the steric demand of the bis(phenolate) ligand is increased either by the length of the bridge or by bulky *ortho*-substituents in the phenoxy unit. The influence of the bridging moiety is most significant (Table 2).

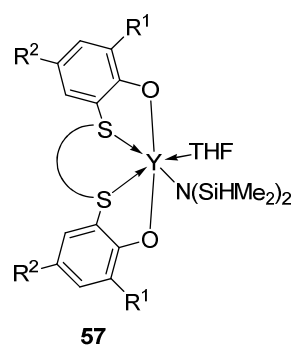


**Figure 29.** Yttrium Complexes Supported by 1, $\omega$ -Dithiaalkanediyli-Bridged Bis(phenolate) Ligands.<sup>94</sup>

**Table II.** Heteroselectivity during the ROP of *rac*-LA using [OSSO]Y complexes.<sup>94</sup>

bridge	R <sup>1</sup>	R <sup>2</sup>	$P_r$
-(CH <sub>2</sub> ) <sub>2</sub> -	<sup>t</sup> Bu	Me	0.68
-(CH <sub>2</sub> ) <sub>2</sub> -	cumyl	cumyl	0.71
	<sup>t</sup> Bu	Me	0.72
-(CH <sub>2</sub> ) <sub>3</sub> -	<sup>t</sup> Bu	<sup>t</sup> Bu	0.84
	<sup>t</sup> Bu	Me	0.85
	cumyl	cumyl	0.86
	<sup>t</sup> Bu	Me	0.88

In 2012, Williams *et al.*<sup>95</sup> prepared highly active yttrium “phosphasalen” initiators (**58** and **59**, Figure 30) for the stereocontrolled ROP of *rac*-LA. Changing the phosphasalen structure enabled access to significant isoselectivities ( $P_m$  up to 0.84, for complex **58**)<sup>96</sup> or high heteroselectivities ( $P_r$  up to 0.90, for complex **59**). These initiators showed high rates, excellent polymerization control, and tolerance to low loadings. Initiator **58** showed nearly complete conversion of 500 equiv of *rac*-LA in ~ 1 h. Analysis of the conversion vs time data for **58** indicated a first-order dependence of the polymerization rate on the LA concentration, and pseudo-first-order rate constants  $k_{obs} = 6.9 \times 10^{-4}$  and  $7.9 \times 10^{-4} \text{ s}^{-1}$  (0.2 mol %, [LA] = 1M, THF) were obtained. The mechanism for heteroselectivity and isoselectivity suggested for **59** and **58**, respectively, involves chain-end control. Analysis of the polymer produced by **58** by differential scanning calorimetry showed a  $T_m$  value of 178 °C; confirming the formation of a stereoblock polymer in agreement with RMN analysis.

In an attempt to understand the contrasting tacticity control of initiator **58** vs. **59**, the structures of these complexes were investigated in solid state and in solution. The coordination geometry of **58** and **59** are quite different indeed, with the former containing a hexacoordinate Y and the latter a pentacoordinate Y. Thus, the authors tentatively attributed the isoselectivity observed for **58** to more sterically congested and constrained active site compared with that in **59**.

Coates' and Carpentier' groups also reported salen-like yttrium complexes (**60** and **61**, respectively; Figure 30). In comparison with those of Williams described above, the Y-salen initiator **60** required 14 h at 70 °C in toluene to reach complete conversion of *meso*-LA at a higher initiator loading (1 mol%).<sup>97</sup> Yttrium-“half-salen” complex **61** (1 mol %) required 3 days to reach complete conversion of *rac*-LA. In both cases only atactic PLAs were obtained.<sup>78c</sup>

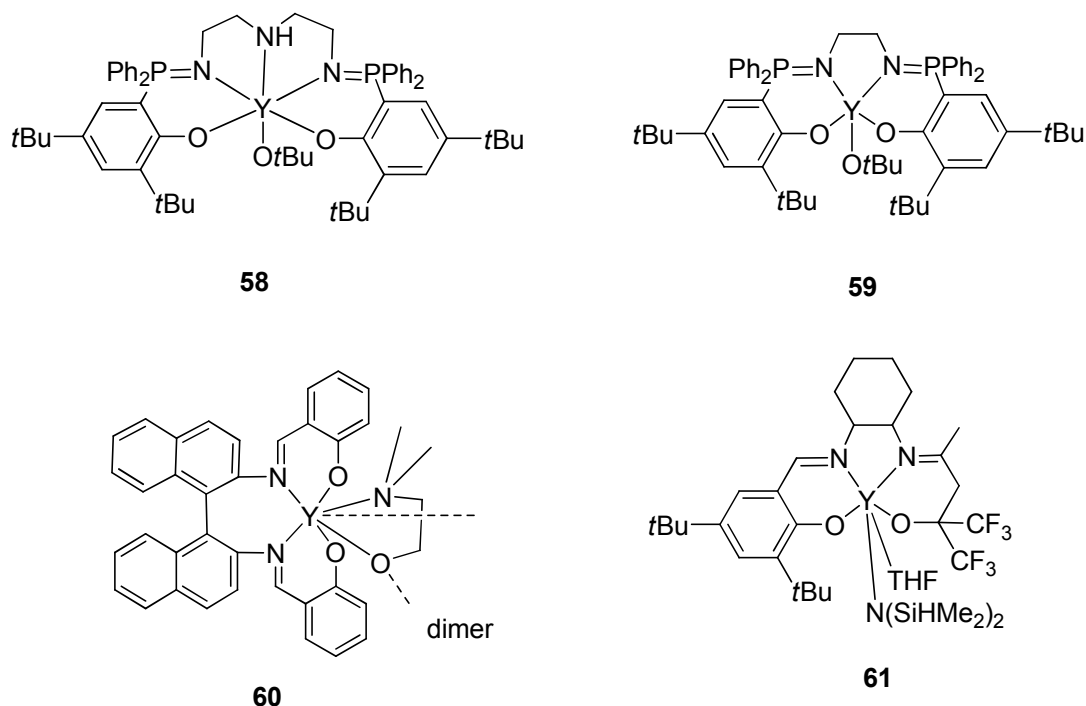
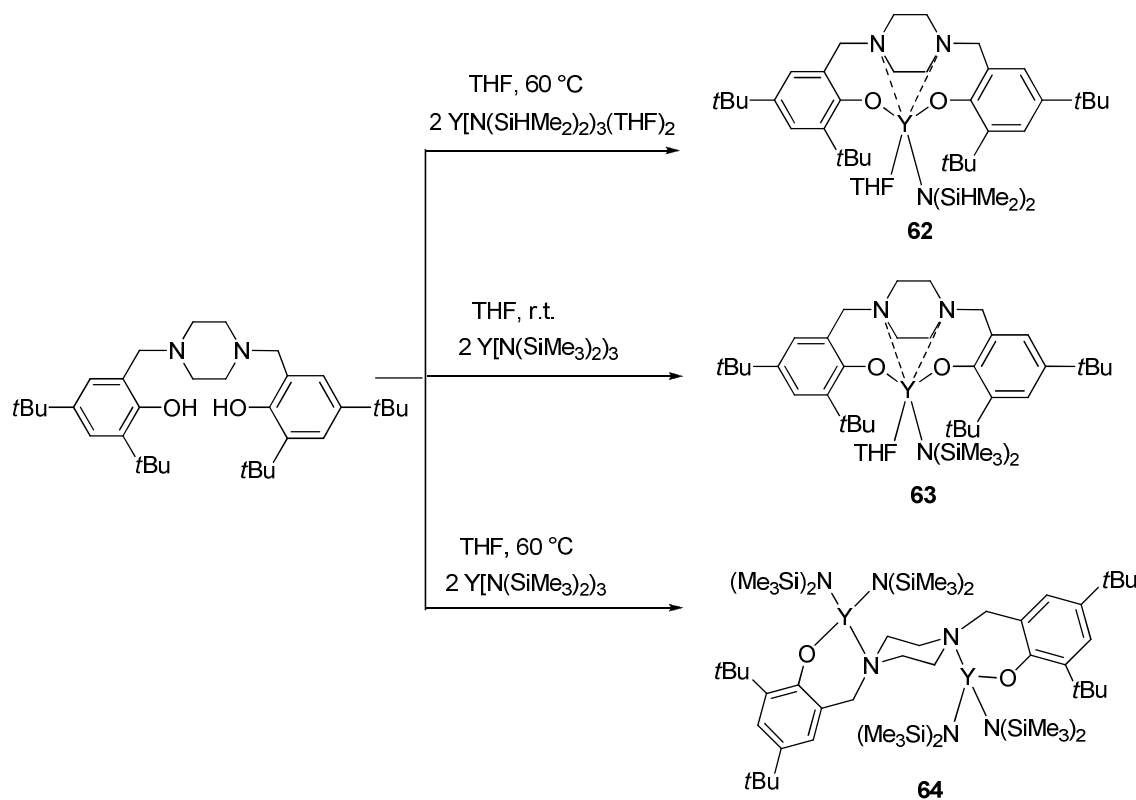


**Figure 30.** SALEN-Like Yttrium Complexes (**58-61**).<sup>78c,95-97</sup>

In 2012, Shen *et al.*<sup>98</sup> prepared a series of bimetallic and monometallic yttrium complexes (**62–64**) stabilized by a piperazine-bridged bis(phenolate) ligand (Scheme 15). The formation of bimetallic yttrium amido complexes was significantly influenced by the reaction temperature and the steric bulkiness of the amido group. For the bulky bis(TMS)-amido group, the bimetallic yttrium bisamido complex **64** was isolated when the reaction was conducted at 60 °C; in contrast, when the reaction was conducted at room temperature, only the monometallic yttrium complex **63** was isolated. For the less bulky bis(dimethylsilyl)amido group, only the monometallic yttrium complex **62** could be prepared. With all of these complexes (**62–64**), the L-LA ROP proceeded rapidly at 60 °C in toluene or THF for an initial monomer concentration of 1 mol.L<sup>-1</sup> (e.g. 95% conversion in 30 min at a monomer-to-initiator ratio = 300 using complex **63**, and 98% conversion in 10 min at [L-LA]<sub>0</sub>/[Y]<sub>0</sub> = 2000 using complex **64**). These complexes were also active for the *rac*-LA ROP, affording only moderate heterotactic PLAs (*P<sub>T</sub>* up to 0.68).



**Scheme 15.** Yttrium Piperazine-Bis(Phenolate) Complexes (**62-64**).<sup>98</sup>

## 1.5. STRUCTURAL, MECHANISTIC AND COMPUTATIONAL STUDIES ON WELL-DEFINED INITIATORS FOR THE ROP OF LACTIDES AND $\beta$ -BUTYROLACTONE

As briefly reviewed in the above sections, over the past decade, many studies have focused on the development of structurally well-defined metal pre(catalysts)/initiators for the ROP of cyclic esters in order to get insights about the complexity of the ROP mechanism and to enable catalyst design on a rational basis, especially for the stereocontrol polymerization of *rac*-LA and *rac*-BBL. For example, popular metal-ligand frameworks such as  $\beta$ -diketiminato- or hydro-tris(pyrazolyl)borate (Tp)-supported  $\text{Zn}^{99}$ ,  $\text{Mg}^{100}$ ,  $\text{Ca}^{101}$  complexes proved useful in establishing a correlation between reactivity and electronegativity while simultaneously providing information about the relative nucleophilicities of various M–X polymerization initiators. Although chalcogen-bridged (bis)phenolate complexes of Ti yielded insight into the

solvent dependence of ROP,<sup>102</sup> similar Ln-(bis)phenolate and more recently amino-(bis)phenolate complexes<sup>45,88,89</sup> revealed the influence of steric bulkiness on catalyst activities.

Al complexes bearing (bis)phenolate,<sup>74</sup> thiophenolate,<sup>76</sup> porphyrin,<sup>50b,c</sup> and salen<sup>97,103</sup> ligands have been also thoroughly studied, yielding extensive insight into structure–activity relationships, ligand reactivity, and transesterification mechanisms.

One particular mechanistic aspect which is still of debate concerns both the potential chelation of the growing polymer chain donor sites and the effect of chelating groups on the reactivity of the active species. However, to date, examples of fully structurally characterized (pre)catalysts/initiators which may act as model complexes mimicking intermediate species involved in the initiation and propagation steps in the ROP of cyclic esters remain rare (Figure 31).

In 2005, Lewinski *et al.*<sup>104</sup> documented the isolation and structural characterization of an intermediate formed by primary insertion of a lactide (LA) molecule into the Al–OR bond of a dialky-aluminum derivative of 2-methoxyethanol (**65**, Figure 31). Compound **65** exists as a dimer, with five-coordinate chelate aluminum centers, as confirmed by an X-ray diffraction study and IR spectroscopy in CH<sub>2</sub>Cl<sub>2</sub> solution. In 2007, Dagorne *et al.*<sup>105</sup> described a five-coordinated Al-lactate cation with a coordinated THF molecule to the metal center (**66**, Figure 31) derived from a monoinsertion of L-Lactide into the Al–O*i*Pr bond of an Al-alkoxide cationic complex incorporating the sterically bulky aminophenolate bidentate ligand 6-(CH<sub>2</sub>NMe<sub>2</sub>)<sub>2</sub>-CPh<sub>3</sub>-4-Me-C<sub>6</sub>H<sub>2</sub>O<sup>-</sup> (*N,O*).

In 2006, Gibson *et al.*<sup>106</sup> reported a Sn(II) (isopropyl (*S*)-lactate) complex supported by a β-diketiminate ligand (**67**, Figure 31). An X-Ray structural determination showed that the lactate ligand forms a five-membered chelate ring with a weak donor bond from the carbonyl oxygen atom to the tin center. To probe the coordination of lactate ligand in solution, <sup>1</sup>H NOESY and COSY NMR spectra were recorded. These data showed that the

methine hydrogen of the [Sn–OCHMe] lactate fragment closely approaches two of the aryl-*i*Pr substituents. Furthermore, evidence for weak coordination of oxygen of the carbonyl group to the metal center in the solution state was suggested by an  $^{119}\text{Sn}$  NMR chemical shift of  $-265.3$  ppm.

Also, in 2006, Okuda *et al.*<sup>107</sup> reported a Sc(III) (*R*)-*tert*-butyl lactate dithia-bis(phenolate) complex (**68**) which possesses a dimeric structure in the solid state (Figure 31). When complex **68** was used for the ROP of *rac*-LA, a highly heterotactic PLA was obtained ( $P_r = 0.93$ ). The authors observed that Ln-complexes with relatively long dithia bridges (three or four carbons atoms) feature high fluxionality in solution (according to  $^1\text{H}$  NMR experiments) affording PLAs with higher heterotacticities (*vide supra*, Table II), while complexes with a dithiaethylenyl bridge are more rigid and lead to lower heteroselectivities. Thus, they claim that a dynamic monomer-recognition process involving interconversion of the ligand configuration from *A* into *A* would lead to high heterotactic selectivity.

In 2007, Nomura *et al.*<sup>58</sup> reported an homochiral heteroleptic Al(III) methyl (*S*)-lactate complex supported by a salen ligand (**69**, Figure 31). Complex **69** has an hexacoordinate aluminum center with a  $\kappa^4$ -salen-ligand and a  $\kappa^2$ -*O*-lactate moiety, as evidenced in the solid state by an X-ray diffraction study, and in solution by  $^{13}\text{C}$  NMR spectroscopy; the carbonyl carbon of **69** appears at  $\delta = 189.2$  ppm. Its large downfield shift relative to the carbonyl carbon of free methyl lactate ( $\delta = 176.1$  ppm) suggests that the oxygen atom of the carbonyl group should be coordinated by the Al atom in solution. In the same study, the authors induced in reaction the isospecific achiral salen-aluminum complex **70** (Scheme 16) at room temperature with one equivalent of LLA to afford quantitatively the insertion product **70**, as confirmed by NMR spectroscopy (Scheme 16). After the first monomer inserts into the Al–OBn bond of the achiral complex **70**, a chirality derived from the monomer is introduced into the complex. In this process, the metal center and/or the ligand conformation may

construct the strictly rigid chiral environment, which cannot be inverted by the exchange of the chiral sense of the polymer terminus. In this case, the stereoselective ROP of *rac*-LA proceeds *via* enantiomorphic site-control. The ROP was also examined by the homochiral complex **69** *via* monitoring the reaction of 20 equiv of *rac*-LA and 1 equiv of complex **69**. If the chiral environment around the metal center is rigid, the polymerization rate constant should be drastically diminished once the favored monomer LLA has been almost consumed at around 50% monomer conversion. However, they observed that the rate constant before and after 50% monomer conversion did not change until 84% monomer conversion. The enantiomeric excess of the remaining monomer reaches a maximum of 13%, which indicates that, essentially, reactions of both LLA and DLA take place simultaneously in this system. If the polymerization proceeds *via* an enantiomorphic site-control, the enantiomeric excess should have increased with monomer conversion, as reported by Spassky.<sup>44</sup> Thus, the chiral environment of the metal complex is flexible and the chiral geometry of the metal complex can be inverted by introduction of the opposite chiral sense of the polymer terminus during the propagation reactions. Because the origin of the chiral differentiation of the racemic monomers comes from the chiral sense of the last inserted monomer, they conclude that the stereoselective polymerization of *rac*-LA using achiral complex **70** takes place *via* a chain-end control.

In 2008, Carpentier *et al.*<sup>78b</sup> reported the Y(III) (R)-*tert*-butyl lactate diimino-dialkoxo complex **72** (Figure 31). A single-crystal diffraction study revealed that **72** is dinuclear in the solid state, with bridging  $\mu, \kappa^2$  *O,O,O,O*-lactate units and a tetracoordinated  $\{\text{ON}^{\text{Et}}\text{NO}\}$  unit. Complex **72** proved to be an active catalyst/initiator for the controlled ROP of both *rac*-LA and *rac*- $\beta$ -BL, but affording only atactic PLAs and PHBs.

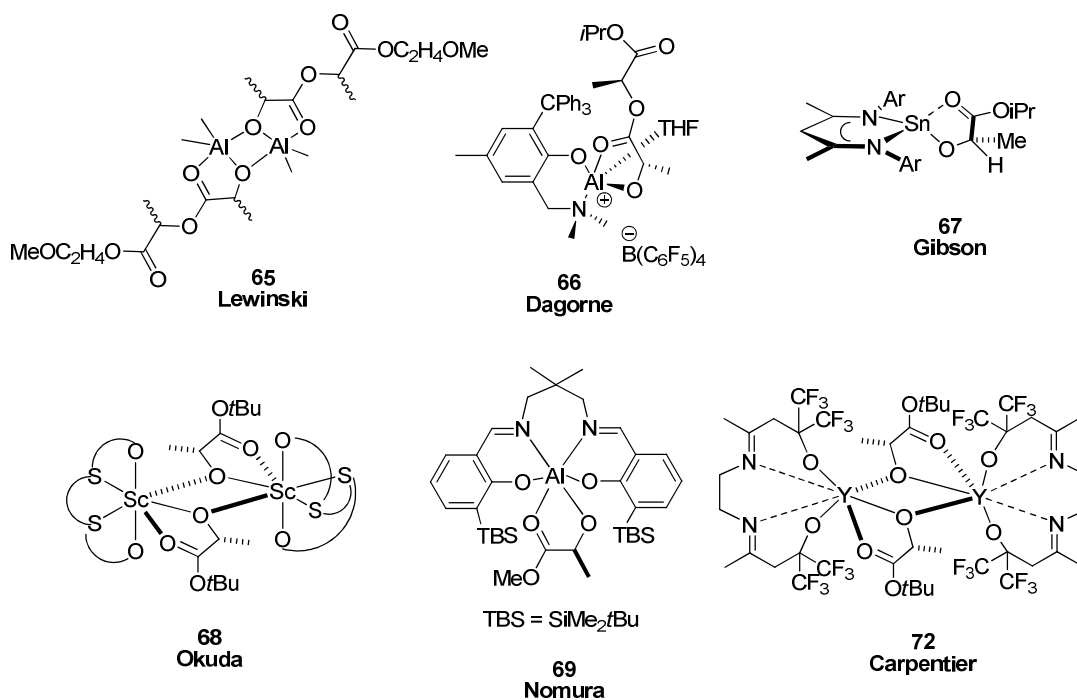
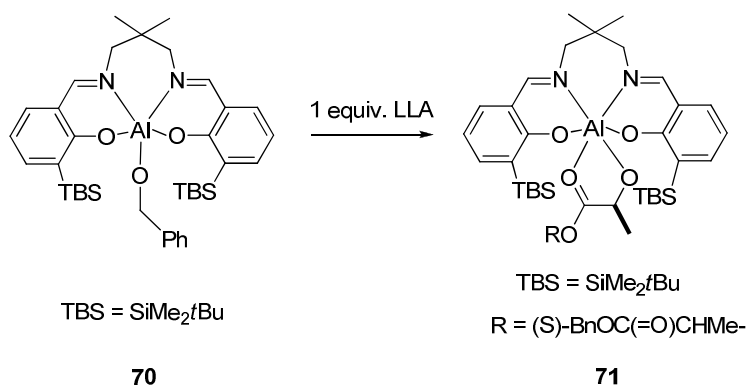


**Figure 31.** Rare Examples of Metal Complexes (**65-69**) and (**72**) Fully Characterized in Solid State and in Solution.<sup>58,78b,104-107</sup>



**Scheme 16.** The Reaction of (**70**) and One Equivalent of LLA at Ambient Temperature Affords Complex (**71**).<sup>58</sup>

In 2010, Phomphrai *et al.*<sup>108</sup> prepared the Al(III) (*S,S*) isopropyl lactidate diamino-bis(phenolate) complex **73** (Figure 32) by two different routes: (a) a reaction between  $\text{L}^2\text{Al-OiPr}$  and 1 equiv of L-LA at  $70^\circ\text{C}$ , (b) treatment of isopropyl lactyllactate with  $\text{L}^2\text{Al-Me}$ , resulting in the product **73** as observed by  $^1\text{H}$  NMR in both cases. Furthermore, a reaction between  $\text{L}^2\text{Al-OiPr}$  and 1.5 equiv of L-LA at  $70^\circ\text{C}$  gave the ring-opened product along with



the unreacted LA. Then, they concluded that the initiation of the first LA insertion of complex  $L^2Al-OiPr$  is much faster than the subsequent propagation.

In 2012, Carpentier *et al.*<sup>66</sup> prepared aluminum dilactate imino-phenoxy complexes **74a–b** (Figure 32). The  $^1H$  NMR spectra of  $\{ON^{Bn}\}Al(iPr (S)\text{-lactate})_2$  (**74a**) and  $\{ON^{pipeBn}\}Al(iPr (S)\text{-lactate})_2$  (**74b**) in benzene- $d_6$  at room temperature are similar. The observation of a series of sharp resonances in both cases is consistent with the existence of single monomeric species in solution. In particular, the methyl phenoxy hydrogens come out as singlets ( $\delta$  1.8 and 1.95 ppm, respectively). In compounds **74a–b**, the two lactate moieties are magnetically inequivalent, as indicated by a series of six doublets, assigned to the methyl groups and two heptets and two quartets for the methine hydrogens of the *iPr* and lactate moieties, respectively. These observations suggested that the lactate moieties are each simply  $\kappa^1$ -O-coordinated to the Al center, as expected for usual four-coordinate Al complexes.

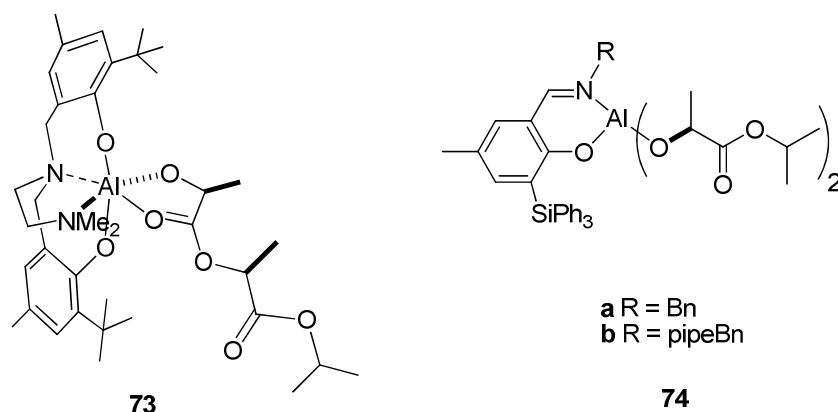
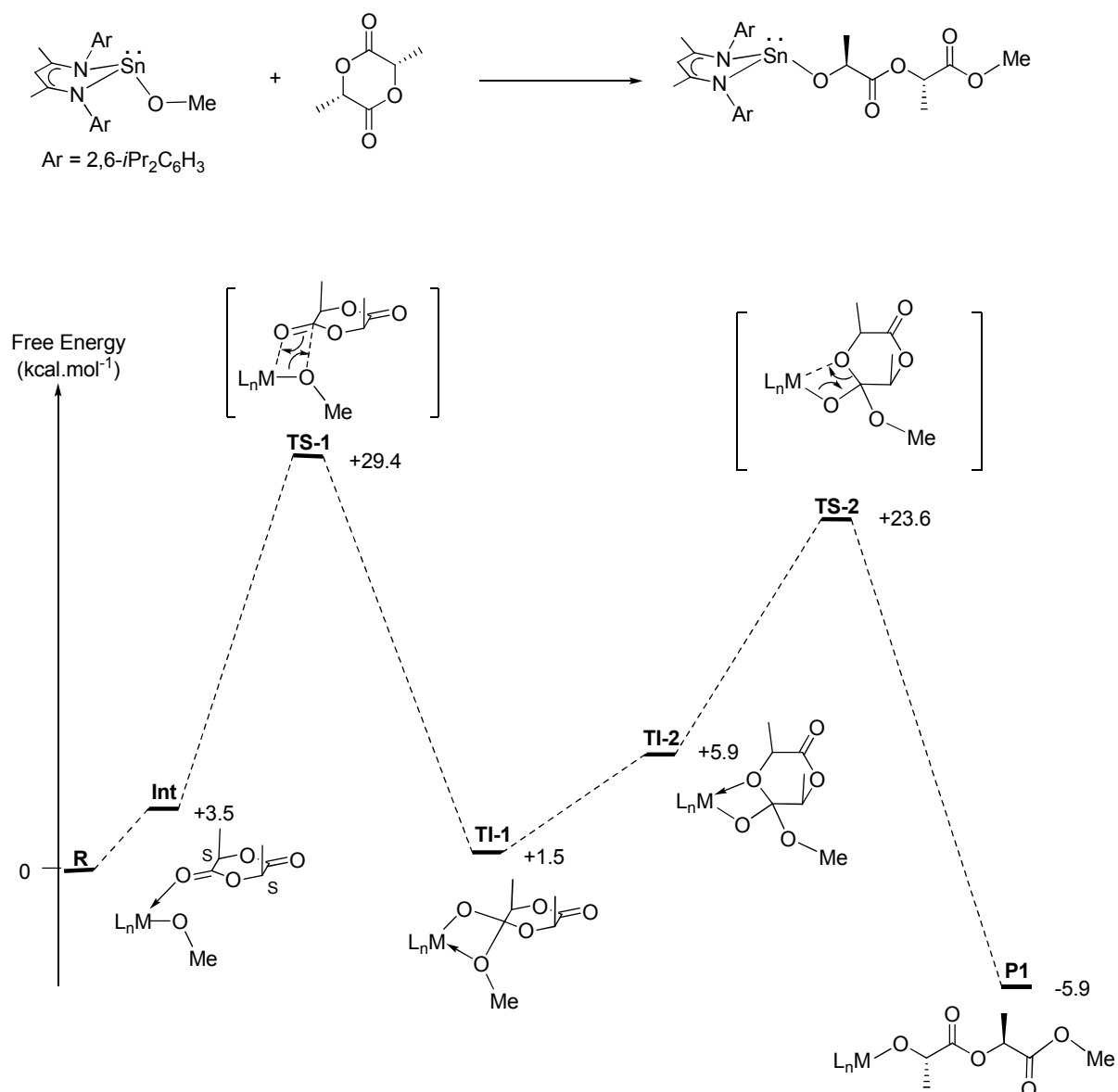


**Figure 32.** Aluminum Lactidate and Dilactate Complexes (**73-74**).<sup>66,108</sup>

The ROP of *rac*-LA was investigated also by theoretical methods. Rzepa, Gibson *et al.*<sup>106,109</sup> reported the studies of the ROP at the  $\beta$ -diketiminate magnesium and tin centers to understand the elementary steps as well as the mechanism of heterotactic stereocontrol of this species in the polymerization of *rac*-LA. Scheme 17 depicts the free energy levels implied in the ring-opening of the first monomer unit insertion and the schematic representation of stationary points, and also two transition states **TS-1** and **TS-2**. In these computations, the

coordination of the monomer to the metal site is strongly affected by the geometric constraints imposed by the tin lone pair and binds weakly to a site *trans* to a nitrogen donor of the BDI ligand (**Int**). Then, the first transition state (**TS-1**) can be described as a four-membered cycle of the metal-alkoxide bond and the C=O carbonyl bond. The tetrahedral intermediate thus generated (**TI-1**) exhibits a Sn $\cdots$ OMe interaction of 3.23 Å (distance comparable to the long Sn $\cdots$ O<sub>carbonyl</sub> interaction the group observed in the solid state of the complex). The rotation around the O<sub>alkoxide</sub>-C vector next affords **TI-2**, which reduces the Sn $\cdots$ OMe bond length (2.93 Å). Cleavage of the six-membered heterocycle then would occur on passing through the four-membered cyclic transition state **TS-2**. Extrusion of the PLA chain from the tin coordination sphere would occur by dissociation of the carbonyl donor interaction and migration of the Sn-alkoxide bond to a resting coordination site similar to the starting complex, to produce **P1** containing a five-membered Sn-lactate, with a long Sn $\cdots$ O<sub>carbonyl</sub> interaction of 2.88 Å.



**Scheme 17.** Free energy changes along the reaction for the first insertion of a monomer unit.<sup>106,109</sup>

In 2012, Jones *et al.*<sup>110</sup> investigated by DFT calculations the influence of the steric shielding of the aluminum center for two aluminum-salalen complexes (**14a** and **14c**, Figure 12). The motivation for this study was that, experimentally, complex **14c** produces heterotactic PLA, while **14a** leads to an isotactic bias (*vide supra*). The actual initiating moiety for the polymerization with **14a,c** is believed to be the –OCH<sub>2</sub>Ph residue (produced from *in situ* alcoholysis). Then, the model complexes were designed by substitution of the Me groups attached to the Al with a OBn residue. The computations suggested that the

polymerization proceeds through a chain-end control mechanism: the experimentally observed polymer tacticities could be confirmed theoretically by comparing calculated activation enthalpies with different sequences of consecutive D- and L-LA insertion. The subtle difference of having a second *t*Bu in the active center of **14a** steers the tacticity of the growing chain towards isotactic enrichment by dissecting the incoming LAs for their “fit” into the reaction chamber. So far, it could be proved theoretically that the *ortho* substituent of the ligand is extremely critical for the positioning of the new incoming LA.

In 2013, Maron *et al.*<sup>111</sup> described detailed theoretical studies involving initiating/propagating steps for the *rac*-BBL ROP initiated by a highly syndiospecific mononuclear (salan)Y(OiPr) (**75**) (Figure 33). Their aim was to obtain a greater understanding of the complexity associated with metal-alkoxide mediated ROP, as well as to address the stereoselectivity exhibited by the salan metal systems (*vide supra* for salan Al-catalyzed ROP of *rac*-LA). Furthermore, this salanY(OiPr) afforded highly alternating PHAs (up to 94% alternation) as reported by Coates *et al.*, in 2009.<sup>18</sup>

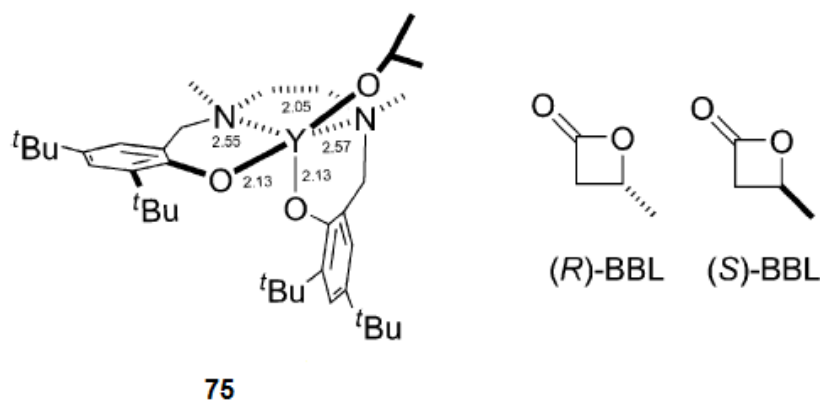
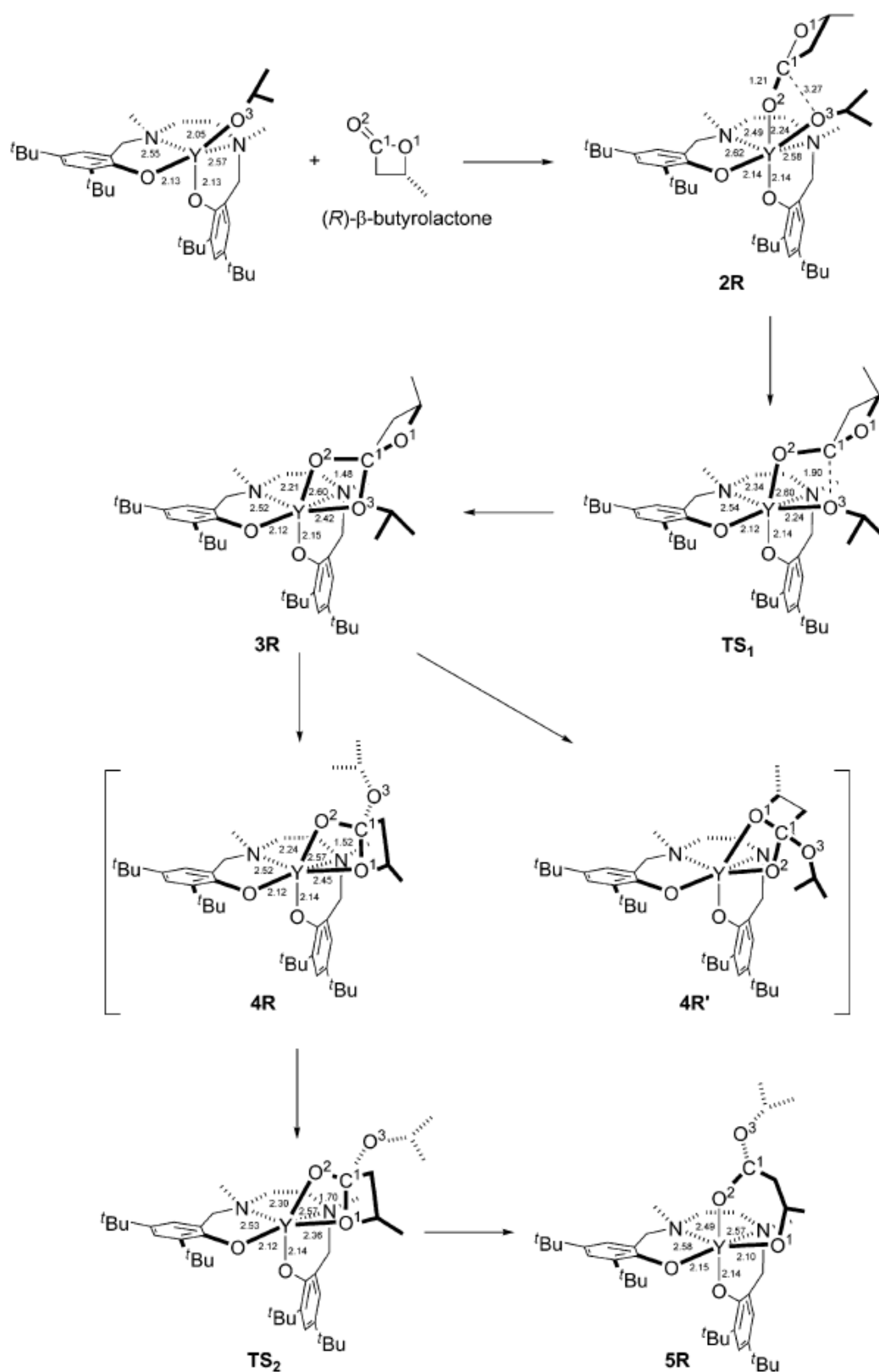


**Figure 33.** Complex (**75**) and Monomer Involved.<sup>18,111</sup>

The reaction sequence together with the corresponding optimized structures of the first insertion is depicted in Scheme 18 (using (*R*)-BBL, as example). The free energy pathways for both (*R*)- and (*S*)-BBL have thus been determined (Figure 34).



**Scheme 18.** Schematic Representation of the First Step of the ROP Mechanism of *(R)*-β-Butyrolactone by an Y-Salan Alkoxide Initiator (**75**) Computed at the DFT level.<sup>111</sup> Bond Lengths are Given in Angstroms.

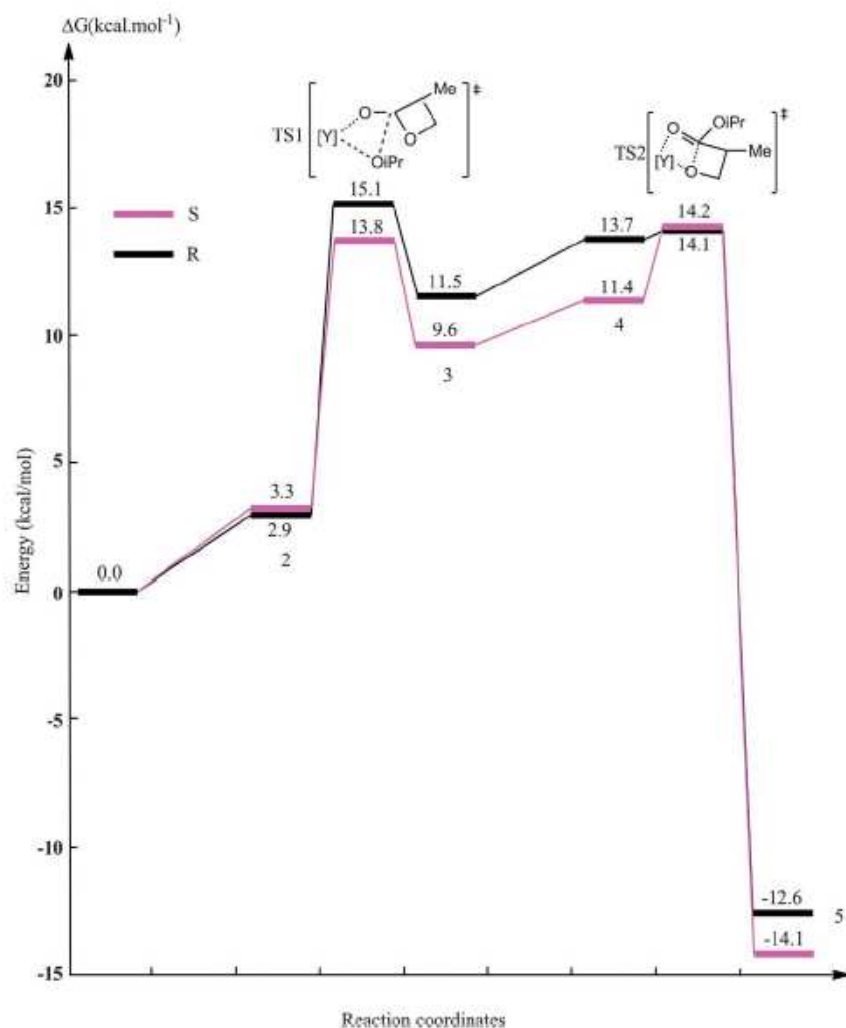


**Figure 34.** Free Energy Profile for the Initiation Step of the ROP of  $\beta$ -Butyrolactone Catalyzed by the Yttrium Complex (**75**).<sup>111</sup>

The reaction begins with the coordination of the *exo*-carbonyl group of (*R*)-BBL to the yttrium center. The formation of the adduct (**2R**) is marginally endergonic (2.9 kcal mol<sup>-1</sup>), indicating a strong interaction between BBL and the yttrium complex as the loss of entropy is almost fully compensated. The yttrium metal centre thus becomes six-coordinated. The transformation of **2R** into **3R** occurs through **TS1** and involves the addition of the Y–O<sup>3</sup> onto the C<sup>1</sup>–O<sup>2</sup> double bond and formation of a planar four-member ring (nucleophilic addition). The reaction requires low activation energy (15.1 kcal mol<sup>-1</sup> with respect to the entrance channel). The conversion of **3R** to **4R** involves the rotation of the four-member ring of the BBL around the C<sup>1</sup>–O<sup>2</sup> bond resulting in the replacement of the Y–O<sup>3</sup> bond by the Y–O<sup>1</sup> one

(Scheme 18). Two isomers **4R** and **4R'** can be generated when the BBL ring rotates either left or right. From these two isomers, the ring opening occurs and involves the transition state (**TS2**) with the formation of a  $sp^3$  hybridized  $C^1$  atom. In this process, the transition state arising from **4R** ( $0.4 \text{ kcal mol}^{-1}$  with respect to **4R** and  $14.2 \text{ kcal mol}^{-1}$  with respect to the entrance channel) is lower in energy than that coming from **4R'**. The coordination of  $O^1$  and  $O^2$  to Y remains in **5R** and is favourable by  $12.6 \text{ kcal mol}^{-1}$  with respect to the entrance channel (Figure 34). (*S*)-BBL reacted with the yttrium complex in a similar way. The only difference is that (*S*)-BBL simply rotates in the opposite direction (with respect to (*R*)-BBL) before **TS2** to reach a more stable transition state by reducing the steric constraint. The product (**5S**) keeps the coordination of  $O^1$  and  $O^2$  with Y. Thus, as anticipated, (*R*)-BBL and (*S*)-BBL can both initiate the ROP with a similar efficiency.

The second step of the reaction appeared slightly more complicated than the first one since either (*R*)-BBL or (*S*)-BBL can react with the two products (**5R** and **5S**) of the first step. Moreover, the second insertion can occur either from the front-side or from the back-side with respect to the plane defined by  $O^4$ , Y and  $O^3$  (**5R**, Scheme 18). Therefore, the four possible associations of monomers (*RR*, *RS*, *SR* and *SS*) for both front-side and back-side processes were computed. Overall, the authors concluded that the syndiotactic polymer chain is preferred over the isotactic one whatever the nature of the first inserted monomer. The mechanism for the syndiotactic polymer formation can occur either from a front-side or from a back-side insertion and is controlled both kinetically and thermodynamically. The latter is associated with formation of a six-membered Y-alkoxybutyrate ring rather than an eight-member ring.

## CHAPTER 2. OBJECTIVES

A first aim of this work was to prepare a series of well-defined Al- and Y- complexes supported by tridentate pyridine–bis(phenolate) and –bis(naphtholate) ligands and evaluate their reactivity and selectivity toward *rac*-lactide and *rac*- $\beta$ -butyrolactone. Our objectives were to reach eventually high activities combined with high stereoselectivities, and to further document –with raw catalytic data- which factors control those properties; this shall be made in light of previous catalytic and DFT studies which have, in particular, revealed the key role of substituents placed on phenolate rings, with yet unclear stereo-electronic effects in the ROP of *rac*- $\beta$ -butyrolactone.

A second main aim of this work was to prepare, isolate and characterize well-defined Al- and Y- $\{\alpha$ - or  $\beta$ - alkoxy esters} derivatives in order to get better insights about the complexity of the ring-opening polymerization mechanism, especially for the stereocontrolled polymerization. The latter  $\alpha$ - or  $\beta$ - alkoxy ester units have been selected to mimic the last monomer unit inserted in the growing polymer chain in the ROP of lactide and  $\beta$ -butyrolactone. Virtually no examples of intermediates involved in the ROP of  $\beta$ -butyrolactone are actually known.



### 3. EXPERIMENTAL

#### 3.1 GENERAL PROCEDURES

All manipulations were performed under a purified argon atmosphere using standard Schlenk techniques or in a glove box. Solvents were distilled from Na/benzophenone (THF, Et<sub>2</sub>O) and Na/K alloy (toluene, pentane, hexane) under argon, degassed thoroughly and stored under argon prior to use. Deuterated solvents (benzene-*d*<sub>6</sub>, toluene-*d*<sub>8</sub>; >99.5% D, Eurisotop) were vacuum-transferred from Na/K alloy (or from CaH<sub>2</sub> for CD<sub>2</sub>Cl<sub>2</sub>) into storage tubes. Pyridine-*d*<sub>5</sub> was stored under argon and kept over activated 4 Å molecular sieves. Benzyl and isopropyl alcohols (Acros) were distilled over Mg turnings under argon atmosphere and kept over activated 4 Å molecular sieves. 4-Methyl-2-(2-phenylpropan-2-yl)phenol,<sup>112</sup> bis(naphthol) pro-ligands {ONO<sup>SiR<sub>3</sub></sup>}H<sub>2</sub><sup>113</sup> and Y(N(SiHMe<sub>2</sub>)<sub>2</sub>)<sub>3</sub>.THF<sup>114</sup> were prepared using reported procedures. *rac*-Lactide (*rac*-LA) was received from Acros, and L-lactide (L-LA) and D-lactide (D-LA) were kindly provided by Total Petrochemicals. Purification of *rac*-LA, L-LA or D-LA required a three step procedure involving first a recrystallization from a hot, concentrated *i*PrOH solution (80 °C), followed by two subsequent recrystallizations in hot toluene (100 °C). After purification, *rac*-LA was stored at a temperature of –30 °C in the glovebox. Racemic β-butyrolactone (Aldrich) was freshly distilled from CaH<sub>2</sub> under nitrogen and degassed thoroughly by freeze-vacuum-thaw cycles prior to use. Other starting materials were purchased from Acros, Strem, Aldrich and Alpha Aesar and used as received.

NMR spectra of complexes were recorded on Bruker AC-300, Avance DRX 400 and AM-500 spectrometers in Teflon-valved NMR tubes at 25 °C unless otherwise indicated. <sup>1</sup>H and <sup>13</sup>C chemical shifts are reported in ppm vs. SiMe<sub>4</sub> and were determined by reference to the residual solvent peaks. Assignment of resonances for complexes was made from 2D <sup>1</sup>H–<sup>13</sup>C HMQC and HMBC NMR experiments. Coupling constants are given in hertz. <sup>19</sup>F NMR chemical shifts were determined by external reference to an aqueous solution of NaBF<sub>4</sub>.

Elemental analyses (C, H, N) were performed using a Flash EA1112 CHNS Thermo Electron apparatus and are the average of two independent determinations.

The X-ray diffraction analyses were performed by Dr. Thierry Roisnel at the University of Rennes. Suitable single-crystals were mounted onto a glass fiber using the “oil-drop” method. Diffraction data were collected at 100 K using an APEXII Bruker-AXS diffractometer with graphite-monochromatized Mo K $\alpha$  radiation ( $k = 0.71073 \text{ \AA}$ ). A combination of  $\omega$ - and  $\phi$ -scans was carried out to obtain at least a unique data set. The structure was solved by direct methods using the SIR97 program,<sup>115</sup> and then refined with full-matrix least-square methods based on  $F^2$  (SHELX-97)<sup>116</sup> with the aid of the WINGX program.<sup>117</sup> Many hydrogen atoms could be found from the Fourier difference analysis. Other hydrogen atoms were placed at calculated positions and forced to ride on the attached atom. The hydrogen atom contributions were calculated but not refined. All non-hydrogen atoms were refined with anisotropic displacement parameters. The locations of the largest peaks in the final difference Fourier map calculation as well as the magnitude of the residual electron densities were of no chemical significance. Crystal data and details of data collection and structure refinement for the different compounds are given in Table 1A (*See the Annexes*).

## 3.2 PRO-LIGAND SYNTHESIS

**3.2.1 1-(Methoxymethyl)-4-methyl-2-(2-phenylpropan-2-yl)benzene:** To a suspension of NaH (3.20 g, 133.34 mmol) in DMF (100 mL), under argon flow, was added dropwise a solution of 4-Methyl-2-(2-phenylpropan-2-yl)phenol (20.0 g, 88.37 mmol) in DMF (100 mL) at 0 °C. After stirring for 4 h at room temperature, methoxymethyl chloride (13.64 g, 141.33 mmol) was added slowly, and the reaction mixture was stirred for 18 h. The reaction mixture was carefully diluted with water (ca. 1 L). And organic materials were extracted with CH<sub>2</sub>Cl<sub>2</sub> (3  $\times$  100 mL). The combined organic extracts were washed with water (2  $\times$  500 mL) and

brine, and dried over  $\text{MgSO}_4$ . The solution was evaporated to dryness at  $80\text{ }^\circ\text{C}$  to give a colorless oily product (21.0 g, 77.67 mmol, 88%), which was used without further purification.  $^1\text{H}$  NMR (300 MHz,  $\text{CDCl}_3$ , 298 K):  $\delta$  7.34 (s, 1H, Haro), 7.22 (br s, 4H, Haro), 7.13-6.91 (m, 3H, Haro), 4.56 (s, 2H,  $\text{OCH}_2\text{OCH}_3$ ), 3.00 (s, 3H,  $\text{OCH}_2\text{OCH}_3$ ), 2.40 (s, 3H,  $\text{CH}_3$ ), 1.72 (s, 6H,  $\text{CH}_3$ ).

**3.2.2 {ONO<sup>Me,Cumyl</sup>}H<sub>2</sub> (**1c**):** A solution of *sec*-BuLi (30.0 mL of a 1.3 M solution in hexane, 39.0 mmol) was added dropwise over 20 min to a stirred solution of 1-(methoxymethyl)-4-methyl-2-(2-phenylpropan-2-yl)benzene (9.50 g, 35.1 mmol) in THF (100 mL) at  $-78\text{ }^\circ\text{C}$ . After stirring overnight at room temperature, a dark solution was obtained to which was added a solution of  $\text{ZnCl}_2$  (4.79 g, 35.1 mmol) in THF (*ca.* 30 mL) at  $-78\text{ }^\circ\text{C}$  over 30 min. Then the resulting solution was gently warmed up to room temperature. To the resulting organozinc solution, a suspension of  $\text{Pd}_2(\text{dba})_3$  (0.16 g, 0.35 mmol), S-Phos (0.326 g, 0.70 mmol) and 2,6-dibromopyridine (4.16 g, 17.6 mmol) was added. The reaction mixture was stirred for 72 h at  $64\text{ }^\circ\text{C}$ , then cooled to room temperature, diluted with water (200 mL), and finally extracted with  $\text{CH}_2\text{Cl}_2$  ( $3 \times 50\text{ mL}$ ). After evaporation to dryness, the crude material was recrystallized in ethyl acetate to give a white powder (7.00 g, 65%). The resulting solid was dissolved in a mixture of 36% aq. HCl (20 mL),  $\text{CHCl}_3$  (30 mL), and EtOH (40 mL), and the solution was refluxed for 24 h. The reaction mixture was cooled to  $0\text{ }^\circ\text{C}$  and carefully reacted with a concentrated solution of NaOH (30 mL). Then, a concentrated solution of  $\text{NH}_4\text{Cl}$  was added to adjust the pH value to 7–8. The product was extracted with  $\text{CH}_2\text{Cl}_2$  ( $3 \times 20\text{ mL}$ ), and the combined organic extracts were dried over  $\text{MgSO}_4$  and finally evaporated to afford **1c** as a white solid (5.8 g, 97%).  $^1\text{H}$  NMR (500 MHz,  $\text{CDCl}_3$ , 298 K):  $\delta$  9.80 (br s, 2H, OH), 7.82 (t,  $^3J = 7.8\text{ Hz}$ , 1H), 7.55 (d,  $^3J = 7.65\text{ Hz}$ , 2H), 7.38–7.22 (m, 14H), 2.44 (s, 6H,  $\text{CH}_3$ ), 1.78 (s, 12H,  $\text{CH}_3$ ).  $^{13}\text{C}\{^1\text{H}\}$  NMR (125 MHz,  $\text{CDCl}_3$ , 298 K):  $\delta$  156.5, 152.5, 150.7,

139.0, 137.2, 129.7, 128.0, 127.9, 127.1, 125.7, 125.4, 122.4, 120.1 ( $C_{\text{aro}}$ ), 42.3 ( $C(\text{CH}_3)_2$ ), 29.8 ( $C(\text{CH}_3)_2$ ), 21.2 ( $\text{CH}_3$ ).

### 3.3 COMPLEXES SYNTHESIS

**Preparation of Aluminum Complexes Bearing Ortho-Substituted Tridentate 2,6-Bis(naphtholate)Pyridine  $\{\text{ONO}^{\text{SiR}_3}\}_2$  where  $\text{SiR}_3 = \text{SiPh}_3$  or  $\text{Si}^i\text{BuMe}_2$  and 2,6-Bis(phenolate)Pyridine  $\{\text{ONO}^{\text{Me,Cumyl}}\}_2$  pro-ligands.**

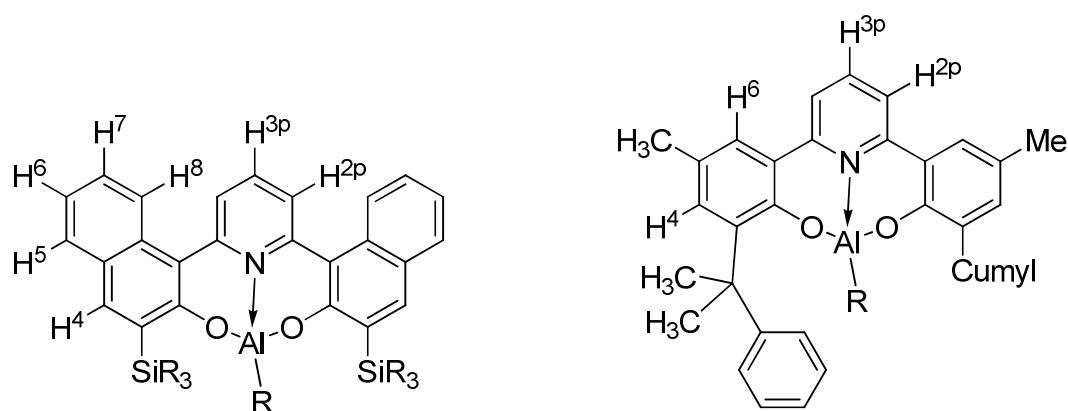


**Figure 35.** Numbering scheme of 1,1-bis(naphtholate)-1',1'pyridine ligand (left) and 1,1-bis(phenolate)-1',1'pyridine ligand (right).

**3.3.1  $\{\text{ONO}^{\text{SiPh}_3}\}_2\text{AlMe}$  (**2a**):** A solution of  $\text{AlMe}_3$  (1.4 equiv., 0.80 mL of a 1.0 M solution in heptane, 0.80 mmol) was added slowly to a clear solution of  $\{\text{ONO}^{\text{SiPh}_3}\}_2$  (0.500 g, 0.57 mmol) in toluene (ca. 10 mL) at room temperature. The reaction mixture was warmed to 80 °C and stirred overnight. After cooling to ambient temperature, the volatiles were removed in vacuo, and the crude product washed with *n*-hexane (ca. 15 mL) to give, after drying, **2a** as a yellow solid (0.420 g, 80%).  $^1\text{H}$  NMR (500 MHz, benzene- $d_6$ , 298K):  $\delta$  8.22 (s,  $2\text{H}^4$ , Haro), 7.88–7.86 (m, 14H, Haro+ $\text{H}^8$ ), 7.34–7.32 (m, 2H,  $\text{H}^5$ ), 7.23–7.10 (m, 18H, Haro), 7.06–7.00 (m, 6H, Haro), 6.66 (t,  $^3J = 8.1$  Hz, 1H,  $\text{H}^{3p}$ ), –1.26 (s, 3H,  $\text{CH}_3$ ).  $^{13}\text{C}\{^1\text{H}\}$  NMR (125 MHz,

benzene-*d*<sub>6</sub>, 298 K):  $\delta$  162.3 (C-O), 153.9 (C-N), 144.8 (C<sup>4</sup>), 139.2 (C<sup>3p</sup>), 137.1 (Cortho), 135.2, 134.3, 130.4, 130.1, 129.7, 129.6, 127.5, 125.8, 123.45, 123.4, 115.2 (Caro). Anal. calcd. for C<sub>62</sub>H<sub>46</sub>AlNO<sub>2</sub>Si<sub>2</sub>: C, 79.73; H, 5.04; N, 1.52. Found: C, 79.62; H, 5.16; N, 1.34.

**3.3.2 {ONO<sup>SiMe<sub>2</sub>tBu</sup>}AlMe (2b):** This product was prepared as described above for **2a** starting from {ONO<sup>SiMe<sub>2</sub>tBu</sup>}H<sub>2</sub> (0.500 g, 0.85 mmol) and AlMe<sub>3</sub> (1.4 equiv., 1.20 mL of a 1.0 M solution in heptane, 1.20 mmol) in toluene (10 mL) to give **2b** as a yellow solid (0.336 g, 0.53 mmol, 63 %). <sup>1</sup>H NMR (500 MHz, benzene-*d*<sub>6</sub>, 298 K):  $\delta$  8.12 (s, 2H<sup>4</sup>, Haro), 7.91 (d, <sup>3</sup>J = 8.4 Hz, 2H<sup>5</sup>, Haro), 7.66 (d, <sup>3</sup>J = 8.4 Hz, 2H<sup>8</sup>, Haro), 7.29–7.25 (m, 2H<sup>7</sup>, Haro), 7.21–7.16 (m, 2H<sup>6</sup> + 2H<sup>2p</sup>, Haro), 6.76 (t, <sup>3</sup>J = 8.1 Hz, 1H, H<sup>3p</sup>), 1.23 (s, 18H, *t*Bu), 0.61 (s, 6H, Me), 0.56 (s, 6H, Me), –0.50 (s, 3H, Al-*Me*). <sup>13</sup>C{<sup>1</sup>H} NMR (125 MHz, benzene-*d*<sub>6</sub>, 298 K):  $\delta$  162.1 (C-O), 154.4 (C-N), 142.4 (C<sup>4</sup>), 139.4 (C<sup>3p</sup>), 133.8 and 133.5 (Caro), 129.8 and 129.7 (C<sup>8</sup>), 128.4, 127.8, 125.8 (C<sup>2p</sup>), 123.45 and 123.4 (C<sup>5</sup>), 115.0 (Caro), 28.0 (SiC(CH<sub>3</sub>)<sub>3</sub>), 17.9 (SiC(CH<sub>3</sub>)<sub>3</sub>), –3.64 and –4.20 (SiMe<sub>2</sub>), –15.5 (Al-*Me*). Anal. calcd. for C<sub>38</sub>H<sub>46</sub>AlNO<sub>2</sub>Si<sub>2</sub>: C, 72.22; H, 7.34; N, 2.22. Found: C, 72.31; H, 7.28; N, 2.16.

**3.3.3 {ONO<sup>SiPh<sub>3</sub></sup>}Al<sup>*i*</sup>Bu (2c):** This product was prepared as described above for **2a** starting from {ONO<sup>SiPh<sub>3</sub></sup>}H<sub>2</sub> (0.500 g, 0.57 mmol) and Al<sup>*i*</sup>Bu<sub>3</sub> (1.2 equiv., 0.62 mL of a 1.1 M solution in toluene, 0.68 mmol) to give **2c** as a yellow solid (0.439 g, 80 %). <sup>1</sup>H NMR (500 MHz, C<sub>6</sub>D<sub>6</sub>, 298 K):  $\delta$  8.24 (s, 2H<sup>4</sup>, Haro), 7.91–7.89 (m, 14H, Haro), 7.33–7.31 (m, 2H, Haro), 7.23–7.19 (m, 8H, Haro), 7.14–7.11 (m, 14H, Haro), 7.05–7.01 (m, 2H, Haro), 6.67 (t, <sup>3</sup>J = 8.1 Hz, 1H, H<sup>3p</sup>), 1.15 (m, <sup>3</sup>J = 6.5 Hz, 1H, AlCH<sub>2</sub>CH(CH<sub>3</sub>)<sub>2</sub>), 0.47 (d, <sup>3</sup>J = 6.5 Hz, 1H, AlCH<sub>2</sub>CH(CH<sub>3</sub>)<sub>2</sub>), –0.69 (d, <sup>3</sup>J = 7.0 Hz, 1H, AlCH<sub>2</sub>CH(CH<sub>3</sub>)<sub>2</sub>). <sup>13</sup>C{<sup>1</sup>H} NMR (125 MHz, C<sub>6</sub>D<sub>6</sub>, 298 K):  $\delta$  162.6 (C-O), 153.8 (C-N), 144.8 (C<sup>4</sup>), 139.3, 137.2, 136.9, 135.2, 134.3, 130.2, 130.1, 129.6, 129.4, 125.8, 123.4, 123.2, 115.3, 27.6, 25.4.

**3.3.4 {ONO<sup>Me,Cumyl</sup>}AlMe (2d):** This product was prepared as described above for **2a**, starting from {ONO<sup>Me,Cumyl</sup>}H<sub>2</sub> (**1c**, 0.300 g, 0.57 mmol) and AlMe<sub>3</sub> (1.4 equiv., 0.80 mL of a 1.0 M solution in heptane, 0.80 mmol). When the solution was cooled down to room temperature, a pale yellow microcrystalline solid was obtained. Then solvents were removed by filtration, and the resulting product **2d** washed with cold *n*-hexane and dried under vacuum (0.248 g, 77%). <sup>1</sup>H NMR (500 MHz, CD<sub>2</sub>Cl<sub>2</sub>, 298 K): δ 7.89 (t, <sup>3</sup>J = 8.1 Hz, 1H, H<sup>3p</sup>), 7.54 (d, <sup>3</sup>J = 8.1 Hz, 2H, H<sup>2p</sup>), 7.46 (s, 2H, H<sup>4</sup>), 7.32 (s, 2H, H<sup>6</sup>), 7.24 (m, 8H, H *o*- + *m*-cumyl), 7.14 (m, 2H, H *p*-cumyl), 2.39 (s, 6H, CH<sub>3</sub> aryl), 1.70 (s, 6H, CH<sub>3</sub> cumyl), 1.65 (s, 6H, CH<sub>3</sub> cumyl), -1.87 (s, 3H, Al-CH<sub>3</sub>). <sup>13</sup>C{<sup>1</sup>H} NMR (125 MHz, CD<sub>2</sub>Cl<sub>2</sub>, 298 K): δ 155.1 (C-O), 154.9 (C-N), 151.4, 141.9, 141.7, 131.8, 128, 127.7, 127.5, 126.1, 125.2, 122.6, 121.6 (C<sub>aro</sub>), 42.4 (C(CH<sub>3</sub>)<sub>2</sub>), 30.5 (C(CH<sub>3</sub>)<sub>2</sub>), 28.5 (C(CH<sub>3</sub>)<sub>2</sub>), 21.2 (CH<sub>3</sub>), -17.3 (Al-CH<sub>3</sub>). Anal. calcd. for C<sub>38</sub>H<sub>38</sub>AlNO<sub>2</sub>: C, 80.40; H, 6.75; N, 2.47. Found: C, 80.34; H, 6.8; N, 2.19.

**3.3.5 NMR-scale generation of {ONO<sup>SiPh<sub>3</sub></sup>}AlO<sup>*i*</sup>Pr (3a):** A J-Young NMR tube was charged with {ONO<sup>SiPh<sub>3</sub></sup>}AlMe (0.045 g, 0.049 mmol). Toluene-*d*<sub>8</sub> *ca.* (0.65 mL) was added in, and the tube was shaken. Then, via a microsyringe, <sup>*i*</sup>PrOH (5.0 μL, 65.3 μmol) was added into the solution. The tube was shaken and allowed to react at 80 °C for 18 h for completion. <sup>1</sup>H NMR spectroscopy revealed the release of methane gas and full conversion of the reagents to give the desired product **3a**. <sup>1</sup>H NMR (500 MHz, toluene-*d*<sub>8</sub>, 298 K): δ 8.05 (s, 2H, H<sup>4</sup>), 7.91 (d, <sup>3</sup>J = 8.5 Hz, 2H, H<sup>8</sup>), 7.85–7.83 (m, 12H, Haro), 7.29 (d, <sup>3</sup>J = 8.1 Hz, 2H, H<sup>5</sup>), 7.22–7.13 (m, 24H, Haro), 6.81 (t, <sup>3</sup>J = 7.8 Hz, 1H, H<sup>3p</sup>), 3.55 (m, 1H, OCHMe<sub>2</sub>), 0.59 (d, <sup>3</sup>J = 5.0 Hz, 6H, OCHMe<sub>2</sub>). <sup>13</sup>C{<sup>1</sup>H} NMR (125 MHz, toluene-*d*<sub>8</sub>, 298 K): δ 163.1 (C-O), 144.9, 137.8, 137.5, 137.2, 135.5, 134.3, 129.9, 129.6, 129.4, 128.3, 128.0, 127.8, 125.6, 123.3, 123.2 (Caro), 63.9

(OCHMe<sub>2</sub>), 27.6 (OCHMe<sub>2</sub>). Anal. calcd. for C<sub>64</sub>H<sub>50</sub>AlNO<sub>3</sub>Si<sub>2</sub>: C, 79.72; H, 5.23; N, 1.45. Found: C, 82.18; H, 4.85; N, 1.28.

**3.3.6 {ONO<sup>SiPh<sub>3</sub></sup>}Al(*i*Pr (*S*)-lactate) (4a):** Toluene (*ca.* 5 mL) was vacuum-condensed in a Schlenk flask containing {ONO<sup>SiPh<sub>3</sub></sup>}AlMe (0.354 g, 0.385 mmol). Then, via a microsyringe, isopropyl (*S*)-lactate (52  $\mu$ L, 0.390 mmol) was added into the solution. The reaction mixture was warmed to 80 °C and stirred for 18 h. After cooling to ambient temperature, the volatiles were removed in vacuo, and the crude product washed with *n*-hexane (*ca.* 15 mL) and dried *in vacuo* to give **4a** as a yellow solid (0.345 g, 86 %). <sup>1</sup>H NMR (500 MHz, toluene-*d*<sub>8</sub>, 298 K):  $\delta$  8.08 (d, <sup>3</sup>*J* = 8.5 Hz, 1H, H<sup>8</sup>), 8.03 (s, 1H, H<sup>4</sup>), 7.99 (d, <sup>3</sup>*J* = 8.5 Hz, 1H, H<sup>8'</sup>), 7.92 (s, 1H, H<sup>4</sup>), 7.76–7.74 (m, 12H, Haro), 7.40 (dd, <sup>3</sup>*J* = 8.0 Hz and <sup>4</sup>*J* = 0.8 Hz, 1H, H<sup>2p</sup>), 7.31 (br d, <sup>3</sup>*J* = 7.8 Hz, 1H, H<sup>5</sup>), 7.30 (br d, <sup>3</sup>*J* = 7.5 Hz, 1H, H<sup>5'</sup>), 7.26 (dd, <sup>3</sup>*J* = 8.0 and <sup>4</sup>*J* = 0.8 Hz, 1H, H<sup>2p</sup>), 7.20–6.96 (m, 22H, Haro), 6.86 (t, <sup>3</sup>*J* = 8.0 Hz, 1H, H<sup>3p</sup>), 4.01 (q, <sup>3</sup>*J* = 6.9 Hz, 1H, (OCH(CH<sub>3</sub>))), 3.17 (sept, <sup>3</sup>*J* = 6.2 Hz, 1H, (C(O)OCHMe<sub>2</sub>)), 0.79 (d, <sup>3</sup>*J* = 6.9 Hz, 3H, (OCH(CH<sub>3</sub>))), 0.41 (d, <sup>3</sup>*J* = 6.2 Hz, 3H, (C(O)OCHMe<sub>2</sub>)), 0.29 (d, <sup>3</sup>*J* = 6.2 Hz, 3H, (C(O)OCHMe<sub>2</sub>)). <sup>13</sup>C{<sup>1</sup>H} NMR (125 MHz, toluene-*d*<sub>8</sub>, 298 K):  $\delta$  189.5 (COO), 164.1 (C-O), 164.0 (C-O), 154.9 (C-N), 154.7 (C-N), 144.9 (C<sup>4</sup>), 144.5 (C<sup>4</sup>), 137.8, 137.4, 137.2, 137.0, 136.9 (C<sup>3p</sup>), 136.3, 135.1, 134.7, 129.5, 129.4, 129.3, 129.2, 128.8, 128.5, 128.3, 128.0, 127.9, 127.6, 125.6, 125.5, 125.4, 124.5, 124.3, 122.8, 122.7, 115.6, 115.5 (Caro), 75.4 (COOCHMe<sub>2</sub>), 68.8 (OCH(CH<sub>3</sub>)), 21.7 (OCH(CH<sub>3</sub>)), 21.4 (COOCHMe<sub>2</sub>), 20.5 (COOCHMe<sub>2</sub>).

**3.3.7 {ONO<sup>SiMe<sub>2</sub>tBu</sup>}Al(*i*Pr (*S*)-lactate) (4b):** This product was prepared as described above for **4a** starting from {ONO<sup>SiMe<sub>2</sub>tBu</sup>}AlMe (0.176 g, 0.278 mmol) and isopropyl (*S*)-lactate (37.2  $\mu$ L, 0.279 mmol). The reaction mixture was stirred for 18 h at 25 °C. The volatiles were removed in vacuo, and the crude product washed with *n*-hexane (*ca.* 10 mL) and dried *in*

*vacuo* to give **4b** as a yellow solid (0.166 g, 85 %).  $^1\text{H}$  NMR (500 MHz, toluene- $d_8$ , 298 K):  $\delta$  8.08 (d,  $^3J = 8.7$  Hz, 1H, H<sup>8</sup>), 8.05 (s, 1H, H<sup>4</sup>), 8.04 (d, 1H, H<sup>8'</sup>), 8.02 (s, 1H, H<sup>4'</sup>), 7.64 (m, 2H, H<sup>5</sup>), 7.34 (dd,  $^3J = 8.0$  Hz and  $^4J = 1.0$  Hz, 1H, H<sup>2p</sup>), 7.31 (dd,  $^3J = 8.0$  Hz and  $^4J = 1.0$  Hz, 1H, H<sup>2p'</sup>), 7.26–7.22 (m, 2H, H<sup>7</sup>), 7.16–7.13 (m, 2H, H<sup>6</sup>), 6.79 (t,  $^3J = 8.0$  Hz, 1H, H<sup>3p</sup>), 5.52 (sept,  $^3J = 6.2$  Hz, 1H, (C(O)OCHMe<sub>2</sub>), 3.82 (q,  $^3J = 6.9$  Hz, 1H, (OCH(CH<sub>3</sub>))), 1.18 (two singlets overlapped, 18H, SiMe<sub>2</sub>tBu), 1.08–1.06 (two doublets overlapped,  $^3J = 5.9$  Hz, 6H, (OCH(CH<sub>3</sub>)<sub>2</sub>)), 0.67 (d,  $^3J = 6.9$  Hz, 3H, (OCH(CH<sub>3</sub>))), 0.64 (s, 3H, SiMeMetBu), 0.58 (s, 3H, SiMeMetBu), 0.54 (s, 3H, SiMe'MetBu), 0.54 (s, 3H, SiMeMe'tBu).  $^{13}\text{C}\{^1\text{H}\}$  NMR (125 MHz, toluene- $d_8$ , 298 K): 190.0 (COO), 164.1 (C-O), 164.0 (C-O), 154.6 (C-N), 140.7 (C<sup>4</sup>), 140.6 (C<sup>4'</sup>), 137.8, 136.9 (C<sup>3p</sup>), 134.5, 134.4, 132.0 (C<sup>3</sup> ipso), 131.8 (C<sup>3'</sup> ipso), 129.4, 129.3, 129.2, 128.5, 128.3, 127.1, 127.0, 125.6, 125.4, 125.0, 124.6 (C<sup>8</sup>), 124.5 (C<sup>8'</sup>), 122.6, 114.9 (C<sup>1</sup> ipso), 114.6 (C<sup>1'</sup> ipso), 73.8 (C(O)OCHMe<sub>2</sub>), 68.5 (OCH(CH<sub>3</sub>)), 28.1 (C(CH<sub>3</sub>)<sub>3</sub>), 28.05 (C(CH<sub>3</sub>)<sub>3</sub>), 22.0 (OCH(CH<sub>3</sub>)<sub>2</sub>), 21.9 (OCH(CH<sub>3</sub>)<sub>2</sub>), 21.6 (OCH(CH<sub>3</sub>)), 18.1 (C(CH<sub>3</sub>)<sub>3</sub>), 18.08 (C(CH<sub>3</sub>)<sub>3</sub>), -2.9 (SiMeMetBu), -2.93 (SiMeMetBu), -3.83 (SiMe'tBu). Anal. calcd. for C<sub>43</sub>H<sub>54</sub>AlNO<sub>5</sub>Si<sub>2</sub>: C, 69.04; H, 7.28; N, 1.87. Found: C, 68.93; H, 7.36; N, 1.66.

**3.3.8 {ONO<sup>Me,Cumyl</sup>}Al(*i*Pr (*S*)-lactate) (**4d**):** This product was prepared as described above for **4a** starting from {ONO<sup>Me,Cumyl</sup>}AlMe (**2d**, 0.114 g, 0.200 mmol) and isopropyl (*S*)-2-lactate (27  $\mu\text{L}$ , 0.202 mmol) to give **4d** as a pale yellow powder in quantitative yield (0.136 g, 99%).  $^1\text{H}$  NMR (500 MHz, toluene- $d_8$ , 298 K):  $\delta$  7.57 (m, 4H, H *o*-cumyl), 7.29 (m, 6H, H<sup>4</sup> + H *m*-cumyl), 7.09 (m, 2H, H *p*-cumyl), 6.95 (s, 1H, H<sup>6</sup>), 6.91 (s, 1H, H<sup>6'</sup>), 6.55 (t,  $^3J = 8.0$  Hz, 1H, H<sup>3p</sup>), 6.48 (d,  $^3J = 7.8$  Hz, 1H, H<sup>2p</sup>), 6.42 (d,  $^3J = 7.8$  Hz, 1H, H<sup>2p'</sup>), 5.37 (hept,  $^3J = 6.3$  Hz, 1H, C(O)OCH(CH<sub>3</sub>)<sub>2</sub>), 4.00 (q,  $^3J = 6.6$  Hz, 1H, OCH(CH<sub>3</sub>)), 2.24 (s, 3H, CH<sub>3</sub> aryl), 2.23 (s, 3H, CH<sub>3</sub> aryl), 2.00 (s, 3H, CH<sub>3</sub> cumyl), 1.99 (s, 3H, CH<sub>3</sub> cumyl), 1.83 (s, 3H, CH<sub>3</sub> cumyl), 1.82 (s, 3H, CH<sub>3</sub> cumyl), 1.12 (2d overlapped,  $^3J = 6.3$  Hz, 6H, C(O)OCH(CH<sub>3</sub>)<sub>2</sub>), 0.91 (d,  $^3J$



= 6.7 Hz, 3H, OCH(CH<sub>3</sub>)). <sup>13</sup>C{<sup>1</sup>H} NMR (125 MHz, toluene-*d*<sub>8</sub>, 298 K): δ 189.5 (COO), 157.3 (C<sub>aro</sub>), 157.2 (C<sub>aro</sub>), 154.5 (CN), 154.4 (C'N), 151.5 (CO), 151.4 (C'O), 140.0 (C<sub>aro</sub>), 139.8 (C<sub>aro</sub>), 139.6 (C<sup>3p</sup>), 130.7 (C<sup>4</sup>), 130.6 (C<sup>4'</sup>), 129.2 (C<sub>aro</sub>), 128.3 (C<sub>aro</sub>), 127.6 (C<sup>6</sup>), 127.4 (C<sup>6'</sup>), 126.9 (C<sub>aro</sub>), 126.8 (C<sub>aro</sub>), 122.9 (C<sub>aro</sub>), 122.8 (C<sub>aro</sub>), 120.8 (C<sup>2p</sup>), 120.6 (C<sup>2p'</sup>), 73.8 (C(O)OCHMe<sub>2</sub>), 68.8 (OCH(CH<sub>3</sub>)), 42.6 (C(CH<sub>3</sub>)<sub>2</sub>), 42.5 (C'(CH<sub>3</sub>)<sub>2</sub>), 32.4 (CH<sub>3</sub> cumyl), 32.3 (CH<sub>3</sub> cumyl), 27.6 (CH<sub>3</sub> cumyl), 27.5 (CH<sub>3</sub> cumyl), 21.8 (OCH(CH<sub>3</sub>), 21.6 (C(O)OCHMe<sub>2</sub>), 21.5 (C(O)OCHMe<sub>2</sub>), 21.2 (CH<sub>3</sub> aryl). Anal. calcd. for C<sub>43</sub>H<sub>46</sub>AlNO<sub>5</sub>: C, 75.53; H, 6.78; N, 2.05. Found: C, 75.37; H, 6.86; N, 1.85.

**3.3.9 {ONO<sup>SiPh<sub>3</sub></sup>}Al((*R*)-OCH(CH<sub>3</sub>)CH<sub>2</sub>COOMe) (5a):** This product was prepared as described above for **4a** starting from {ONO<sup>SiPh<sub>3</sub></sup>}AlMe (0.045 g, 48.9 μmol) and methyl (*R*)-3-hydroxybutyrate (7.0 μL, 62.5 μmol). After cooling to ambient temperature, the toluene solution was concentrated to *ca.* (1 mL). Slow evaporation of the solution gave **5a** as yellow crystals (0.025 g, 50%). <sup>1</sup>H NMR (500 MHz, CD<sub>2</sub>Cl<sub>2</sub>, 298 K): δ 8.26 (d, <sup>3</sup>J = 8.6 Hz, 1H, H<sup>8</sup>), 8.23 (d, <sup>3</sup>J = 8.6 Hz, 1H, H<sup>8'</sup>), 7.89–7.80 (t + 2 dd overlapped, 3H, H<sup>2p</sup>+H<sup>3p</sup>), 7.74 (s, 1H, H<sup>4</sup>), 7.67 (s, 1H, H<sup>4'</sup>), 7.57–7.53 (m, 14H, Haro SiPh<sub>3</sub> + H<sup>5</sup>/H<sup>5'</sup>), 7.50–7.47 (m, 2H, H<sup>7</sup>/H<sup>7'</sup>), 7.40–7.37 (m, 6H, Haro SiPh<sub>3</sub>), 7.26–7.23 (m, 14H, Haro SiPh<sub>3</sub> + H<sup>6</sup>/H<sup>6'</sup>), 3.44 (m, 1H, OCH(Me)), 2.51 (s, 3H, CH<sub>2</sub>COOMe), 1.42 (dd, 1H, <sup>3</sup>J = 2.1 Hz, <sup>2</sup>J = 16.8 Hz, CHHCOOMe), 1.19 (dd, 1H, <sup>3</sup>J = 10.5 Hz, <sup>2</sup>J = 16.8 Hz, CHHCOOMe), 0.60 (d, 3H, <sup>3</sup>J = 6.1 Hz, OCH(Me)). <sup>13</sup>C{<sup>1</sup>H} NMR (125 MHz, CD<sub>2</sub>Cl<sub>2</sub>, 298 K): δ 180.8 (COO), 163.5 (C-O), 163.2 (C-O), 155.24 (C-N), 155.21 (C-N), 144.6 (C<sup>4</sup>), 144.4 (C<sup>4'</sup>), 137.5, 136.9, 136.2, 136.1, 134.8, 129.64, 129.6, 128.7, 128.66, 128.1, 128.0, 127.9, 127.86, 127.7, 127.64, 126.4, 126.3, 124.3, 124.25, 122.9, 122.8, 115.7, 115.1 (Caro), 63.0 (OCH(Me)), 53.9 (CH<sub>2</sub>COOMe, overlapped with CD<sub>2</sub>Cl<sub>2</sub>), 41.3 (CH<sub>2</sub>COOMe), 25.5 (OCH(Me)).

**3.3.10**  $\{\text{ONO}^{\text{Me,Cumyl}}\}\text{Al}((R)\text{-OCH}(\text{CH}_3)\text{CH}_2\text{COOMe})$  (**5d**): A J-Young NMR tube was charged with  $\{\text{ONO}^{\text{Me,Cumyl}}\}\text{AlMe}$  (0.0127 g, 22.4  $\mu\text{mol}$ ). Toluene- $d_8$  (ca. 0.65 mL) was added in, and the tube was shaken. Then, via a microsyringe, methyl (*R*)-3-hydroxybutyrate (2.5  $\mu\text{L}$ , 22.4  $\mu\text{mol}$ ) was added into the suspension. The tube was shaken and warmed at 80 °C for 5 h.  $^1\text{H}$  NMR spectroscopy revealed the release of methane and completion of the reaction. Evaporation of volatiles in vacuum left **5d** as an impure pale yellow solid. Analytically pure crystals of **5d** suitable for X-ray diffraction were obtained by recrystallization from a concentrated  $\text{CH}_2\text{Cl}_2$  solution layered with hexane at room temperature.  $^1\text{H}$  NMR (500 MHz,  $\text{CD}_2\text{Cl}_2$ , 298 K):  $\delta$  7.83 (t,  $^3J = 8.15$  Hz, 1H,  $\text{H}^{3\text{p}}$ ), 7.65 (m, 2H,  $\text{H}_{\text{aro}}$ ), 7.45 (m, 2H,  $\text{H}_{\text{aro}}$ ), 7.26–7.07 (m, 12H,  $\text{H}_{\text{aro}}$ ), 3.91 (s, 3H,  $\text{CH}_2\text{COOCH}_3$ ), 3.47 (m, 1H,  $\text{OCH}(\text{CH}_3)$ ), 2.35 (s, 3H,  $\text{CH}_3$ ), 2.32 (s, 3H,  $\text{CH}_3$ ), 1.95 (dd,  $^3J = 2.9$  Hz and  $^2J = 16.4$  Hz, 1H,  $\text{CHHCOOCH}_3$ ), 1.77 (s, 3H,  $\text{CH}_3$ ), 1.72 (s, 3H,  $\text{CH}_3$ ), 1.68 (s, 3H,  $\text{CH}_3$ ), 1.63 (s, 3H,  $\text{CH}_3$ ), 0.65 (d,  $^3J = 6.2$  Hz, 3H,  $\text{OCH}(\text{CH}_3)$ ). The second  $\text{CHHCOOCH}_3$  overlapped with the methyl signals.

**3.3.11**  $\{\text{ONO}^{\text{SiPh}_3}\}\text{Al}((rac)\text{-OCH}(\text{CF}_3)\text{CH}_2\text{COOEt})$  (**6a**): A solution of ethyl 3-hydroxy-4,4,4-trifluorobutyrate (10.9 mg, 58.7  $\mu\text{mol}$ ) in toluene- $d_8$  (ca. 0.3 mL) was added to a suspension of  $\{\text{ONO}^{\text{SiPh}_3}\}\text{AlMe}$  (0.045 g, 48.9  $\mu\text{mol}$ ) in toluene- $d_8$  (ca. 0.4 mL). The resulting suspension was transferred in a J-Young NMR tube and heated at 80 °C for 40 h.  $^1\text{H}$  NMR spectroscopy revealed the release of methane and completion of the reaction. The resulting solution was layered with hexane (ca. 1 mL) and left at room temperature to give yellow crystals of **6a** (0.032 g, 60%).  $^1\text{H}$  NMR (500 MHz,  $\text{CD}_2\text{Cl}_2$ , 298 K):  $\delta$  8.28 (d, 1H,  $^3J = 8.6$  Hz), 8.18 (d, 1H,  $^3J = 8.5$  Hz), 7.95–7.91 (m, 2H), 7.82–7.8 (m + 1 s, 2H,  $\text{H}^{4+}$  aro), 7.61 (s, 1H,  $\text{H}^4$ ), 7.60–7.47 (m, 14H, Haro), 7.42–7.38 (m, 6H, Haro), 7.31–7.13 (m, 14H, Haro + 5 H for 1 molecule of toluene), 3.37 (m, 1H,  $\text{OCH}(\text{CF}_3)$ ), 2.86–2.80 (m, 1H,  $\text{CH}_2\text{COOCHHCH}_3$ ),

2.69–2.62 (m, 1H, CH<sub>2</sub>COOCHHCH<sub>3</sub>), 1.34 (dd, 1H, <sup>3</sup>J = 2.25 Hz and <sup>2</sup>J = 17.1 Hz CHHCOOEt), 1.19 (dd, 1H, <sup>3</sup>J = 11.1 Hz and <sup>2</sup>J = 17.1 Hz, CHHCOOEt), 0.81 (t, 3H, <sup>3</sup>J = 7.1 Hz, CH<sub>2</sub>COOCH<sub>2</sub>CH<sub>3</sub>). <sup>13</sup>C{<sup>1</sup>H} NMR (125 MHz, CD<sub>2</sub>Cl<sub>2</sub>, 298 K): δ 178.1 (COO), 162.7 (C-O), 162.3 (C-O), 155.58 (C-N), 155.57 (C-N), 145.0 (C<sup>4</sup>), 144.4 (C<sup>4</sup>), 137.8, 136.9, 136.8, 136.2, 135.7, 134.8, 134.6, 129.7, 129.3, 129.25, 129.0, 128.6, 128.2, 128.1, 128.01, 127.98, 127.6, 127.1, 126.7, 126.5, 124.5, 124.2, 123.1, 123.0 (Caro), 66.9 (<sup>2</sup>J<sub>CF</sub> = 0.25 Hz, OCH(CF<sub>3</sub>)), 64.3 (COOCH<sub>2</sub>CH<sub>3</sub>), 32.6 (CH<sub>2</sub>COOEt), 13.1 COOCH<sub>2</sub>CH<sub>3</sub>). <sup>19</sup>F{<sup>1</sup>H}NMR (185 MHz, CD<sub>2</sub>Cl<sub>2</sub>, 298 K): δ –81.94.

**3.3.12 {ONO<sup>Me,Cumyl</sup>}Al((rac)-OCH(CF<sub>3</sub>)CH<sub>2</sub>COOEt) (6d):** This product was prepared as described above for **6a** starting from {ONO<sup>Me,Cumyl</sup>}AlMe (0.0256 g, 45.1 μmol) and (±)-ethyl 3-hydroxy-4,4,4-trifluorobutyrate (9.2 mg, 45.1 μmol). The J-Young NMR tube was heated at 80 °C for 17 h. <sup>1</sup>H NMR spectroscopy revealed the release of methane gas and completion of the reaction. The product is slightly soluble in toluene and it precipitates with conversion of the starting **2d**. The supernatant solution was removed by filtration and, the resulting precipitate was dried under vacuum to give **6d** as a pale yellow solid (0.020 g, 60%). <sup>1</sup>H NMR (500 MHz, CD<sub>2</sub>Cl<sub>2</sub>, 298 K): δ 7.81 (t, <sup>3</sup>J = 8.3 Hz, 1H, H<sup>3p</sup>), 7.65 (d, 1H, <sup>3</sup>J = 8.3 Hz, H<sup>2p</sup>), 7.63 (d, 1H, <sup>3</sup>J = 8.2 Hz, H<sup>2p'</sup>), 7.45 (2 singlets, 2H, H<sup>6</sup>), 7.31–7.07 (m, 12H, H<sup>4</sup>, H<sup>4'</sup> and other aro), 4.34 (2 quadruplets overlapped, 2H, <sup>3</sup>J = 7.2 Hz, COOCH<sub>2</sub>CH<sub>3</sub>), 3.56 (m, 1H, <sup>3</sup>J = 9.1 Hz and <sup>3</sup>J = 3.1 Hz, OCH(CF<sub>3</sub>)), 2.37 (s, 3H, CH<sub>3</sub>), 2.34 (s, 3H, CH<sub>3</sub>), 1.98 (dd, 1H, <sup>3</sup>J = 3.1 Hz, <sup>2</sup>J = 16.5 Hz, CHHCOOEt), 1.84 (dd, <sup>3</sup>J = 9.1 Hz and <sup>2</sup>J = 16.5 Hz, 1H, CHHCOOCH<sub>2</sub>CH<sub>3</sub>), 1.81 (s, 3H, CH<sub>3</sub>), 1.75 (s, 3H, CH<sub>3</sub>), 1.67 (s, 3H, CH<sub>3</sub>), 1.63 (s, 3H, CH<sub>3</sub>), 1.49 (t, <sup>3</sup>J = 7.2 Hz, 3H, CH<sub>2</sub>COOCH<sub>2</sub>CH<sub>3</sub>). <sup>13</sup>C{<sup>1</sup>H} NMR (125 MHz, CD<sub>2</sub>Cl<sub>2</sub>, 298 K): δ 178.9 (COO), 157.6 and 157.05 (CO), 156.3 and 156.25 (CN), 152.4 and 152.1 (C quaternary aro), 139.5 (CH<sup>3p</sup>), 139.4 and 139.3 (C quaternary aro), 132.1 and 132.0 (CH<sup>4</sup>),

129.4 and 128.6 ( $C^5$ ), 128.00 (CH aro), 127.5 and 127.4 ( $CH^6$ ), 126.2 and 126.15 (CH cumyl), 126.1 and 126.00 (CH cumyl), 125.3 and 125.2 (CH cumyl), 122.5 and 122.0 (C quaternary aro), 121.0 and 120.8 ( $CH^{2p}$ ), 67.4 (q,  $^2J = 31.2$  Hz, OCH(CF<sub>3</sub>)), 64.8 (COOCH<sub>2</sub>CH<sub>3</sub>), 42.8 and 42.7 (C(CH<sub>3</sub>)<sub>2</sub>), 33.6 (CH<sub>2</sub>COOEt), 32.3 and 30.8 (C(CH<sub>3</sub>)<sub>2</sub>), 29.9 and 28.6 (C(CH<sub>3</sub>)<sub>2</sub>'), 21.2 and 21.1 (CH<sub>3</sub> phenyl), 13.8 (COOCH<sub>2</sub>CH<sub>3</sub>).  $^{19}F\{^1H\}$  NMR (185 MHz, CD<sub>2</sub>Cl<sub>2</sub>, 298 K):  $\delta$  -81.87 ppm.

### 3.3.13 NMR-scale generation of the propagating species formed from (S)-4a and L-LA

**(7a):** In the glove box, a J-Young NMR tube was charged with (S)-**4a** (0.0338 g, 0.0326 mmol) and L-lactide (0.024 g, 0.166 mmol) in toluene-*d*<sub>8</sub> (0.7 mL) or CD<sub>2</sub>Cl<sub>2</sub> (0.7 mL). The NMR tube was sealed, shaken, and allowed to stand at room temperature for 20 days (for CD<sub>2</sub>Cl<sub>2</sub>) and at 80 °C for 18 h (for toluene- *d*<sub>8</sub>). After this time period, the mixture was composed of 42% of propagating species **7a**, 33% of L-LA and 25% of (S)-**4a**.  $^1H$  NMR (500 MHz, toluene-*d*<sub>8</sub>, 298 K): Aromatic signals of the product and starting complex **4a** overlapped:  $\delta$  5.05–4.97 (m, 12H, **Hf**), 4.89 (q,  $^3J = 7.1$  Hz, 1H, **Hh**), 4.84 (q,  $^3J = 6.2$  Hz, 1H, **Hj**), 4.09 (q,  $^3J = 6.8$  Hz, 1H, **Ha**), 3.67 (q,  $^3J = 6.9$  Hz, 1H, **Hd**), 1.44–1.35 (m, (it seems 3 doublets, they are related with the unit sequence), 36 H, **Mee**)), 1.15–1.12 (d, 3H, **Hg** + d, 6H, (C(O)OCH*Me*) from **L-LA** overlapped), 0.95-0.89 (3d overlapped, 9H, **Hi** + **Hb**), 3.67 (d,  $^3J = 6.9$  Hz, 3H, **Hc**).  $^{13}C\{^1H\}$  NMR (125 MHz, toluene-*d*<sub>8</sub>, 298 K):  $\delta$  189.2 (COOCH**a**), 169.8 (COOCH**f**), 169.78 (COO), 169.67 (COO), 169.66 (COO), 169.4 (COOCH**h**), 167.7 (COOCH**d**), 163.9 (C-O), 163.8 (C-O), 154.67 (C-N), 154.5 (C-N), 144.8 (C<sup>4</sup>), 144.2 (C<sup>4</sup>), 137.4, 137.14, 136.7, 136.2, 135.07, 134.5, 129.6, 124.3, 124.1, 122.9, 122.8, 115.6, 115.4 (Caro), some signals could not be identified because they overlapped with the signals of the deuterated solvent, 73.4 (CH**d**), 69.7 (CH**h**), 69.3 (CH**f**), 68.9 (CH**j**), 68.8 (CH**a**), 21.93 (CH**b**<sub>3</sub>), 21.5 and 21.44 (CH**i**<sub>3</sub>), 16.7 and 16.6 (CH**e**<sub>3</sub>), 16.5 (CH**g**<sub>3</sub>), 16.4 (CH**c**<sub>3</sub>).

### 3.3.14 NMR-scale generation of the first insertion product from (*R*)-**5a** and L-LA (**8a**):

In the glove box, a J-Young NMR tube was charged with (*R*)-**5a** (0.030 g, 29.35  $\mu\text{mol}$ ),  $\text{CD}_2\text{Cl}_2$  (0.7 mL), and L-lactide (0.0057 g, 39.62  $\mu\text{mol}$ ). The tube was sealed, shaken, and allowed to stand at room temperature for 23 h. After this time period, the mixture was composed of 32% of **8a**, 42% of L-LA and 26% of **5a**.  $^1\text{H}$  NMR (500 MHz,  $\text{CD}_2\text{Cl}_2$ , 298 K): Aromatic signals for the product and the starting complex **5a** overlapped,  $\delta$  5.25 (m, 1H,  $^3J = 6.3$  Hz, He), 4.19 (q, 1H,  $^3J = 6.9$  Hz, Ha), 3.7 (s, 3H,  $\text{OCHi}_3$ ), 3.25 (q, 1H,  $^3J = 6.9$  Hz, Hd), 2.67 (dd, 1H,  $^3J = 7.2$  Hz and  $^2J = 16.0$  Hz, Hg), 2.55 (dd, 1H,  $^3J = 5.8$  Hz and  $^2J = 16.0$  Hz, Hh), 1.29 (d, 3H,  $^3J = 6.3$  Hz, Hf), 0.89 (d, 3H,  $^3J = 7.0$  Hz, Hb), 0.36 (d, 3H,  $^3J = 6.9$  Hz, Hc).  $^{13}\text{C}\{^1\text{H}\}$  NMR (125 MHz,  $\text{CD}_2\text{Cl}_2$ , 298 K):  $\delta$  188.7 (COOCHa), 170.2 (COOChi<sub>3</sub>), 167.7 (COOCHd), 163.6 (C-O), 163.4 (C-O), 154.8 (C-N), 154.7 (C-N), 144.7 (C<sup>4</sup>), 144.1(C<sup>4</sup>), 137.3, 137.1, 136.8, 136.77, 136.7, 136.4, 135.7, 129.7, 129.63, 129.25, 128.45, 128.13, 127.96, 127.71, 127.68, 126.26, 126.2, 124.33, 124.1, 123.05, 123.0, 115.2, 115.16 (Caro), 74.4 (CHd), 69.2 (CHe), 68.8 (CHa), 52.1 (OChi<sub>3</sub>), 40.6 (CH<sub>2</sub>COOMe), 21.8 (CHb<sub>3</sub>), 19.8 (CHf<sub>3</sub>), 15.85 (CHc<sub>3</sub>).

### Preparation of Yttrium Complexes Bearing Pyridine-Bis(phenolate) $\{\text{ONO}^{\text{Me,Cumyl}}\}_2$ pro-ligand.

**3.3.15  $\{\text{ONO}^{\text{Me,Cumyl}}\}_2\text{Y}[\text{N}(\text{SiHMe}_2)_2](\text{THF})(\text{Et}_2\text{O})$  (**9**):** A Schlenk flask was charged with  $\{\text{ONO}^{\text{Me,Cumyl}}\}_2$  (**1c**, 331 mg, 0.63 mmol) and  $\text{Y}[\text{N}(\text{SiHMe}_2)_2]_3(\text{THF})$  (350 mg, 0.63 mmol), and diethyl ether (15 mL) was vacuum-condensed in. The reaction mixture was gently warmed to room temperature and stirred overnight. After filtration, the clear solution was concentrated and placed at  $-30$  °C, which eventually afforded **9** as yellow crystals (130 mg, 23%). **9a**:  $^1\text{H}$  NMR (500 MHz, toluene-*d*<sub>8</sub>, 298 K):  $\delta$  7.37–7.35 (m, 6H, aro), 7.09–6.89 (m,

11H, aro), 4.68 (br s, 2H, Si-*H*), 3.22 (q,  $^3J = 7.0$  Hz, 4H, Et<sub>2</sub>O), 3.15 (br m,  $\alpha$ -CH<sub>2</sub>, 4H, THF), 2.33 (s, 6H, Me), 1.93 (s, 12H, Me), 1.06 (br s, 6H, Et<sub>2</sub>O), 0.99 (br m,  $\beta$ -CH<sub>2</sub>, 4H, THF), 0.26 (br s, 12H, SiHMe<sub>2</sub>). Note that this compound is however not very stable in toluene-*d*<sub>8</sub>, and slowly transforms into another, yet unidentified species at room temperature (*ca.* 13% after 15 min at 25 °C) and even more so at higher temperature (27% conversion after 4 h at 90 °C). Characteristic signals for the decomposition species formed at room temperature:  $\delta$  7.59 (2H, aro), 7.41 (2H, aro), 7.28 (m, 2H, aro), 7.17 (m, 2H, aro), 7.11 (m, 2H, aro), 6.85 (m, 1H, aro), 6.81 (d,  $^3J = 1.85$  Hz, 1H, aro), 6.76 (d,  $^3J = 2.3$  Hz, 1H, aro), 6.47 (dd,  $^3J = 2.4$  Hz and  $^4J = 0.5$  Hz, 1H, aro), 6.39 (dd,  $^3J = 6.6$  Hz,  $^4J = 2.1$  Hz, 1H, aro), 4.77 (m, 2H, Si-*H*), 2.42 (s, 3H, Me), 2.33 (s, 3H, Me), 1.96 (s, 3H, Me), 1.90 (s, 3H, Me), 1.79 (s, 3H, Me), 0.04 (d,  $^3J = 3.0$  Hz, 6H, SiHMe<sub>2</sub>), -0.08 (d,  $^3J = 3.0$  Hz, 6H, SiHMe<sub>2</sub>). Compound **9** is much more stable in pyridine-*d*<sub>5</sub>, in which it does react, at least for several hours at room temperature. <sup>1</sup>H NMR (500 MHz, pyridine-*d*<sub>5</sub>, 298 K):  $\delta$  7.63 (d,  $^3J = 7.9$  Hz, 4H, H *o*-cumyl), 7.48 (s, 2H, H<sup>4</sup>), 7.37–7.29 (m, 5H, H *m*-cumyl + H<sup>3p</sup>), 7.18–7.16 (m, 2H, H *p*-cumyl), 7.06 (d,  $^3J = 7.9$  Hz, 2H, H<sup>2p</sup>), 6.9 (s, 2H, H<sup>6</sup>), 4.77 (br m, 2H, Si-*H*), 3.64 (br m,  $\alpha$ -CH<sub>2</sub>, 4H, free THF), 3.35 (q,  $^3J = 7.0$  Hz, 4H, free Et<sub>2</sub>O), 2.35 (s, 6H, CH<sub>3</sub>), 2.13 (s, 12H, CH<sub>3</sub> cumyl), 1.60 (br m,  $\beta$ -CH<sub>2</sub>, 4H, free THF), 1.11 (t,  $^3J = 7.0$  Hz, 4H, free Et<sub>2</sub>O), 0.20 (d,  $^3J = 2.8$  Hz, 12H, SiHMe<sub>2</sub>). <sup>13</sup>C{<sup>1</sup>H} NMR (125 MHz, pyridine-*d*<sub>5</sub>, 298 K):  $\delta$  161.7 (C-N), 158.8 (C-O), 158.77 (C-O), 153.2, 138.1, 137.5, 131.8, 130.1 (C<sup>6</sup>), 129.1 (C<sup>4</sup>), 128.1, 126.8, 125.06, 124.1, 67.8 ( $\alpha$ -CH<sub>2</sub>, free THF), 65.8 (OCH<sub>2</sub>, free Et<sub>2</sub>O), 43.2 (C(CH<sub>3</sub>)<sub>2</sub>), 31.3 (C(CH<sub>3</sub>)<sub>2</sub>), 25.8 ( $\beta$ -CH<sub>2</sub>, free THF), 21.0 (CH<sub>3</sub>), 15.52 (CH<sub>3</sub>, free Et<sub>2</sub>O), 4.1 (SiHMe<sub>2</sub>).

**3.3.16** {ONO<sup>Me,Cumyl</sup>}Y((*R*)-OCH(CH<sub>3</sub>)CH<sub>2</sub>COOMe) (**10**): In the glove box, methyl (*R*)-3-hydroxybutyrate (1.4  $\mu$ L, 13  $\mu$ mol) was added to a solution of {ONO<sup>Me,Cumyl</sup>}Y[N(SiHMe<sub>2</sub>)<sub>2</sub>](THF)(Et<sub>2</sub>O) (**9**, 0.0116 g, 13  $\mu$ mol) in C<sub>6</sub>D<sub>6</sub> (*ca.* 0.7 mL).

After 10 min, the reaction was complete as evidenced by  $^1\text{H}$  NMR. Evaporation of volatiles in vacuum left **10** as a pale yellow solid in quantitative yield (6,35 mg, 99 %).  $^1\text{H}$  NMR (500 MHz, toluene- $d_8$ , 258 K):  $\delta$  7.48 (d,  $^3J = 7.6$  Hz, 2H, Haro), 7.35 (d,  $^3J = 7.6$  Hz, 2H, Haro), 7.20–6.93 (m, 13H, Haro), 2.96 (br m, 1H, OCH(Me)), 2.89 (s, 3H,  $\text{CH}_2\text{COOCH}_3$ ), 2.43 (br dd,  $^3J = 14.4$  Hz, 1H, CHHCOOMe), 2.31 (s, 3H,  $\text{CH}_3$ ), 2.27 (s, 3H,  $\text{CH}_3$ ), 2.03 (s, 3H,  $\text{CH}_3$ ), 1.99 (s, 3H,  $\text{CH}_3$ ), 1.74 (br dd,  $^2J = 14.4$  Hz, 1H, CHHCOOMe), 1.66 (s, 3H,  $\text{CH}_3$ ), 1.58 (s, 3H,  $\text{CH}_3$ ), 0.87 (d,  $^3J = 5.7$  Hz, 3H, OCH( $\text{CH}_3$ )).  $^{13}\text{C}\{^1\text{H}\}$  NMR (100 MHz, toluene- $d_8$ , 258 K):  $\delta$  180.1 (COO), 163.0, 162.9, 159.2, 158.5, 152.0, 151.5, 138.01 ( $\text{C}^{3\text{p}}$ ), 137.4, 136.95, 136.9, 136.6, 131.6, 131.35, 131.15, 131.0, 128.9, 128.0, 127.7, 127.6, 126.8, 125.1, 125.0, 124.8, 123.5, 123.3, 123.2, 122.9, 65.07 OCH(Me), 53.4 ( $\text{COOCH}_3$ ), 43.5 ( $\text{C}(\text{CH}_3)_2$ ), 43.3 ( $\text{C}(\text{CH}_3)_2$ ), 42.4 ( $\text{CH}_2\text{COOMe}$ ), 31.4 ( $\text{CH}_3$ ), 30.9 ( $\text{CH}_3$ ), 29.3 ( $\text{CH}_3$ ), 26.5( $\text{CH}_3$ ), 23.5 ( $\text{CH}_3$ ), 21.0 ( $\text{CH}_3$ ), 20.8 ( $\text{CH}_3$ ).

**3.3.17**  $\{\text{ONO}^{\text{Me,Cumyl}}\}\text{Y}((S,S)\text{-OCH}(\text{CH}_3)\text{CO}_2\text{CH}(\text{CH}_3)\text{CO}_2\text{Me})$  (**11**): This product was prepared as described above for **10**, starting from  $\{\text{ONO}^{\text{Me,Cumyl}}\}\text{Y}[\text{N}(\text{SiHMe}_2)_2](\text{THF})(\text{Et}_2\text{O})$  (**9**, 0.030 g, 33.6  $\mu\text{mol}$ ) and methyl (*S,S*)-lactyllactate (6.0 mg, 33.6  $\mu\text{mol}$ ) in THF- $d_8$  (0.7 mL) for 30 min at room temperature.  $^1\text{H}$  NMR spectroscopy revealed the release of  $\text{HN}(\text{SiHMe}_2)_2$  and  $\text{Et}_2\text{O}$  and formation of **11** along with another species yet unidentified (33–40%). Compound **11** is not stable in solution at room temperature and transforms over 18 h into other species; probably arising from transesterification reactions. Characteristic data for **11**:  $^1\text{H}$  NMR (500 MHz, THF- $d_8$ , 298 K):  $\delta$  7.63 (t,  $^3J = 7.9$  Hz, 1H,  $\text{H}^{3\text{p}}$ ), 7.22–6.77 (m, 16H, Haro), 4.90–4.85 (two quadruplets overlapped,  $^3J = 6.9$  Hz, 2H, OCH( $\text{CH}_3$ ) $\text{CO}_2\text{CH}(\text{CH}_3)\text{CO}_2\text{Me}$ ), 4.44 (m,  $^3J = 3.0$  Hz, 2H,  $\text{HN}(\text{SiHMe}_2)_2$ ), 3.67 (s, 3H,  $\text{COOCH}_3$ ), 3.36 (q,  $^3J = 7$  Hz, 3H,  $\text{OCH}_2\text{CH}_3$ , free  $\text{Et}_2\text{O}$ ), 2.22–2.20 (m, 6H, *p*- $\text{CH}_3$  of phenolate), 1.69–1.65 (m, 12 H,  $\text{CH}_3$  of cumyl), 1.56 (d,  $^3J = 7.0$  Hz, 3H,  $\text{CH}(\text{CH}_3)$ ), 1.49 (d,

$^3J = 6.9$  Hz, 3H, CH(CH<sub>3</sub>)), 1.09 (t,  $^3J = 7.0$  Hz, 3H, OCH<sub>2</sub>CH<sub>3</sub>, free Et<sub>2</sub>O), 0.09 (d,  $^3J = 3.1$  Hz, 12H, HN(SiHMe<sub>2</sub>)<sub>2</sub>). <sup>13</sup>C{<sup>1</sup>H} NMR (125 MHz, THF-*d*<sub>8</sub>, 298 K): δ 190.0 (OCH(CH<sub>3</sub>)CO<sub>2</sub>CH(CH<sub>3</sub>)CO<sub>2</sub>Me), 169.0 (OCH(CH<sub>3</sub>)CO<sub>2</sub>CH(CH<sub>3</sub>)CO<sub>2</sub>Me), 162.1 and 162.0 (CN), 158.8 and 158.7 (CO), 154.7 and 154.6 (C quat aro), 153.5 and 153.4 (C quat aro), 136.5 (CH<sup>3p</sup>), 130.6 and 130.5 (CH), 129.15 and 129.1 (C quat aro), 128.0 and 127.8 (CH), 126.2 and 126.15 (C quat aro), 125.2 and 125.15 (CH), 125.1 and 125.0 (CH), 123.15 and 123.1 (CH), 122.5 and 122.3 (CH<sup>2p</sup>), 73.0 (OCH(CH<sub>3</sub>)CO<sub>2</sub>CH(CH<sub>3</sub>)CO<sub>2</sub>Me), 69.9 (OCH(CH<sub>3</sub>)CO<sub>2</sub>CH(CH<sub>3</sub>)CO<sub>2</sub>Me), 42.1 and 41.9 (C(CH<sub>3</sub>)<sub>2</sub>), 51.0 (OCH<sub>3</sub>), 29.1 and 29.0 (C(CH<sub>3</sub>)<sub>2</sub>), 23.2 (OCH(CH<sub>3</sub>)CO<sub>2</sub>CH(CH<sub>3</sub>)CO<sub>2</sub>Me), 20.1 and 20.3 (CH<sub>3</sub>), 16.0 (OCH(CH<sub>3</sub>)CO<sub>2</sub>CH(CH<sub>3</sub>)CO<sub>2</sub>Me). Characteristic signals for the another species formed in THF (500 MHz, THF-*d*<sub>8</sub>, 298 K): δ 7.73 (t,  $^3J = 8$  Hz, 1H, H<sup>3p</sup>), 7.30 (d,  $^3J = 8$  Hz, 2H, H<sup>2p</sup>), 7.54 (m,  $^3J =$  Hz, 2H, SiH), 1.81 (s, 12H, CH<sub>3</sub> of cumyl), 0.12 (d,  $^3J = 3.1$  Hz, 12H, -N(SiHMe<sub>2</sub>)<sub>2</sub>). Some other signals overlapped with those of **11**.

### 3.4 REACTIVITY TOWARD LACTIDES AND β-BUTYROLACTONE

#### 3.4.1 Typical Procedure for *rac*-Lactide Polymerization

In a typical experiment (Table 5, entry 23), [{ONO<sup>SiPh<sub>3</sub></sup>}Al(*i*Pr (*S*)-lactate)] (10.0 mg, 9.65 μmol) and *rac*-Lactide (139 mg, 0.965 mmol, 100 equiv vs. Al) were charged in a Schlenk flask in the glovebox. Toluene (0.5 mL) was then added, and the flask was immersed in an oil bath preset at the desired temperature. The reaction mixture was stirred over the appropriated time (17 h; note that reaction times have not been systematically optimized). The reaction was quenched by addition of an excess of H<sub>2</sub>O (*ca.* 2 mL of a 10 % H<sub>2</sub>O solution in THF). The resulting mixture was then concentrated under vacuum and the conversion was determined by <sup>1</sup>H NMR analysis of the residue. Finally, the crude polymer was redissolved in



CH<sub>2</sub>Cl<sub>2</sub> and purified upon precipitation in pentane (*ca.* 30 mL), filtered and dried under vacuum. The recovered polymer was then analyzed by NMR and SEC.

### 3.4.2. Typical Procedure for *rac*-Lactide Polymerization in presence of ROH (R = Bn; *i*Pr)

The procedure is similar to described above, except for addition of alcohol (0.653 mg, 11.0 μmol of *i*PrOH, 1 equiv vs. Al) to a solution of [{ONO<sup>SiPh<sub>3</sub></sup>}AlMe] (10.0 mg, 11.0 μmol) in toluene (0.55 mL). The resulting mixture was stirred at room temperature for 5 min, and then *rac*-Lactide (156 mg, 1.09 mmol, 100 equiv vs. Al) was rapidly added to.

### 3.4.3. Typical Procedure for *rac*-β-butyrolactone Polymerization

In a typical experiment (Table 10, entry 12), in the glove-box, a Schlenk flask was charged with a solution of {ONO<sup>Me,Cumyl</sup>}Y[N(SiHMe<sub>2</sub>)<sub>2</sub>](THF)(Et<sub>2</sub>O) (10.0 mg, 11.2 μmol) in toluene (0.56 mL). Into this solution was rapidly syringed in *rac*-β-butyrolactone (96.4 mg, 1.12 mmol, 100 equiv vs. Y) with stirring. The reaction mixture was stirred at room temperature for 45 min. The reaction was quenched by addition of an excess of H<sub>2</sub>O (*ca.* 2 mL of a 10 % H<sub>2</sub>O solution in THF). After a small sample of the crude material was removed for characterization by <sup>1</sup>H NMR, the crude polymer was precipitated in pentane (*ca.* 50 mL), filtered and dried under vacuum. The polymer was then analyzed by NMR and SEC.

## 3.5 POLYMER CHARACTERIZATION

### 3.5.1 Size Exclusion Chromatography (SEC)

Molecular weights of PLAs were determined by size exclusion chromatography (SEC) in THF at 30 °C (flow rate = 1.0 mL·min<sup>-1</sup>) on a Polymer Laboratories PL50 apparatus equipped with a refractive index detector and two ResiPore 300 × 7.5 mm columns. The

polymer samples were dissolved in THF (2 mg.mL<sup>-1</sup>). The number average molecular masses ( $M_n$ ) and polydispersity indexes ( $M_w/M_n$ ) of the polymers were calculated with reference to a universal calibration vs. polystyrene standards.  $M_n$  values of PLAs were corrected with Mark-Houwink factor of 0.58, to account for the difference in hydrodynamic volumes between polystyrene and polylactide.<sup>45c,118</sup>

### 3.5.2 Nuclear Magnetic Resonance (NMR)

Monomer conversions were calculated from <sup>1</sup>H NMR spectra of the crude reaction mixtures in CDCl<sub>3</sub>, from the integration (Int.) ratio Int. polymer/[Int. polymer + Int. monomer], using the methyl hydrogen resonances for PLA at  $\delta$  1.49 ppm and for LA at  $\delta$  1.16 ppm, the methine hydrogen resonances for PHB at  $\delta$  5.25 ppm and for *rac*-BL at  $\delta$  4.66 ppm.

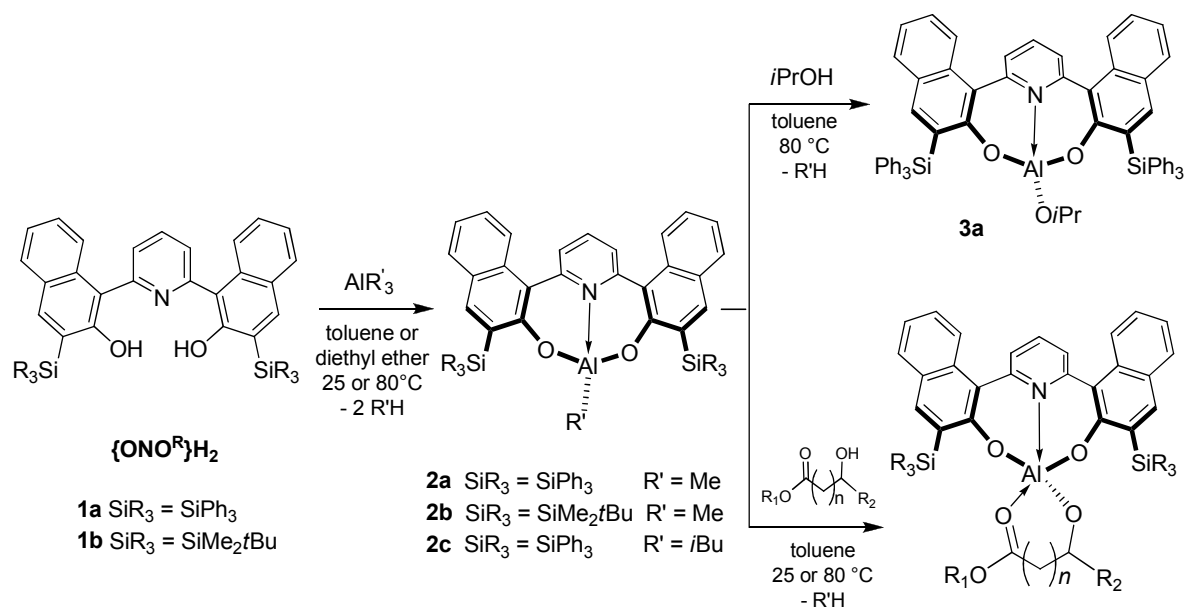
Molar masses of PLAs samples were determined by <sup>1</sup>H NMR spectroscopy in CDCl<sub>3</sub> taking into account the relative intensities of signals for the chain end and the main chain ester units.

The microstructure of PLAs was determined by homodecoupling <sup>1</sup>H NMR spectroscopy at 25 °C in CDCl<sub>3</sub>, with a Bruker AC-500 spectrometer. The microstructure of PHBs was determined by analyzing the carbonyl and methylene regions of <sup>13</sup>C{<sup>1</sup>H} NMR spectra at 40 °C in CDCl<sub>3</sub> with a Bruker AC-500 operating at 125 MHz, using *ca.* 0.2 mol.L<sup>-1</sup> solutions of PHB (reprecipitated with pentane from a dichloromethane solution).<sup>41</sup>

## 4. RESULTS AND DISCUSSION

### 4.1 Discrete lactate and $\beta$ -alkoxy-butyrate Aluminum bis(phenolate)-pyridine complexes: Models for mechanistic investigations in the Ring-Opening Polymerization of lactides.

Aluminum(III) complexes of the type  $\{L\}_2AlR'$  were synthesized by one-pot  $\sigma$ -bond metathesis reaction of  $\{ONO^{SiR_3}\}_2H_2$  pro-ligands ( $SiR_3 = SiPh_3$ , **1a**;  $SiMe_2tBu$ , **1b**) with  $AlR'_3$  ( $R' = Me, iBu$ ).<sup>119</sup> Then, in order to obtain Al-alkoxide, -lactate and  $\beta$ -alkoxy-butyrate compounds, the parent methyl complexes  $\{ONO^{SiR_3}\}_2AlMe$  (**2a**, **2b**) were reacted with the corresponding alcohol and  $\alpha$ - and  $\beta$ -hydroxy-esters  $R''OH$  ( $R'' = iPr$ , **3a**;  $(S)$ - $CH(Me)CO_2iPr$ , **4a**, **4b**;  $(R)$ - $CH(Me)CH_2CO_2Me$ , **5a**;  $(rac)$ - $CH(CF_3)CH_2CO_2Et$ , **6a**) (Scheme 19).



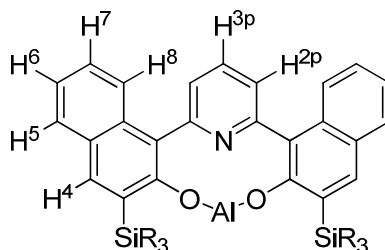
**Scheme 19.** Preparation of Aluminum Complexes (**2-6**) Featuring Bis(Naphtholate)-Pyridine Ligands.

#### 4.1.1 Preparation of alkyl $\{\text{ONO}^{\text{SiR}_3}\}\text{AlR}'$ Complexes ( $\text{R}' = \text{Me}$ , $\text{SiR}_3 = \text{SiPh}_3$ , **2a**; $\text{SiMe}_2\text{tBu}$ , **2b**; $\text{R} = i\text{Bu}$ , $\text{SiR}_3 = \text{SiPh}_3$ , **2c**).

The reaction of the bis(naphthol)-pyridine pro-ligand  $\{\text{ONO}^{\text{SiR}_3}\}_2$  ( $\text{SiR}_3 = \text{SiPh}_3$ , **1a**;  $\text{SiMe}_2\text{tBu}$ , **1b**) with 1.2 equiv. of  $\text{AlR}'_3$  in toluene at 80 °C or in diethyl ether at 20 °C afforded selectively the corresponding Al(III)-alkyl compounds  $\{\text{ONO}^{\text{SiPh}_3}\}\text{AlMe}$  (**2a**),  $\{\text{ONO}^{\text{SiMe}_2\text{tBu}}\}\text{AlMe}$  (**2b**) and  $\{\text{ONO}^{\text{SiPh}_3}\}\text{Al}i\text{Bu}$  (**2c**), which were isolated as yellow solids in 80 %, 63 % and 80 % yields, respectively (Scheme 19). These compounds, which are air- and moisture-sensitive, are readily soluble in aromatic hydrocarbons (benzene, toluene). Also, compound **2b** is slightly soluble in aliphatic hydrocarbons (hexane, pentane). Compounds **2a**, **2b** and **2c** were characterized in solution by NMR spectroscopy and in the solid state by a single-crystal X-ray diffraction study for **2a**.

The  $^1\text{H}$  and  $^{13}\text{C}\{^1\text{H}\}$  NMR spectra of **2a**, **2b** and **2c**<sup>†</sup> feature each one set of resonances, consistent with the existence of a single monomeric species exhibiting a  $C_s$ -symmetric structure in  $\text{C}_6\text{D}_6$  solution at room temperature. The  $^1\text{H}$  NMR spectra of **2a**, **2b** and **2c** feature a singlet for the naphtholate  $\text{H}^4$  at  $\delta$  8.22,  $\delta$  8.12 and 8.24 ppm, respectively, and a triplet for the pyridine  $\text{H}^{3p}$  at  $\delta$  6.66,  $\delta$  6.76 and 6.67 ppm, respectively, in a diagnostic 2:1 intensity ratio, as expected for a  $C_s$ -symmetric structure. The methyl resonance for **2a** and **2b** appears at  $\delta$  -1.26 and -0.50 ppm, respectively. Also, the  $^1\text{H}$  NMR spectrum of **2c** contains three resonances for the  $i\text{Bu}$  fragment as a multiplet ( $\text{Al}-\text{OCH}_2\text{CH}(\text{CH}_3)_2$ ) at  $\delta$  1.15 ppm, a

<sup>†</sup> Numbering scheme of 1,1-bis(naphtholate)-1',1' pyridine ligand



doublet (Al–OCH<sub>2</sub>CH(CH<sub>3</sub>)<sub>2</sub>) at  $\delta$  0.47 ppm and a doublet (Al–OCH<sub>2</sub>CH(CH<sub>3</sub>)<sub>2</sub>) at  $\delta$  –0.69 ppm (*see the Annexes*).

Single crystals of **2a** suitable for X-ray diffraction studies were successfully prepared by recrystallization from a concentrated toluene/hexane solution (30:70) at room temperature. The molecular structure of **2a**, with selected bond distances and angles, are given in Figure 36. The main crystallographic details are reported in Table 1A (*See the Annexes*). Complex **2a** features a monomeric structure in the solid state. The Al atom is four-coordinated by the tridentate {ONO<sup>SiPh<sub>3</sub></sup>}<sup>2-</sup> ligand and the methyl group. The geometry around the Al atom is better described as distorted tetrahedral with bond angles in the range 94.15(7)–119.39(9) °. The Al–O naphtholate bond lengths in **2a** are similar (1.7445(14) and 1.7588(14) Å) and fall within the range (1.714(4)–1.7842(10) Å) observed for related Al-bis(phenolate) complexes.<sup>120,121</sup> The naphtholate groups twist in the same direction from the plane of the pyridine linker, affording a C<sub>s</sub>-symmetric structure with a dihedral angle of 47°, similar to those observed in related group 3 metal complexes prepared by Grunova *et al.* (49–84°).<sup>91</sup>

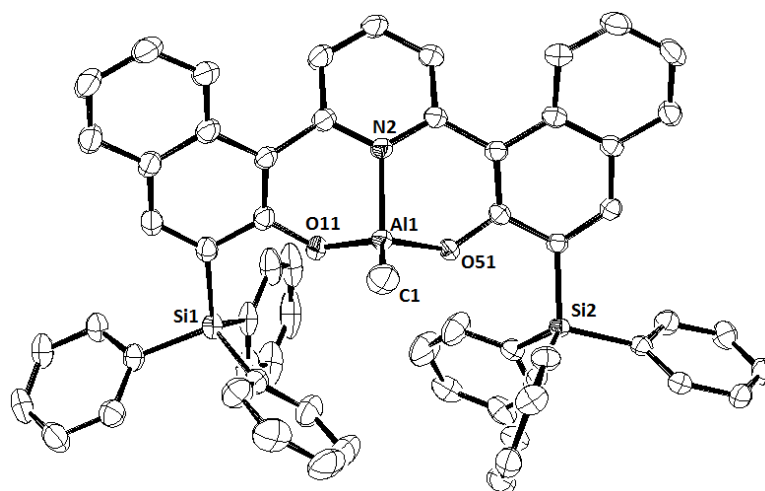


**Figure 36.** Molecular structure of {ONO<sup>SiPh<sub>3</sub></sup>}AlMe (**2a**, 2C<sub>7</sub>H<sub>8</sub>) (all solvents molecules and hydrogen atoms are omitted for clarity; thermal ellipsoids drawn at 50% probability). Selected bond distances (Å) and angles (deg): Al(1)–O(51), 1.7445(14); Al(1)–O(11), 1.7588(14); Al(1)–N(2), 1.9394(15); Al(1)–C(1), 1.922(2); O(51)–Al(1)–O(11), 110.18(7);

O(51)–Al(1)–C(1), 115.85(9); O(11)–Al(1)–C(1), 119.39(9); C(1)–Al(1)–N(2), 117.05(9); O(51)–Al(1)–N(2), 95.95(6); O(11)–Al(1)–N(2), 94.15(7).

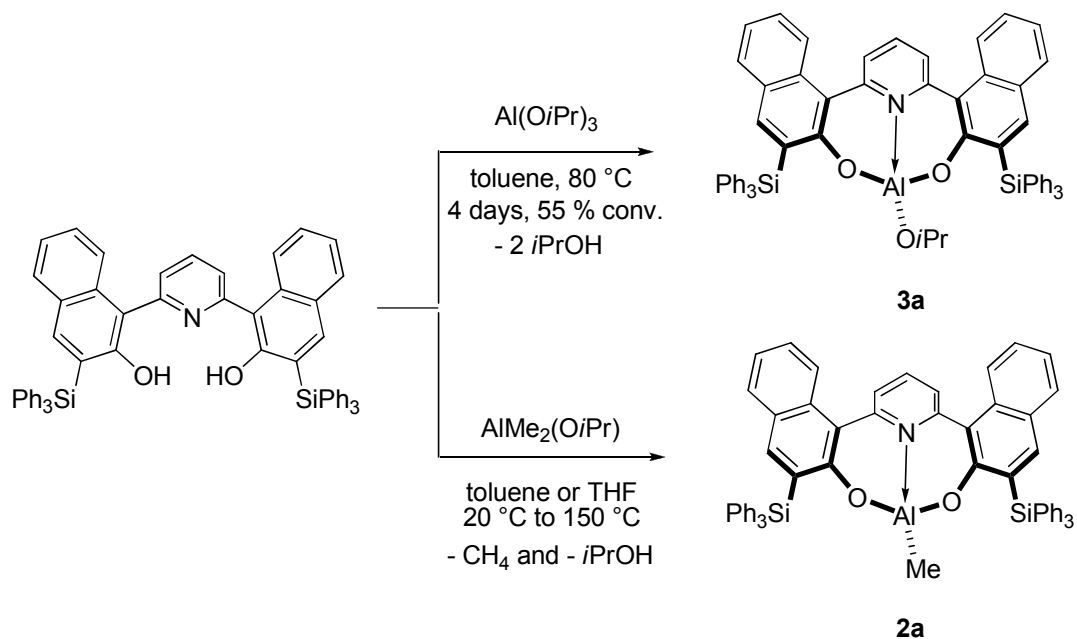
#### 4.1.2 Preparation of $\{\text{ONO}^{\text{SiR}^3}\}\text{AlOR}$ ( $\text{R} = i\text{Pr}$ , **3a**; (*S*)- $\text{CH}(\text{Me})\text{CO}_2i\text{Pr}$ , **4a**, **4b**; (*R*)- $\text{CH}(\text{Me})\text{CH}_2\text{CO}_2\text{Me}$ , **5a**; (*rac*)- $\text{CH}(\text{CF}_3)\text{CH}_2\text{CO}_2\text{Et}$ , **6a**).

The Al-methyl complexes **2a** and **2b** were transformed into Al-alkoxide complexes via methane elimination upon reaction with the corresponding alcohol, as shown in Scheme 19. The reaction between **2a** and isopropanol proceeded slowly in toluene at 80 °C: 50% conversion was observed after 20 h, which yielded, after purification, the isopropoxide complex **3a** as a yellow solid in 45% yield. This compound is air- and moisture-sensitive and is readily soluble in aromatic hydrocarbons (benzene, toluene). The identity of **3a** was assigned on the basis of NMR spectroscopy and elemental analysis.

The  $^1\text{H}$  and  $^{13}\text{C}\{^1\text{H}\}$  NMR spectra of **3a** are consistent with the existence of a single species in which both naphtholate groups are magnetically equivalent on the NMR time scale. The  $^1\text{H}$  NMR spectrum in toluene- $d_8$  features a singlet for the naphtholate  $\text{H}^4$  at  $\delta$  8.05 ppm and a triplet for the pyridine  $\text{H}^{3\text{p}}$  at  $\delta$  6.81 ppm in a 2:1 intensity ratio. The resonances for the isopropoxide group were observed as a broad singlet at  $\delta$  3.55 ppm ( $\text{OCH}(\text{CH}_3)_2$ ) and a doublet at  $\delta$  0.59 ppm ( $\text{OCH}(\text{CH}_3)_2$ ).

Other routes were considered for the preparation of complex **3a**, that is the reaction of pro-ligand  $\{\text{ONO}^{\text{SiPh}_3}\}_2$  with  $\text{Al}(\text{O}i\text{Pr})_3$  or  $(i\text{PrO})\text{AlMe}_2$  (Scheme 20). Actually, the alcohol elimination reaction between  $\text{Al}(\text{O}i\text{Pr})_3$  and  $\{\text{ONO}^{\text{SiPh}_3}\}_2$  proceeded significantly more slowly (55% conversion after 4 days at 80 °C in toluene) than the corresponding methane elimination reaction from complex **2a** (*vide supra*, Scheme 1); this may presumably reflect the lower basicity of the former Al precursor. Also, different conditions were explored for the reaction of pro-ligand  $\{\text{ONO}^{\text{SiPh}_3}\}_2$  with  $(i\text{PrO})\text{AlMe}_2$ , i.e. heating at 20-150 °C in toluene or

THF. However, none of the reactions led to the expected isopropoxide complex; instead, and quite surprisingly considering the abovementioned relative reactivity of  $\text{Al}(\text{O}i\text{Pr})_3$  and  $\text{AlMe}_3$  toward  $\{\text{ONO}^{\text{SiPh}_3}\}_2\text{H}_2$ , in all cases the formation of methyl complex  $\{\text{ONO}^{\text{SiPh}_3}\}_2\text{AlMe}$  (**2a**) was observed by  $^1\text{H}$  NMR spectroscopy (Figure 37).



**Scheme 20.** Preparation of Al-Methyl (**2a**) and Al-Isopropoxide (**3a**) Complexes.

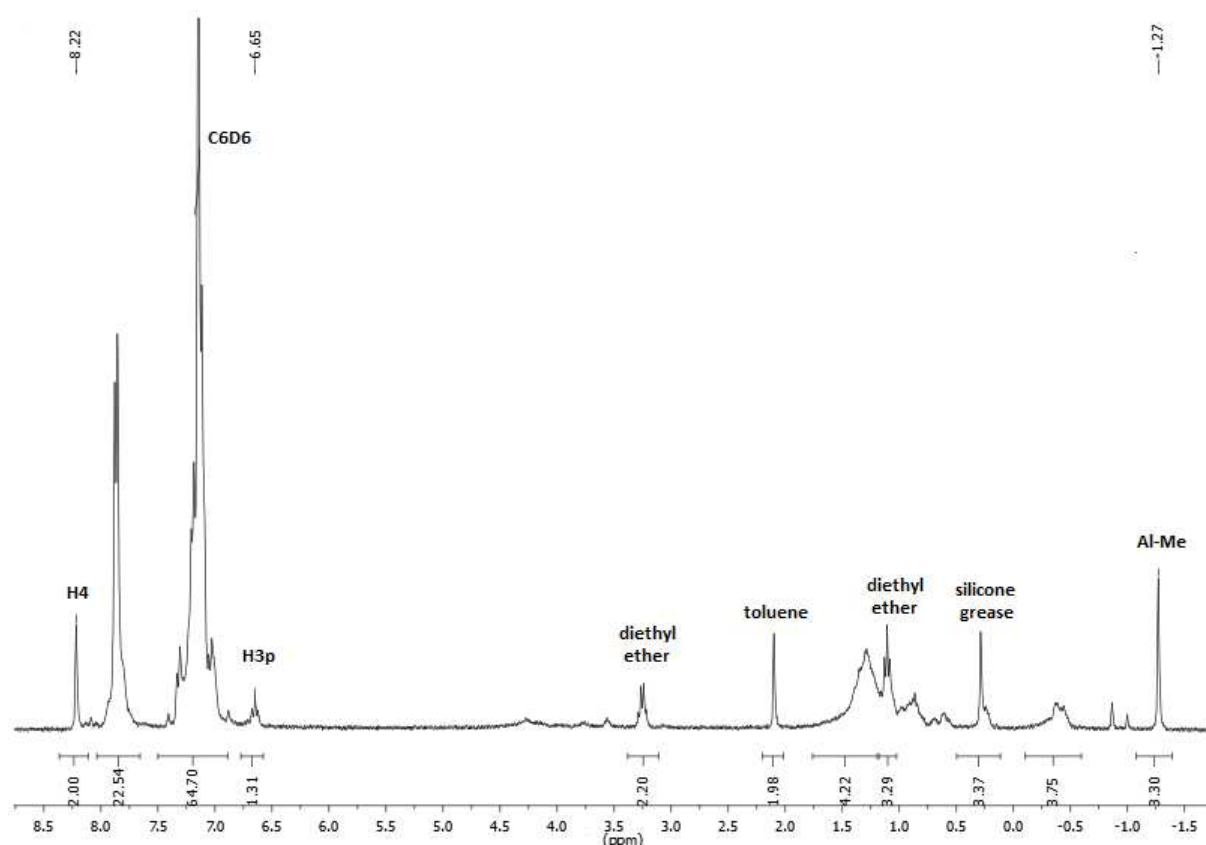


**Figure 37.**  $^1\text{H}$  NMR spectrum (300 MHz,  $\text{C}_6\text{D}_6$ , 298 K) of the crude product of the 1:1 reaction between  $\{\text{ONO}^{\text{SiPh}_3}\}_2\text{H}_2$  and  $(i\text{PrO})\text{AlMe}_2$  (toluene, 80 °C, 4 days).

We also anticipated that Al- $\{\alpha\text{- or } \beta\text{-alkoxy ester}\}$  derivatives may act as good model complexes, mimicking intermediate/active species in the initiation and propagation steps of the ROP of lactides and  $\beta$ -lactones mediated by such Al-alkoxides. So, the reactions between methyl complexes  $\{\text{ONO}^{\text{SiR}^3}\}_2\text{AlMe}$  (**2a** and **2b**) and various  $\alpha$ -hydroxy ester (isopropyl (*S*)-lactate) or  $\beta$ -hydroxy esters (methyl (*R*)-3-hydroxybutyrate and ethyl (*rac*)-3-hydroxy-4,4,4-trifluorobutyrate) were conducted to reach the desired corresponding lactate  $\{\text{ONO}^{\text{SiR}^3}\}_2\text{Al}((S)\text{-OCH}(\text{Me})\text{CO}_2i\text{Pr})$  ( $\text{R} = \text{SiPh}_3$ , **4a**;  $\text{SiMe}_2t\text{Bu}$ , **4b**) and  $\beta$ -alkoxy-butyrate complexes  $\{\text{ONO}^{\text{SiPh}_3}\}_2\text{Al}(\text{OR})$  ( $\text{OR} = (R)\text{-OCH}(\text{Me})\text{CH}_2\text{CO}_2\text{Me}$ , **5a**; (*rac*)- $\text{OCH}(\text{CF}_3)\text{CH}_2\text{CO}_2\text{Et}$ , **6a**) (*vide supra*, Scheme 19). Adjusting the reaction conditions allowed recovering the targeted compounds in 86%, 85%, 50% and 60% isolated yields, respectively.



Compounds **4a**, **5a** and **6a** are readily soluble in polar solvents (dichloromethane, THF). Compounds **4a** and **4b** are also soluble in aromatic hydrocarbons (benzene, toluene), while **6a** is slightly so. Thanks to its TBDMS groups, compound **4b** is also quite soluble in aliphatic hydrocarbons (hexanes, pentane). The identity of **4a**, **4b**, **5a** and **6a** was established by elemental analysis,  $^1\text{H}$  and  $^{13}\text{C}$  NMR spectroscopy in solution, and single-crystal X-ray diffraction studies for **4a**, **5a** and **6a**.

The  $^1\text{H}$  and  $^{13}\text{C}\{^1\text{H}\}$  NMR data for the aluminum(III) (*S*)-lactate (**4a**, **b**) and (*R*)- and (*rac*)- $\beta$ -alkoxy-butyrate (**5a**, **6a**) complexes in toluene- $d_8$ ,  $\text{C}_6\text{D}_6$  and  $\text{CD}_2\text{Cl}_2$ , at room temperature, are indicative of the existence of a single  $C_1$ -symmetric species. In the  $^1\text{H}$  NMR spectra recorded in toluene- $d_8$ , the non-equivalent  $\text{H}^4/\text{H}^{4'}$  and  $\text{H}^8/\text{H}^{8'}$  hydrogens of the naphtholate groups appear as two sets of resonances ( $\delta$  8.03 and 7.92 ppm;  $\delta$  8.08 and 7.99 ppm, respectively for **4a** and  $\delta$  8.05 and 8.02 ppm;  $\delta$  8.02 and 8.04 ppm, respectively for **4b**). The resonances for the isopropyl (*S*)-lactate group were observed as a quartet for the methine  $\text{OCH}(\text{CH}_3)\text{CO}_2i\text{Pr}$  ( $\delta$  4.01 for **4a** and  $\delta$  3.82 ppm for **4b**), a septet for the other methine  $\text{OCH}(\text{CH}_3)\text{CO}_2\text{CH}(\text{CH}_3)_2$  ( $\delta$  3.17 for **4a** and  $\delta$  5.52 ppm for **4b**), a doublet for the methyl group associated with the chiral center ( $\text{OCH}(\text{CH}_3)\text{CO}_2i\text{Pr}$ ) ( $\delta$  0.79 for **4a** and  $\delta$  0.64 ppm for **4b**) and two doublets for the non-equivalent methyl  $\text{OCH}(\text{CH}_3)\text{CO}_2\text{CH}(\text{CH}_3)_2$  ( $\delta$  0.41 and  $\delta$  0.29 ppm for **4a** and  $\delta$  1.08 and  $\delta$  1.06 ppm for **4b**). The significant difference in the chemical shifts for the methine resonance of the isopropyl group, in those two compounds ( $\delta$  3.17 for **4a** and  $\delta$  5.52 ppm for **4b**) probably stems from, at least in part, from anisotropic effects induced by the phenyl groups of the naphtholate *ortho*-substituents in the former compound. It could also reflect the existence of interactions between those isopropyl C–H and the  $\pi$ -system of one of the phenyl groups of the  $-\text{SiPh}_3$  substituent, as observed in the solid state (*vide infra*). NOESY experiments demonstrate the spatial proximity ( $d < 5 \text{ \AA}$ ) between hydrogens of the phenyl groups and isopropyl C–H (Figure 38).<sup>122</sup>

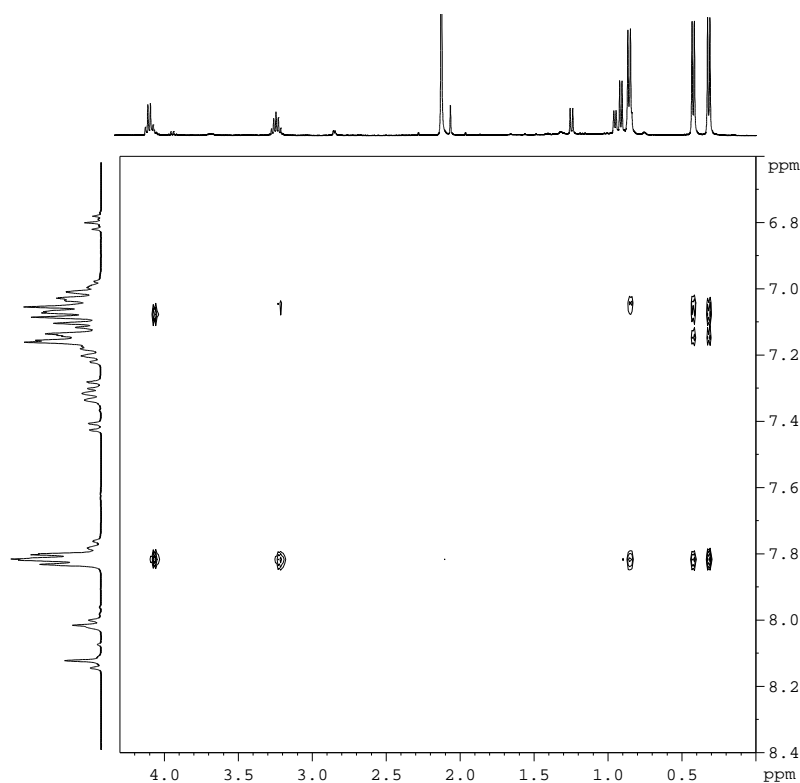


**Figure 38.**  $^1\text{H}$ - $^1\text{H}$  NOESY NMR spectrum (toluene- $d_8$  at 25°C, 400 MHz) of the  $\{\text{ONO}^{\text{SiPh}_3}\}\text{Al}((S)\text{-OCH}(\text{CH}_3)\text{CO}_2i\text{Pr})$  (**4a**).

In the  $^1\text{H}$  NMR spectrum (*see the Annexes*) of **5a** in  $\text{CD}_2\text{Cl}_2$ , the non-equivalent  $\text{H}^4/\text{H}^4'$  hydrogens of the naphtholate groups were observed at  $\delta$  7.74 and 7.67 ppm. The resonances for the (*R*)- $\beta$ -alkoxy-butyrate group were observed as a multiplet and a doublet for the methine and methyl hydrogens associated to the chiral center ( $\text{OCH}(\text{Me})\text{CH}_2\text{CO}_2\text{Me}$ ,  $\delta$  3.44 ppm;  $\text{OCH}(\text{CH}_3)\text{CH}_2\text{CO}_2\text{Me}$ ,  $\delta$  0.60 ppm), two doublets of doublet for the diastereotopic methylene hydrogens ( $\text{OCH}(\text{Me})\text{CHHCO}_2\text{Me}$ ,  $\delta$  1.42 and 1.19 ppm), and a single resonance for the methyl ester group ( $\text{OCH}(\text{Me})\text{CH}_2\text{CO}_2\text{CH}_3$ ,  $\delta$  2.51 ppm).

In the  $^1\text{H}$  NMR spectrum (*see the Annexes*) of **6a** in  $\text{CD}_2\text{Cl}_2$ , the non-equivalent  $\text{H}^4/\text{H}^4'$  and  $\text{H}^8/\text{H}^8'$  hydrogens of the naphtholate groups were observed at  $\delta$  7.8 and 7.6 ppm and  $\delta$  8.27 and 8.17 ppm, respectively. The resonances for the fluorinated *rac*- $\beta$ -alkoxy-butyrate group were observed as a multiplet for the methine hydrogen ( $\text{OCH}(\text{CF}_3)\text{CH}_2\text{CO}_2\text{Et}$ ,  $\delta$  3.37 ppm), two doublets of doublet for the diastereotopic methylene hydrogens

(OCH(CF<sub>3</sub>)CHHCO<sub>2</sub>Et,  $\delta$  1.33 and  $\delta$  1.18 ppm); the methylene hydrogens of the ethyl ester group (CO<sub>2</sub>CHHCH<sub>3</sub>) are also diastereotopic, giving rise to an eight-line pattern ( $\delta$  2.83 and 2.66 ppm), and a triplet for the methyl group (OCH(CF<sub>3</sub>)CH<sub>2</sub>CO<sub>2</sub>CH<sub>2</sub>CH<sub>3</sub>,  $\delta$  0.81 ppm).

In the <sup>19</sup>F{<sup>1</sup>H} NMR spectrum of complex **6a**, a single resonance for the CF<sub>3</sub> group was observed at  $\delta$  -81.93 ppm, clearly shifted from the resonance in the starting reagent (*rac*-CF<sub>3</sub>CH(OH)C(O)OEt;  $\delta$  -80.18 ppm).

In the <sup>13</sup>C{<sup>1</sup>H} NMR spectra of these complexes in toluene-*d*<sub>8</sub>, the resonance for the carbonyl group was observed in the range  $\delta$  177.0-190.0 ppm (Table 3)<sup>123</sup> significantly shifted downfield from the corresponding resonance in the initial alcohol reagent ( $\delta$  175.0 ppm). These data suggest that the carbonyl group in those complexes is coordinated to the Al atom in solution, forming mononuclear species, as observed in the solid state (*vide infra*).

**Table III:** Comparison of the <sup>13</sup>C{<sup>1</sup>H} NMR chemical shifts (ppm) for carbonyl groups in aluminum-{alkoxy ester} complexes **4a**, **4b**, **5a** and **6a**, and the corresponding hydroxy-ester reagent.

	<b>4a</b>	<b>4b</b>	<b>5a</b>	<b>6a</b>
$\delta$ for C=O complex	189.5	190.0	180.0	177.0
$\delta$ for C=O initial reagent ROH	175.0	175.0	172.5	170.1

The variable temperature <sup>1</sup>H NMR spectra of lactate complex **4a** in toluene-*d*<sub>8</sub> in the temperature range 298-373 K are shown in Figure 39. These spectra, which are representative also for  $\beta$ -alkoxy-butyrates compounds **5a** and **6a** complexes, revealed no dynamic phenomena. This suggests that no interconversion exists between overall dissymmetric species having different geometries (symmetries) of the coordinated ONO fragment (*i.e.*, C<sub>1</sub><sup>Cs</sup>-ONO  $\rightleftharpoons$  C<sub>1</sub><sup>C2-ONO</sup>).

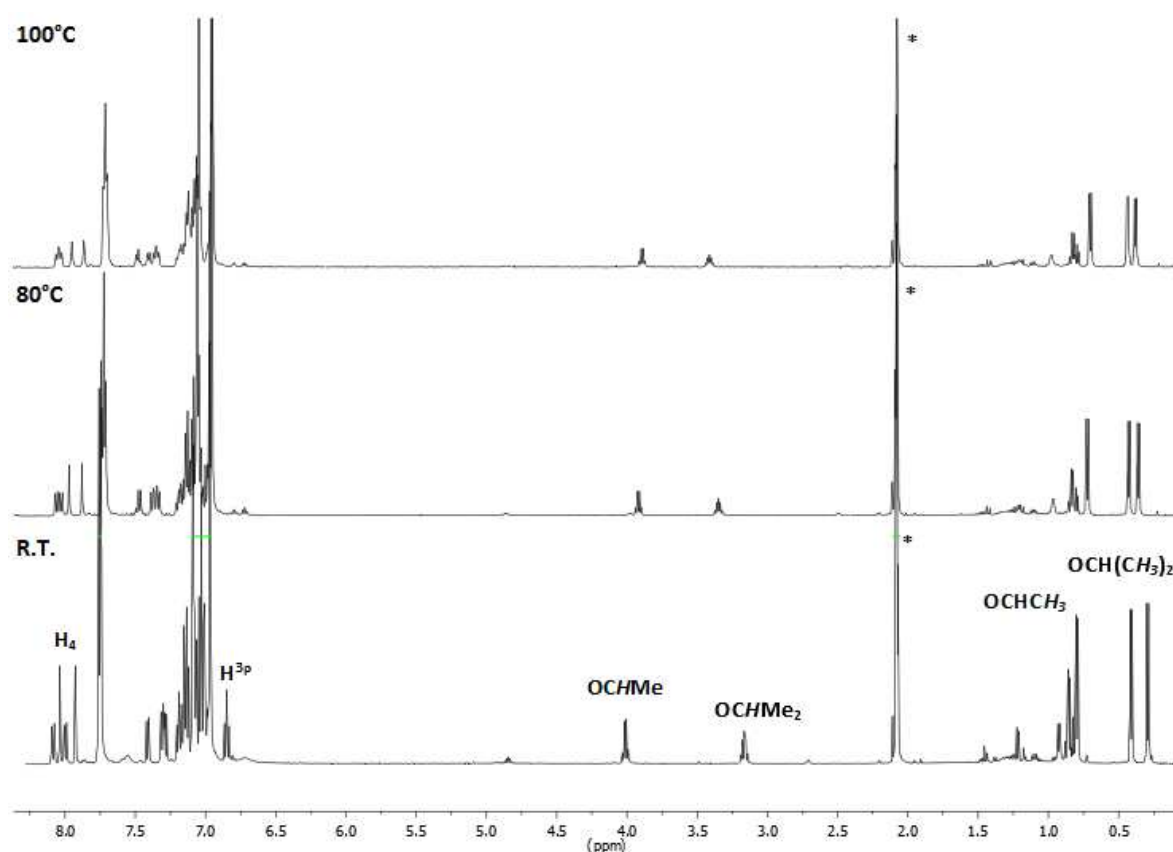


**Figure 39.** Variable Temperature  $^1\text{H}$  NMR spectra (500 MHz, toluene- $d_8$ ) of  $\{\text{ONO}^{\text{SiPh}_3}\}\text{Al}((S)\text{-OCH}(\text{Me})\text{CO}_2i\text{Pr})$  (**4a**); bottom, 298 K; middle, 353 K; top, 373 K (\* stands for residual solvent resonances).

The molecular structures of complexes **4a**, **5a** and **6a** were established by X-ray crystallography. Single crystals suitable for such X-ray diffraction studies were grown from concentrated toluene solutions layered with hexane at room temperature. The molecular structures, and selected bond distances and angles for these compounds are given in Figures 40, 41 and 42. The main crystallographic details are reported in Table 1A (*see the Annexes*).

In the solid-state, **4a**, **5a** and **6a** are monomeric with a five-coordinated aluminum center. Their geometry is best described as slightly distorted trigonal bipyramidal (trigonal index,  $\tau = 0.89\text{--}0.93$  for these three complexes).<sup>124</sup> In all cases, the axial positions are

occupied by a nitrogen atom (N2) and a carbonyl oxygen atom (O71), with N–Al–O angles in the range 175.62(11)–176.9(3)°. <sup>125</sup> The other oxygen atoms (O(11), O(51) and O(74)) occupy the equatorial positions with O–Al–O angles ranging from 114.9(3) to 123.3(4)°. The Al–O(carbonyl) bond distances (Al(1)–O(71), 2.018(5) Å, **4a**; 1.993(2) Å, **5a**; 2.030(2) Å, **6a**) (Table 4) are slightly shorter than those in [Me<sub>2</sub>Al(ethyl lactate)]<sub>2</sub> (2.157(2) Å) and [Me<sub>2</sub>Al(μ-OCH(Me)COO)<sub>2</sub>O(CH<sub>2</sub>)<sub>2</sub>OMe]<sub>2</sub> (2.147(4) Å). <sup>104</sup> In comparison, in the six-coordinated Al-{salen}((*S*)-OCH(Me)CO<sub>2</sub>Me) complex described by Nomura *et al.*, <sup>58</sup> the carbonyl oxygen of lactate occupies the sixth position at the Al center with a Al–O bond length of 2.165 Å slightly longer than in the present compounds. The Al–O(phenoxide) bond distances for **4a**, **5a** and **6a** are in the range 1.761(6)–1.780(2) Å and compare well to those for aluminum amino-bis(phenolate) complexes (1.748(3)–1.782(1) Å). <sup>108,126</sup>

More singularly, the molecular structures of complexes **4a**, **5a** and **6a** feature close contacts (Table 4) between the π-system of one of the SiPh<sub>3</sub> phenyl groups and C–H of the isopropyl group in **4a** (Figure 40), C–H of the ester methyl and methylene groups in **5a** (Figure 41), and C–H of the methine, methylene and ester ethyl groups in **6a** (Figure 42) present in the (*S*)-lactate and β-alkoxy-esters moieties, respectively. These observations are important when considering C–H•••π-system interactions, which can occur only when the π-system is close enough to the C–H unit. <sup>89,109,127</sup>

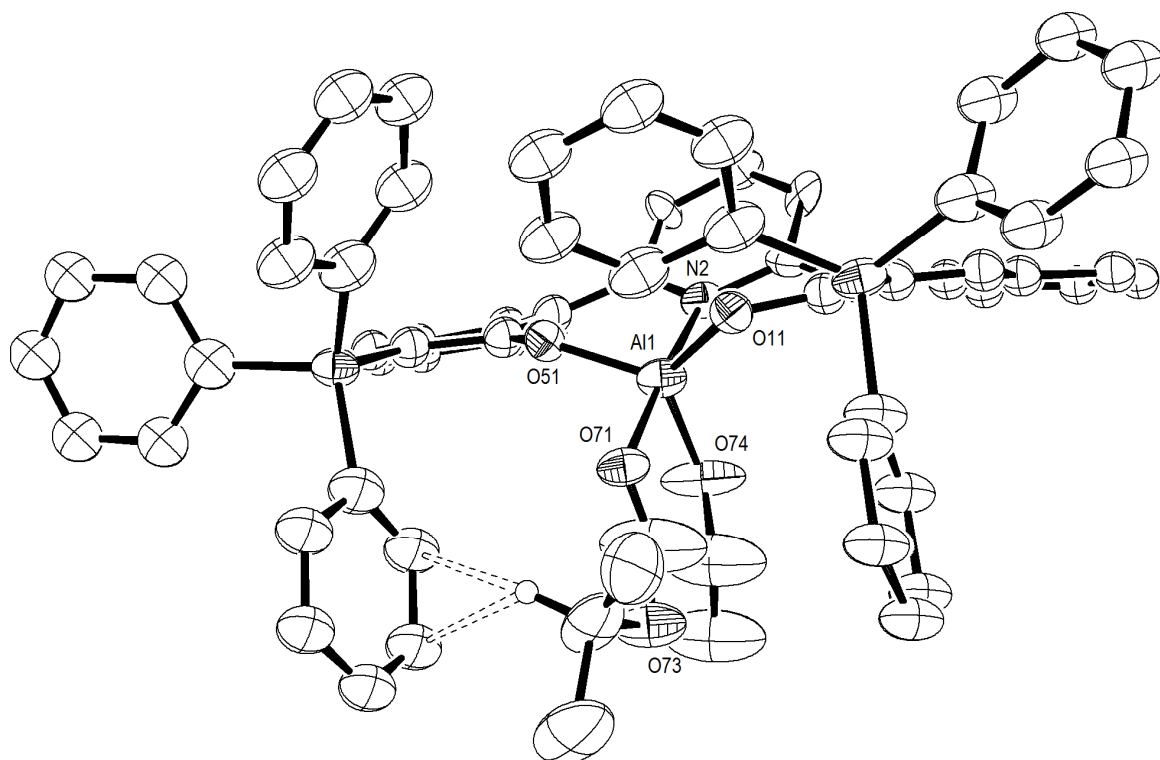


**Figure 40.** Molecular structure of  $\{\text{ONO}^{\text{SiPh}_3}\}\text{Al}((S)\text{-OCH}(\text{Me})\text{CO}_2i\text{Pr})$  (**4a**) (thermal ellipsoids drawn at 50 % probability level; all solvents molecules and hydrogen atoms, except that of the isopropyl moiety of the isopropyl (*S*)-lactate group, are omitted for clarity). Selected bond distances (Å) and angles (deg): Al–O(74), 1.745(6); Al–O(11), 1.761(6); Al–O(51), 1.777(6); Al–O(71), 2.018(5); Al–N, 2.018(6); N–Al–O(71), 176.9(3); O(51)–Al–O(11), 114.9(3); O(51)–Al–O(74), 123.3(4); O(11)–Al–O(74), 121.2(4); O(74)–Al–O(71), 84.1(3); O(11)–Al–O(71), 89.0(2); O(51)–Al–O(71), 89.7(2); O(74)–Al–N, 93.1(3); O(11)–Al–N, 91.5(3); O(51)–Al–N, 92.9(3).

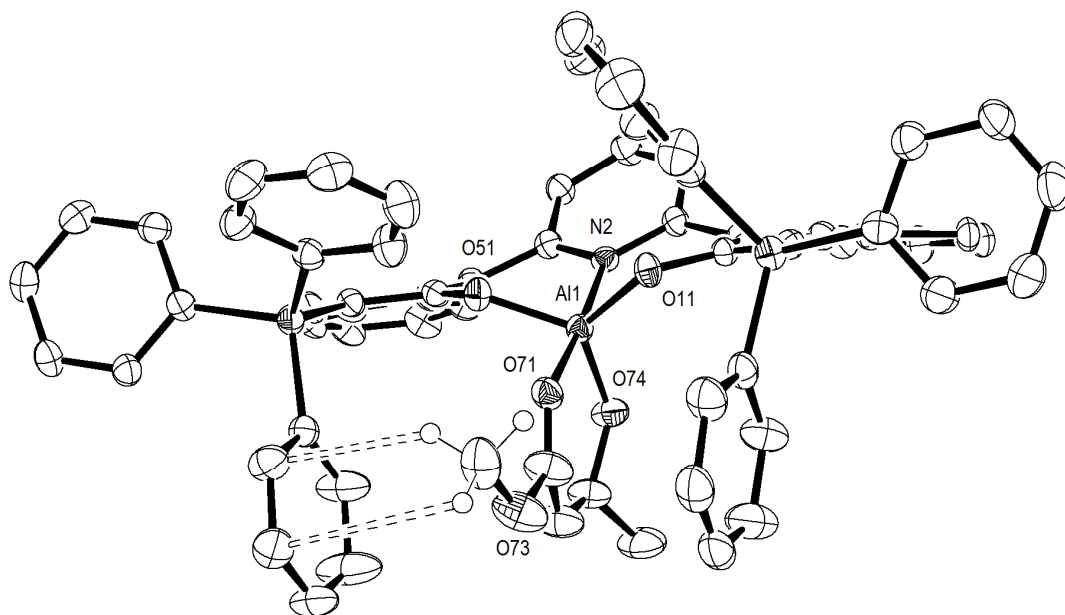


**Figure 41.** ORTEP drawing of  $\{\text{ONO}^{\text{SiPh}_3}\}\text{Al}((R)\text{-OCH}(\text{Me})\text{CH}_2\text{CO}_2\text{Me})$  (**5a**) (thermal ellipsoids drawn at 50 % probability level; all solvents molecules and hydrogen atoms, except that of the methoxy moiety of the (*R*)- $\beta$ -alkoxy-butyrate group, are omitted for clarity). Selected bond distances (Å) and angles (deg): Al–O(74), 1.729(2); Al–O(51), 1.779(2); Al–O(11), 1.780(2); Al–O(71), 1.993(2); Al–N, 2.023(3); O(74)–Al–O(51), 121.83(12); O(74)–Al–O(11), 122.35(12); O(51)–Al–O(11), 115.77(11); O(71)–Al–N, 175.62(11); O(51)–Al–O(71), 86.37(10); O(74)–Al–O(71), 92.90(11); O(11)–Al–O(71), 88.15(10); O(74)–Al–N, 91.15(11); O(51)–Al–N, 90.08(11); O(11)–Al–N, 91.09(11).

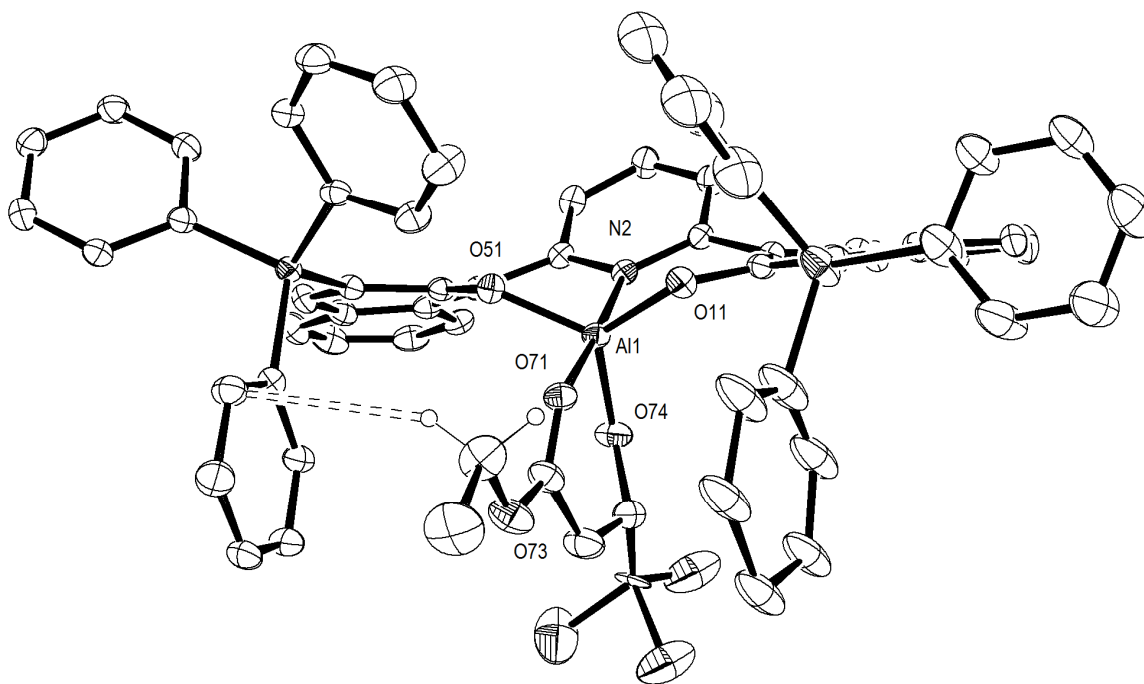


**Figure 42.** ORTEP drawing of  $\{\text{ONO}^{\text{SiPh}_3}\}\text{Al}((\text{rac})\text{-OCH}(\text{CF}_3)\text{CH}_2\text{CO}_2\text{Et})$  (**6a**) (thermal ellipsoids drawn at 30 % probability level; hydrogen atoms, except that of the ethyl group of the *rac*- $\beta$ -alkoxy-trifluorobutyrate are omitted for clarity). Selected bond distances ( $\text{\AA}$ ) and angles (deg): Al–O(74), 1.755(2); Al–O(11), 1.767(2); Al–O(51), 1.777(2); Al–O(71), 2.030(2); Al–N, 2.017(2); O(74)–Al–O(11), 120.62(12); O(74)–Al–O(51), 120.86(12); O(11)–Al–O(51), 118.23(11); O(74)–Al–N, 92.14(10); O(11)–Al–N, 91.86(10); O(51)–Al–N, 91.28(10); O(74)–Al–O(71), 91.20(10); O(11)–Al–O(71), 87.82(10); O(51)–Al–O(71), 85.63(10); N–Al–O(71), 176.29(10).



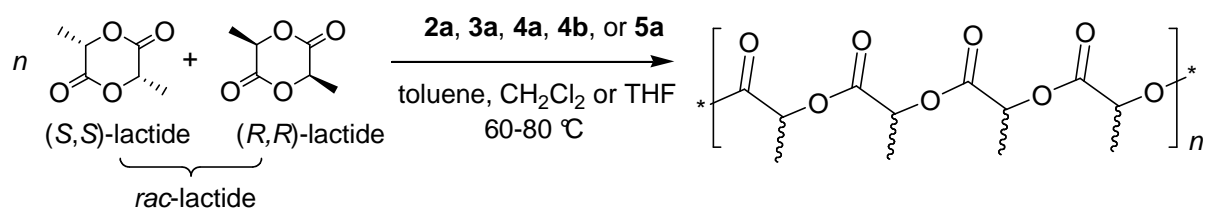
**Table IV:** Selected bond lengths (Å) around the Al center for compounds **2a**, **4a**, **5a** and **6a**, and close contacts (Å) for compounds **4a**, **5a** and **6a**.

Bond	2a	4a	5a	6a
Al–O(11)	1.7445(14)	1.761(6)	1.779(2)	1.767(2)
Al–O(51)	1.7588(14)	1.777(6)	1.780(2)	1.777(2)
Al–N	1.9394(15)	2.018(6)	2.023(3)	2.017(2)
Al–C(1)	1.9220(2)	-	-	-
Al–O(71) (carbonyl)	-	2.018(5)	1.993(2)	2.030(2)
Al–O(74)	-	1.745(6)	1.729(2)	1.755(2)
C–H•••π (OCH(CH <sub>3</sub> ) CO <sub>2</sub> CH(CH <sub>3</sub> ) <sub>2</sub> )	-	3.731	-	-
C–H•••π (OCH(CH <sub>3</sub> ) CO <sub>2</sub> CH(CH <sub>3</sub> ) <sub>2</sub> )	-	3.088	-	-
C–H•••π (OCH(CH <sub>3</sub> ) CO <sub>2</sub> CH(CH <sub>3</sub> ) <sub>2</sub> )	-	2.846	-	-
C–H•••π (OCH(CH <sub>3</sub> )CH <sub>2</sub> CO <sub>2</sub> CH <sub>3</sub> )	-	-	3.329	-
C–H•••π (OCH(CH <sub>3</sub> )CH <sub>2</sub> CO <sub>2</sub> CH <sub>3</sub> )	-	-	2.597	-
C–H•••π (OCH(CH <sub>3</sub> )CH <sub>2</sub> CO <sub>2</sub> CH <sub>3</sub> )	-	-	2.851	-
C–H•••π (OCH(CF <sub>3</sub> )CH <sub>2</sub> CO <sub>2</sub> CH <sub>2</sub> CH <sub>3</sub> )	-	-	-	2.822
C–H•••π (OCH(CF <sub>3</sub> )CH <sub>2</sub> CO <sub>2</sub> CH <sub>2</sub> CH <sub>3</sub> )	-	-	-	3.172
C–H•••π (OCH(CF <sub>3</sub> )CH <sub>2</sub> CO <sub>2</sub> CH <sub>2</sub> CH <sub>3</sub> )	-	-	-	3.052
C–H•••π (OCH(CF <sub>3</sub> )CH <sub>2</sub> CO <sub>2</sub> CH <sub>2</sub> CH <sub>3</sub> )	-	-	-	3.070

#### 4.1.3 Studies on the ring-opening polymerization of *rac*-lactide with aluminum bis(naphtholate) complexes.

Alkoxide complexes of aluminum are well-established catalysts/initiators for the ROP of lactide.<sup>54,97</sup> Activity (mol<sub>monomer</sub>/mol<sub>metal</sub>.h), productivity (mol<sub>monomer</sub>/mol<sub>metal</sub>), degree of control/livingness, and stereoselectivity in the case of chiral monomers depend crucially on ancillary ligands that define the sterics and electronics around the active metal center. We were therefore interested in evaluating the catalytic abilities of the new aluminum complexes, considering that (i) alkoxide aluminum complexes bearing (bis)phenolate ligands have been shown to have valuable catalytic abilities, especially for controlling the stereoselective ROP of *rac*-lactide,<sup>44,55,71</sup> and (ii) scandium, yttrium and lanthanum amido complexes supported by the tridentate pyridine-bis(naphtholate) ligands used in this study have been previously shown to feature high activities and stereocontrol toward *rac*-lactide.<sup>91</sup>

The *catalytic* abilities of  $\{\text{ONO}^{\text{SiPh}_3}\}\text{AlMe}$  (**2a**),  $\{\text{ONO}^{\text{SiPh}_3}\}\text{AlO}i\text{Pr}$  (**3a**),  $\{\text{ONO}^{\text{SiR}_3}\}\text{Al}((S)\text{-OCH}(\text{Me})\text{CO}_2i\text{Pr})$  ( $\text{SiR}_3 = \text{SiPh}_3$ , **4a**;  $\text{SiMe}_2i\text{Bu}$ , **4b**) and  $\{\text{ONO}^{\text{SiPh}_3}\}\text{Al}((R)\text{-OCH}(\text{Me})\text{CH}_2\text{CO}_2\text{Me})$  (**5a**) to promote the ROP of *rac*-lactide was thus examined (Scheme 21). The performance of methyl complex **2a** was also tested in the presence of  $\text{PhCH}_2\text{OH}$  or  $i\text{PrOH}$  as co-initiator/chain transfer agent. Representative results obtained in those polymerization experiments are summarized in Table 5.



**Scheme 21.** Ring-Opening Polymerization of *rac*-Lactide Initiated by Complexes **2-5**.

**Table V.** ROP of *rac*-lactide promoted by {ONO<sup>SiR3</sup>}AIR complexes.

Entry	Cat	[LA]/[Al] /[ROH]	ROH	solvent	Temp (°C)	Time (h)	Conv <sup>b</sup> (%)	$M_{n,calc}$ <sup>c</sup> (kDa)	$M_{n,GPC}$ <sup>d</sup> (kDa)	$M_{n,NMR}$ <sup>e</sup> (kDa)	$M_w/M_n$ <sup>d</sup>	$P_r$ <sup>f</sup>
1	<b>2a</b>	20:1:0	-	tol	60	10	-	-	-	-	-	-
2	<b>2a</b>	20:1:0	-	tol	80	17	55	1.6	15.0	nd	1.52	0.50
3	<b>2a</b>	50:1:0	-	tol	80	17	47	3.4	29.6	nd	1.55	0.54
4	<b>2a</b>	100:1:0	-	tol	25	17	-	-	-	-	-	-
5	<b>2a</b>	100:1:0	-	tol	60	17	28	4.0	10.5	nd	1.16	0.55
6	<b>2a</b>	100:1:0	-	tol	80	17	72	10.4	43.3	nd	1.39	0.55
7	<b>2a</b>	500:1:0	-	tol	80	17	42	30.3	69.5	nd	1.18	0.54
8	<b>2a</b>	100:1:1	BnOH	tol	60	17	70	10.1	6.2	6.7	1.06	0.56
9	<b>2a</b>	100:1:1	BnOH	tol	80	6	80	11.5	6.8	11.2	1.06	0.53
10	<b>2a</b>	100:1:1	BnOH	tol	80	17	100	14.4	7.4	12.0	1.13	0.51
11	<b>2a</b>	500:1:1	BnOH	tol	80	17	78	56.2	24.7	nd	1.08	0.55
12	<b>2a</b>	100:1:1	<sup>i</sup> PrOH	tol	60	17	63	9.1	10.5	13.8	1.07	0.56
13	<b>2a</b>	100:1:1	<sup>i</sup> PrOH	THF	60	17	44	6.3	5.0	7.2	1.06	0.59
14	<b>2a</b>	100:1:1	<sup>i</sup> PrOH	CH <sub>2</sub> Cl <sub>2</sub>	60	17	44	6.3	3.0	5.6	1.08	0.57
15	<b>2a</b>	100:1:1	<sup>i</sup> PrOH	tol	80	6	89	12.8	15.5	nd	1.08	0.59
16	<b>2a</b>	100:1:1	<sup>i</sup> PrOH	tol	80	17	100	14.4	10.9	14.4	1.19	0.55
17	<b>2a</b>	250:1:1	<sup>i</sup> PrOH	tol	80	17	91	36.0	26.6	nd	1.08	0.55
18	<b>2a</b>	500:1:1	<sup>i</sup> PrOH	tol	80	17	60	43.2	25.0	nd	1.08	0.56
19	<b>2a</b>	500:1:1	<sup>i</sup> PrOH	tol	80	23	94	67.7	40.3	nd	1.17	0.56
20	<b>3a</b>	100:1:0	-	tol	80	17	50	7.2	16.5	nd	1.12	0.54
21	<b>4a</b>	100:1:0	-	tol	80	4.5	80	11.5	7.2	9.6	1.09	0.55
22	<b>4a</b>	100:1:0	-	tol	80	9.5	95	13.7	8.7	8.8	1.09	0.58
23	<b>4a</b>	100:1:0	-	tol	80	17	100	14.4	9.3	15.1	1.10	0.55
24	<b>4a</b>	500:1:0	-	tol	80	19.5	76	54.7	34.0	nd	1.14	0.55
25	<b>4b</b>	100:1:0	-	tol	25	17	-	-	-	-	-	-
26	<b>4b</b>	100:1:0	-	tol	80	4.5	95	13.7	9.5	9.8	1.04	0.60
27	<b>4b</b>	100:1:0	-	tol	80	17	100	14.4	13.8	9.0	1.19	0.61
28	<b>5a</b>	100:1:0	-	tol	80	3	72	10.4	7.1	6.05	1.07	0.55
29	<b>5a</b>	100:1:0	-	tol	80	10	96	13.8	9.0	8.75	1.11	0.55
30	<b>5a</b>	100:1:0	-	tol	80	17	100	14.4	9.8	9.7	1.2	0.57
31	<b>5a</b>	500:1:0	-	tol	80	17	92	66.3	30.7	nd	1.12	0.53
32	<b>5a</b>	1000:1:0	-	tol	80	22	74	106.7	42.15	nd	1.10	0.55

<sup>a</sup> General conditions: [*rac*-LA] = 2.0 mol.L<sup>-1</sup>. <sup>b</sup> Conversion of lactide as determined by <sup>1</sup>H NMR on the crude reaction mixture. <sup>c</sup>  $M_n$  values calculated considering one polymer chain per metal-center from the relation:  $M_{n,calc} = conv \times [LA]_0/[Al]_0 \times 144$ . <sup>d</sup> Experimental  $M_n$  and

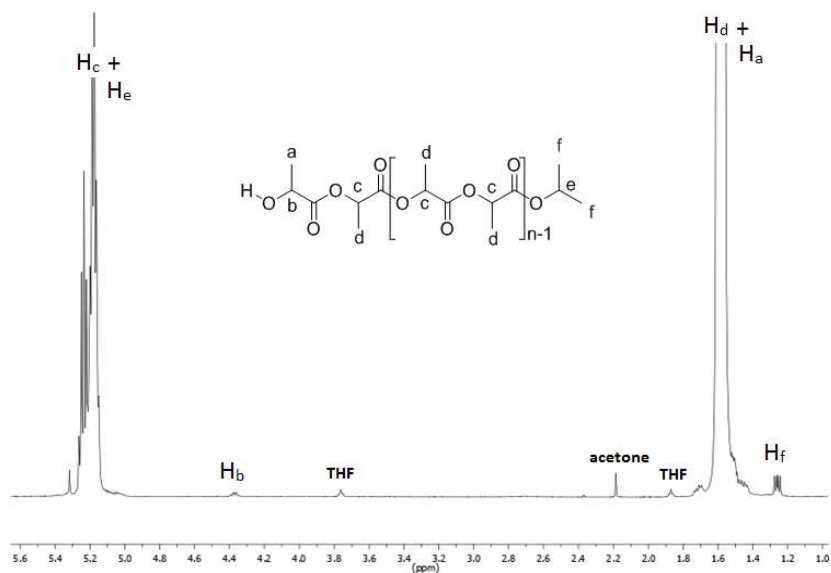
$M_w/M_n$  values determined by GPC in THF vs. PS standards;  $M_n$  values are corrected with a 0.58 factor. <sup>e</sup> Experimental  $M_n$  values determined by <sup>1</sup>H NMR analysis of the reprecipitated polymer. <sup>f</sup>  $P_r$  is the probability of racemic linkage, as determined by <sup>1</sup>H NMR homo-decoupled experiments.

All complexes proved to be active at 80 °C in toluene. The molecular weight distributions were all unimodal, ranging from  $M_w/M_n = 1.06$  to 1.55, indicative of a single-site behavior. When the polymerization was promoted by methyl complex **2a**, without added alcohol, we observed a linear relationship between the monomer-to-metal ratio and the number-average molecular weight ( $M_n$ ) (compare 2, 3, 6 and 7); however the much larger values of  $M_{n,exp}$  as compared to  $M_{n,calc}$  values in those cases indicate a low initiation efficiency (IF = 11-44 %); this is in line with the poor nucleophilicity generally attributed to Al-*Me* moieties. On the other hand, the ROP promoted by **2a** in the presence of 1 equiv. of ROH (to prepare *in-situ* the active species), or with discrete (*S*)-lactate (**4a**) and (*R*)- $\beta$ -alkoxy-butyrate (**5a**) complexes, showed that the molecular weight increases linearly with time and that experimental and calculated  $M_n$  values matched quite well (entries 9-10, 21-23, 28-30). For **4a**, increase of the *rac*-LA loading from 100 to 500 equiv. led to proportionally higher molecular weights PLAs (entries 21, 24). These data illustrate the good degree of control over the polymerization provided by **4a** and **5a**.

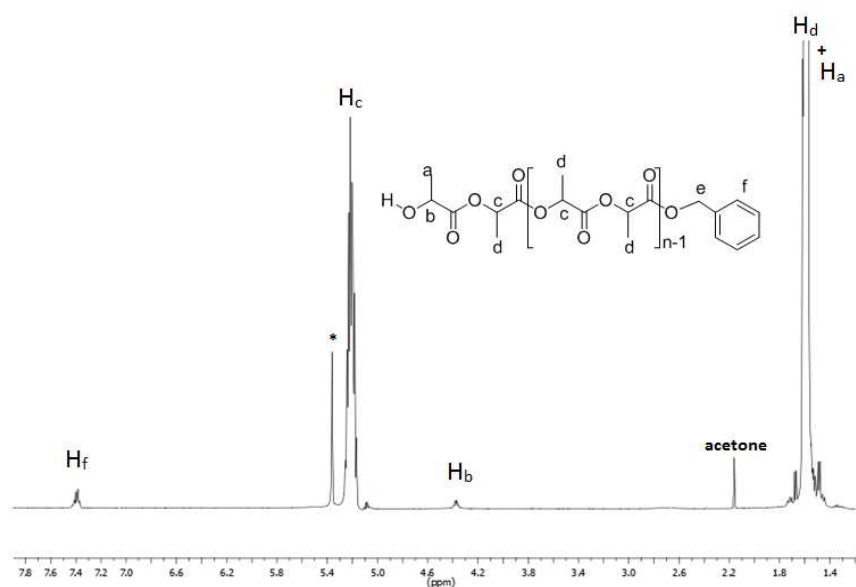
For relatively low molecular weight polymers, the  $M_n$  values were also determined by <sup>1</sup>H NMR spectroscopy (in CDCl<sub>3</sub> or CD<sub>2</sub>Cl<sub>2</sub>), taking into account the polymers end-groups (Figures 43 and 44). These values generally matched quite well the calculated ones.

Surprisingly, we observed quite different conversion and  $M_{n,exp}$  values for the PLAs produced from (i) the Al-isopropoxide species *in situ* generated by adding 1 equiv. of isopropanol to the aluminum methyl complex **2a** and (ii) that obtained from the isolated

isopropoxide complex **3a** (compare the entries 16 and 20). One possible explanation is the existence of dimeric Al-isopropoxide species instead of monomeric ones in the latter case. Indeed, we didn't run DOSY experiments neither get suitable crystals for X-ray diffraction studies in order to understand this polymerization activity of the complex **3a**.



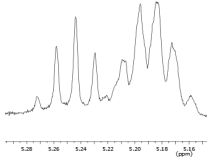
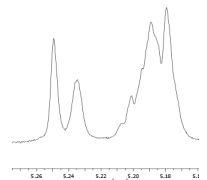
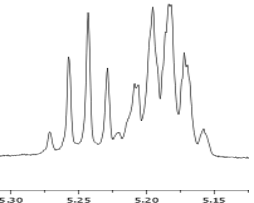
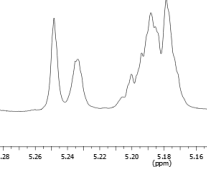
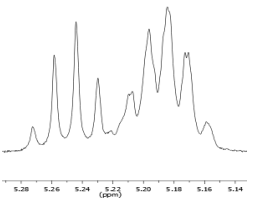
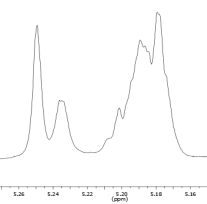
**Figure 43.** <sup>1</sup>H NMR spectrum (500 MHz, CDCl<sub>3</sub>, 298 K) of a poly(lactide) produced from the {ONO<sup>SiPh<sub>3</sub></sup>}AlMe (**2a**)/iPrOH (1:1) system (Table 3, entry 16).



**Figure 44.** <sup>1</sup>H NMR spectrum (500 MHz, CD<sub>2</sub>Cl<sub>2</sub>, 298 K) of a poly(lactide) generated from the {ONO<sup>SiPh<sub>3</sub></sup>}AlMe (**2a**)/BnOH (1:1) system (Table 3, entry 9).

The homo-decoupled  $^1\text{H}$  NMR spectra of the methine region of the PLAs samples derived from **2a/ROH**, **4a** and **4b** in toluene at 80 °C (Table 6) are consistent with the formation of polymer chains that are most predominantly atactic, with a slightly bias toward heterotactic ( $P_r$  max = 0.61, Table 5, entry 27). In striking difference with the series of  $\{\text{ONO}^{\text{SiPh}_3}\}\text{Ln}[\text{N}(\text{SiMe}_2\text{H})_2](\text{THF})$  complexes reported by Grunova *et al.*<sup>91</sup> which led to highly heterotactic enriched PLAs, these aluminum complexes  $\{\text{ONO}^{\text{SiPh}_3}\}\text{Al}(\text{X})$  are less active and do not induce high stereocontrol, despite the smaller ionic radius of Al (for penta-coordinate complexes: Al(III) = 0.48 Å; Sc (III) = 0.745 Å; for six-coordinate complex Y(III) = 0.90 Å).<sup>128</sup>

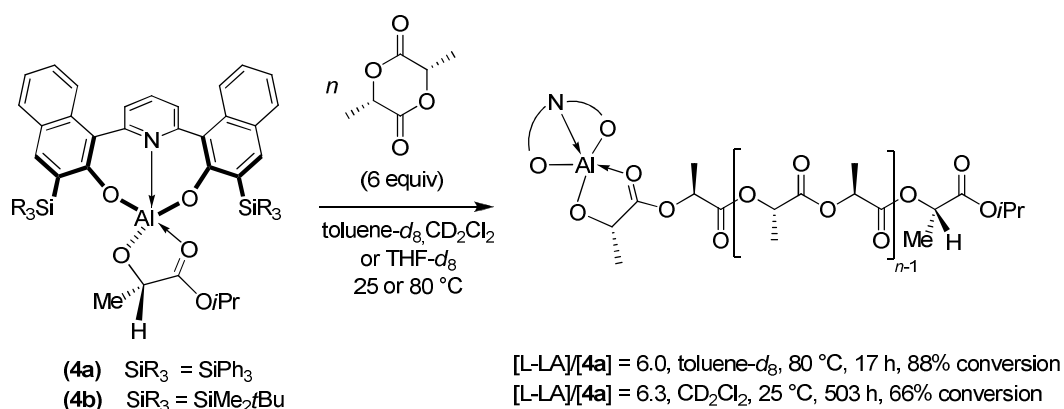
**Table VI:** Methine region of  $^1\text{H}$  NMR and  $^1\text{H}$  homo-decoupled NMR spectra of different PLAs.

Experiment	$^1\text{H}$ NMR	$^1\text{H}\{^1\text{H}\}$ NMR
16		
23		
27		

#### 4.1.4 Reactivity studies and mechanistic considerations on ring-opening polymerization of D-, L- and *rac*-lactide.

##### 4.1.4.1 Studies of the reactivity of Al(III)-(isopropyl (*S*)-lactate) complexes **4a** and **4b**.

Al(III) isopropyl (*S*)-lactate complexes  $\{\text{ONO}^{\text{R}}\}\text{Al}((\text{S})\text{-OCH}(\text{CH}_3)\text{CO}_2i\text{Pr})$  **4a** and **4b** were synthesized as model compounds to get a better understanding of the reactivity of the propagating species. Reactions of (*S*)-**4a** or (*S*)-**4b** with D-, L- and *rac*-lactide monomers in toluene-*d*<sub>8</sub>, CD<sub>2</sub>Cl<sub>2</sub> and THF-*d*<sub>8</sub> were monitored by <sup>1</sup>H NMR spectroscopy (Table 7, Scheme 22).



**Scheme 22.** General Scheme for the Reactions between Al-Isopropyl (*S*) Lactate Complexes (**4a-b**) and L-LA.

**Table VII.** Reactions between D-, L- and *rac*-Lactide Monomers and Complexes (*S*)-**4a** and (*S*)-**4b**.

		toluene- <i>d</i> <sub>8</sub> (25; 80°C)	CD <sub>2</sub> Cl <sub>2</sub> (25°C)	THF- <i>d</i> <sub>8</sub> (25°C)
( <i>S</i> )- <b>4a</b>	<b>L-LA</b>	1.8 to 6.0 equiv.	1.35 to 6.3 equiv.	-
( <i>S</i> )- <b>4a</b>	<b>D-LA</b>	1.1 equiv.	-	-
( <i>S</i> )- <b>4a</b>	<b><i>rac</i>-LA</b>	1.1 equiv.	1.2 equiv.	1.7 equiv.
( <i>S</i> )- <b>4b</b>	<b><i>rac</i>-LA</b>	1.1 equiv.	-	-

A first series of experiments was conducted at room temperature over short reaction times in order to possibly observe intermediates such as monomer adducts. The <sup>1</sup>H NMR

spectrum of a reaction mixture of complex (*S*)-**4a** with 1.1 equiv. of *rac*-LA in toluene-*d*<sub>8</sub> after 30 min at 25 °C showed a split of the resonances for both the methine and methyl groups of the *rac*-LA monomer (each as two broadened quartets). When enantiomerically-pure L-LA (1.8 equiv.) or D-LA (1.1 equiv.) was used instead of *rac*-LA, only one of these resonances was observed (Figure 45). These observations suggest interaction of the monomer with the chiral complex, with formation of possible diastereomeric (*S*,L) and (*S*,D) six-coordinated adducts. Surprisingly yet, at the same time, we did not observe any significant change in the resonance set of the initial complex, indicating minor (if any) changes in the coordination sphere of (*S*)-**4a**, and arguing against coordination of the monomer onto the Al center.

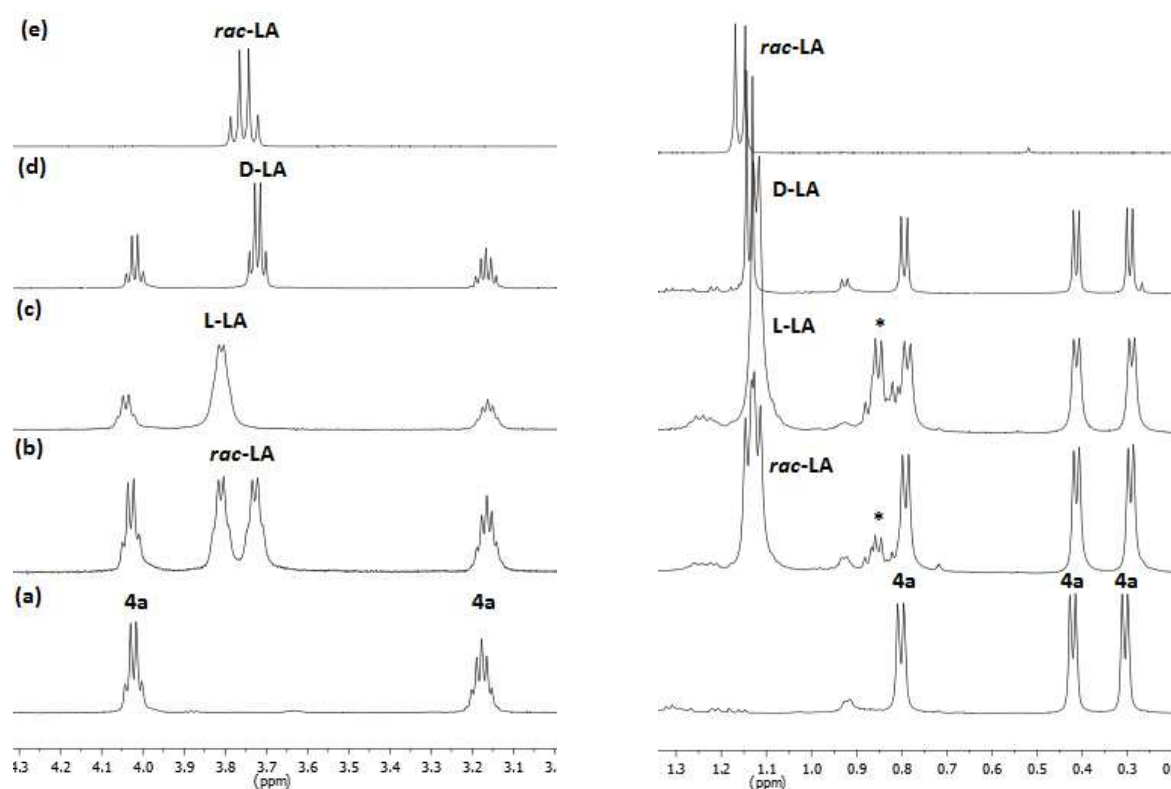


**Figure 45.** Details of the methine (left) and methyl (right) regions of the <sup>1</sup>H NMR spectra (500 MHz, toluene-*d*<sub>8</sub>, 298 K) of (a) (*S*)-**4a**, and mixtures of (*S*)-**4a** with (b) 1.1 equiv. of *rac*-LA, (c) 1.8 equiv. of L-LA, (d) 1.1 equiv. of D-LA, and (e) of *rac*-LA alone (\*stands for residual hexane resonances).



In contrast to the above reaction between **4a** and *rac*-LA, no splitting of the LA methine resonances was observed when we monitored by  $^1\text{H}$  NMR the reaction of a 1:1.1 mixture of (*S*)-**4b**/*rac*-LA (Figure 46). It is worth noting that the only difference between these two systems, **4a** vs. **4b**, lies in the  $\text{SiPh}_3$  vs.  $\text{Si}i\text{BuMe}_2$  substituent. These observations suggest that the lactide enantiomers may interact with the phenyl groups of the  $\text{SiPh}_3$  substituents in the “second-coordination” sphere of the Al complex. Also, it may suggest that the  $\text{C-H}\cdots\pi$  interactions observed in the solid state persist in solution and play a role in the differentiation of the two enantiomers of lactide; anyway, the exact nature of those likely weak interactions observed in solution remain obscure thus far.

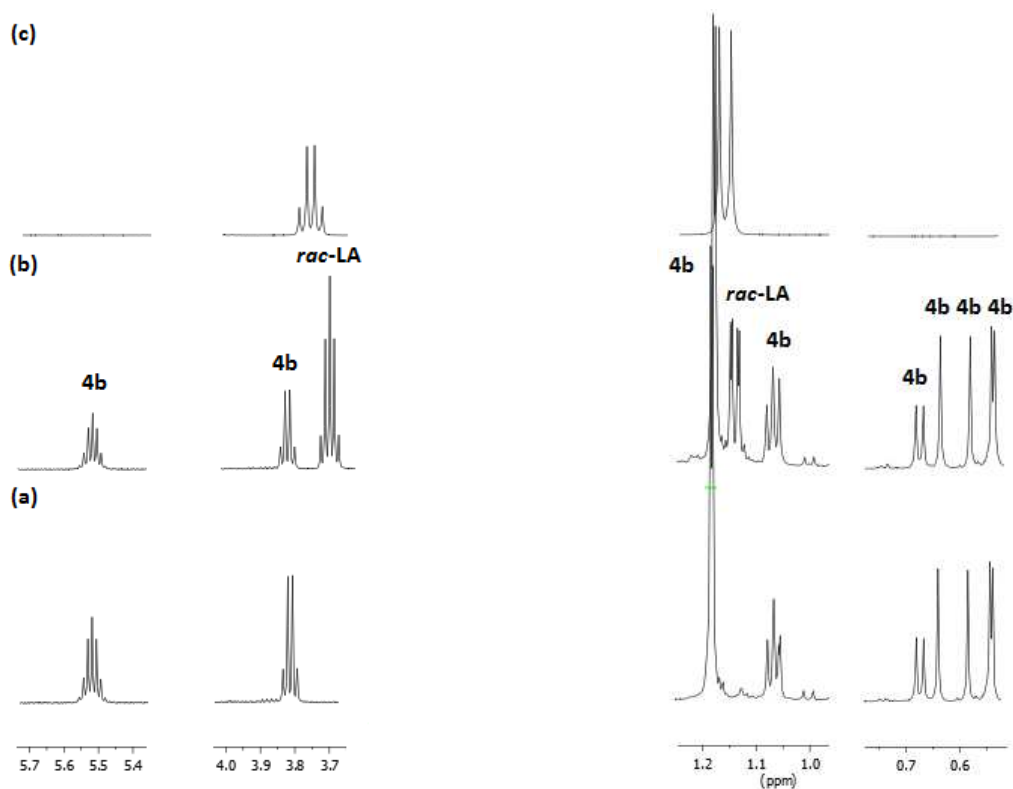


**Figure 46.** Details of the  $^1\text{H}$  NMR spectra (500 MHz, toluene- $d_8$ , 298 K) (a) (*S*)-**4b**, (b) a 1:1.1 (*S*)-**4b**/*rac*-LA reaction mixture after 30 min at 25 °C, and (d) *rac*-LA.

When the  $^1\text{H}$  NMR spectra of such mixtures were recorded in THF- $d_8$  or  $\text{CD}_2\text{Cl}_2$  instead of toluene- $d_8$ , the split of the LA methine resonances in the (*S*)-**4a**/*rac*-LA (1:1.2 or 1:1.7) mixture was not observed, only minor splitting of the LA methyl resonances was observed in  $\text{CD}_2\text{Cl}_2$  or THF- $d_8$  (Figures 47 and 48, respectively).

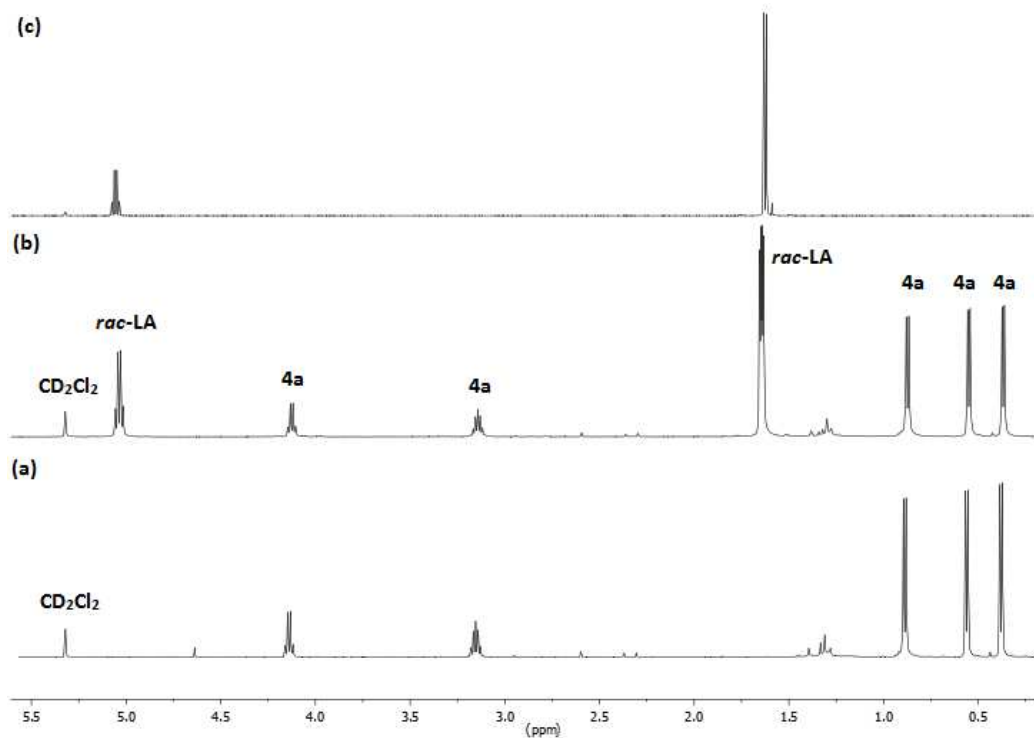


**Figure 47.** Details of the  $^1\text{H}$  NMR spectra (500 MHz,  $\text{CD}_2\text{Cl}_2$ , 298 K) of (a) (*S*)-**4a**, (b) a 1:1.2 (*S*)-**4a**/*rac*-LA mixture, and (c) *rac*-LA.

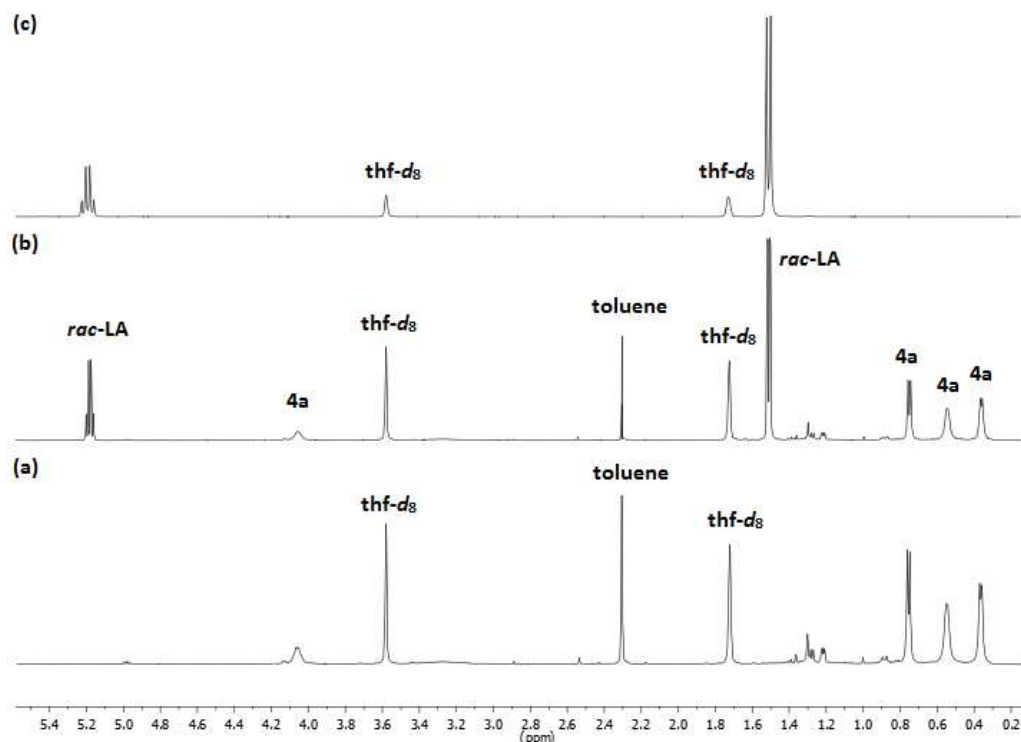


**Figure 48.** Details of the <sup>1</sup>H NMR spectra (500 MHz, THF-*d*<sub>8</sub>, 298 K) (a) (*S*)-**4a**, (b) a 1:1.7 mixture of (*S*)-**4a** and *rac*-LA, and (c) *rac*-LA.

Monitoring of the propagation step was attempted by <sup>1</sup>H NMR spectroscopy in CD<sub>2</sub>Cl<sub>2</sub> in which the polymerization reaction proceeded slowly at room temperature. Selected spectra of a 1:6.26 reaction mixture of (*S*)-**4a**/L-LA, recorded over a time period of 503 h with a final 66% conversion of L-LA, are shown in Figures 49-51. In the early stage, resonances for (*S*)-**4a** (*C-H* quartet and CH<sub>3</sub> doublet related to the chiral center (δ 4.16 and δ 0.9 ppm), the -OCHMe<sub>2</sub> septet at δ 3.19 and -OCH(CH<sub>3</sub>)<sub>2</sub> doublets at δ 0.59 and δ 0.41 ppm), and for the non-consumed monomer (the methine *C-H* resonance visible as a quartet at δ 5.09) were observed. As the polymerization started, these resonances progressively were replaced by a new set of resonances assignable to propagating species. These include a broad resonance at δ 5.2 ppm, assigned to the methine of propagating PLA oligomers, as confirmed by <sup>13</sup>C, <sup>1</sup>H-<sup>1</sup>H COSY, <sup>13</sup>C-<sup>1</sup>H HMQC and <sup>13</sup>C-<sup>1</sup>H HMBC NMR experiments (*see the Annexes*).

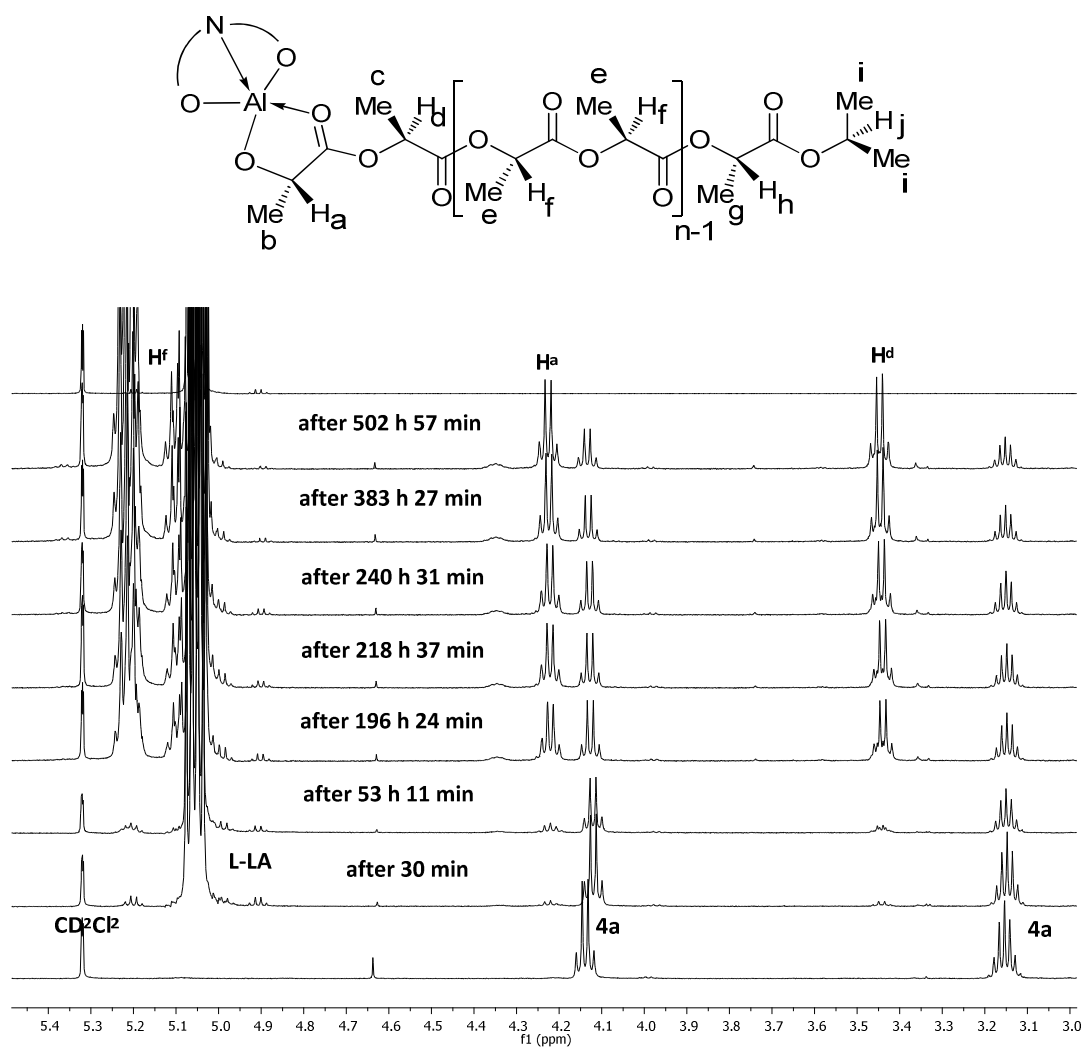


**Figure 49.** Details of the low-field aliphatic region of the  $^1H$  NMR spectra (500 MHz,  $CD_2Cl_2$ , 298 K) of a 1:6.26 mixture of (*S*)-**4a** and L-LA kept at 25 °C. The bottom spectrum is that of pure (*S*)-**4a**.

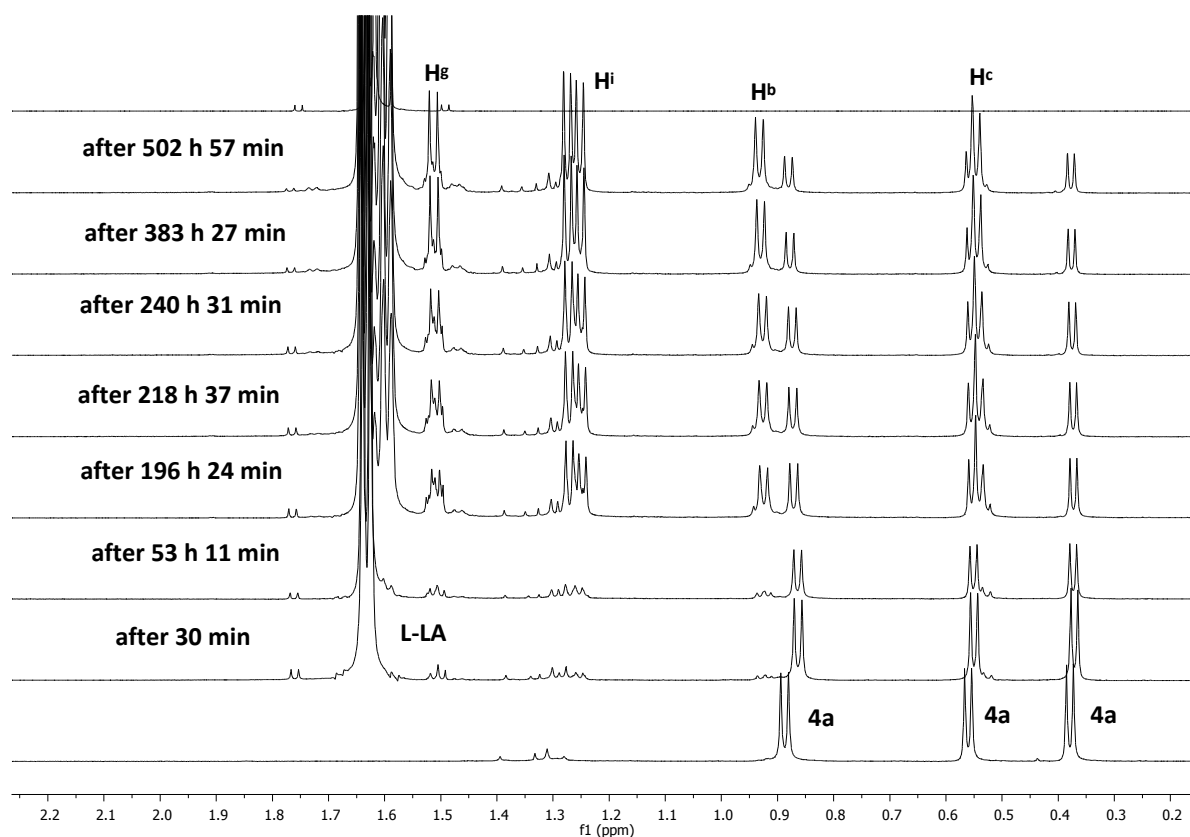


**Figure 50.** Details of the high-field aliphatic region of the  $^1\text{H}$  NMR spectrum (500 MHz,  $\text{CD}_2\text{Cl}_2$ , 298 K) of a 1:6.26 mixture of **4a** and L-LA kept at 25 °C. The bottom spectrum is that of pure **4a**.

The reaction of a 1:6 mixture of (*S*)-**4a**/L-LA in toluene- $d_8$  at 80 °C for 17 h, giving a final 88% conversion of L-LA, was monitored by  $^1\text{H}$  NMR (Figure 52). We could observe in the  $^1\text{H}$  NMR spectrum in toluene- $d_8$ , the resonance of the  $\text{CO}_2i\text{Pr}$  end-group,  $\text{H}_j$ , as a septet at  $\delta$  4.84 ppm; the corresponding doublet resonances are observed at  $\delta$  0.94 and 0.91 ppm. The observation of ester chain termini implies that ring-opening of the cyclic ester monomer occurs via cleavage of an acyl-oxygen bond, as proposed for metal-alkoxide initiating systems.<sup>106</sup>

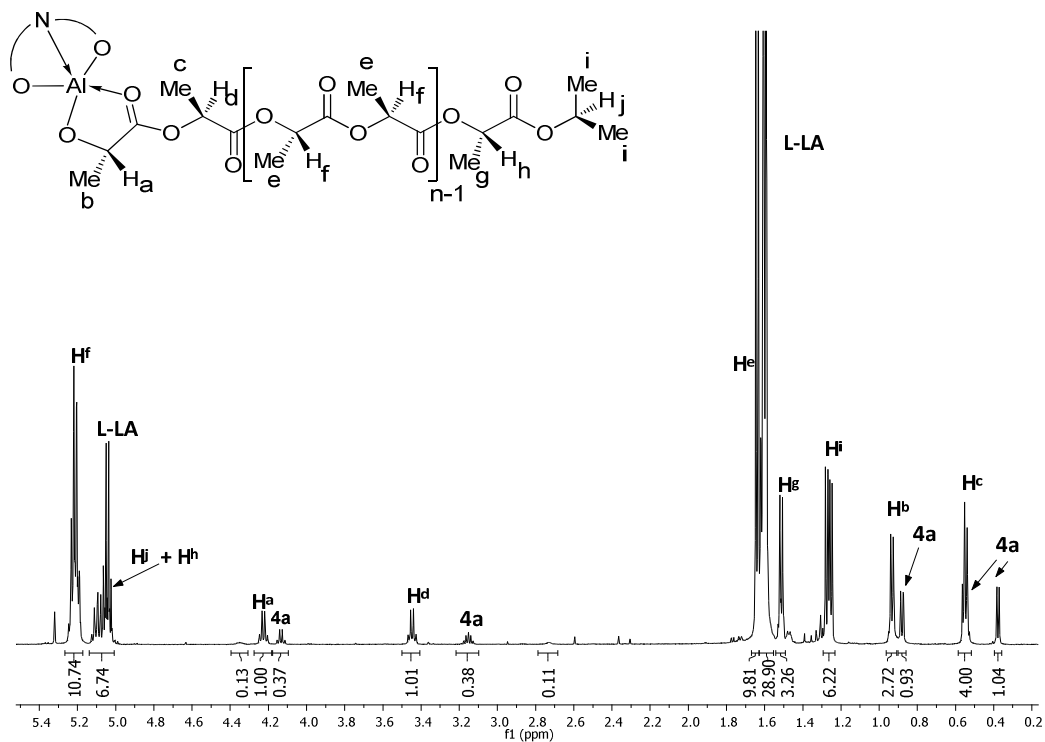


**Figure 51.** Detail of the aliphatic region of the  $^1\text{H}$  NMR spectrum (500 MHz,  $\text{CD}_2\text{Cl}_2$ , 298 K) of a 1:6.26 **4a**/L-LA mixture after 503 h at 25 °C (66% conversion of L-LA).

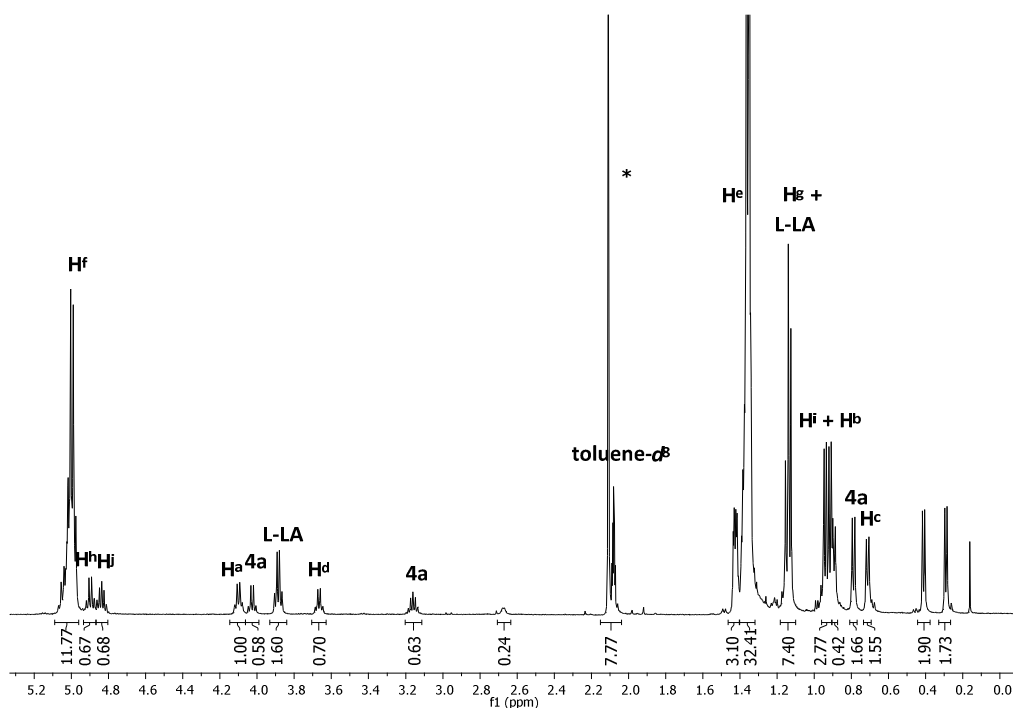


**Figure 52.** Detail of the aliphatic region of the  $^1\text{H}$  NMR spectrum (500 MHz,  $\text{toluene-}d_8$ , 298 K) of the reaction mixture **4a**/L-LA (1:6 equiv.) after 17 h at 80 °C (88% conversion of L-LA) (\*stands for residual solvent resonances).

The conversion of L-lactide by complex (*S*)-**4a** as a function of time was monitored by <sup>1</sup>H NMR spectroscopy (Tables 8 and 9, Figures 53 – 56). A pseudo first-order kinetics in monomer was observed, with  $k_{app} = 3.6 \times 10^{-5} \text{ min}^{-1}$  (in CD<sub>2</sub>Cl<sub>2</sub> at 25 °C) and  $6 \times 10^{-4} \text{ s}^{-1}$  or  $3.6 \times 10^{-2} \text{ min}^{-1}$  (in toluene-*d*<sub>8</sub> at 80 °C). Further studies should be extended to L, D and *rac*-Lactide in order to better understand the kinetics of the polymerization.

**Table VIII.** Kinetic monitoring (<sup>1</sup>H NMR) of the reaction mixture of **4a**/L-LA (1:6.26) in CD<sub>2</sub>Cl<sub>2</sub> at 25 °C.

t (h)	Conv. <sup>a</sup> (%)	[LA] <sub>t</sub>	[LA] <sub>0</sub> /[LA] <sub>t</sub>	ln [LA] <sub>0</sub> /[LA] <sub>t</sub>
0	0	0.3932	1.0000	0.0000
53 h 11 min	2.5	0.3833	1.0261	0.0258
196 h 24 min	29	0.2791	1.4132	0.3458
218 h 37 min	33	0.2634	1.4937	0.4012
240 h 31 min	39	0.2398	1.6389	0.4940
383 h 27 min	57	0.1691	2.3366	0.8487
502 h 57 min	66	0.1337	2.9500	1,0818

<sup>a</sup>Conversion of L-LA as determined from the intensities of methyl resonances of L-LA and those of oligomers.

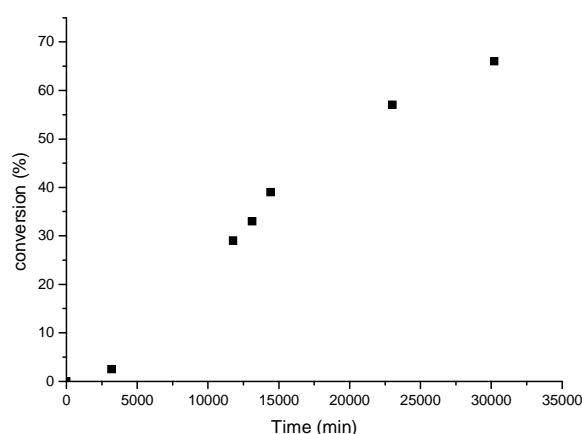


**Figure 53.** Plot of L-LA conversion vs. time for the reaction mixture of **4a**/L-LA (1:6.26) in CD<sub>2</sub>Cl<sub>2</sub> at 25 °C, [LA]<sub>0</sub> = 0.3932 mol.L<sup>-1</sup>.

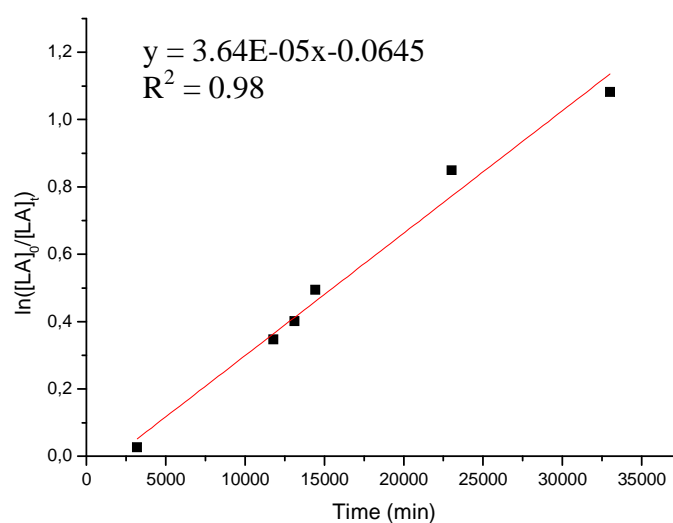


**Figure 54.** Semi-logarithmic plot of L-LA conversion vs. time initiated by complex (S)-**4a** (25 °C, CD<sub>2</sub>Cl<sub>2</sub>, [LA]<sub>0</sub> = 0.3932 mol.L<sup>-1</sup>).

**Table IX.** Kinetic monitoring (<sup>1</sup>H NMR) of the reaction of **4a**/L-LA (1:5) mixture in toluene-*d*<sub>8</sub> at 80 °C.

t (s)	Conv <sup>a</sup> (%)	[LA] <sub>t</sub>	[LA] <sub>0</sub> /[LA] <sub>t</sub>	ln [LA] <sub>0</sub> /[LA] <sub>t</sub>
0	0	0.269	1.000	0.000
288	1	0.266	1.011	0.011
790	8	0.247	1.011	0.011
1292	21	0.212	1.269	0.238
1794	38	0.167	1.611	0.477
2356	53	0.126	2.135	0.758
2798	66	0.091	2.956	1.084
3300	77	0.062	4.339	1.468
3802	83	0.046	5.848	1.766
4304	87	0.035	7.686	2.039
4806	93	0.019	14.158	2.650
5307	93	0.019	14.158	2.650
5809	93	0.019	14.158	2.650

<sup>a</sup>Conversion of L-LA as determined from the intensities of methyl resonances of L-LA and those of oligomers.



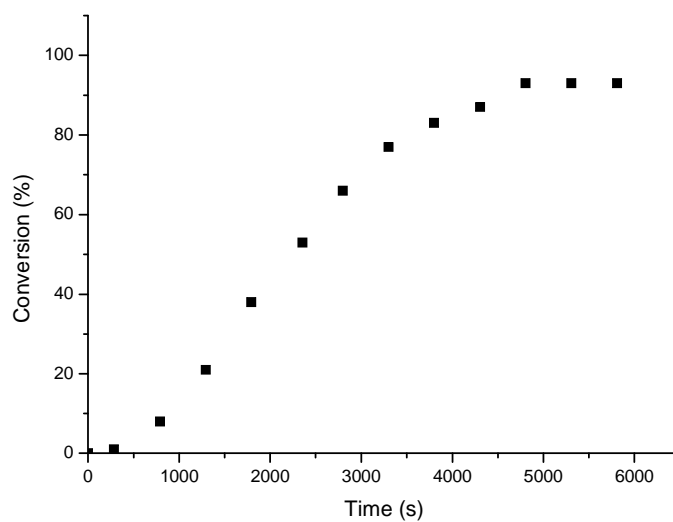


**Figure 55.** Plot of L-LA conversion vs. time for the reaction mixture of **4a**/L-LA (1:5) at 80 °C in toluene- $d_8$ ,  $[LA]_0 = 0.269 \text{ mol.L}^{-1}$ .

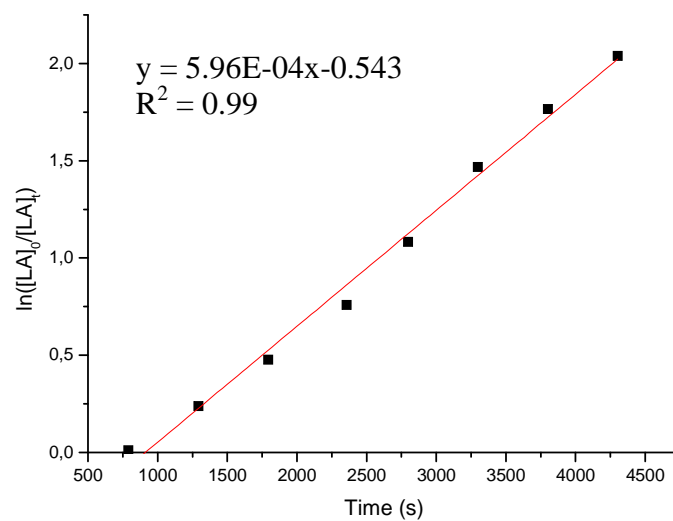
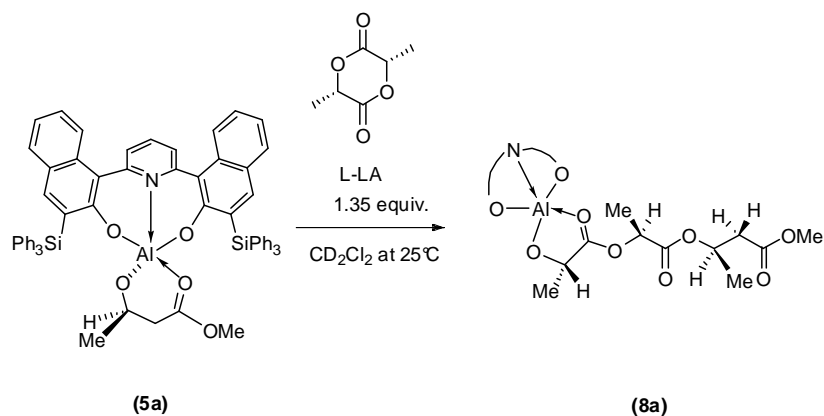


**Figure 56.** Semi-logarithmic plot of L-LA conversion vs time initiated by complex (*S*)-**4a** (80 °C, toluene- $d_8$ ,  $[LA]_0 = 0.269 \text{ mol.L}^{-1}$ ).

#### 4.1.4.2 Studies of the reactivity of Al(III)-(methyl (*R*)- $\beta$ -alkoxy-butyrates) complex **5a**.

In attempts to catch the first insertion product, we monitored by  $^1\text{H}$  NMR spectroscopy the room temperature reaction of a 1:1.35 mixture of (*R*)-**5a**/L-LA in  $\text{CD}_2\text{Cl}_2$ . NMR spectra were recorded over a period of 12 days (Scheme 23). Note that this monitoring could not be performed in toluene due to the very poor solubility of **5a** in this solvent.



**Scheme 23.** Reaction between 1 equiv of Al-(methyl (*R*)- $\beta$ -alkoxy-butyrates) (**5a**) and 1.35 equiv of L-LA giving the product of the first insertion of the LA molecule (**8a**).

In the early stages of the reaction, resonances for **5a** (C-H multiplet and  $\text{CH}_3$  doublet related to the chiral center ( $\delta$  3.44 and 0.6 ppm), the -OMe singlet at  $\delta$  2.51 ppm and the -CHH two doublet of doublet for diastereotopic methylenic protons ( $\delta$  1.42 and 1.19 ppm), and for unconsumed monomer (the methine C-H resonance visible as a quartet at  $\delta$  5.04 ppm) were observed (Figure 57). After 23 h, these resonances decreased in intensity and were replaced by a set of resonances assignable to the first insertion product. The resonance for the methoxycarbonyl fragment was shifted significantly downfield ( $\Delta\delta = 1.19$  ppm) from that in **5a**; the same trend was observed for the two doublets of doublet of the methylene group ( $\Delta\delta = 1.31$  ppm) (Figure 58). Prolonging the reaction over 23 h resulted in the formation of a second species that built up with time. To better visualize the presence of this second species, the  $^1\text{H}$  NMR spectrum of the reaction after 21 days is shown in Figure 59. We suspect that this new species may be the product of intra- or intermolecular side reactions.

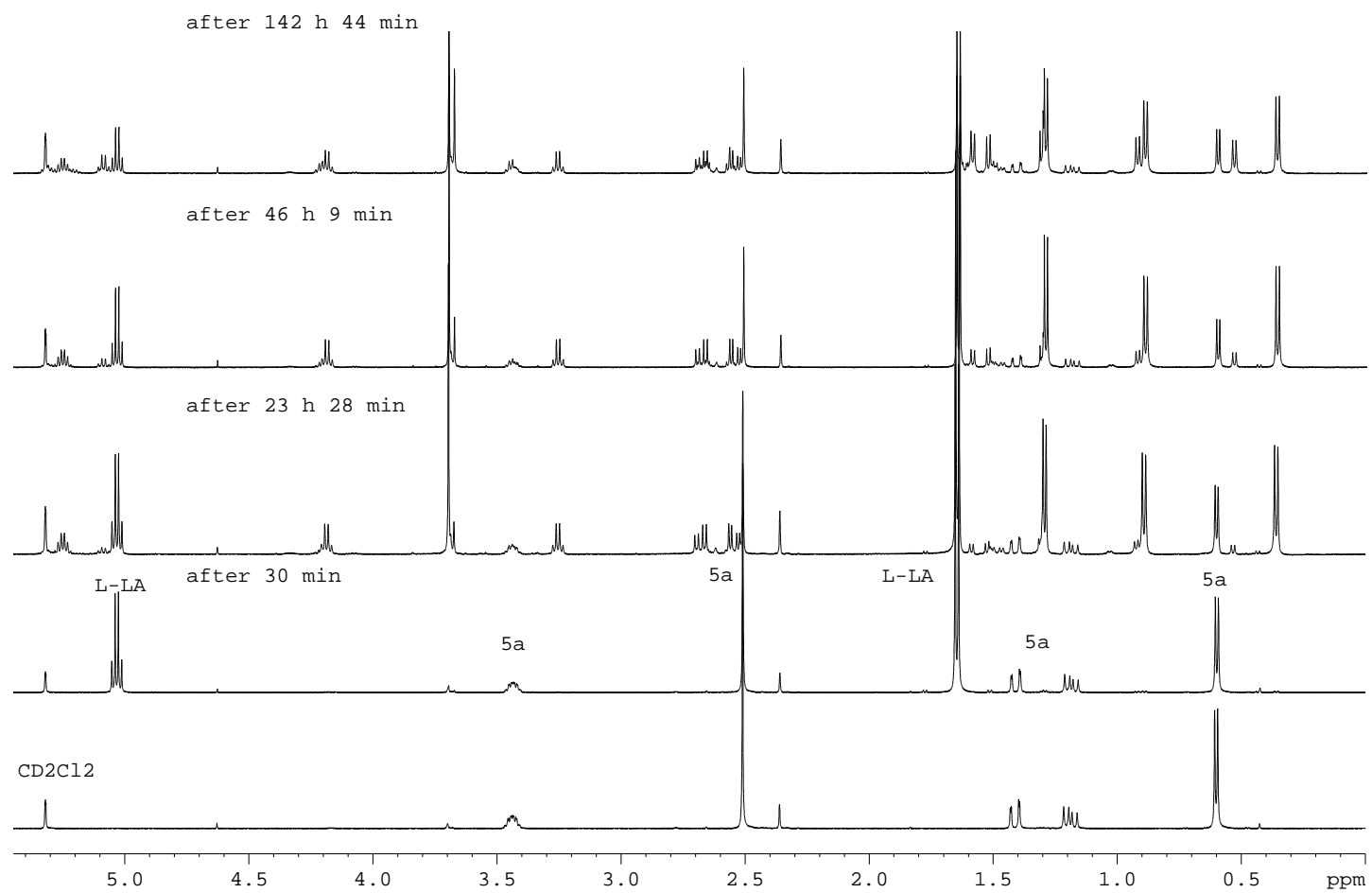


**Figure 57.**  $^1\text{H}$  NMR monitoring (500 MHz,  $\text{CD}_2\text{Cl}_2$ , 298 K) of the reaction of a 1:1.35 mixture of (*R*)-**5a** and L-LA in  $\text{CD}_2\text{Cl}_2$  at 25 °C (\* stands for residual solvent resonances). The bottom spectrum is that of pure (*R*)-**5a**.

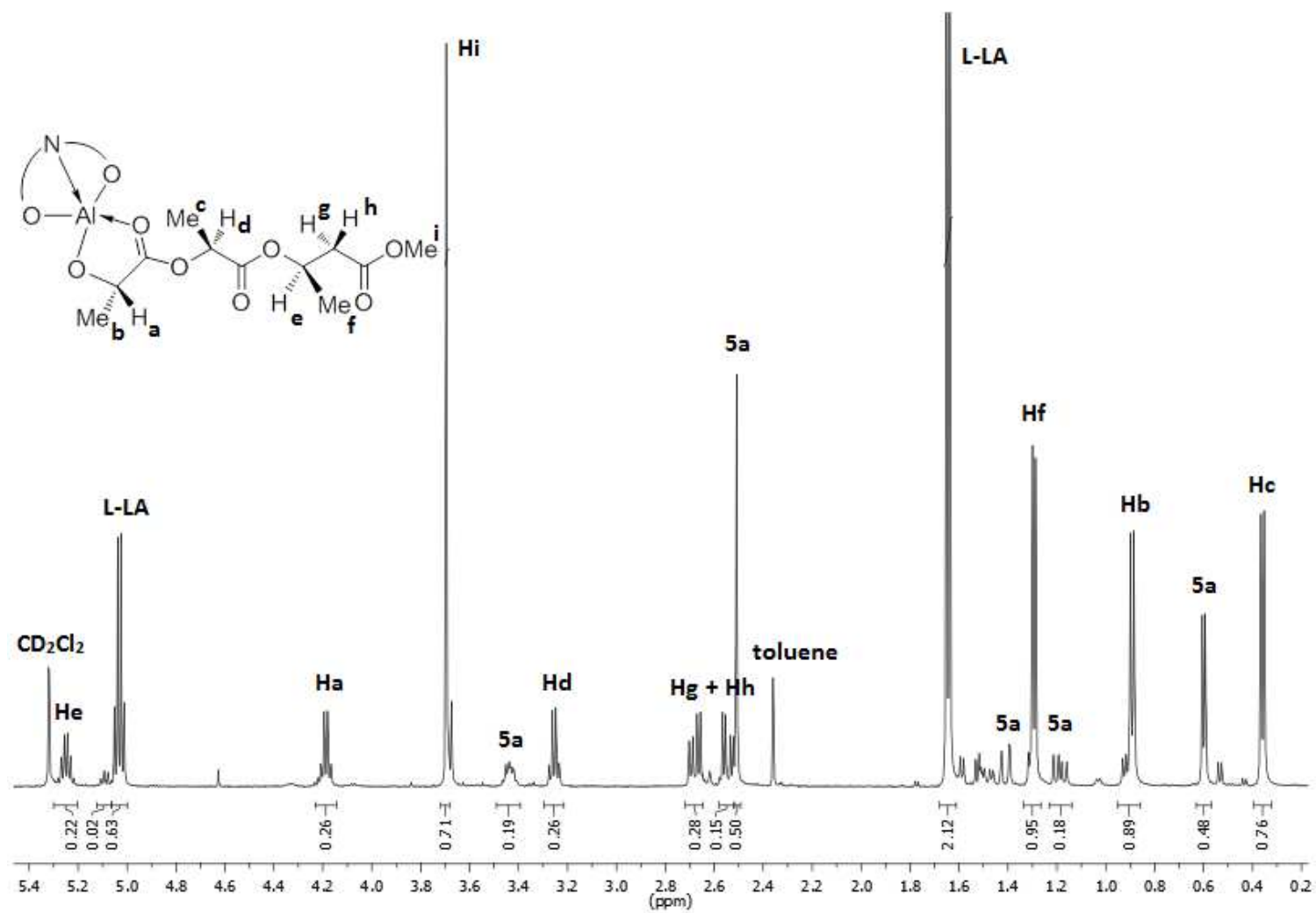


**Figure 58.** <sup>1</sup>H NMR spectrum (500 MHz, CD<sub>2</sub>Cl<sub>2</sub>, 298 K) of the 1:1.35 reaction of a mixture of (*R*)-**5a** and L-LA after 23 h at 25 °C (\* stands for residual solvent resonances).

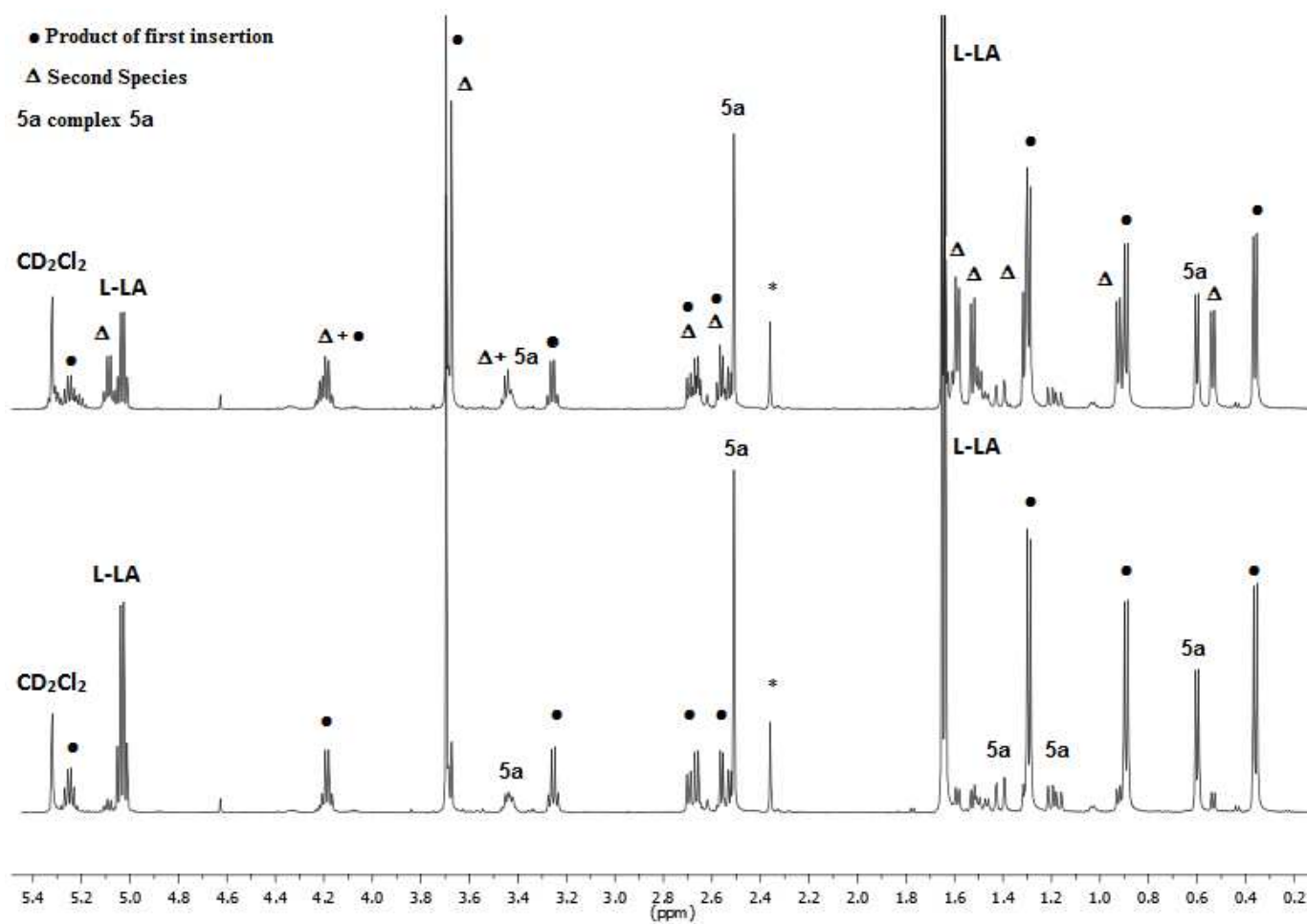


**Figure 59.**  $^1\text{H}$  NMR spectra (500 MHz,  $\text{CD}_2\text{Cl}_2$ , 298 K) of the 1:1.35 reaction of a mixture of (*R*)-**5a** and L-LA after (bottom) 23 h and (top) 21 days at 25 °C (\* stands for residual solvent resonances).

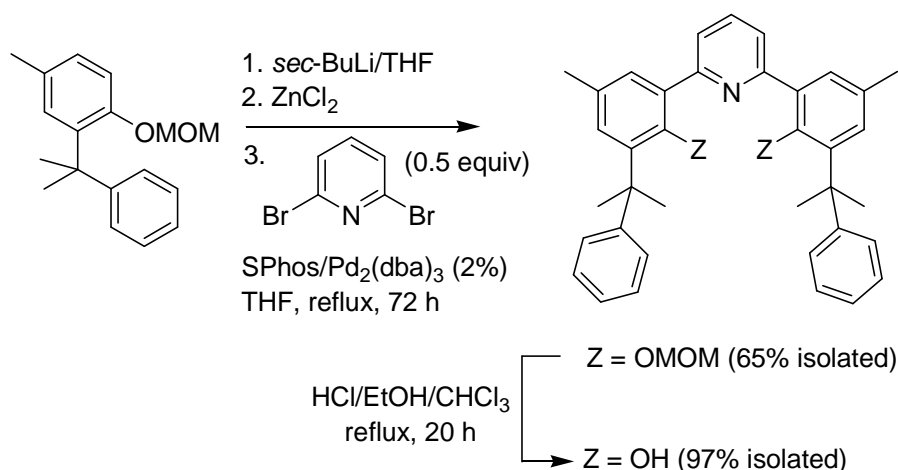
## 4.2 Well-defined Al- and Y- Complexes Bearing a Tridentate Cumyl Ortho-Substituted Bis(phenoxy)pyridine ligand.

This section addresses a different issue in the ROP of *rac*-lactide and *rac*-BBL in bis(phenolate)-metal systems, which is the origin of the stereoselectivity. Preliminary experimental and computational works in the group of Jean-François Carpentier have suggested that the presence of aryl substituents on the phenolate rings may play a significant role in this stereocontrol, via weak attractive C-H... $\pi$  interactions between those aryl groups and C-H moieties of the monomer moieties in the growing polymer chain.<sup>89</sup>

Accordingly, the aim of this work was to prepare a series of well-defined Al- and Y-complexes supported by tridentate pyridine-bis(phenolate) ligands having cumyl substituents and to assess the exact nature of interactions between those substituents and  $\alpha$ - or  $\beta$ - alkoxy esters moieties coordinated onto the metal center. The latter  $\alpha$ - or  $\beta$ - alkoxy ester units have been selected to mimic the last monomer unit inserted in the growing polymer chain in the ROP of lactide and  $\beta$ -butyrolactone.

### 4.2.1 Preparation of the new pro-ligand {ONO<sup>Me,Cumyl</sup>}H<sub>2</sub>

The preparation of the new diprotio pro ligand {ONO<sup>Me,Cumyl</sup>}H<sub>2</sub> was successfully achieved starting from the methoxymethyl-protected 2-cumyl-4-methyl-phenol, followed by Negishi cross-coupling reaction using a Pd-Phos catalyst, in a similar synthetic protocol as previously described for those 2,6-bis(naphthol)pyridine pro-ligands (Scheme 24).<sup>113</sup>



**Scheme 24.** Preparation of Pro-Ligand {ONO<sup>Me,Cumyl</sup>}H<sub>2</sub> (**1c**).

Pro-ligand {ONO<sup>Me,Cumyl</sup>}H<sub>2</sub> was recovered in 65 % yield as a colorless, crystalline compound soluble in polar solvents as (CHCl<sub>3</sub>, CH<sub>2</sub>Cl<sub>2</sub>, THF) and in toluene at 80 °C, but sparingly soluble at room temperature. This compound was characterized by <sup>1</sup>H and <sup>13</sup>C NMR spectroscopy. The NMR spectra (*see the Annexes*) at 25 °C in CDCl<sub>3</sub> show single sets of resonances. Crystallographic data and structural determination details for **1c** are summarized in Table 1A (*see the Annexes*).

Single crystals suitable for X-ray diffraction studies were successfully prepared by crystallization from dichloromethane. The molecule of pro-ligand **1c** adopts in the solid state an approximated (noncrystallographic) C<sub>2</sub> symmetry, in which the phenol groups are twisted from the pyridine plane in the opposite directions (Figure 60). The short distance of 3.412 Å between the oxygen atoms in **1c** apparently results from the small torsion angles of 23.55 and 23.21° between the planes of the pyridine unit and the phenol fragments.

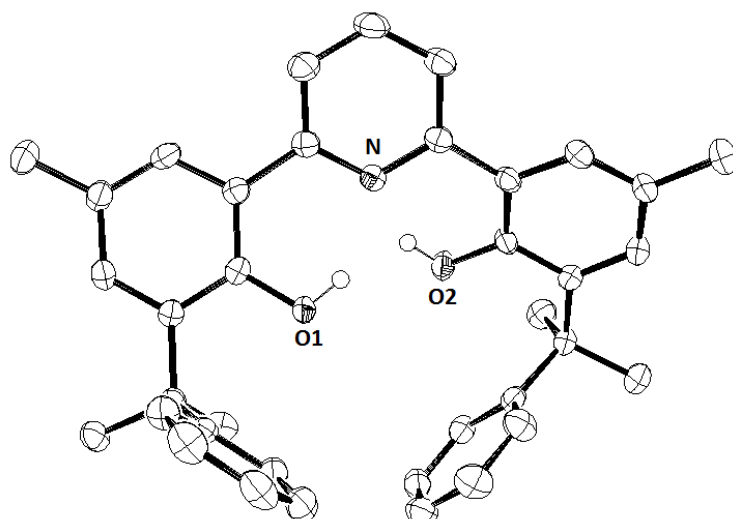
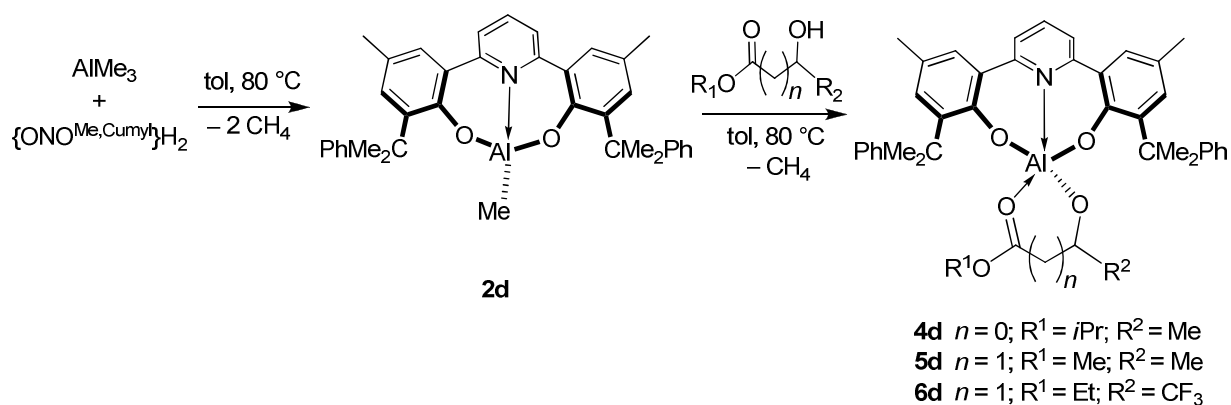


**Figure 60.** Molecular structure of pro-ligand  $\{\text{ONO}^{\text{Me,Cumyl}}\}\text{H}_2$  (all hydrogens atoms, except those of hydroxyl groups, are omitted for clarity; thermal ellipsoids drawn at 50 % probability). Selected bond distances (Å) and angles (deg):  $\text{H}(\text{O}(1))\text{-N} = 1.919$ ;  $\text{H}(\text{O}(2))\text{-N} = 1.985$ ;  $\angle \text{Py-Ph}(1) = 23.55$ ;  $\angle \text{Py-Ph}(2) = 23.21$ .

#### 4.2.2 Preparation of $\{\text{ONO}^{\text{Me,Cumyl}}\}\text{AlOR}$ ( $\text{R} = \text{Me}$ , **2d**; (*S*)- $\text{CH}(\text{Me})\text{CO}_2i\text{Pr}$ , **4d**; (*R*)- $\text{CH}(\text{Me})\text{CH}_2\text{CO}_2\text{Me}$ , **5d**; (*rac*)- $\text{CH}(\text{CF}_3)\text{CH}_2\text{CO}_2\text{Et}$ , **6d**).

In the previous section, we described the synthesis and the structure characterization of silyl *ortho*-substituted tridentate 2,6-bis(naphtholate)pyridine Al(III) complexes. These compounds were tested in the ROP of *rac*-lactide showing good control over the polymerization. Also, structural investigations revealed short contacts between the  $\pi$ -system of one of the phenyl substituents of the naphtholate groups and C-H of the isopropyl group of the lactate substituent (for **4a**) and C-H of the methylenic and methyl groups of the butyrate fragment (for **5a**). Seeking for better insights into such type of interactions, we prepared complexes **4d**, **5d** and **6d** (Scheme 25) supported by the tridentate ligand  $(\text{ONO}^{\text{Me,Cumyl}})^{2-}$ .





**Scheme 25.** Synthesis of Aluminum Complexes (**2-6**) Supported by the  $\{\text{ONO}^{\text{Me,Cumyl}}\}^{2-}$  Ligand.

Complex **2d** was synthesized by heating at 80 °C of a toluene solution of the pro-ligand  $\{\text{ONO}^{\text{Me,Cumyl}}\}\text{H}_2$  with 1.4 equiv. of  $\text{AlMe}_3$  (*vide supra*, Scheme 7); and isolated as an air- and moisture-sensitive colorless crystals in 77 % yield. This product is soluble in polar solvents as  $\text{CH}_2\text{Cl}_2$  at room temperature and in aromatic hydrocarbons (benzene, toluene) at 60 °C. The identity of **2d** was established on the basis of  $^1\text{H}$  and  $^{13}\text{C}$  NMR spectroscopy (*see the Annexes*).

Aluminum derivatives of lactate (**4d**) and  $\beta$ -alkoxy-butyrate (**5d** and **6d**) were prepared by methane elimination from the reaction of **2d** with 1 equiv. of the corresponding hydroxy-ester ((*S*)- $\text{CH}(\text{Me})\text{CO}_2iPr$ , **4d**; (*R*)- $\text{CH}(\text{Me})\text{CH}_2\text{CO}_2\text{Me}$ , **5d**; (*rac*)- $\text{CH}(\text{CF}_3)\text{CH}_2\text{CO}_2\text{Et}$ , **6d**) (*vide supra*, Scheme 7). The reactions proceeded at 80 °C in toluene to afford complexes **4d-6d**, as air-sensitive, colorless solids, isolated in 80 % (for **4d**). Complexes **4d-6d** were characterized in solution by NMR spectroscopy (*see the Annexes*). It was not possible to purify the complex **5d** for the use in polymerization. In an attempt made to purify the complex **5d**, small amounts of crystals were successfully isolated; crystals suitable for X-Ray diffraction studies were grown from concentrated  $\text{CD}_2\text{Cl}_2$  solution layered by hexane at room temperature. The main crystallographic details are reported in Table 1A

(see the Annexes). The molecular structure of **5d**, and selected bond distances and angles for this compound are given in Figure 61.

The  $^1\text{H}$  and  $^{13}\text{C}\{^1\text{H}\}$  NMR data for the aluminum(III) (*S*)-lactate (**4d**) and (*R*)- and (*rac*)- $\beta$ -alkoxy-butyrates (**5d**, **6d**) complexes in toluene- $d_8$  and  $\text{CD}_2\text{Cl}_2$ , at room temperature, are indicative of the existence of a single  $C_1$ -symmetric species. In the spectrum of the  $^1\text{H}$  NMR of complex **4d**, the resonances for the isopropyl (*S*)-lactate group were observed as a quartet for the methine  $\text{OCH}(\text{CH}_3)\text{CO}_2i\text{Pr}$  ( $\delta$  4.00 ppm), a septet for the other methine  $\text{OCH}(\text{CH}_3)\text{CO}_2\text{CH}(\text{CH}_3)_2$  ( $\delta$  5.37 ppm), a doublet for the methyl group associated with the chiral center ( $\text{OCH}(\text{CH}_3)\text{CO}_2i\text{Pr}$ ) ( $\delta$  0.91 ppm), and two doublets overlapped for the non-equivalent methyl  $\text{OCH}(\text{CH}_3)\text{CO}_2\text{CH}(\text{CH}_3)_2$  ( $\delta$  1.12 ppm).

It is worth to note that, there is a significant difference in the chemical shifts for the methine resonance of the isopropyl group among the three aluminum (*S*)-lactate complexes, observed at  $\delta$  3.17,  $\delta$  5.52 and  $\delta$  5.37 ppm for **4a**, for **4b** and **4d**, respectively.

In the  $^1\text{H}$  NMR spectrum of **5d** in  $\text{CD}_2\text{Cl}_2$ , the resonances for the (*R*)- $\beta$ -alkoxy-butyrates group were observed as a multiplet and a doublet for the methine and methyl hydrogens, respectively, associated to the chiral center ( $\text{OCH}(\text{Me})\text{CH}_2\text{CO}_2\text{Me}$ ,  $\delta$  3.47 ppm;  $\text{OCH}(\text{CH}_3)\text{CH}_2\text{CO}_2\text{Me}$ ,  $\delta$  0.65 ppm), one doublet of doublet for the diastereotopic methylene hydrogens ( $\text{OCH}(\text{Me})\text{CHHCO}_2\text{Me}$ ,  $\delta$  1.95 ppm; the second would be overlapped), and a single resonance for the methyl ester group ( $\text{OCH}(\text{Me})\text{CH}_2\text{CO}_2\text{CH}_3$ ,  $\delta$  3.91 ppm). In comparison with the complex (*R*)-**5a**, the resonance for the methyl ester group is significantly shielded ( $\text{OCH}(\text{Me})\text{CH}_2\text{CO}_2\text{CH}_3$ ,  $\delta$  2.51 ppm).

In the  $^1\text{H}$  NMR spectrum of **6d** in  $\text{CD}_2\text{Cl}_2$  the resonances for the fluorinated *rac*- $\beta$ -alkoxy-butyrates group were observed as a multiplet for the methine hydrogen ( $\text{OCH}(\text{CF}_3)\text{CH}_2\text{CO}_2\text{Et}$ ,  $\delta$  3.56 ppm), two doublets of doublet for the diastereotopic methylene

hydrogens ( $\text{OCH}(\text{CF}_3)\text{CHHCO}_2\text{Et}$ ,  $\delta$  1.99 and  $\delta$  1.85 ppm), two multiplets for the diastereotopic methylene hydrogens of the ethyl ester group ( $\text{CO}_2\text{CHHCH}_3$ ) ( $\delta$  4.35 ppm, overlapped), and a triplet for the methyl group ( $\text{OCH}(\text{CF}_3)\text{CH}_2\text{CO}_2\text{CH}_2\text{CH}_3$ ,  $\delta$  1.49 ppm). In comparison with the bis(naphtholate)  $\text{Al}((rac)\text{-OCH}(\text{CF}_3)\text{CH}_2\text{COOEt})$  (**6a**) complex, we observed chemical shifts significantly different, principally for the diastereotopic methylene hydrogens of the ethyl ester group ( $\text{CO}_2\text{CHHCH}_3$ ) ( $\delta$  2.83 and 2.66 ppm for **6a**).

The solid-state structure of **5d** features a monomeric molecule with an aluminum center in a slightly distorted trigonal bipyramidal geometry, penta-coordinated by the  $\{\text{ONO}^{\text{Me,Cumyl}}\}^{2-}$  ligand and the (*R*)- $\beta$ -alkoxy-butyrate moiety. In addition, **5d** adopts two different structures in the crystal unit: in one the cumyl groups points in the same direction of the (*R*)- $\beta$ -alkoxy-butyrate moiety, and in the second one the aryl groups of **5d** are turned in the opposite direction with respect to the (*R*)- $\beta$ -alkoxy-butyrate group (Figure 61). The axial positions are occupied by a nitrogen atom and a carbonyl oxygen atom (O71 and O10), with N–Al–O angles ( $171.00(11)$  and  $176.44(10)$ )°. The other oxygen atoms (O(11), O(51) and O(74)) occupy the equatorial positions with O–Al–O angles ranging from  $118.16(12)$  to  $122.96(11)$ °. The Al–O(carbonyl) bond distances Al–O(71),  $2.006(2)$  and Al(2)–O(10),  $2.057(2)$  compare well with the Al(*R*)- $\beta$ -alkoxy-butyrate supported by (bis)naphtholate ligand (Al–O =  $1.993(2)$  Å) (*vide supra*, Figure 41).

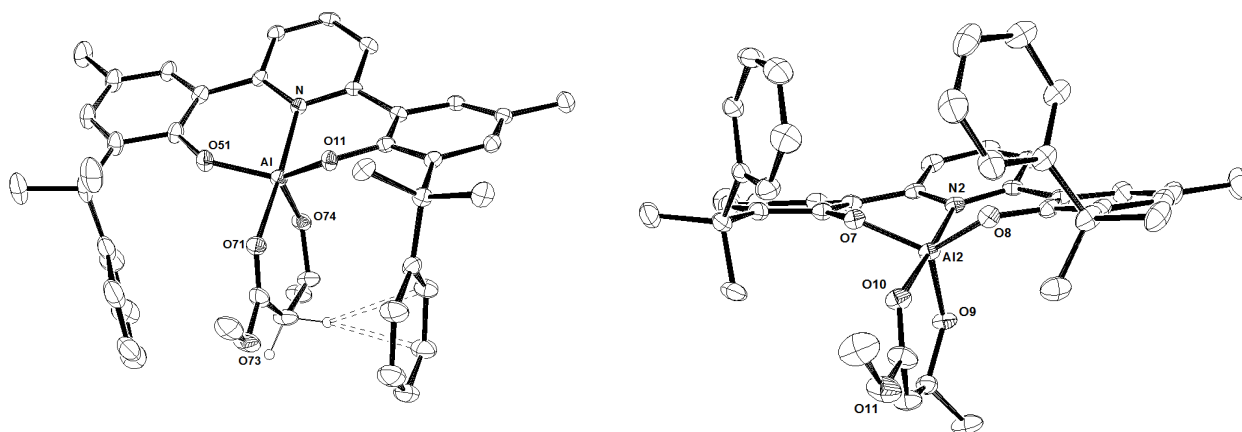


**Figure 61.** ORTEP drawing of  $\{\text{ONO}^{\text{Me,Cumyl}}\}\text{Al}((R)\text{-OCH}(\text{Me})\text{CH}_2\text{CO}_2\text{Me})$  (**5d**) (thermal ellipsoids drawn at 50 % probability level; all solvents molecules and hydrogen atoms, except that of the methylene of the (*R*)- $\beta$ -alkoxy-butyrate group, are omitted for clarity, omitted for clarity. Selected bond distances ( $\text{\AA}$ ) and angles (deg): (on the left): Al–O(74)= 1.745(2); Al–O(51)= 1.757(2); Al–O(11)= 1.762(2); Al–O(71)= 2.006(2); Al–N= 2.017(2); O(74)–Al–O(51)= 118.16(12); O(74)–Al–O(11)= 118.18(11); O(51)–Al–O(11)= 122.96(11); O(71)–Al–N= 171.00(11); O(51)–Al–O(71)= 84.58(10); O(74)–Al–O(71)= 93.40(10); O(11)–Al–O(71)= 84.05(10); O(74)–Al–N= 95.44(10); O(51)–Al–N= 92.72(10); O(11)–Al–N= 90.26(10). (on the right): Al(2)–O(9)= 1.743(2); Al(2)–O(8)= 1.757(2); Al(2)–O(7) = 1.771(2); Al(2)–N(2)= 1.996(3); Al(2)–O(10)= 2.057(2); O(9)–Al(2)–O(8)= 120.76(12); O(9)–Al(2)–O(7)= 119.58(11); O(8)–Al(2)–O(7)= 119.06(11); O(9)–Al(2)–N(2)= 92.25(10); O(8)–Al(2)–N(2)= 92.62(11); O(7)–Al(2)–N(2)= 92.83(11); O(9)–Al(2)–O(10)= 91.27(10); O(8)–Al(2)–O(10)= 85.07(10); O(7)–Al(2)–O(10)= 85.95(10); N(2)–Al(2)–O(10)= 176.44(10).

### 4.2.3 Studies of the reactivity of Al(III)-(isopropyl (*S*)-lactate) complex **4d** toward L- and *rac*-Lactides.

In the previous studies of reactivity of bis(naphtholate) Al(III) (*S*)-lactate complexes, we observed in the  $^1\text{H}$  NMR spectrum for the reaction mixture of complex (*S*)-**4a** with 1.1 equiv. of *rac*-LA in toluene- $d_8$  after 30 min at 25 °C a split of the resonances for both the methine and methyl groups of the *rac*-LA monomer (each as two broadened quartets). On the other hand, no significant splitting of the LA methine resonances was observed when we monitored by  $^1\text{H}$  NMR the reaction of a 1:1.1 mixture of (*S*)-**4b**/*rac*-LA. The only difference between these two systems, **4a** vs. **4b**, lies in the nature of  $\text{SiR}_3$  substituent ( $\text{SiPh}_3$  vs.  $\text{Si}i\text{BuMe}_2$ ). In order to investigate possible interactions between the  $\pi$ -system of the cumyl substituent present in (*S*)-**4d** complex and the lactate moiety that could eventually differentiate the two enantiomers from *rac*-LA, we monitored the reaction of (*S*)-**4d** with *rac*-lactide in toluene- $d_8$  after 30 min at room temperature. In this case, we didn't observe a significant splitting of the LA methine resonances (Figure 62). However, we noticed changes in the chemical shifts of signals in the aromatic region (Figure 63).

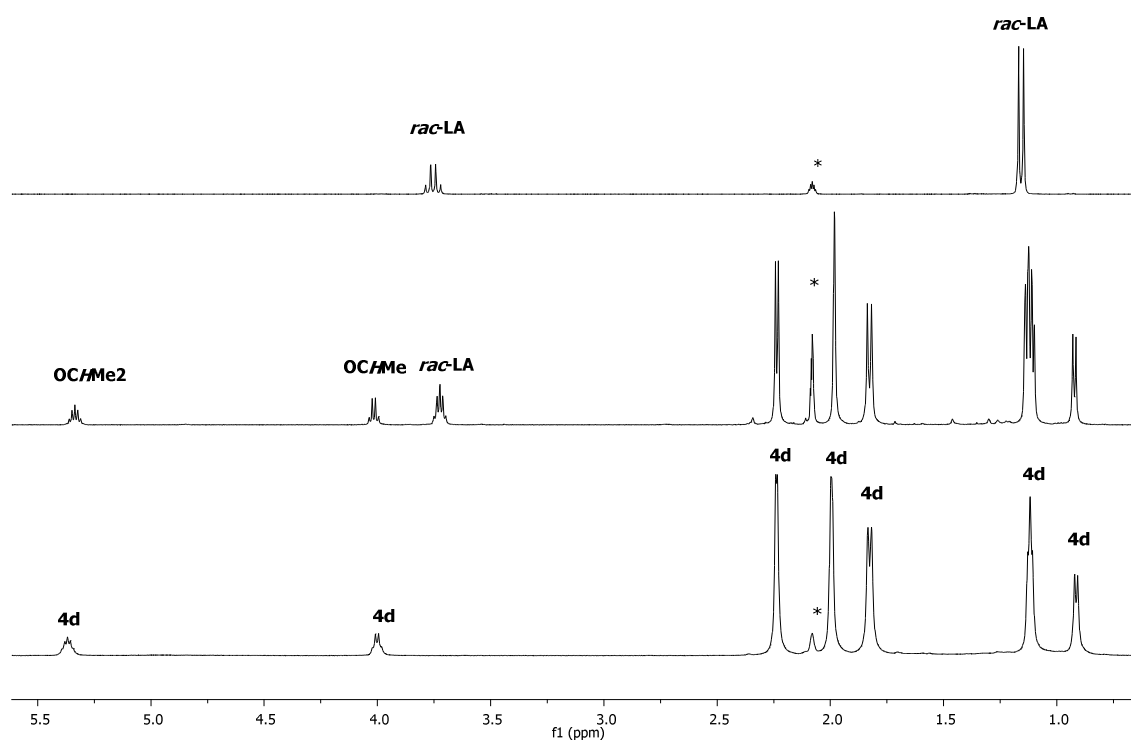


**Figure 62.** Detail of the aliphatic region of the  $^1\text{H}$  NMR spectrum (500 MHz, toluene- $d_8$ , 298 K) of; bottom, (*S*)-**4d**, and mixtures of (*S*)-**4d** with; middle, 1 equiv. of *rac*-LA and; top, of *rac*-LA (\*stands for residual solvent resonances).

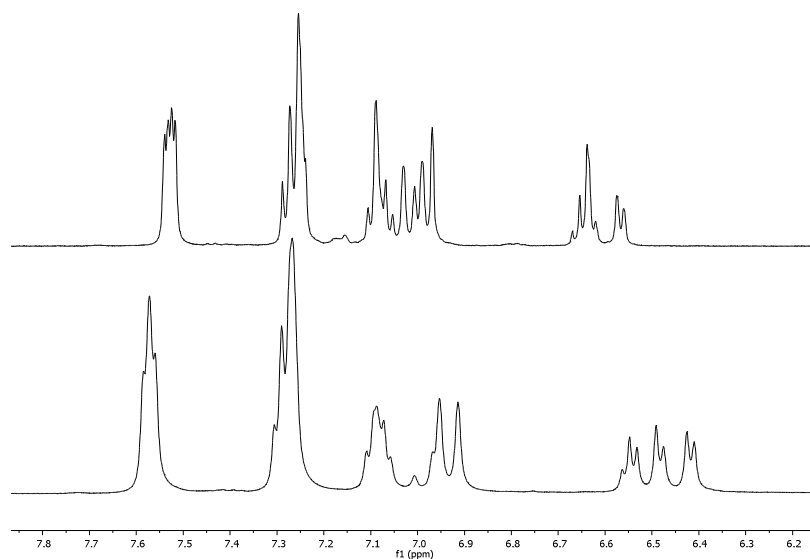
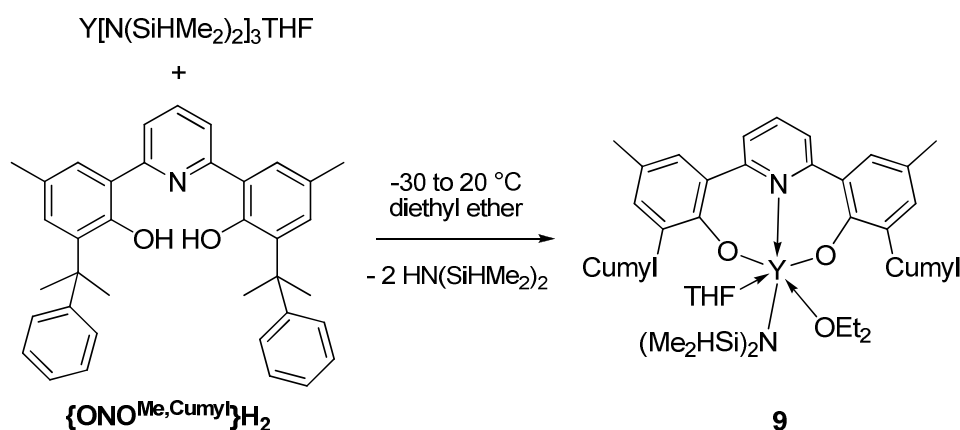


**Figure 63.** Detail of the aromatic region of the  $^1\text{H}$  NMR spectrum (500 MHz, toluene- $d_8$ , 298 K) of the reaction mixture; bottom, (*S*)-**4d**, and mixtures of (*S*)-**4d** with; top, 1 equiv. of *rac*-LA.

Moreover, the (*S*)-**4d** complex was tested in ROP of *rac*-Lactide [*rac*-LA]/[(*S*)-**4d** = 100] giving rise to atactic polymers ( $P_r = 0.5$ ). Thus, the above results, such as polymerization outcome using (*S*)-**4d**, NMR analysis of these Al(III) lactate and  $\beta$ -alkoxy-esters derivatives and X-ray diffraction studies of (*R*)-**5d** suggest absence of any weak stabilizing interaction of the *CH* of the lactate and  $\beta$ -alkoxy-esters moieties and the  $\pi$ -system of the cumyl groups present in the ligand.

#### 4.2.4 Preparation of yttrium complexes supported by tridentate pyridine-bis(phenolate) $\{\text{ONO}^{\text{Me,Cumyl}}\}_2^-$ ligand.

An yttrium complex of the new ligand  $\{\text{ONO}^{\text{Me,Cumyl}}\}_2^-$  was also prepared via a  $\sigma$ -bond metathesis approach. The amine elimination reaction between the silylamido precursor  $[\text{Y}(\text{N}(\text{SiHMe}_2)_2)_3(\text{THF})]$  and pro-ligand  $\{\text{ONO}^{\text{Me,Cumyl}}\}_2\text{H}_2$  in diethyl ether afforded the monosilylamido complex  $\{\text{ONO}^{\text{Me,Cumyl}}\}_2\text{Y}[\text{N}(\text{SiHMe}_2)_2](\text{THF})(\text{Et}_2\text{O})$  (**9**), with concomitant release of 2 equiv. of bis(dimethylsilyl)amine (Scheme 26). Compound **9** is readily soluble in usual organic solvents (THF, toluene, benzene).



**Scheme 26.** Synthetic Route for Y-Amido Complex (**9**).

The  $^1\text{H}$  and  $^{13}\text{C}$  NMR spectra of **9** in toluene- $d_8$  or  $\text{C}_6\text{D}_6$  at room temperature all contain two sets of resonances, indicative of the presence of one  $\text{C}_s$ -symmetric species (**9A**) as major component and one second species (**9B**) resulting from the decomposition of **9A**. In the  $^1\text{H}$  NMR spectrum (*see the Annexes*) we observed the presence of one coordinated THF and one coordinated diethyl ether molecules for **9A**. The chemical shift for the  $\text{SiH}$  ( $\delta$  4.85 for **9B** and 4.80 ppm for **9A** at 298 K in  $\text{C}_6\text{D}_6$ ), which is shifted upfield when compared to the chemical shift in  $[\text{Y}\{\text{N}(\text{SiHMe}_2)_2\}_3(\text{THF})]$  precursor ( $\delta$  4.99 ppm), argue against a strong  $\beta(\text{Si-H})$  agostic interaction with the yttrium center in solution.<sup>129</sup>

The VT-NMR spectra (500 MHz, toluene- $d_8$ , 298–363 K) show an increase from 1/8 to 1/4 of the decomposition product **9B** and the formation of another unidentified species (**9C**) after heating the compound **9** to 363 K (Figure 64). The bottom spectrum shows the dynamic behavior of the  $\text{Et}_2\text{O}$  molecule. Besides, we observe in the middle and top spectra that an increase of the temperature favors the dissociation of the labile  $\text{Et}_2\text{O}$  molecule with concomitant formation of **B** and **C** as decomposition products (Figure 64).

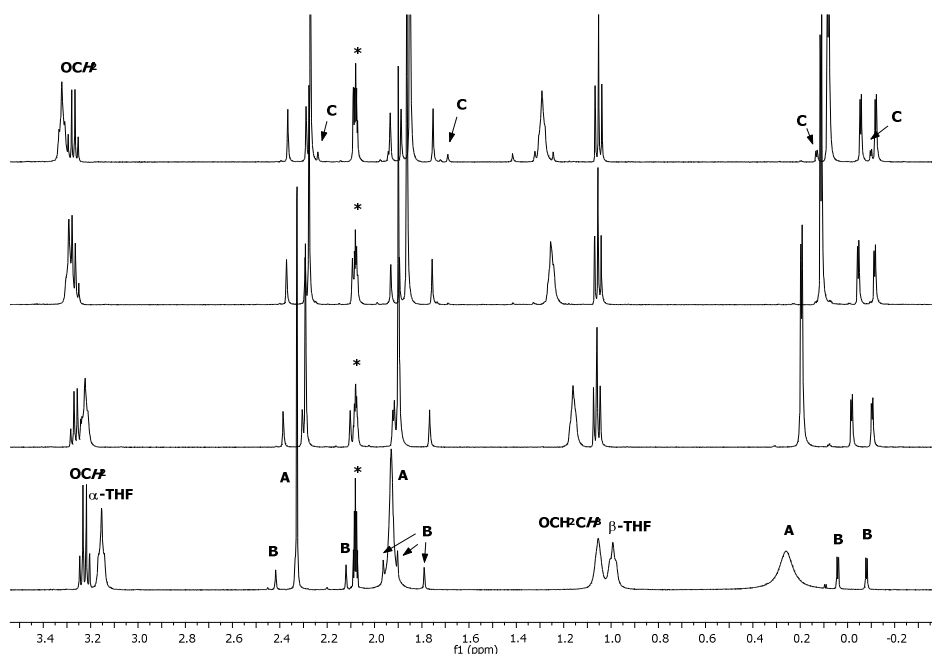


**Figure 64.** Details of the aliphatic region of the VT- $^1\text{H}$  NMR spectra (500 MHz, toluene- $d_8$ , 298–363 K) of  $\{\text{ONO}^{\text{Me,Cumyl}}\}\text{Y}[\text{N}(\text{SiHMe}_2)_2](\text{THF})(\text{Et}_2\text{O})$  (**9**); bottom, 298 K; middle, 333



and 353 K; top, 363 K. (A)  $C_5$ -symmetric species. (B and C) Decomposition products (\*refers to residual solvent resonances).

In order to stabilize complex **9**, we have run  $^1\text{H}$  NMR in pyridine- $d_5$ .<sup>130</sup> Predominantly, the  $^1\text{H}$  and  $^{13}\text{C}$  NMR spectra of **9** in pyr- $d_5$  are consistent with a single hexacoordinated  $C_5$ -symmetric species, which is stable for several days at room temperature. Thanks to the strong basicity of pyridine, the THF and diethyl ether were displaced from the yttrium coordination sphere. Indeed, in the  $^1\text{H}$  NMR spectrum (*see the Annexes*) of **9** in Pyr- $d_5$  at room temperature, signals for free THF and  $\text{Et}_2\text{O}$  molecules were observed.

Single crystals of **9** suitable for an X-ray diffraction analysis were obtained by recrystallization from a diethyl ether solution at  $-30\text{ }^\circ\text{C}$ . Crystallographic data and structural determination details are summarized in Table 1A (*see the Annexes*), and important bond distances and angles are given in Figure 65. The solid-state structure of **9** features a monomeric structure with an yttrium center in a distorted octahedral geometry, six-coordinated by the  $\{\text{ONO}^{\text{Me,Cumyl}}\}^{2-}$  ligand, the bis(dimethylsilyl)amido group, a THF and a diethyl ether molecules (Figure 65). The THF and diethyl ether ligands are located *trans* to each other and *cis* to the silylamido ligand, as indicated by corresponding angles [ $\text{O}(71)\text{--Y--O}(61)$   $162.75(9)$ ,  $\text{O}(71)\text{--Y--N}(3)$   $98.90(9)$ ,  $\text{O}(61)\text{--Y--N}(3)$   $98.33(9)^\circ$ ]. Also, the two oxygen donors of the bis(phenolate) ligand are in a *trans* position [ $\text{O}(11)\text{--Y--O}(51)$   $153.77(7)^\circ$ ]. The  $\text{Y--O}(\text{ligand})$  ( $2.1427(19)$  and  $2.144(2)$  Å) bond distances as well as the  $\text{Y--N}(\text{silylamido})$  ( $2.268(3)$  Å) bond distance, fall into the range of distances observed in related amido-yttrium complexes supported by tridentate bis(naphtholate)-pyridine and tetradentate bis(phenolate)<sup>41,88,89,94,98</sup> ligands. Further features such as a  $\text{Si}(1)\text{--N}(3)\text{--Si}(2)$  angle of  $122.63(16)^\circ$  that is just slightly larger than for an ideal  $\text{sp}^2$  hybridization and long, equivalent  $\text{Y}\cdots\text{Si}$  ( $3.4276(10)$  and  $3.4158(11)$  Å) distances exclude a  $\beta(\text{Si--H})$  diasteric interaction in complex **9**.<sup>131</sup>

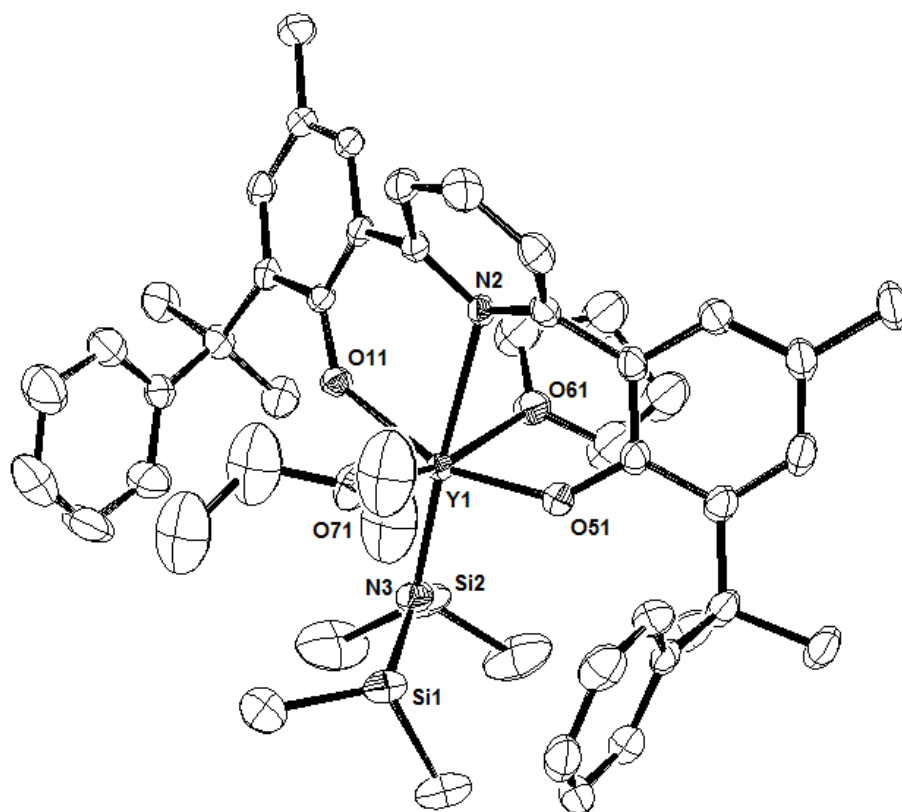
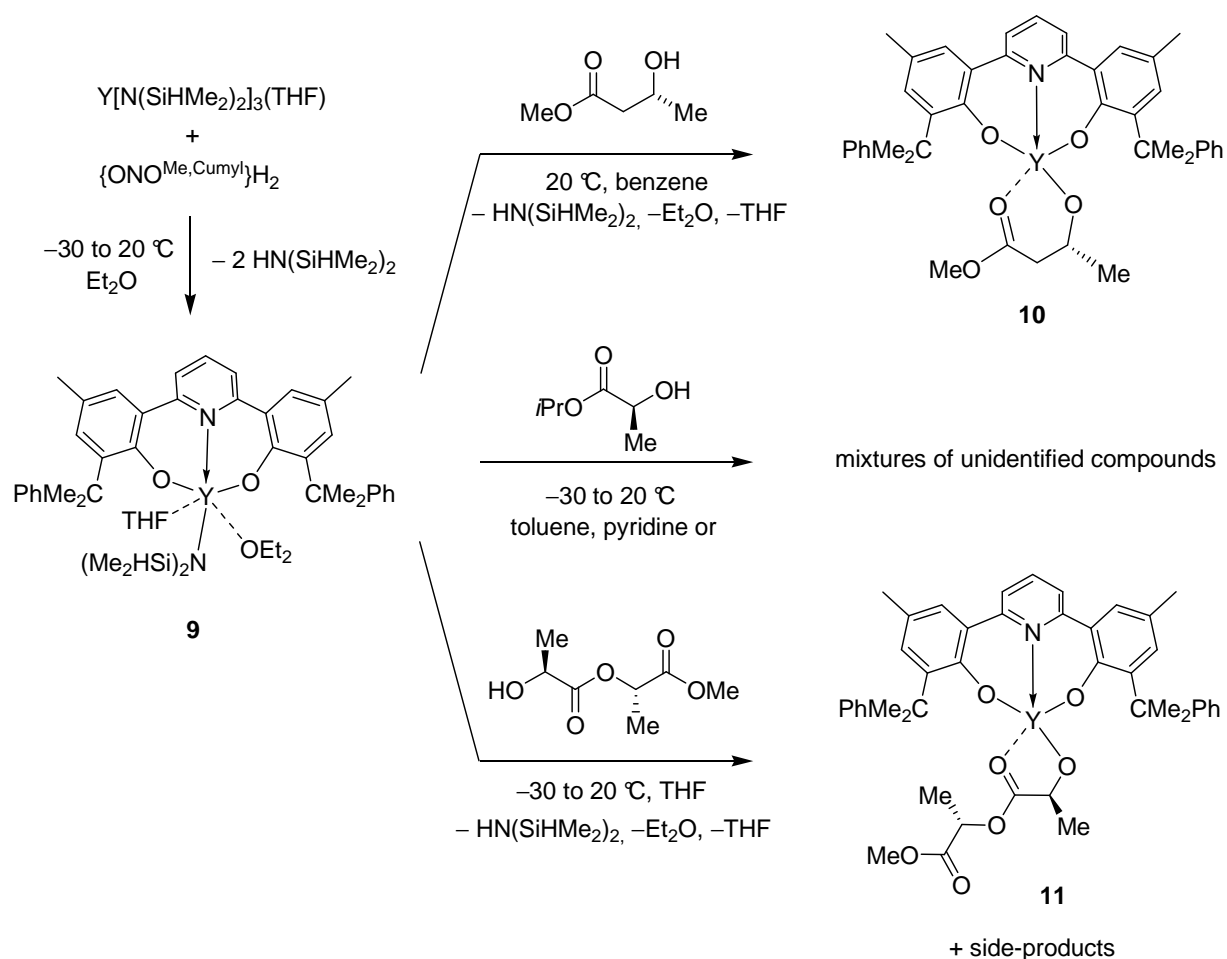


**Figure 65.** ORTEP drawing of  $\{\text{ONO}^{\text{Me,Cumyl}}\}\text{Y}[\text{N}(\text{SiHMe}_2)_2](\text{THF})(\text{Et}_2\text{O})$  (**9**) (thermal ellipsoids drawn at 50% probability level; all hydrogen atoms are omitted for clarity). Selected bond distances ( $\text{\AA}$ ) and angles (deg):  $\text{Y}(1)\text{--O}(11) = 2.1427(19)$ ;  $\text{Y}(1)\text{--O}(51) = 2.144(2)$ ;  $\text{Y}(1)\text{--O}(61) = 2.366(2)$ ;  $\text{Y}(1)\text{--O}(71) = 2.358(2)$ ;  $\text{Y}(1)\text{--N}(2) = 2.615(2)$ ;  $\text{Y}(1)\text{--N}(3) = 2.268(3)$ ;  $\text{Y}(1)\text{--Si}(1) = 3.4276(10)$ ;  $\text{Y}(1)\text{--Si}(2) = 3.4158(11)$ ;  $\text{N}(2)\text{--Y}(1)\text{--N}(3) = 176.57(9)$ ;  $\text{O}(11)\text{--Y}(1)\text{--O}(51) = 153.77(7)$ ;  $\text{O}(71)\text{--Y}(1)\text{--O}(61) = 162.75(9)$ ;  $\text{O}(11)\text{--Y}(1)\text{--N}(2) = 76.32(7)$ ;  $\text{O}(11)\text{--Y}(1)\text{--N}(3) = 106.16(8)$ ;  $\text{O}(11)\text{--Y}(1)\text{--O}(61) = 90.60(8)$ ;  $\text{O}(11)\text{--Y}(1)\text{--O}(71) = 85.44(8)$ ;  $\text{O}(51)\text{--Y}(1)\text{--N}(2) = 77.76(7)$ ;  $\text{O}(51)\text{--Y}(1)\text{--N}(3) = 99.91(9)$ ;  $\text{O}(51)\text{--Y}(1)\text{--O}(61) = 88.43(8)$ ;  $\text{O}(51)\text{--Y}(1)\text{--O}(71) = 87.77(8)$ ;  $\text{O}(71)\text{--Y}(1)\text{--N}(2) = 83.58(8)$ ;  $\text{O}(71)\text{--Y}(1)\text{--N}(3) = 98.90(9)$ ;  $\text{O}(61)\text{--Y}(1)\text{--N}(2) = 79.17(7)$ ;  $\text{O}(61)\text{--Y}(1)\text{--N}(3) = 98.33(9)$ ;  $\text{Si}(2)\text{--N}(3)\text{--Y}(1) = 118.58(14)$ ;  $\text{Si}(1)\text{--N}(3)\text{--Y}(1) = 118.78(14) = \text{Si}(2)\text{--N}(3)\text{--Si}(1) = 122.63(16)$ .

Yttrium derivatives containing a  $\beta$ -alkoxy-butyrates (**10**) and a (*S,S*) methyl lactidate (**11**) moiety were prepared by treatment of complex **9** with 1 equiv. of methyl (*R*)-3-hydroxybutyrate and 1 equiv. of methyl (*S,S*)-lactylactate in toluene or benzene, and THF-*d*<sub>8</sub>, respectively, at room temperature (Scheme 27). The methyl (*R*)-alkoxy-butyrates complex **10** was isolated in quantitative yield, while lactylactate complex **11** was generated only in a *J*-Young NMR tube. It is worth to note that **10** is, as our knowledge, the first example of a well-defined yttrium alkoxy-butyrates complex



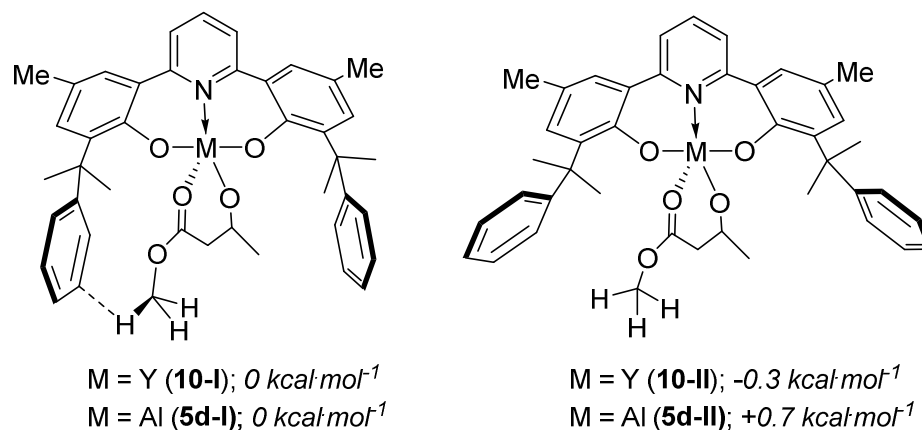
**Scheme 27.** Synthesis of Yttrium Complexes Supported by the  $\{\text{ONO}^{\text{Me,Cumyl}}\}_2^{2-}$  Ligand (**1c**).

The resonances in the  $^1\text{H}$  and  $^{13}\text{C}\{^1\text{H}\}$  NMR spectra of complex **10** in toluene- $d_8$  at room temperature are noticeably broadened, reflecting the existence of a dynamic behavior under these conditions. Decrease of the temperature down to 258 K allowed freezing this dynamic process, resulting in a sharp set of resonances, consistent with a single  $C_1$ -symmetric species. The  $^1\text{H}$  NMR spectrum of **10** in toluene- $d_8$  at 258 K (*see the Annexes*) displays six singlets ( $\delta$  2.31, 2.27, 2.02, 1.99, 1.66 and 1.58 ppm) for the six non-equivalent methyl groups in the  $\{\text{ONO}^{\text{Me,Cumyl}}\}$  ligand unit. The resonances for the (*R*)- $\beta$ -alkoxy-butyrate group were observed as a broad singlet and a doublet for the methine and methyl hydrogens associated to the chiral center ( $\text{OCH}(\text{CH}_3)\text{CH}_2\text{CO}_2\text{Me}$ ,  $\delta$  2.96 and 0.87 ppm, respectively), two doublets of doublet for the diastereotopic methylene hydrogens ( $\text{OCH}(\text{Me})\text{CHHCO}_2\text{Me}$ ,  $\delta$  2.43, 1.75 ppm), and a singlet resonance for the methyl ester group ( $\text{OCH}(\text{Me})\text{CH}_2\text{CO}_2\text{CH}_3$ ,  $\delta$  2.89 ppm).

In a previous study, Carpentier *et al.*<sup>89</sup> demonstrated by means of DFT computations that, in yttrium amino-alkoxy-bis(phenolate) complexes,  $\text{C}-\text{H}\cdots\pi$  interactions between methylenic hydrogens of the alkoxy-butyrate moieties and certain carbon atoms (typically, *ortho*- and *meta*-) of phenyl rings of the cumyl substituents can be remarkably stabilizing (by 5–12 kcal·mol<sup>-1</sup>). Herein, we have used the same computational approach to assess the stabilization ability of cumyl groups in complexes **10** and **5d**. Thus, the molecular structure of yttrium and aluminum complexes adopting both geometries observed for **5d** in the solid state (Figure 61, *vide supra*, Scheme 28) were optimized. Unexpectedly, the only close contacts detected involved hydrogens of the OMe group of the alkoxy-butyrate moiety and the *meta*-carbon atoms of phenyl rings of the cumyl substituents (2.74–2.77 Å) (see optimized geometries **10-I** and **5d-I**). However, only insignificant differences were found between the total electron energies values calculated for geometries **I** and **II** of complexes **10** and **5d**

(0.3–0.7 kcal·mol<sup>-1</sup>), which argues against strong stabilizing interactions in these molecules.

This is in line with the observation of two conformations in the solid state structure of **5d**.



**Scheme 28.** Model geometries computed to assess possible C–H··· $\pi$  interactions in **5d** and **10**.

Interestingly though, the NOESY data obtained for complex **10** in toluene-*d*<sub>8</sub> at 253 K (*see the Annexes*) also suggest close contacts between hydrogens of the OMe group of the alkoxy-butyrate moiety and phenyl hydrogens of the cumyl substituents on the NMR-time scale.

Complex **11** decomposes in THF solution over a few hours at room temperature; the yttrium co-product(s) eventually formed in this solution could not be identified by <sup>1</sup>H NMR. Perhaps the yttrium co-products result from transesterification reactions, but this is not clear yet. We also observed that exposure of solid **11** under high vacuum results in the formation of unidentified products. Due to the instability of complex **11** in solution, it was characterized by multinuclear NMR spectroscopy in THF-*d*<sub>8</sub> at ambient temperature (*see the Annexes*), using a freshly prepared sample. As complex **11** mimics the first insertion product of the LA ROP, we were interested in probing the existence, and eventual nature and extension of a metallacycle formed between the yttrium center and the lactidate fragment.

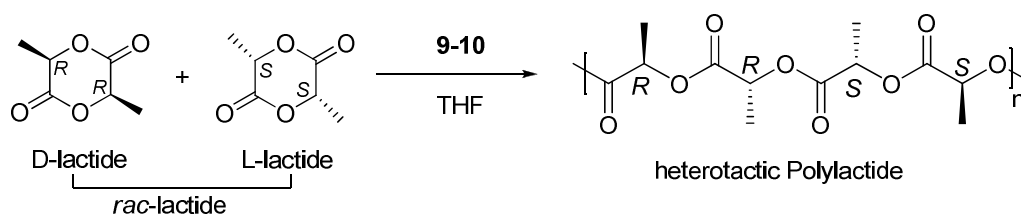
The multinuclear NMR spectra of **11** (*see the Annexes*), showed that the two signals for the carbonyl groups appear at  $\delta$  190.0 (OCH(CH<sub>3</sub>)C(=O)OCH(CH<sub>3</sub>)COOMe) and 169.0 (OCH(CH<sub>3</sub>)C(=O)OCH(CH<sub>3</sub>)COOMe) ppm. In comparison, the carbonyl carbons of the initial methyl (*S,S*)-lactyllactate reagent in the <sup>13</sup>C {<sup>1</sup>H} NMR spectrum appear at  $\delta$  175.1 (internal) and 170.0 (terminal) ppm. Thus, the carbonyl carbon of complex **11** ( $\delta$  190.0 ppm) significantly shifted downfield from the free reagent, suggesting that this internal carbonyl group is coordinated to the Y center forming a five-membered ring, instead a eight-membered ring in solution.

Attempts to generate an yttrium isopropyl (*S*)-lactate derivative complex from {ONO<sup>Me,Cumyl</sup>}Y[N(SiHMe<sub>2</sub>)<sub>2</sub>](THF)(Et<sub>2</sub>O) and 1 equiv. of isopropyl (*S*)-lactate, under various conditions, were unsuccessful (Scheme 27, *vide supra*).

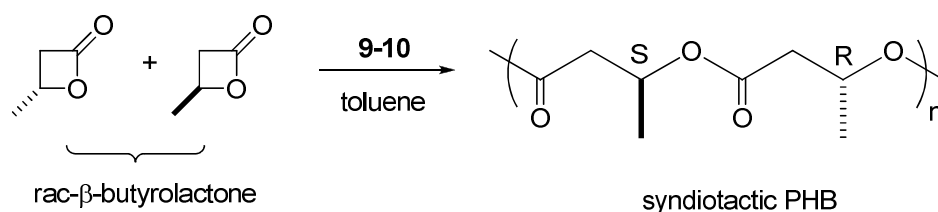
#### 4.2.5 Studies on the Ring-Opening Polymerization of *rac*-lactide and *rac*- $\beta$ -Butyrolactone with Yttrium Pyridine-Bis(phenolate) Complexes.

Discrete group 3 metal complexes are well-established catalysts-initiators for the ring-opening polymerization (ROP) of lactones and related monomers such as lactide (LA) and  $\beta$ -butyrolactone (BBL). We were therefore interested in evaluating the performances of the new yttrium pyridine-bis(phenolate) complexes prepared, considering that (i) yttrium complexes **9** and **10** possess a potentially active nucleophilic group (i.e., amido and  $\beta$ -alkoxy-butyrate, respectively)<sup>89</sup> and (ii)  $\beta$ -alkoxy-butyrate complex **10** is assumed to be an early intermediate in the ROP of  $\beta$ -butyrolactone or, more exactly, to mimic the active species with a growing PHB chain in such a process.<sup>111</sup>

Complexes **9** and **10** were thus assessed in the ROP of *rac*-lactide (Scheme 29) and *rac*- $\beta$ -butyrolactone (Scheme 30). Representative results are summarized in Table 10.



**Scheme 29.** Ring-Opening Polymerization of *rac*-Lactide Initiated by Complexes **9-10**.



**Scheme 30.** Ring-Opening Polymerization of *rac*- $\beta$ -BL Initiated by Complexes **9-10**.

**Table X.** ROP of *rac*-Lactide and *rac*- $\beta$ -butyrolactone Initiated by Complexes **9** and **10**<sup>a</sup>.

entry	compd	Monomer (M)	[M]/[Y]	solvent	Time (min)	Conv <sup>b</sup> (%)	M <sub>n,calc</sub> <sup>c</sup> (kDa)	M <sub>n,exp</sub> <sup>d</sup> (kDa)	M <sub>n,NMR</sub> <sup>e</sup> (kDa)	M <sub>w</sub> /M <sub>n</sub> <sup>d</sup>	P <sub>r</sub> <sup>f</sup>
1	<b>9</b>	<i>rac</i> -LA	100	toluene	10	41	5.9	10.9	-	1.91	0.60
2	<b>9</b>	<i>rac</i> -LA	500	toluene	50	67	48.2	60.6	-	1.88	0.60
3 <sup>g</sup>	<b>9</b>	<i>rac</i> -LA	100	toluene	13	55	7.9	9.0	-	1.94	0.79
4	<b>9</b>	<i>rac</i> -LA	100	pyridine	30	90	13.0	18.3	-	1.47	0.77
5	<b>9</b>	<i>rac</i> -LA	100	THF	6	94	13.5	30.6	-	1.98	0.96
6	<b>9</b>	<i>rac</i> -LA	500	THF	10	75	54.0	79.0	-	2.02	0.96
7	<b>9</b>	<i>rac</i> -LA	1000	THF	15	70	100.8	165.9	-	1.75	0.94
8 <sup>h</sup>	<b>9</b>	<i>rac</i> -LA	100	THF	13	64	9.2	4.2	6.4	1.14	0.87
9	<b>10</b>	<i>rac</i> -LA	100	toluene	10	87	12.5	9.4	13.9	1.49	0.55
10	<b>10</b>	<i>rac</i> -LA	100	THF	90	94	13.5	8.8	15.8	1.38	0.84
11	<b>10</b>	<i>rac</i> -LA	500	THF	330	65	46.8	25.1	-	1.29	0.88
12	<b>9</b>	<i>rac</i> -BBL	100	toluene	45	43	3.7	20.1	-	1.15	0.81
13	<b>9</b>	<i>rac</i> -BBL	250	toluene	90	39	8.4	44.3	-	1.43	-
14	<b>9</b>	<i>rac</i> -BBL	500	toluene	230	25	10.7	41.7	-	2.10	-
15	<b>9</b>	<i>rac</i> -BBL	100	pyridine	130	100	8.6	27.3	-	1.28	0.59
16	<b>9</b>	<i>rac</i> -BBL	100	pyridine	10	82	7.0	23.4	-	1.11	-
17 <sup>g</sup>	<b>9</b>	<i>rac</i> -BBL	200	toluene	1	100	17.2	28.1	-	2.40	0.86
18 <sup>h</sup>	<b>9</b>	<i>rac</i> -BBL	100	toluene	45	89	7.6	-	-	-	-
19 <sup>h</sup>	<b>9</b>	<i>rac</i> -BBL	500	toluene	230	62	26.7	27.6	-	1.07	0.81
20	<b>10</b>	<i>rac</i> -BBL	100	toluene	45	35	3.0	6.4	3.2	1.05	0.80
21 <sup>i</sup>	<b>10</b>	<i>rac</i> -BBL	100	toluene	1080	81	7.0	16.1	11.5	1.13	0.80
22	<b>10</b>	<i>rac</i> -BBL	250	toluene	90	28	6.0	11.0	7.5	1.05	-
23 <sup>i</sup>	<b>10</b>	<i>rac</i> -BBL	250	toluene	1080	93	20.0	35.0	26.5	1.10	-
24 <sup>i</sup>	<b>10</b>	<i>rac</i> -BBL	500	toluene	1080	81	34.8	66.0	40.2	1.15	-

<sup>a</sup> General conditions:  $[rac\text{-LA}]_0 = 2.0 \text{ mol.L}^{-1}$  or  $[rac\text{-BBL}]_0 = 3.0 \text{ mol.L}^{-1}$ , and room temperature. <sup>b</sup> Conversion of monomer as determined by  $^1\text{H}$  NMR on the crude reaction mixture. <sup>c</sup> Calculated  $M_n$  values considering one polymer chain per Y center. <sup>d</sup> Experimental  $M_n$  and  $M_w/M_n$  values determined by GPC in THF vs. PS standards;  $M_n$  values are corrected with a 0.58 factor for PLAs, and uncorrected for PHBs. <sup>e</sup> Experimental  $M_n$  values determined by  $^1\text{H}$  NMR analysis of the reprecipitated polymer. <sup>f</sup>  $P_r$  is the probability of racemic linkage, as determined by  $^1\text{H}$  NMR homo-decoupled experiments. <sup>g</sup> The polymerization was carried out in the presence of 5 equiv of pyridine vs Y. <sup>h</sup> The polymerization was carried out in the presence of 1 equiv of *i*PrOH vs Y. <sup>i</sup> No stirring; a highly viscous reaction mixture was observed after the reaction time.

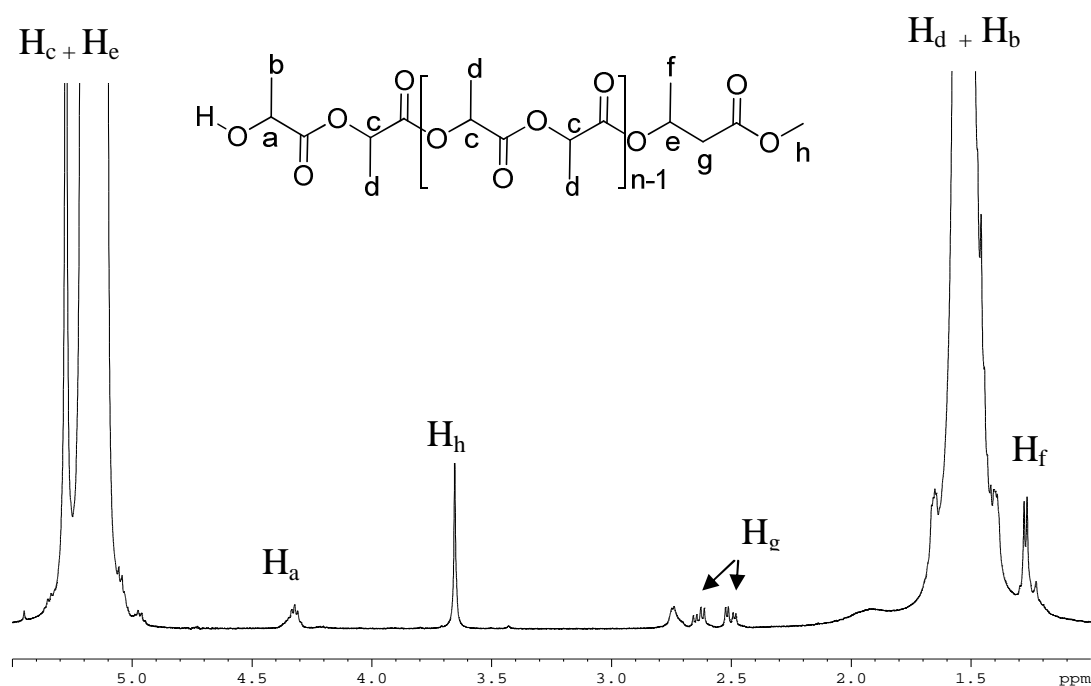
Both complexes **9** and **10** are active in the ROP of *rac*-LA at ambient temperature. Complex **9** is highly active in THF solution; polymerizations of 1000 equiv of *rac*-LA in THF reached 70% conversion in only 15 min (entry 7). Complex **10** proved to be even more active than **9** in toluene solution (compare entry 1 vs entry 9) but less active than **9** in THF solution (compare entry 5 vs entry 10). In toluene, we assume that this difference in apparent catalytic activities reflects more the higher nucleophilicity of the butyrate group as initiating group (as compared to amido). Perhaps, these differences in reactivity arise from the chelating butyrate group, leaving **10** less nucleophilic than expected.

We also observed that, for complex **9**, the number-average molecular weight values determined by GPC ( $M_n$  (exp)) almost doubled in comparison with the calculated  $M_n$  values (compare entries 1-2 and 5-7). At the same time, experimental  $M_n$  values are in linear dependence on the monomer conversions for different monomer loadings (compare entries 5–7). The molecular weight distributions are rather broad (although unimodal), in the range

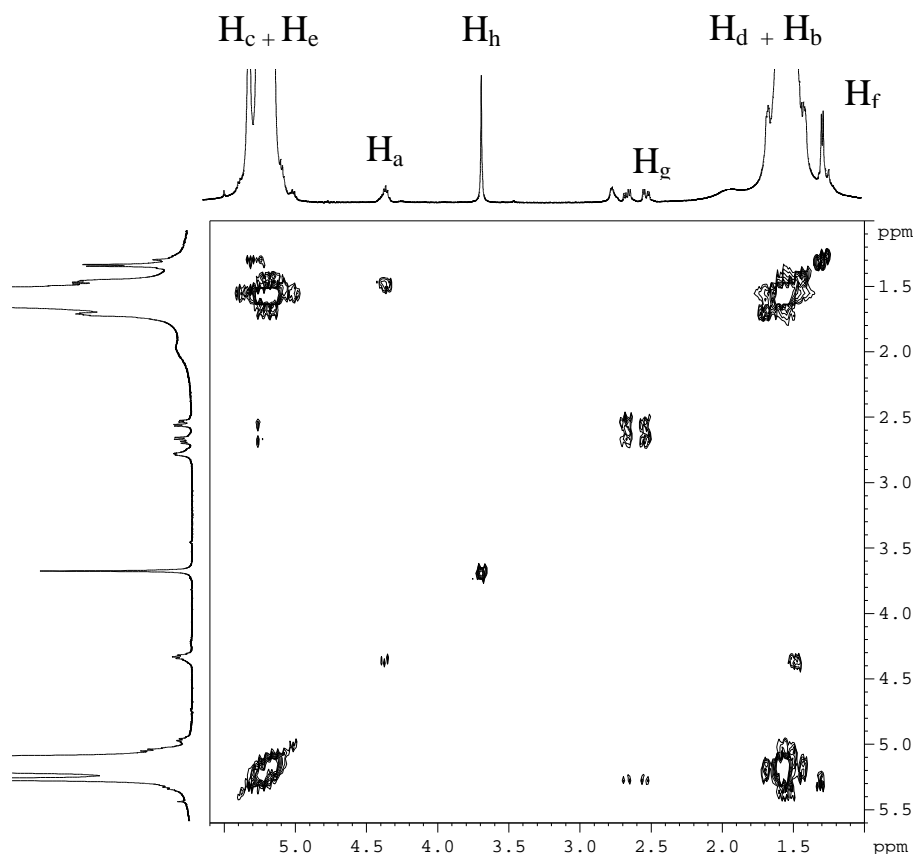


( $M_w/M_n = 1.75\text{--}2.02$ ). In the polymerizations of *rac*-LA mediated by complex **10**, the experimental  $M_n$  values are in quite good agreement with the calculated ones for a single-site catalyst (entries 9–10). In addition, the polydispersities are narrower ( $M_w/M_n = 1.29\text{--}1.49$ ). The somewhat decrease of the molecular weights (compare entries 9–10 vs. 11) for larger monomer loadings ( $[rac\text{-LA}]_0/[Y] = 500$ ) suggests that significant transesterification reactions take place under these conditions. Similar side-reactions were observed using Al(III) bis(naphtholate)-pyridine  $\beta$ -alkoxy-butyrate complex [(*R*)-**5d**] in the ROP of lactides (*vide supra*).

For relatively low molecular weight PLAs produced by **10**, the  $M_n$  values were also determined by  $^1\text{H}$  NMR spectroscopy in  $\text{CDCl}_3$ , taking into account the polymers end-groups (Figures 66 and 67). These values generally matched quite well the calculated ones.



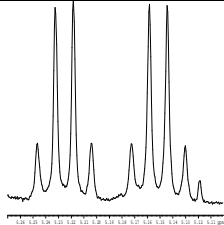
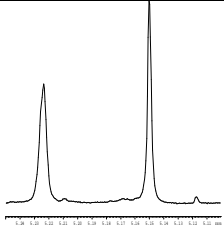
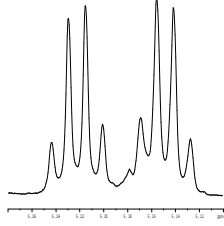
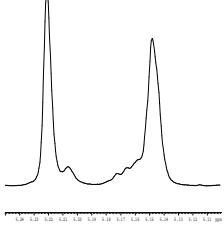
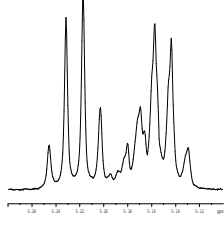
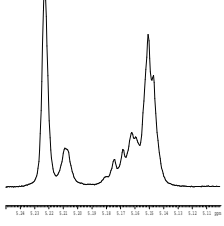
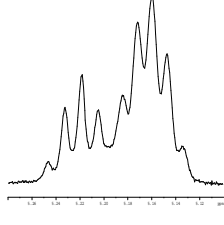
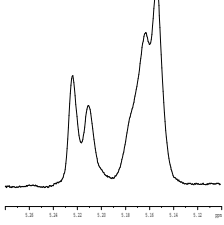
**Figure 66:**  $^1\text{H}$  NMR spectrum (500 MHz,  $\text{CDCl}_3$ , 298 K) of a PLA produced from  $\{\text{ONO}^{\text{Me,Cumyl}}\}_2\text{Y}((R)\text{-OCH}(\text{CH}_3)\text{CH}_2\text{COOMe})$  (**10**) (Table **10**, entry 10).



**Figure 67.**  $^1\text{H}$ - $^1\text{H}$  COSY NMR spectrum (500 MHz,  $\text{CDCl}_3$ , 298 K) of a PLA produced from  $\{\text{ONO}^{\text{Me,Cumyl}}\}\text{Y}((R)\text{-OCH}(\text{CH}_3)\text{CH}_2\text{COOMe})$  (**10**) (Table 10, entry 10).

Interestingly, homo-decoupled  $^1\text{H}$  NMR spectra (homodecoupling of the methine resonances) showed that some of the PLAs formed with these systems had highly heterotactic microstructures (Table 11). The probability of racemic linkage ( $P_r$ ) ranged from 0.55 (nearly atactic) up to 0.96. As we observed with tetradentate bis(phenolato)-lanthanide and the parents tridentate bis(naphtholate)-lanthanide systems, the stereoselectivity strongly depended on the nature of the solvent: almost all the PLAs produced in toluene had atactic microstructures whereas those obtained in THF had in almost all cases heterotactic microstructures.

**Table XI:** Methine region of  $^1\text{H}$  NMR and  $^1\text{H}$  homo-decoupled NMR spectra of different PLAs.

Experiment	$^1\text{H}$ NMR	$^1\text{H}\{^1\text{H}\}$ NMR	$P_r$
5			0.96
11			0.88
4			0.77
9			0.55

Similarly, the ROP of *rac*-BBL promoted by complexes **9** and **10** in toluene allowed the formation of highly syndiotactic PHBs (Figure 68), with  $P_r$  values in the range 0.59–0.86 (entries 12–24).

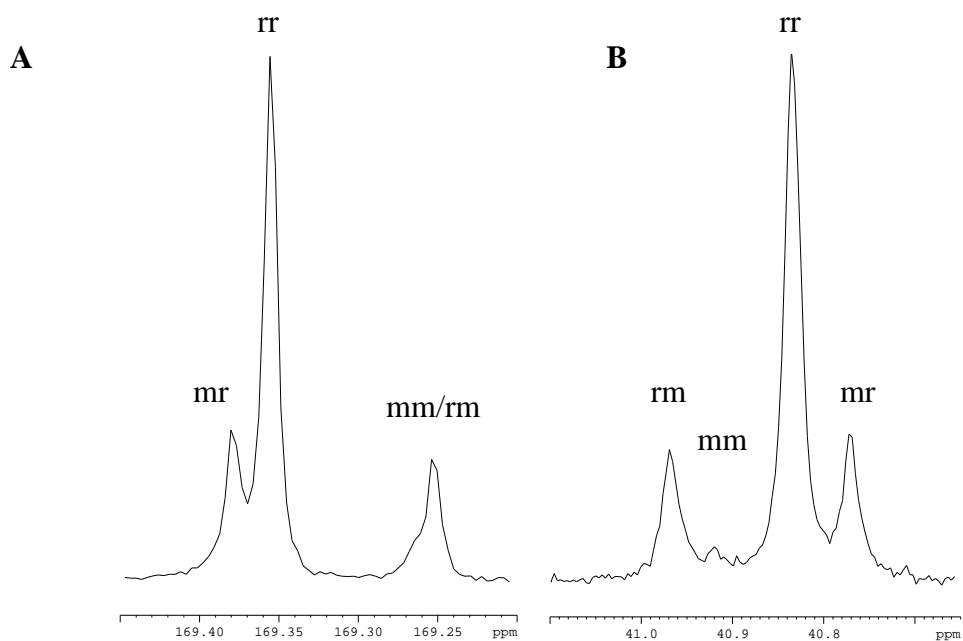


**Figure 68.** Carbonyl (**A**) and Methylene (**B**) regions of the  $^{13}\text{C}\{^1\text{H}\}$  NMR spectrum (100 MHz,  $\text{CDCl}_3$ , 298 K) of a PHB produced from  $\{\text{ONO}^{\text{Me,Cumyl}}\}\text{Y}((R)\text{-OCH}(\text{CH}_3)\text{CH}_2\text{COOMe})$  (**10**) (Table 10, entry 21).

As reflected in entries 12 and 16, the polymerization activity towards BBL depends much on the solvent nature: the polymerization of 100 equiv of *rac*-BBL in pyridine reached 82 % conversion in 10 min, while at  $[\textit{rac}\text{-BBL}]_0/[\text{Y}] = 100$  in toluene, the conversion reached 43% in 45 min). Surprisingly, when *rac*-BBL was polymerized with **9** in the presence of 5 equiv of pyridine (entry 17), a higher activity (the polymerization of 200 equiv of *rac*-BBL in toluene reached 100% in 1 min) and higher stereoselectivity ( $P_T = 0.86$ ) were found; in order to stabilize complex **9**, the active species in these experiments was prepared *in situ* by addition of 5 equiv of pyridine.

The experimental number-average molecular weights for PHBs produced by complex **10** (entries 20–24) are in close agreement with the calculated ones, also calculated by  $^1\text{H}$  NMR taking into account the PHB end-groups (Figure 69 and 70). The molecular weight distributions were unimodal and much narrower ( $M_w/M_n = 1.05\text{--}1.15$ ) than those observed for

PLAs (Table 10). These data evidence a significant degree of control over the polymerization.

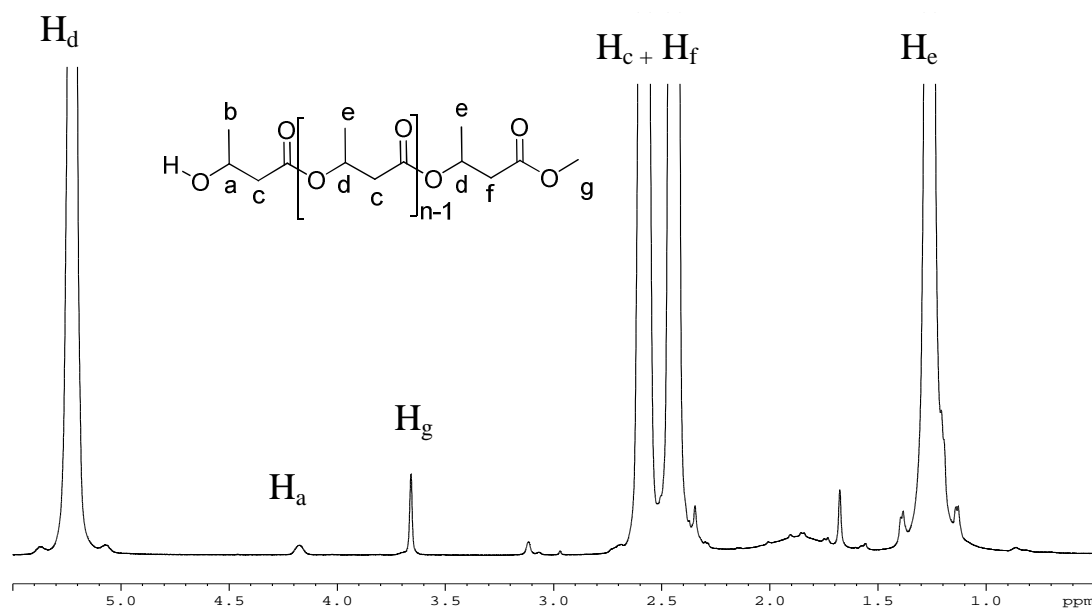


**Figure 69:** <sup>1</sup>H NMR spectrum (500 MHz, CDCl<sub>3</sub>, 298 K) of a PHB produced from {ONO<sup>Me,Cumyl</sup>}Y((R)-OCH(CH<sub>3</sub>)CH<sub>2</sub>COOMe) (**10**) (Table 10, entry 21).

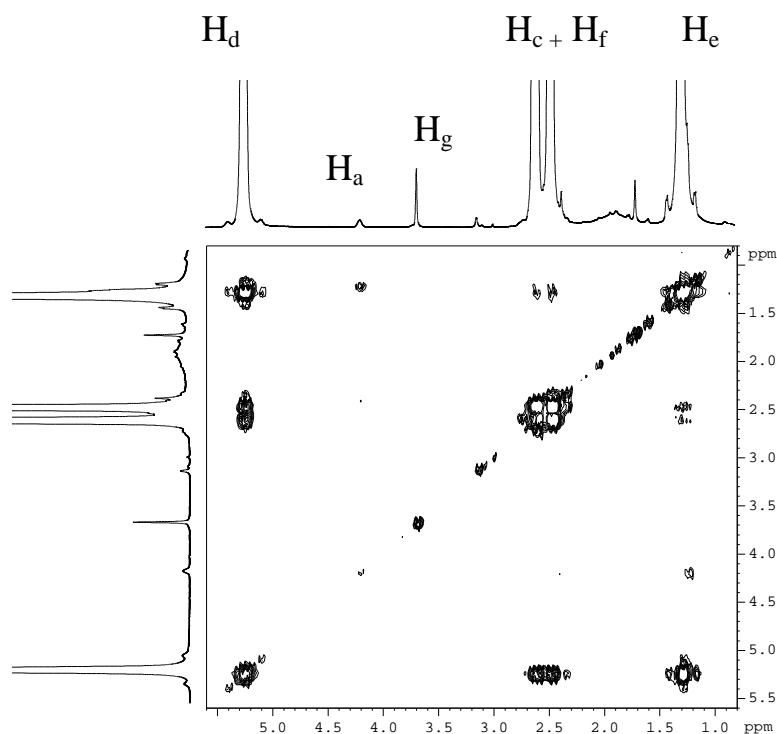


**Figure 70.** <sup>1</sup>H-<sup>1</sup>H COSY NMR spectrum (500 MHz, CDCl<sub>3</sub>, 298 K) of a PHB produced from {ONO<sup>Me,Cumyl</sup>}Y((R)-OCH(CH<sub>3</sub>)CH<sub>2</sub>COOMe) (**10**) (Table 10, entry 21).

## 5. CONCLUSIONS

In conclusion, we have prepared in good yields a series of discrete aluminum complexes supported by tridentate bis(*ortho*-silyl-substituted naphtholate)-pyridine, and a new bis(*ortho*-cumyl-substituted phenolate)-pyridine ligands, *via* the reaction of the corresponding pro-ligand  $\{\text{ONO}^{\text{R}^{\prime}}\}_2$  ( $\text{R}^{\prime} = \text{SiR}_3; \text{Me}, \text{Cumyl}$ ) and  $\text{AlR}_3$  ( $\text{R} = \text{Me}, i\text{Bu}$ ). These Al-alkyl complexes were treated with hydroxy-esters to afford new Al-lactate and - $\beta$ -alkoxy-butyrate complexes. All aluminum complexes adopt either  $C_s$ -symmetric or  $C_1$ -symmetric structures in the solid state, as observed for complexes **2a**, **4a**, **5a**, **6a** and **5d** and in toluene, benzene and  $\text{CH}_2\text{Cl}_2$  solutions as well. Also, we observed close contacts between substituents of those ligands and the lactate and  $\beta$ -alkoxy-butyrate moieties by NOESY NMR experiments and also in solid state. Compounds **2a–5a** are single-site initiators for the ROP of *rac*-LA at 80 °C, affording PLAs with narrow polydispersities and their molecular weights were found in good agreement with the calculated values. Furthermore, we have characterized by NMR a first insertion product of lactide in the ROP using the Al- $\beta$ -alkoxy-butyrate complex.

In parallel, two new yttrium complexes based on the new bis(*ortho*-cumyl-substituted phenolate)-pyridine ligand were synthesized *via* controlled amine-elimination reactions. The polymerizations of *rac*-lactide, when carried out in THF, afforded heterotactic-enriched PLAs ( $P_r$  up to 0.96). These complexes were also active for the ROP of *rac*-BBL, to afford syndiotactic-enriched PHBs ( $P_r$  up to 0.86) when 5 equiv of pyridine were added to **9**.

A unique yttrium complex **10** that contains a  $\beta$ -alkoxy-butyrate moiety has been isolated and characterized in solution. This complex mimics the early intermediate and active species with a growing polymer chain in butyrolactone ring-opening polymerization. In fact, this complex has been shown to be an active and stereoselective catalyst/initiator for the controlled ROP of both lactide and  $\beta$ -butyrolactone. This is the first experimental evidence in

line with the recent theoretical studies demonstrated by Maron *et al.*. In addition, an yttrium lactidate complex **11** was generated *in situ* in THF solution, suggesting coordination of the oxygen from the internal carbonyl group and the formation of a five-membered ring with the metal center.

The degree of stereocontrol in those polymerizations of *rac*-LA using aluminum and yttrium complexes is significantly affected by the nature (and ionic radius) of the metal center (Al, Y), resulting only in atactic PLAs for aluminum complexes.

## 6. REFERENCES AND NOTES

- [1] Mahrova, T. V.; Fukin, G. K.; Cherkasov, A. V.; Trifonov, A. A.; Ajellal, N.; Carpentier, J-F. *Inorg. Chem.* **2009**, *48*, 4258–4266.
- [2] Dechy-Cabaret, O.; Martin-Vaca, B.; Bourissou, D. *Chem. Rev.* **2004**, *104*, 6147–6176.
- [3] Duda, A.; Penczek, S. *Macromolecules* **1990**, *23*, 1636–1639.
- [4] Carpentier, J-F. *Angew. Chem. Int. Ed.* **2010**, *49*, 2662–2663.
- [5] Okada, M. *Prog. Polym. Sci.* **2002**, *27*, 87–133.
- [6] Bouyahyi, M. PhD Thesis. **2009**, University of Rennes 1.
- [7] Williams, C. K. *Chem. Soc. Rev.* **2007**, *36*, 1573–1580.
- [8] Garlotta, D. *J. Polym. Environ.* **2001**, *9*(2), 63–84.
- [9] Gupta, A. P.; Kumar, V. *Eur. Polym. J.* **2007**, *43*, 4053–4074.
- [10] Auras, R.; Lim, L-T.; Selke, S. E. M.; Tsuji, H. Poly(lactid acid): Synthesis, Structures, Properties, Processing, and applications. **2010**, John Wiley & Sons, Inc., Hoboken , New Jersey.
- [11] Kleine, J.; Kleine, H.; Uber, H. *Makromol. Chem.* **1959**, *30*, 23–38.
- [12] Mecking, S. *Angew. Chem. Int. Ed.* **2004**, *43*, 1078–1085.
- [13] Dijkstra, P. J.; Du, H.; Feijen, J. *Polym. Chem.* **2011**, *2*, 520–527.
- [14] Dutta, S.; Hung, W-C; Huang, D.-H.; Lin C.-C *Adv. Polym. Sci.* **2012**, *245*, 219–284.
- [15] Inoue, Y.; Yoshie, N. *Prog. Polym. Sci.* **1992**, *17*, 571–610.
- [16] Frazzetto, G. *Eur. Mol. Bio. Org.* **2003**, *4*, 835–837.
- [17] Carpentier, J.-F. *Macromol. Rapid Commun.* **2010**, *31*, 1696–1705.
- [18] Kramer, J. W.; Treiter, D.S.; Dunn, E. W.; Castro, P. M.; Roisnel, T.; Thomas, C. T.; Coates, G. W. *J. Am. Chem. Soc.* **2009**, *131*, 16042–16044.



- [19] (a) Sosnowski, S.; Gadzinowski, M.; Slomkowski, S. *Macromolecules* **1996**, *29*, 4556–4564. (b) Gadzinowski, M.; Sosnowski, S.; Slomkowski, S. *Macromolecules* **1996**, *29*, 6404–6407.
- [20] (a) Kricheldorf, H.; Dunsing, R. *Makromol. Chem.* **1986**, 1611; (b) Kricheldorf, H.; Kreiser, I. R. *Makromol. Chem.* **1987**, 188.
- [21] Bourissou, D.; Moebis-Sanchez, S.; Martin-Vaca, B. *C. R. Chimie* **2007**, *10*, 775–794.
- [22] Kasperczyk, J. E. *Macromol.* **1995**, *28*, 3937–3939.
- [23] Bero, M.; Dobrzynski, P.; Kasperczyk, J. *J. Polym. Sci. A: Polym. Chem.* **1999**, *37*, 4038–4042.
- [24] Hofman, A., Slomkowski, S., Penczek, S. *Makromol. Chem.*, **1984**, 185:91.
- [25] Ito, K.; Hashizuka, Y.; Yamashita, Y. *Macromolecules* **1977**, *10*:821.
- [26] Normand, M. PhD Thesis. 2012, University of Rennes 1.
- [27] Simon, L.; Goodman, J. M. *J. Org. Chem.* **2007**, *72*, 9656–9662.
- [28] Chuma, A.; Horn, H. W.; Swope, W. C.; Pratt, R. C.; Zhang, L.; Lohleijer, B. G. G.; Wade, C. G.; Waymouth, R. M.; Hedrick, J. L.; Rice, J. E. *J. Am. Chem. Soc.* **2008**, *130*, 6749–6754.
- [29] Pratt, R. C.; Lohmeijer, B. G. G.; Long, D. A.; Lundberg, P. N. P.; Dove, A. P.; Li, H.; Wade, C. G.; Waymouth, R. M.; Hedrick, J. L. *Macromolecules* **2006**, *39*, 7863–7871.
- [30] (a) Piedra-Aroni, E.; Brignou, P.; Amgoune, A.; Guillaume, S. M.; Carpentier, J.-F.; Bourissou, D. *Chem. Comm.* **2011**, *47*, 9828–9830. (b) Brignou, P.; Guillaume, S. M.; Roisnel, T.; Bourissou, D.; Carpentier, J.-F. *Chem. Eur. J.* **2012**, *18*, 9360–9370.
- [31] Dittrich, W.; Schulz, R. C. *Angew. Makromol. Chem.* **1971**, *15*, 109–126.
- [32] Kricheldorf, H. R.; Berl, M.; Scharnagl, N. *Macromolecules* **1988**, *21*, 286–293.
- [33] Dubois, P.; Jacobs, C.; Jérôme, R.; Teyssié, P. *Macromolecules* **1991**, *24*, 2266–2270.
- [34] Ovitt, T. M.; Coates, G. W. *J. Polym. Sci. A Polym. Chem.* **2000**, *38*, 4686–4692.

- [35] Chamberlain, B. M.; Cheng, M.; Moore, D. R.; Ovitt, T. M.; Lobkovsky, E. B.; Coates, G. W. *J. Am. Chem. Soc.* **2001**, *123*, 3229–3238.
- [36] Zell, M. T.; Padden, B.E; Paterick, A. J.; Thakur, K. A. M.; Kean, R. T. Hillmyer, M. A.; Munson, E. J. *Macromolecules*, **2002**, *35*, 7700–7707.
- [37] Biela, T.; Duda, A.; Penczek, S. *Macromolecules* **2006**, *39*, 3710–3713.
- [38] Chisholm, M. H.; Gallucci, J.C. Phomphrai, K. *Inorg. Chem.* **2004**, *43*, 6717-6725.
- [39] Hormnirun, P.; Marshall, E.; Gibson, V. C.; White, A. J. P.; Williams, D. J. *J. Am. Chem. Soc.* **2004**, *126*, 2688–2689.
- [40] Kemnitzer, J. E.; McCarthy, S. P.; Gross, R. A. *Macromolecules* **1993**, *26*, 1221–1229.
- [41] Ajellal, N.; Bouyahyi, M.; Amgoune, A.; Thomas, C. M.; Bondon, A.; Pillin, I.; Grohens, Y.; Carpentier J-F. *Macromolecules*. **2009**, *42*, 987–993.
- [42] (a) Penczek, S.; Biela, T.; Duda, A. *Macromol. Rapid. Commun.* **2000**, *21*, 941–950; (b) Baran, J.; Duda, A.; Kowalski, A.; Szymanski, R.; Penczek, S. *Macromol. Rapid. Commun.* **1997**, *18*, 325–333.
- [43] Jacobson, H.; Stockmayer, W.H. *J. Chem. Phys.* **1950**, *18*, 1600–1606.
- [44] (a) Spassky, N.; Wisniewski, M.; Pluta, C.; Le Borgne, A. *Macromol. Chem. Phys.* **1996**, *197*, 2627–2637. (b) Radano, C.P.; Baker, G.L.; Smith, M.P. *J. Am. Chem. Soc.* **2000**, *122*, 1552–1553.
- [45] (a) Cai, C. X.; Amgoune, A.; Lehmann, C. W.; Carpentier, J. F. *Chem. Commun.*, **2004**, 330–331. (b) Amgoune, A.; Thomas, C. M.; Roisnel, T.; Carpentier, J.-F. *Chem.–Eur. J.*, **2005**, *12*, 169–179. (c) Amgoune, A.; Thomas C. M.; Carpentier, J. F. *Macromol. Rapid Commun.*, **2007**, *28*, 693.
- [46] Degee, P.; Dubois, P.; Jérôme, R.; Jacobsen, S.; Fritz, H.-G. *Macromol. Symp.* **1999**, *144*, 289–302.
- [47] Dubois, P.; Jacobs, C.; Jerome, R.; Teyssie, P. *Macromol.* **1991**, *24*, 2266–2270.

- [48] Degee, P.; Dubois, P.; Jacobsen, S.; Fritz, H. G.; Jerome, R. *J. Polym. Sci., A: Polym. Chem.* **1999**, *37*, 2413–2420.
- [49] Kowalski, A.; Duda, A.; Penczek, S. *Macromol.* **1998**, *31*, 2114–2122.
- [50] (a) Shimasaki, K.; Aida, T.; Inoue, S. *Macromol.* **1987**, *20*, 3076–3080. (b) Trofimoff, L.; Aida, T.; Inoue, S. *Chem. Lett.* **1987**, 991–994. (c) Aida, T.; Inoue, S. *Acc. Chem. Res.* **1996**, *29*, 39–48.
- [51] Emig, N.; Nguyen, H.; Krautscheid, H.; Réau, R.; Cazaux, J.B.; Bertrand, G. *Organometallics*, **1998**, *17*, 3599–3608.
- [52] Leborgne, A.; Vincens, V.; Jouglard, M.; Spassky, N., *Makromol. Chem., Macromol. Symp.* **1993**, *73*, 37–46.
- [53] Montaudo, G.; Montaudo, M. S.; Puglisi, C.; Samperi, F.; Spassky, N.; LeBorgne, A.; Wisniewski, M. *Macromolecules* **1996**, *29*, 6461–6465.
- [54] Zhong, Z.; Dijkstra, J. P.; Feijen, J. *J. Am. Chem. Soc.* **2003**, *125*, 11291–11298.
- [55] Nomura, N.; Ishii, R.; Akakura, M.; Aoi, K. *J. Am. Chem. Soc.* **2002**, *124*, 5938–5939.
- [56] Cross, E. D.; Allan, L. E. N.; Decken, A.; Shaver, M. P. *J. Polym. Sci., A: Polym. Chem.* **2013**, *51*, 1137–1146.
- [57] Tang, Z.; Chen, X.; Pang, X.; Yang, Y.; Zhang, X.; Jing, X. *Biomacromolecules* **2004**, *5*, 965–970.
- [58] Nomura, N.; Ishii, R.; Yamamoto, Y.; Kondo, T. *Chem. – Eur. J.* **2007**, *13*, 4433–4451.
- [59] Chen, H.-L.; Dutta, S.; Huang, P.-Y.; Lin, C.-C. *Organometallics* **2012**, *31*, 2016–2025.
- [60] (a) Pang, X.; Du, H.; Chen, X.; Zhuang, X.; Cui, D.; Jing, X. *J. Polym. Sci., A: Polym. Chem.*, **2005**, *43*, 6605–6612. (b) Pang, X.; Du, H.; Chen, X.; Wang, X.; Jing, X. *Chem.–Eur. J.*, **2008**, *14*, 3126–313
- [61] Whitelaw, E. L.; Loraine, G.; Mahon, M. F.; Jones, M. D. *Dalton Trans.* **2011**, *40*, 11469–11473.

- [62] Du, H.; Velders, A. H.; Dijkstra, P. J.; Sun, J.; Zhong, Z.; Chen, X.; Feijen, J. *Chem. Eur. J.* **2009**, *15*, 9836–9845.
- [63] Hancock, S. L.; Jones, M. D.; Langridge, C. L.; Mahon, M. F. *New J. Chem.* **2012**, *36*, 1891–1896.
- [64] Iwasa, N.; Fujiki, M.; Nomura, K. *J. Mol. Cat. A: Chemical* **2008**, *292*, 67–75.
- [65] Pappalardo, D.; Annunziata, L.; Pellicchia, C. *Macromolecules*. **2009**, *42*, 6056–6062.
- [66] Normand, M.; Dorcet, V.; Kirillov, E.; Carpentier, J.-F. *Organometallics* **2013**, *32*, 1694–1709.
- [67] Yu, X.-F.; Wang, Z.-X. *Dalton Trans.* **2013**, *42*, 3860–3868.
- [68] (a) Darensbourg, D. J.; Karroonnirun, O. *Organometallics* **2010**, *29*, 5627–5634. (b) Darensbourg, D.; Karroonnirun, O.; Wilson, S. J. *Inorg. Chem.* **2011**, *50*, 6775–6787.
- [69] Matsubara, K.; Terata, C.; Sekine, H.; Yamatani, K.; Harada, T.; Eda, K.; Dan, M.; Koga, Y.; Yasuniwa, M. *J. Polym. Sci. Part A: Polym. Chem.* **2012**, *50*, 957–966.
- [70] Bouyhayi, M.; Sarazin, Y.; Casagrande, O. L.; Carpentier, J.-F. *Appl. Organomet. Chem.* **2012**, *26*, 681–688.
- [71] Tang, Z.; Gibson, V. C. *Eur. Polym. J.*, **2007**, *43*, 150–155.
- [72] Lamberti, M.; D’Auria, I.; Mazzeo, M.; Milione, S.; Bertolasi, V.; Pappalardo, D. *Organometallics* **2012**, *31*, 5551–5560.
- [73] Wang, Y.; Ma, H. *J. Organomet. Chem.* **2013**, *731*, 23–28.
- [74] (a) Ko, B.-T.; Wu, C.-C.; Lin, C.-C. *Organometallics* **2000**, *19*, 1864–1869. (b) Chisholm, M. H.; Navarro-Llobet, D.; Simonsick, W. J. *Macromolecules* **2001**, *34*, 8851–8857. (c) Liu, Y.-C.; Ko, B.-T.; Lin, C.-C. *Macromolecules* **2001**, *34*, 6196–6201.
- [75] Chisholm, M. H.; Lin, C.-C.; Gallucci, J. C.; Ko, K.-T.; Lin, B.-T. *Dalton Trans.* **2003**, 406–412.

- [76] Huang, C.-H.; Wang, F.-C.; Ko, B.-T.; Yu, T.-L.; Lin, C.-C. *Macromolecules* **2001**, *34*, 356–361.
- [77] Melillo, Ma. H.; Oliva, G.; Spaniol, L.; Englert, T. P.; Okuda, J. *J. Dalton Trans.* **2005**, 721–727.
- [78] (a) Amgoune, A.; Lavanant, L.; Thomas, C. M.; Chi, Y.; Welter, R.; Dagherne, S.; Carpentier, J.-F. *Organometallics* **2005**, *24*, 6279–6282. (b) Bouyahyi, M.; Grunova, E.; Marquet, N.; Kirillov, E.; Thomas, C. M.; Roisnel, T.; Carpentier, J.-F. *Organometallics* **2008**, *27*, 5815–5825. (c) Alaaeddine, A.; Thomas, C. M.; Roisnel, T.; Carpentier, J. -F. *Organometallics* **2009**, *28*, 1469–1475. (d) Bouyahyi, M.; Roisnel, T.; Carpentier, J.-F. *Organometallics* **2010**, *29*, 491–500. (e) Bouyahyi, M.; Roisnel, T.; Carpentier, J.-F. *Organometallics* **2012**, *31*, 1458–1466.
- [79] Palard, I., Schappacher, M.; Soum, A.; Guillaume, S.M. *Polym. Int.* **2006**, *55*, 1132–1137.
- [80] McLain, S.; Ford, T.; Drysdale, N. *Polym. Prep. Am. Chem. Soc. Polym. Chem.*, **1992**, *33*, 463–464.
- [81] LeBorgne, A.; Pluta, C.; Spassky, N.; *Macromol. Rapid. Commun.* **1994**, *15*, 955–960.
- [82] Alaaeddine, A.; Amgoune, A.; Thomas, C. M.; Dagherne, S.; Bellemin-Laponnaz, S.; Carpentier, J.-F. *Eur.J. Inorg. Chem.* **2006**, *18*, 3652-3658.
- [83] Ajellal, N.; Lyubov, D. M.; Sinenkov, M. A.; Fukin, G. K.; Cherkasov, A. V.; Thomas, C. M.; Carpentier, J. F.; Trifonov, A. A. *Chem. Eur. J* **2008**, *14*, 5440–5448.
- [84] Luo, Y.; Wang, X.; Chen, J.; Luo, C.; Zhang, Y.; Yao, Y. *J. Organomet. Chem.* **2009**, *694*, 1289.
- [85] Wang, Y.; Luo, Y.; Chen, J.; Xue, H.; Liang, H. *New J. Chem.* **2012**, *36*, 933–940.
- [86] Miao, W.; Li, S.; Cui, D.; Huang, B. *J. Organomet. Chem.* **2007**, *692*, 3823.

- [87] Arnold, P. L.; Buffet, J.-C.; Blaudeck, R. P.; Sujecki, S.; Blake, A. J.; Wilson, C. *Angew. Chem. Int. Ed.* **2008**, *47*, 6033–6036.
- [88] Amgoune, A.; Thomas, C. M.; Ilinca, S.; Roisnel, T.; Carpentier, J.-F. *Angew. Chem. Int. Ed.* **2006**, *45*, 2782.
- [89] Bouyahyi, M.; Ajellal, N.; Kirillov, E.; Thomas, C. M.; Carpentier, J.-F. *Chem. Eur. J.* **2011**, *17*, 1872.
- [90] Liu, X.; Shang, X.; Tang, T.; Hu, N.; Pei, F.; Cui, D.; Chen, X.; Jing, X. *Organometallics*, **2007**, *26*, 2747–2757.
- [91] Grunova, E.; Kirillov, E.; Roisnel, T.; Carpentier, J.-F. *Dalton Trans.* **2010**, *39*, 6739–6752.
- [92] Hodgson, L.M.; Platel, R.H.; White, A.J.P.; Williams, C.K. *Macromolecules* **2008**, *41*, 8603–8607.
- [93] Platel, R. H.; White, A. J. P.; Williams, C. K. *Inorg. Chem.* **2011**, *50*, 7718–7728.
- [94] Ma, H.; Spaniol, T.P.; Okuda, J. *Inorg. Chem.* **2008**, *47*, 3328–3339.
- [95] Cao, T. P. A.; Buchard, A.; Le Goff, C. F.; Auffrant, A.; Williams, C. K. *Inorg. Chem.* **2012**, *51*, 2157–2169.
- [96] Bakewell, C.; Cao, T. P. A.; Long, N.; Le Goff, X. F.; Auffrant, A.; Williams, C. K. *J. Am. Chem. Soc.* **2012**, *134*, 20577–20580.
- [97] Ovitt, T. M.; Coates, G. W. *J. Am. Chem. Soc.* **2002**, *124*, 1316–1326.
- [98] Li, W.; Zhang, Z.; Yao, Y.; Zhang, Y.; Shen, Q. *Organometallics* **2012**, *31*, 3499–3511.
- [99] (a) Chisholm, M. H.; Eilerts, N. W.; Huffman, J. C.; Iyer, S. S.; Pacold, M.; Phomphrai, K. *J. Am. Chem. Soc.* **2000**, *122*, 11845–11854. (b) Cheng, M.; Attygalle, A. B.; Lobkovsky, E. B.; Coates, G. W. *J. Am. Chem. Soc.* **1999**, *121*, 11583–11584. (c) Dove, A. P.; Gibson, V. C.; Marshall, E. L.; White, A. J. P.; Williams, D. J. *Dalton Trans.*

- 2004**, 570–578. (d) Helou, M.; Miserque, O.; Brusson, J.-M.; Carpentier, J.-F.; Guillaume, S. M. *Chem. Eur. J.* **2008**, *14*, 8772–8775.
- [100] (a) Chisholm, M. H.; Huffman, J. C.; Phomphrai, K. *J. Chem. Soc., Dalton Trans.* **2001**, 222–224. (b) Chisholm, M. H.; Gallucci, J.; Phomphrai, K. *Inorg. Chem.* **2002**, *41*, 2785–2794.
- [101] (a) Chisholm, M. H.; Eilerts, N. W. *Chem. Commun.* **1996**, 853–854. (b) Chisholm, M. H.; Gallucci, J.; Phomphrai, K. *Chem. Commun.* **2003**, 48–49.
- [102] (a) Nakayama, Y.; Watanabe, K.; Ueyama, N.; Nakamura, A.; Harada, A.; Okuda, J. *Organometallics* **2000**, *19*, 2498–2503. (b) Takashima, Y.; Nakayama, Y.; Watanabe, K.; Itono, T.; Ueyama, N.; Nakamura, A.; Yasuda, H.; Harada, A.; Okuda, J. *Macromolecules* **2002**, *35*, 7538–7544. (c) Takashima, Y.; Nakayama, Y.; Hirao, T.; Yasuda, H.; Harada, A. *J. Organomet. Chem.* **2004**, *689*, 612–619.
- [103] (a) Wisniewski, M.; Borgne, A. L.; Spassky, N. *Macromol. Chem. Phys.* **1997**, *198*, 1227–1238. (b) Bhaw-Luximon, A.; Jhurry, D.; Spassky, N. *Polym. Bull.* **2000**, *44*, 31–38. (c) Nomura, N.; Ishii, R.; Akakura, M.; Aoi, K. *J. Am. Chem. Soc.* **2002**, *124*, 5938–5939.
- [104] Lewinski, J.; Horeglad, P.; Wójcik, K.; Justyniak, I. *Organometallics* **2005**, *24*, 4588–4593.
- [105] Dagorne, S.; Le Bideau, F.; Welter, R.; Bellemin-Laponnaz, S.; Maise-François, A. *Chem. Eur. J.* **2007**, *13*, 3202–3217.
- [106] Dove, A. D.; Gibson, V. C.; Marshall, E. L.; Rzepa, H. S.; White, A. J. P.; Williams, D. J. *J. Am. Chem. Soc.* **2006**, *128*, 9834–9843.
- [107] Ma, H.; Spaniol, T. P.; Okuda, J. *Angew. Chem. Int. Ed.* **2006**, *45*, 7818–7821.
- [108] Phomphrai, K.; Chumsaeng, P.; Sangtrirutnugul, P.; Kongsaree, P.; Pohmakotr, M. *Dalton Trans.* **2010**, *39*, 1865–1871.

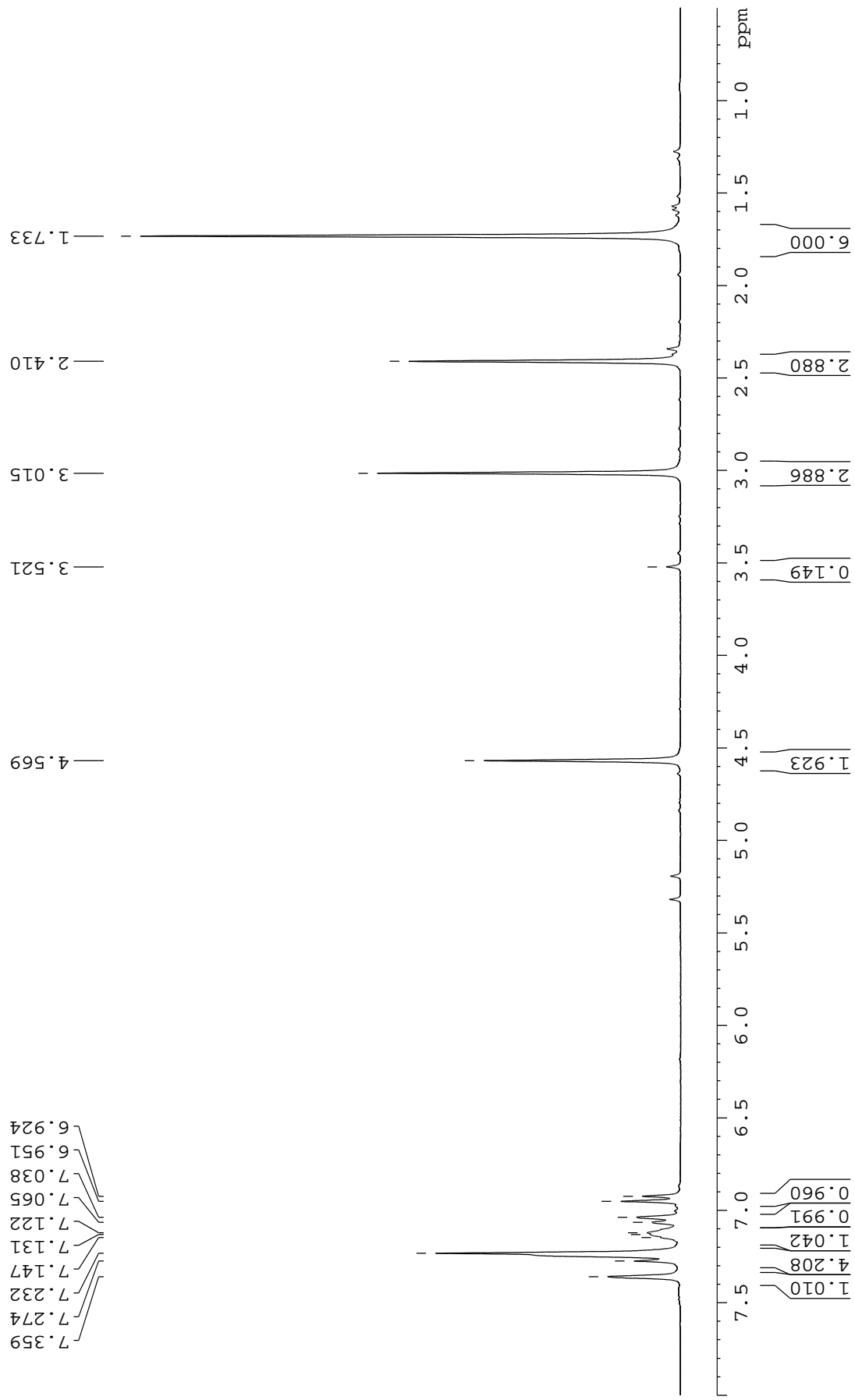
- [109] Marshall, E. L.; Gibson, V. C.; Rzepa, H. S. *J. Am. Chem. Soc.* **2005**, *127*, 6048–6051.
- [110] Vieira, I. dos S.; Whitelaw, E. L.; Jones, M. D.; Herres-Pawlis, S. *Chem. Eur. J* **2013**, *19*, 4712–4716.
- [111] Fang, J.; Tschan, M. J.-L.; Roisnel, T.; Trivelli, X.; Gauvin, R. M.; Thomas, C. T.; Maron, L. *Polym. Chem.* **2013**, *4*, 360–367.
- [112] Kochnev, A. I.; Oleynik, I. I.; Oleynik, I. V.; Ivanchev, S. S.; Tolstikov, G. A. *Russ. Chem. Bull., Int. Ed.*, **2007**, *56*, 1125–1129.
- [113] Kirillov, E.; Roisnel, T.; Razavi, A.; Carpentier, J-F. *Organometallics*, **2009**, *28*, 5036–5051.
- [114] Anwander, R.; Runte, O.; Eppinger, J.; Gertberger, G.; Herdtweck, E.; Spiegler, M. *J. Chem. Soc., Dalton Trans.* **1998**, 847.
- [115] Altomare, A.; Burla, M.C.; Camalli, M.; Cascarano, G.; Giacovazzo, C.; Guagliardi, A.; Moliterni, A.G.G.; Polidori, G.; Spagna, R. *J. Appl. Crystallogr.* **1999**, *32*, 115.
- [116] (a) Sheldrick, G.M. SHELXS-97, Program for the Determination of Crystal Structures, University of Goettingen, Germany, **1997**; (b) Sheldrick, G.M. SHELXL-97, Program for the Refinement of Crystal Structures, University of Goettingen, Germany, **1997**.
- [117] Farrugia, L.J. *J. Appl. Crystallogr.* **1999**, *32*, 837.
- [118] Barakat, I.; Dubois, P.; Jerome, R.; Teyssie, P. *J. Polym. Sci., A: Polym. Chem.* **1993**, *31*, 505.
- [119] Similar reactions with  $\{\text{OSO}^{\text{SiPh}_3}\}_2\text{H}_2$  pro-ligand resulted in instable materials.
- [120] Chen, C.-T.; Huang, C.-A.; Huang B.-H. *Macromolecules* **2004**, *37*, 7968–7973.
- [121] Alcazar-Roman, L. M.; O’Keefe, B. J.; Hillmyer, M. A.; Tolman, W. B. *Dalton Trans.* **2003**, 3082–3087.



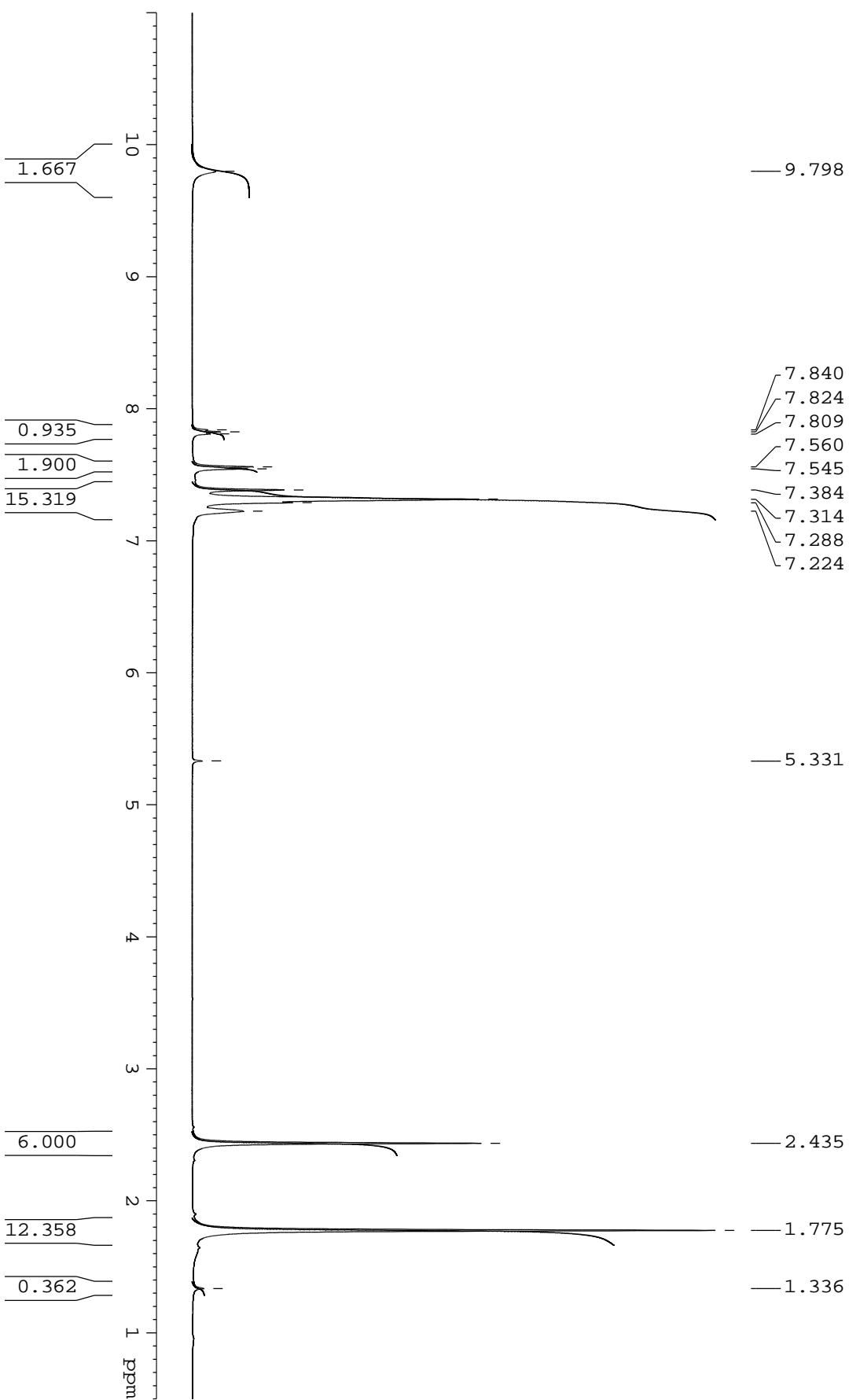
- [122] Silverstein, R. M.; Webster, F. X.; Kiemle, D.; Kiemle, D. J. *Spectrometric identification of organic compounds*. John Wiley & Sons, Inc., **2003**. p. 189.
- [123] The carbonyl carbons of (alkyl lactate)-Al complexes in the  $^{13}\text{C}$  NMR spectrum (C=O...Al) are reported to appear at  $\delta$  181.8–185.3 ppm. See: Ko, B.-T.; Wang, F.-C.; Sun, Y.-L.; Lin, C.-H.; Lin, C. -C.; Kuo, C. -Y. *Polyhedron* **1998**, *17*, 4257–4264.
- [124] In comparison, a dialkyl-aluminum complex of  $\alpha$ -tropolone and ethyl *rac*-lactate shows a much stronger distortion (angle formed by the axial bonds =  $153.8(1)^\circ$ ), which was ascribed to the constraints imposed by the central four-membered and chelating five-membered heterocyclic rings in this compound. See: Addison, A. W.; Rao, T. N.; Reedijk, J.; Van Rijn, J.; Verschoor, G. C. *J. Chem. Soc., Dalton Trans.* **1984**, 1349–1356.
- [125] Lewinski, J.; Zachara, J.; Justyniak, I. *Organometallics* **1997**, *16*, 4597–4605.
- [126] Chen, C-T.; Huang, C-A.; Huang, B-H. *Dalton Trans.* **2003**, 3799–3803.
- [127] (a) Broder, C. K.; Davidson, M. G.; Forsyth, V. T.; Howard, J. A. K.; Lamb, S.; Mason, S. A. *Cryst. Growth Des.* **2002**, *2*, 163. (b) Desiraju, G. R.; Steiner, T. *The Weak Hydrogen Bond*, Oxford University Press, Oxford, **1999**.
- [128] Shannon, R. D. *Acta Cryst.* **1976**, *A32*, 751 – 767.
- [129] Anwander, R.; Runte, O.; Eppinger, J.; Gerstberger, G.; Herdtweck, E.; Spiegler, M. *J. Chem. Soc. Dalton Trans.* **1998**, 847.
- [130] NMR studies in THF- $d_8$  were more complicated than expected. For now, they are not discussed here.
- [131] Hieringer, W.; Eppinger, J.; Anwander, R.; Herrmann, W. A. *J. Am. Chem. Soc.* **2000**, *122*, 11983-11994.

**Table 1A.** Summary of crystal and refinement data for compounds **2a**, **5a**, **6a**, **5d**, **1c** and **9**.

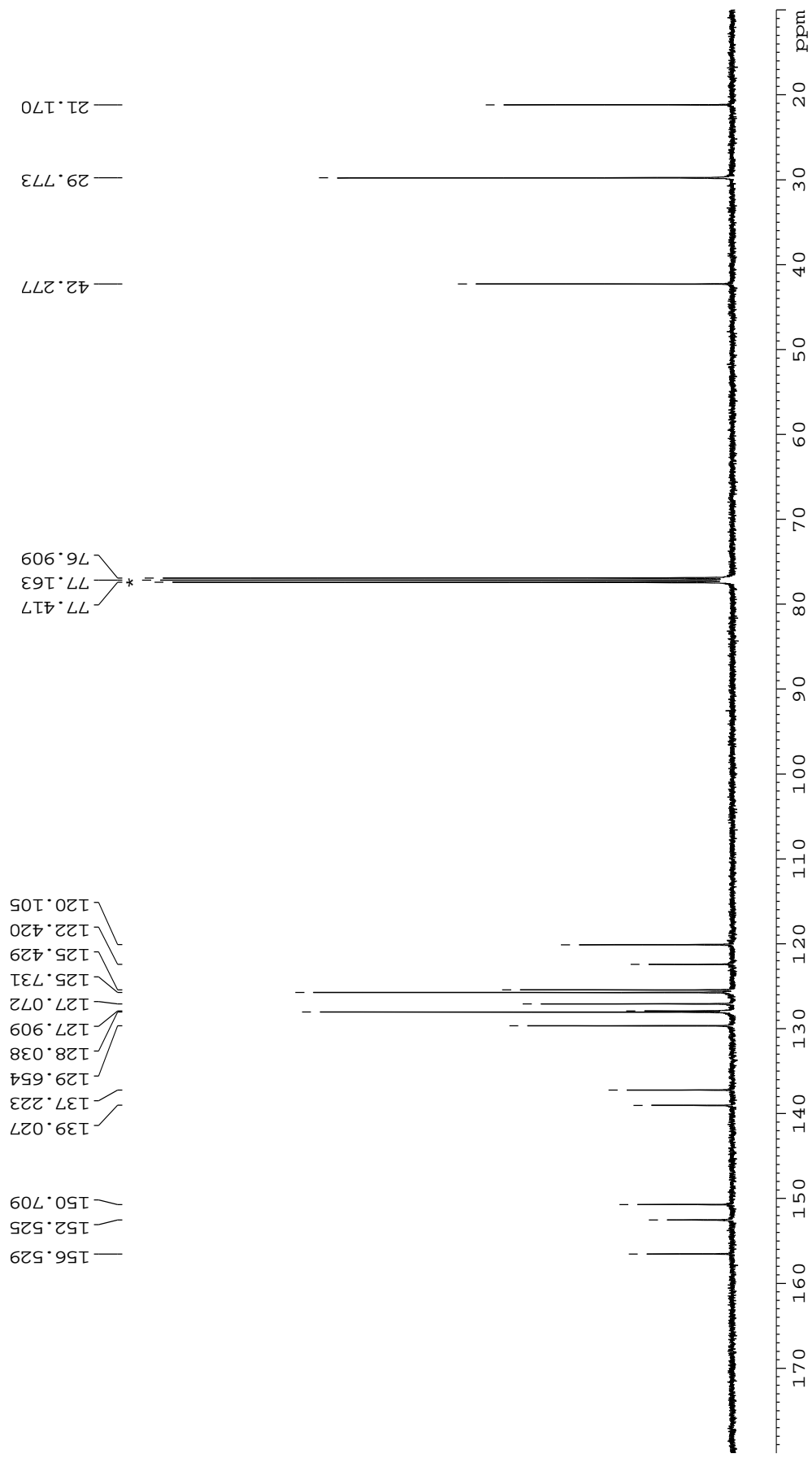
	<b>2a</b>	<b>5a</b>	<b>6a</b>	<b>5d</b>	<b>1c</b>	<b>9</b>
Empirical formula	C <sub>62</sub> H <sub>46</sub> AlNO <sub>2</sub> Si <sub>2</sub>	C <sub>66</sub> H <sub>51</sub> AlNO <sub>5</sub> Si <sub>2</sub>	C <sub>67</sub> H <sub>51</sub> AlF <sub>3</sub> NO <sub>5</sub> Si <sub>2</sub>	C <sub>84</sub> H <sub>88</sub> Al <sub>2</sub> N <sub>2</sub> O <sub>10</sub>	C <sub>37</sub> H <sub>37</sub> NO <sub>2</sub>	C <sub>49</sub> H <sub>67</sub> N <sub>2</sub> O <sub>4</sub> Si <sub>2</sub> Y
Formula weight	920.16	1022.25	1090.25	1339.52	527.68	893.14
Crystal system	Monoclinic	Triclinic	Triclinic	Triclinic	Monoclinic	Monoclinic
Space group	P 2 <sub>1</sub> /c	P -1	P -1	P -1	P 2 <sub>1</sub> /n	P 2 <sub>1</sub> /n
a, Å	11.3014(2)	12.5250(4)	12.613(5)	15.8935(5)	13.1098(12)	12.896(2)
b, Å	18.2532(3)	14.0401(6)	14.577(6)	16.9816(4)	8.0072(7)	25.405(3)
c, Å	27.8300(5)	18.6406(8)	19.572(7)	18.2728(6)	27.619(3)	15.536(2)
α (°)	90	91.530(2)	79.851(18)	107.2690(10)	90	90
β (°)	92.8790(10)	96.906(2)	72.166(15)	107.1600(10)	90.292(4)	110.122(5)
γ (°)	90	99.4860(10)	85.080(16)	114.6260(10)	90	90
Volume, Å <sup>3</sup>	5733.71(17)	3206.1(2)	3370(2)	3750.09(19)	2899.2(5)	4779.3(11)
Z	4	2	2	2	4	4
Density, g.m <sup>-3</sup>	1.066	1.059	1.074	1.186	1.209	1.241
m, mm <sup>-1</sup>	0.117	0.114	0.118	0.098	0.074	1.314
F(000)	1928	1072	1136	1424	1128	1896
Crystal size, mm	0.22 × 0.15 × 0.09	0.27 × 0.22 × 0.14	0.22 × 0.16 × 0.09	0.6 × 0.3 × 0.23	0.57 × 0.08 × 0.05	0.55 × 0.46 × 0.38
θ range, deg	2.93 to 27.48	2.92 to 27.5	2.95 to 27.49	1.33 to 27.52	2.94 to 27.48	2.94 to 27.48
Limiting indices	-8 ≤ h ≤ 14, -23 ≤ k ≤ 20, -35 ≤ l ≤ 34	-12 ≤ h ≤ 16, -18 ≤ k ≤ 16, -24 ≤ l ≤ 24	-16 ≤ h ≤ 16, -18 ≤ k ≤ 18, -25 ≤ l ≤ 25	-20 ≤ h ≤ 17, -20 ≤ k ≤ 22, -23 ≤ l ≤ 23	-16 ≤ h ≤ 16, -9 ≤ k ≤ 10, -35 ≤ l ≤ 35	-16 ≤ h ≤ 16, -27 ≤ k ≤ 32, -30 ≤ l ≤ 20
Reflec. Collected	46721	40484	45953	42735	26552	42223
R <sub>int</sub>	0.0377	0.0589	0.0491	0.044	0.07	0.0531
Reflec. Unique [I > 2σ(I)]	12982	14412	15081	17008	6546	10851
Data/restrains/ param.	12982 / 0 / 614	14412 / 0 / 689	15081 / 0 / 689	17008 / 0 / 913	6546 / 0 / 369	10851 / 0 / 512
Goodness-of-fit on F <sup>2</sup>	1.079	1.081	1.132	1.061	1.012	1.022
R <sub>1</sub> [I > 2σ(I)] (all data)	0.0534 (0.0727)	0.0753 (0.1068)	0.0842 (0.1171)	0.078 (0.119)	0.0546 (0.12)	0.0518 (0.0742)
wR <sub>2</sub> [I > 2σ(I)] (all data)	0.1595 (0.1704)	0.198 (0.2117)	0.2531 (0.2767)	0.2223 (0.2412)	0.1113 (0.144)	0.1261 (0.136)
Largest diff. e.Å <sup>-3</sup>	0.498 and -0.28	0.368 and -0.324	1.041 and -1.047	0.512 and -0.45	0.255 and -0.243	1.397 and -0.993



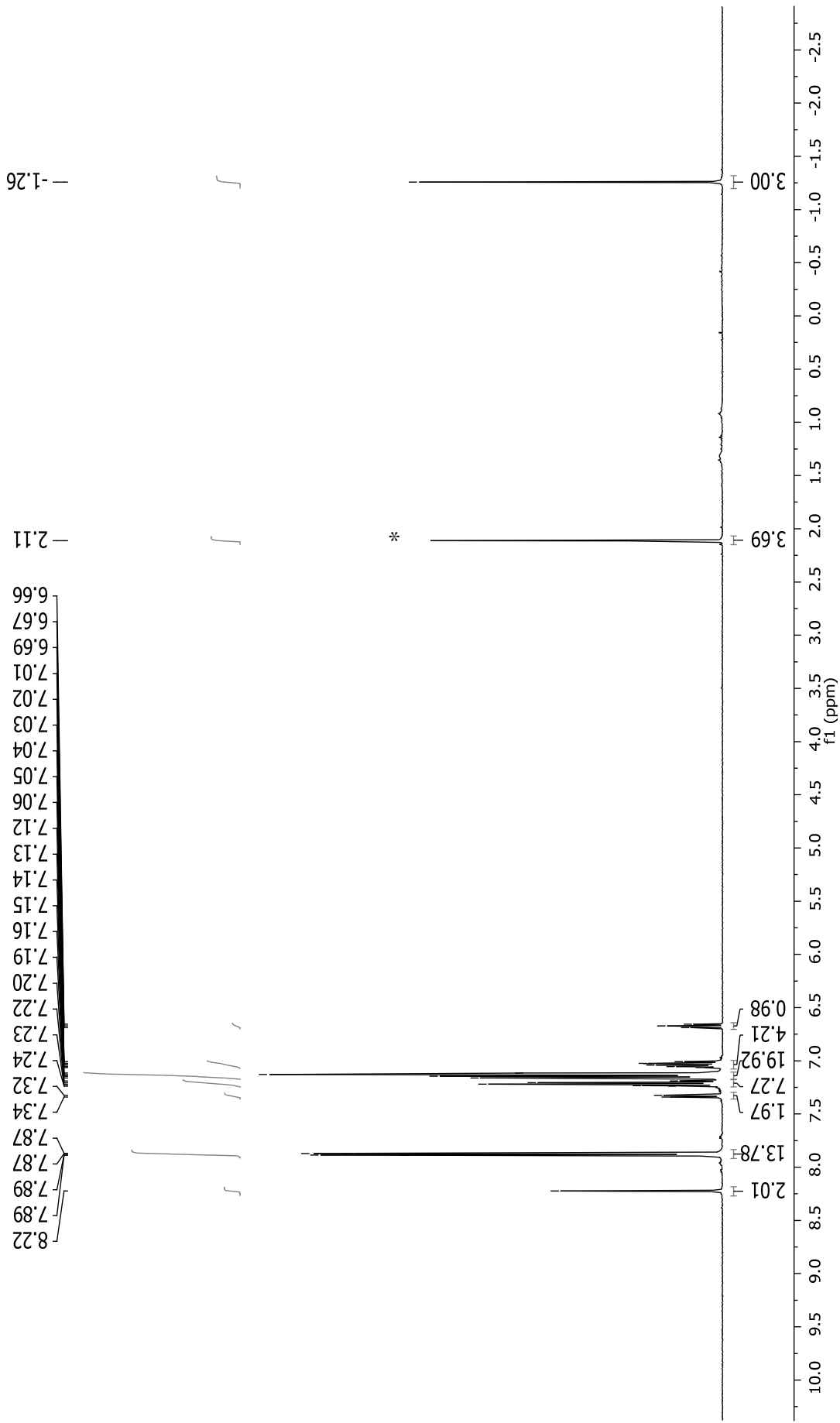
**Figure 1A.**  $^1\text{H}$  NMR spectrum (300 MHz,  $\text{CDCl}_3$ , 298 K) of 1-(methoxymethyl)-4-methyl-2-(2-phenylpropan-2-yl)benzene.



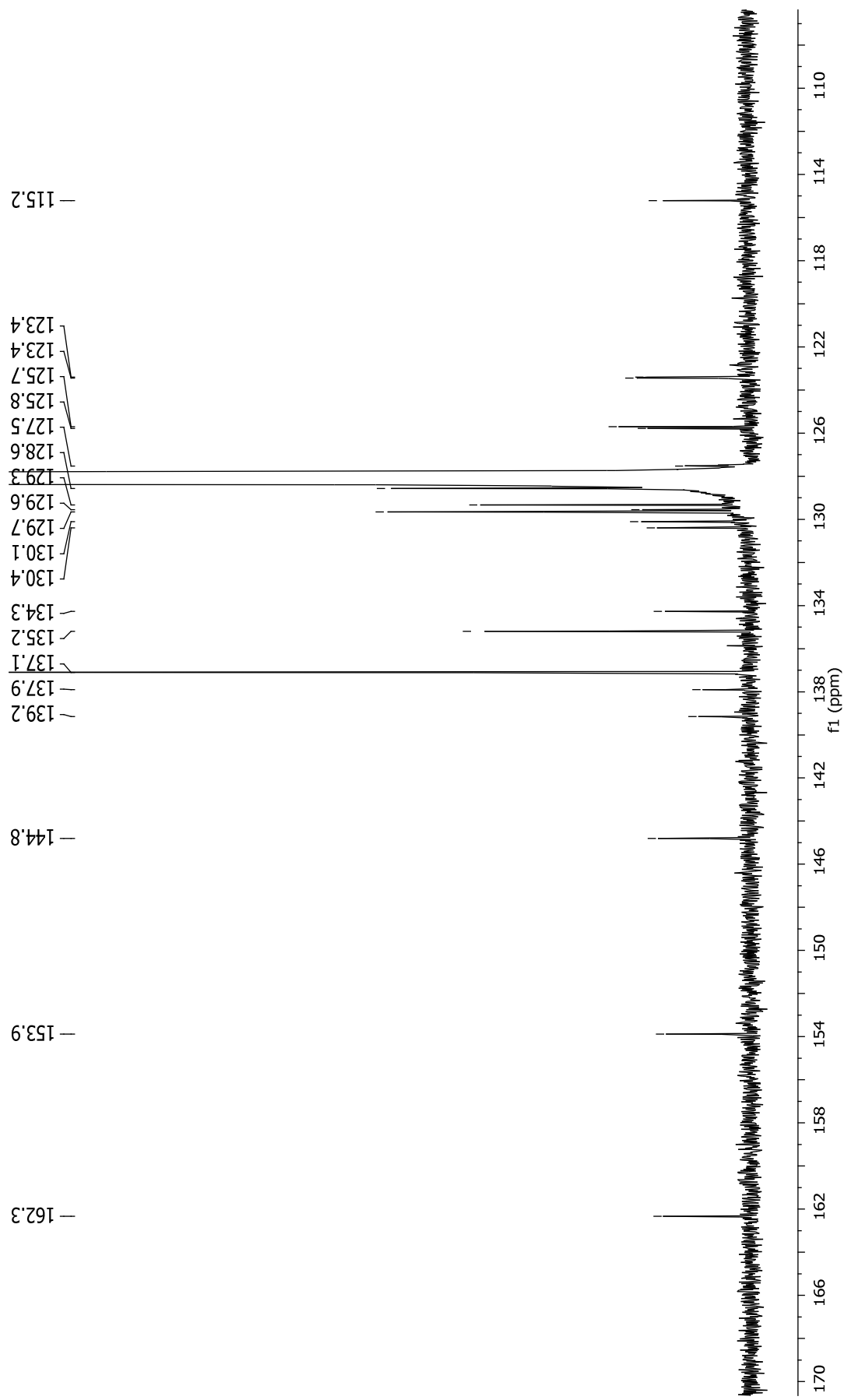
**Figure 2A.**  $^1\text{H}$  NMR spectrum (500 MHz,  $\text{CDCl}_3$ , 298 K) of  $\{(\text{ONO})^{\text{Me,Cunyl}}\}_2\text{H}_2$  (**1c**).



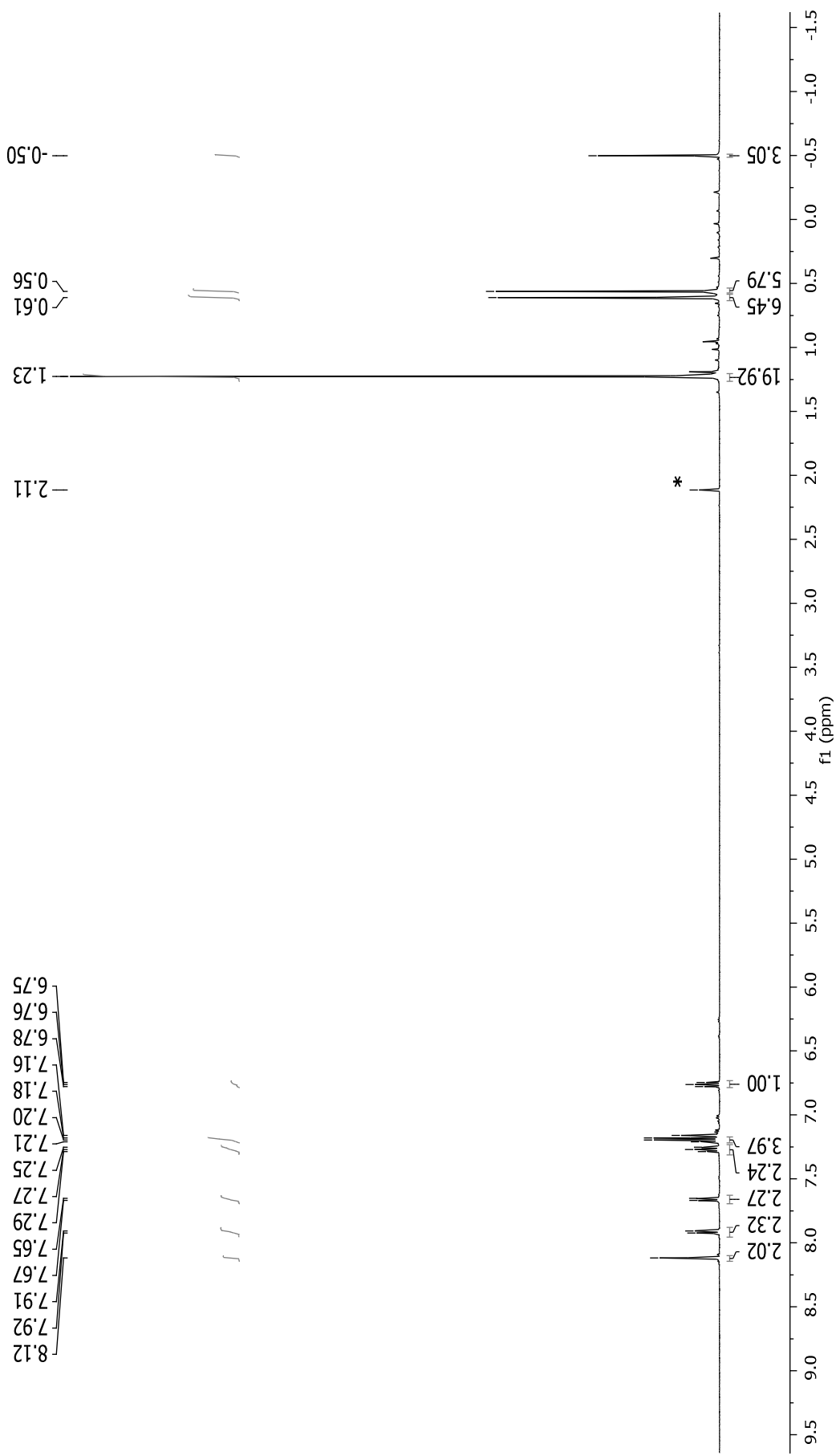
**Figure 3A.**  $^{13}\text{C}\{^1\text{H}\}$  NMR spectrum (125 MHz,  $\text{CDCl}_3$ , 298 K) of  $\{\text{ONO}^{\text{Me,Cumyl}}\}\text{H}_2$  (**1c**) (stands for residual solvent resonances).



**Figure 4A.**  $^1\text{H}$  NMR spectrum (500 MHz,  $\text{C}_6\text{D}_6$ , 298 K) of  $\{\text{ONO}^{\text{SiPh}_3}\}\text{AlMe}$  (**2a**) (\*stands for residual solvent resonances).

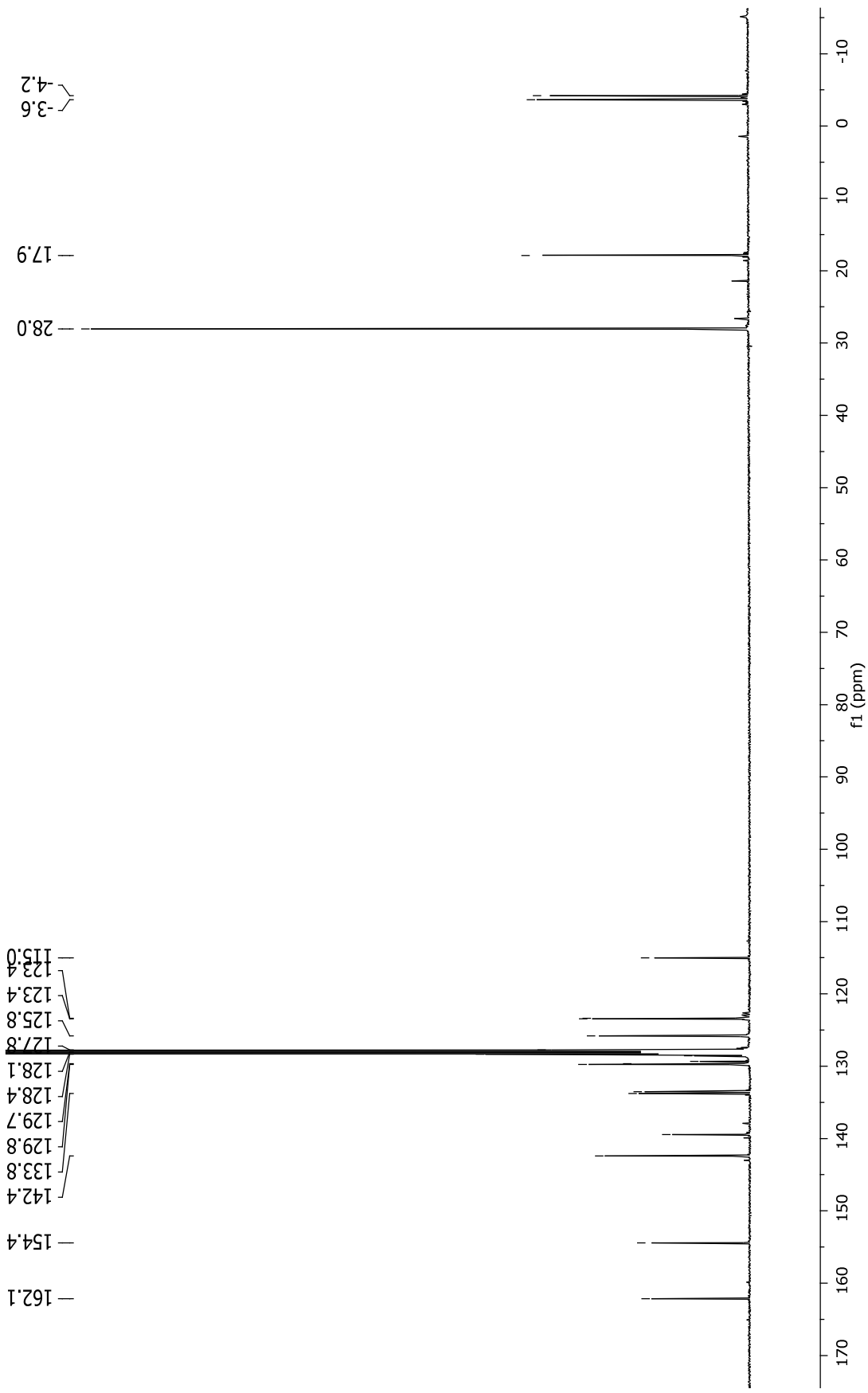


**Figure 5A.** Aromatic selected region of  $^{13}\text{C}\{^1\text{H}\}$  NMR spectrum (125 MHz,  $\text{C}_6\text{D}_6$ , 298 K) of  $\{\text{ONO}^{\text{SiPh}_3}\}\text{AlMe}$  (2a).



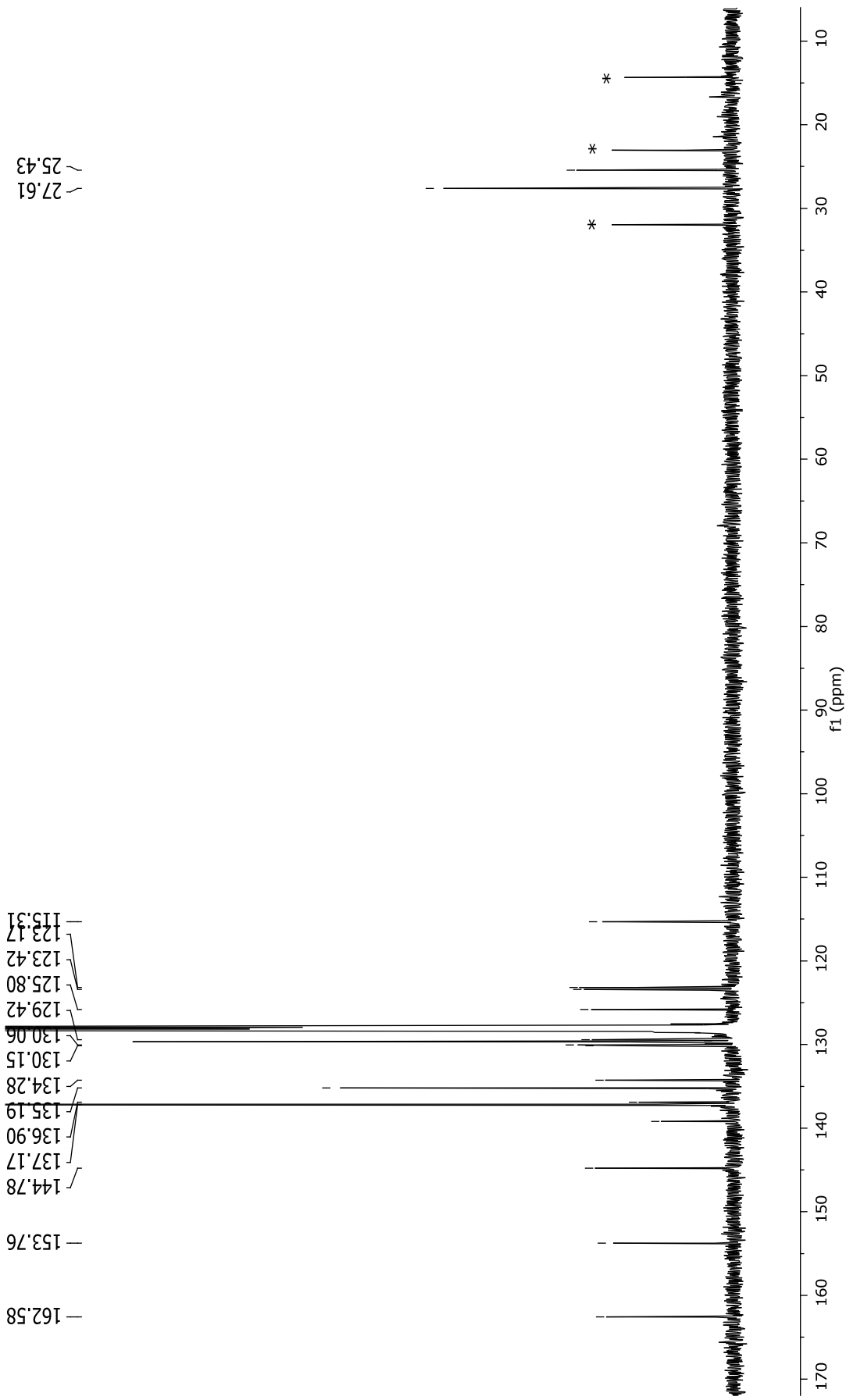
**Figure 6A.** <sup>1</sup>H NMR spectrum (500 MHz, C<sub>6</sub>D<sub>6</sub>, 298 K) of {ONO<sup>SiMe<sub>2</sub>tBu</sup>}AlMe (2b) (\*stands for residual toluene resonance).



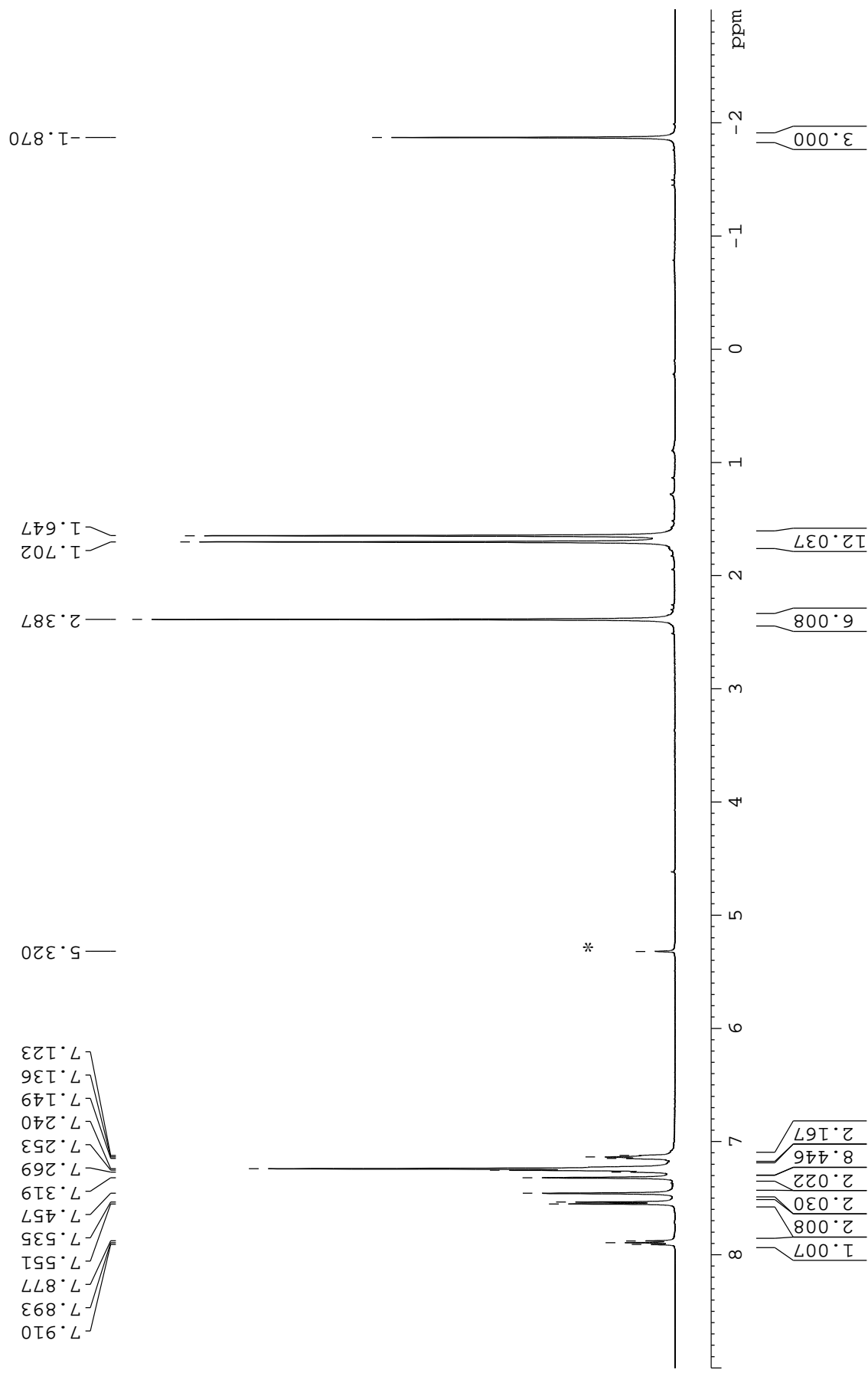


**Figure 7A.**  $^{13}\text{C}\{^1\text{H}\}$  NMR spectrum (125 MHz,  $\text{C}_6\text{D}_6$ , 298 K) of  $\{\text{ONO}^{\text{SiMe}_2\text{tBu}}\}\text{AlMe}$  (**2b**).

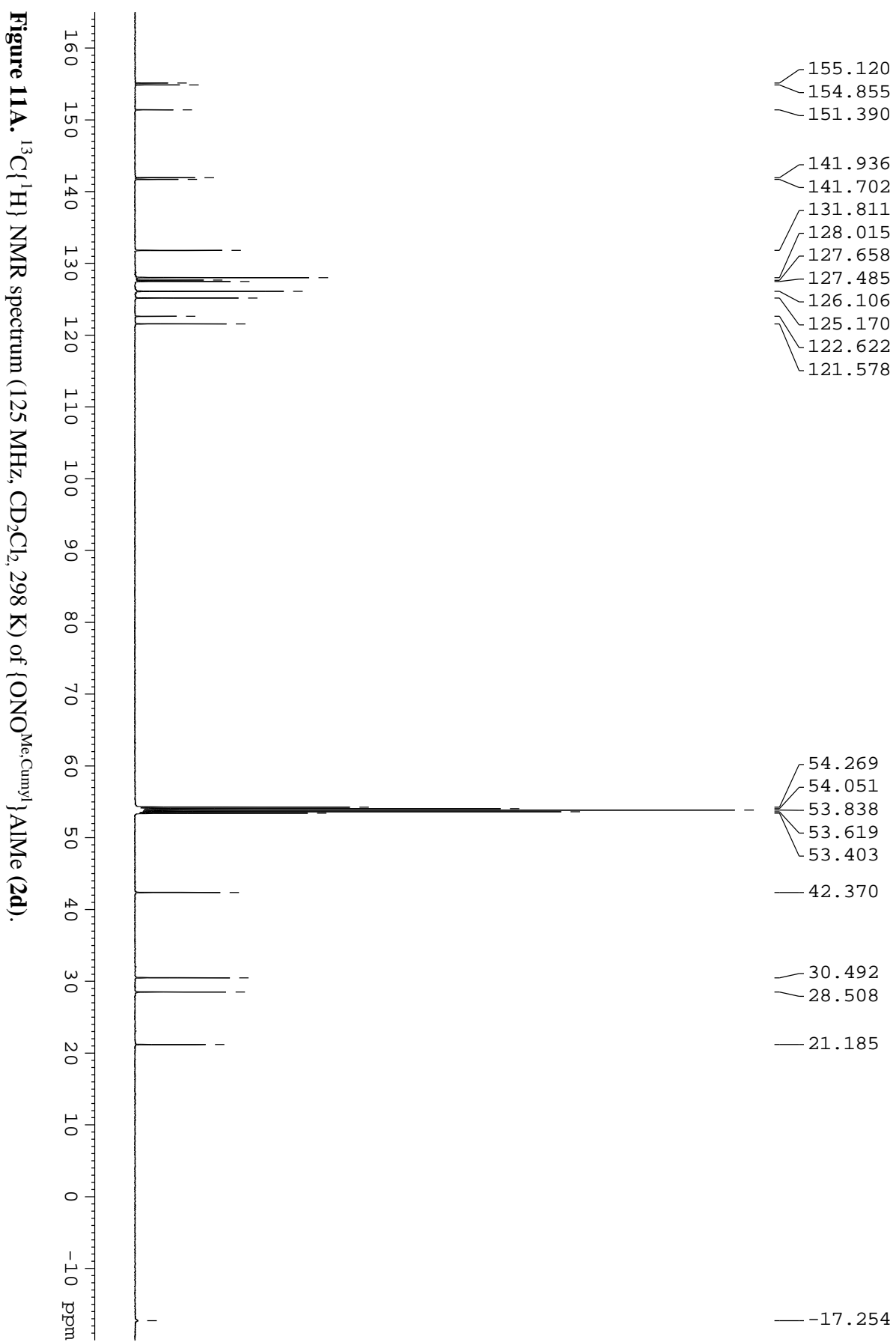




**Figure 9A.**  $^{13}\text{C}\{^1\text{H}\}$  NMR spectrum (125 MHz,  $\text{C}_6\text{D}_6$ , 298 K) of  $\{\text{ONO}^{\text{SiPh}_3}\}_t\text{Al}^i\text{Bu}$  (**2c**) (\*stands for residual hexane resonances).



**Figure 10A.** <sup>1</sup>H NMR spectrum (500 MHz, CD<sub>2</sub>Cl<sub>2</sub>, 298 K) of {ONO<sup>Me,Cumyl</sup>1}AlMe (**2d**) (\*stands for residual solvent resonances).



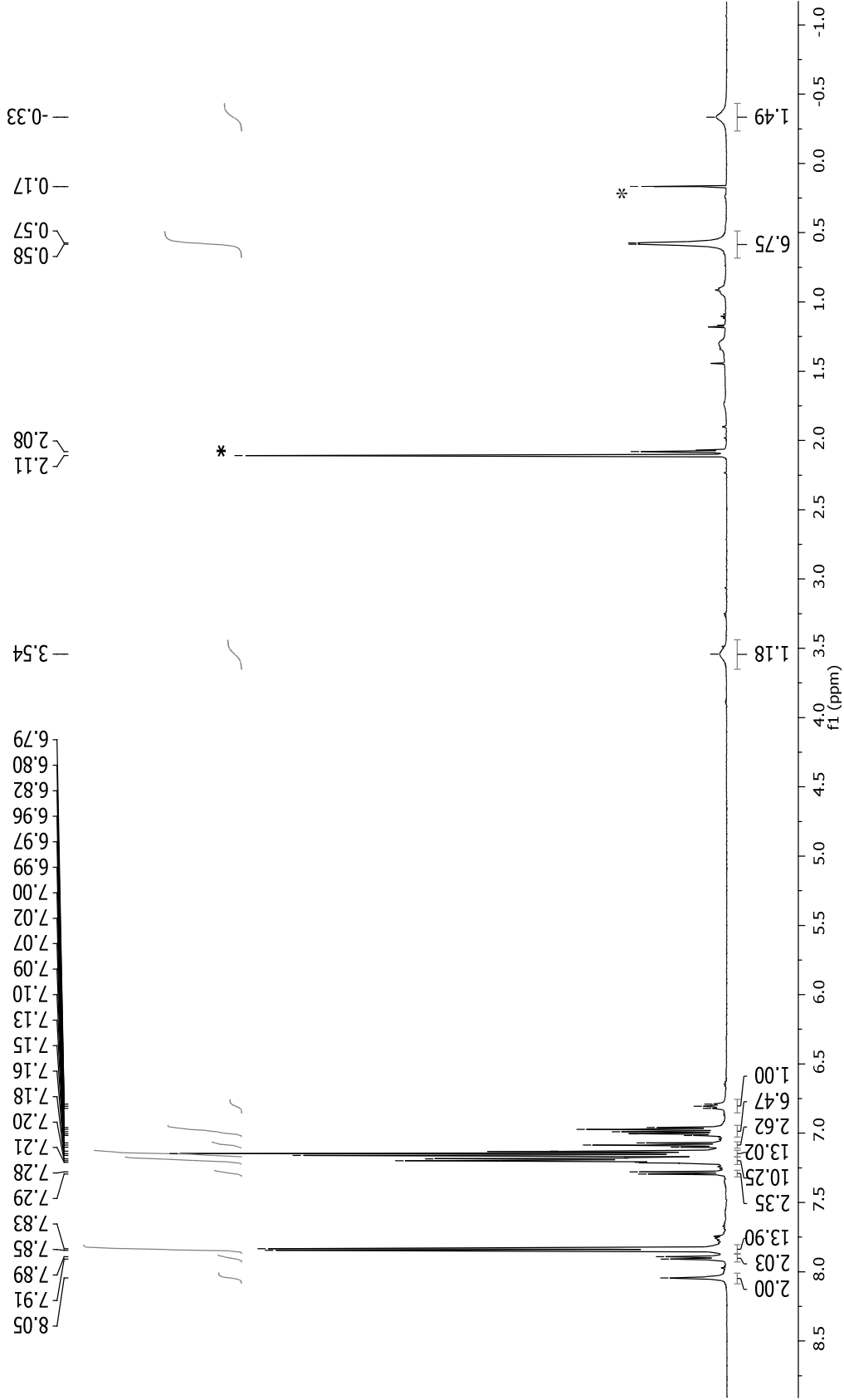


**Figure 12A.**  $^1\text{H}$  NMR spectrum (500 MHz, toluene- $d_8$ , 298 K) of  $\{\text{ONO}^{\text{SiPh}_3}\}_3\text{Al(OiPr)}$  (**3a**) (\*stands for residual toluene resonance and methane release).

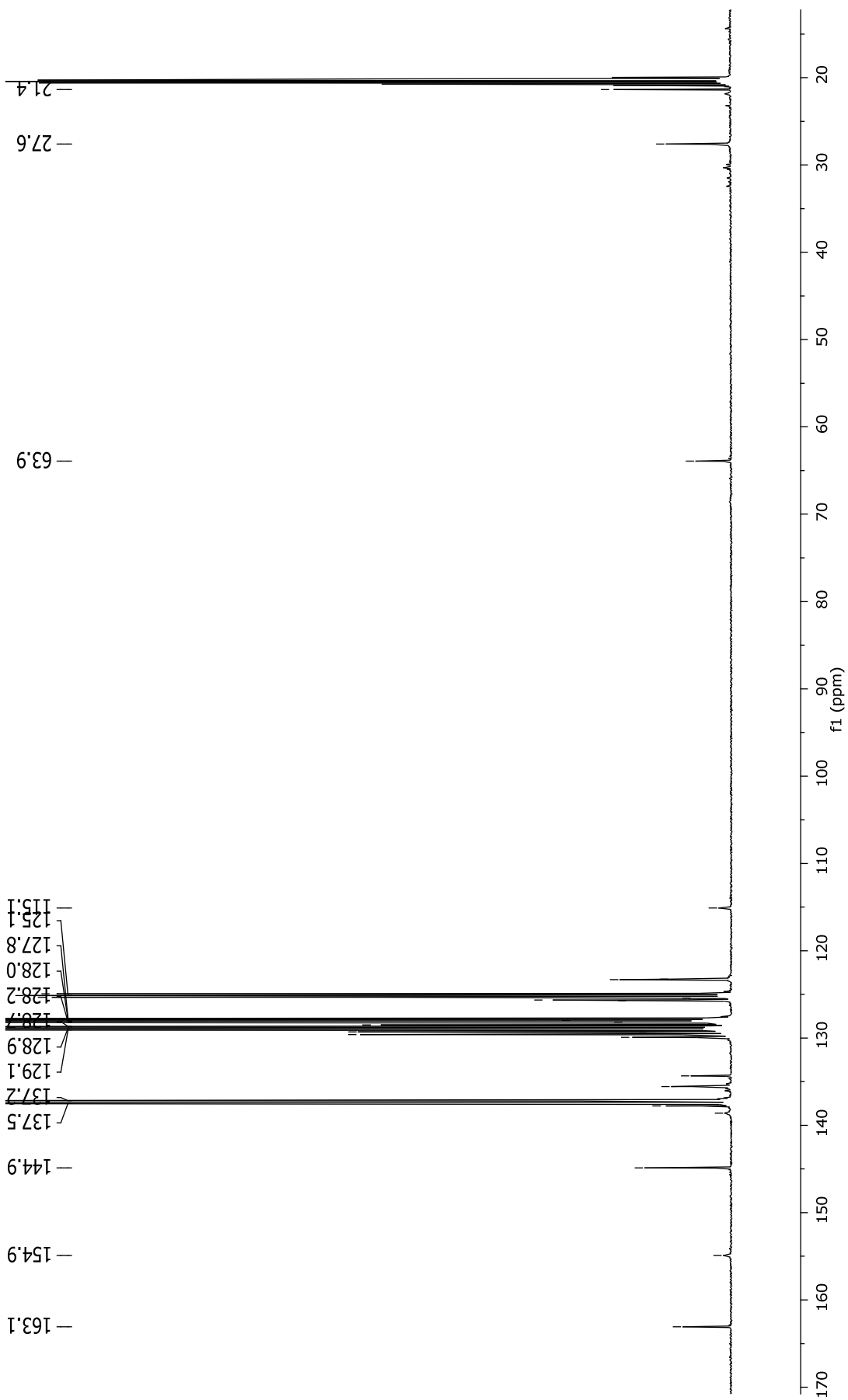


**Figure 13A.**  $^{13}\text{C}\{^1\text{H}\}$  NMR spectrum (125 MHz, toluene- $d_8$ , 298 K) of  $\{\text{ONO}^{\text{SiPh}_3}\text{AlOiPr}\}$  (3a).

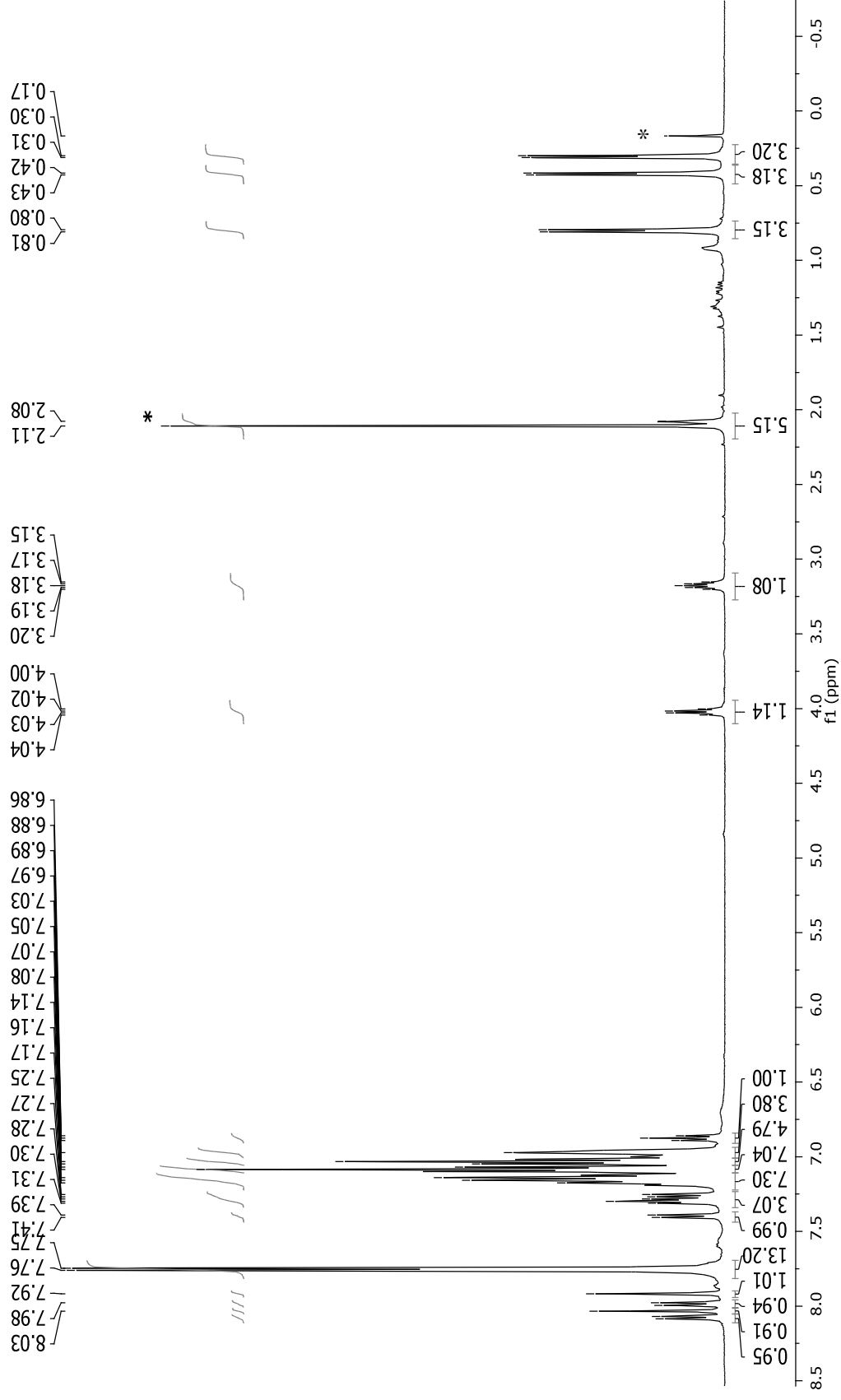


**Figure 14A.**  $^1\text{H}$  NMR spectrum (500 MHz, toluene- $d_8$ , 298 K) of  $\{\text{ONO}^{\text{SiPh}_3}\text{Al}(\text{rPr}(\text{S})\text{-lactate})\text{Al}(\text{rPh})_3\}$  (**4a**) (\*stands for residual toluene resonance and methane reelease).



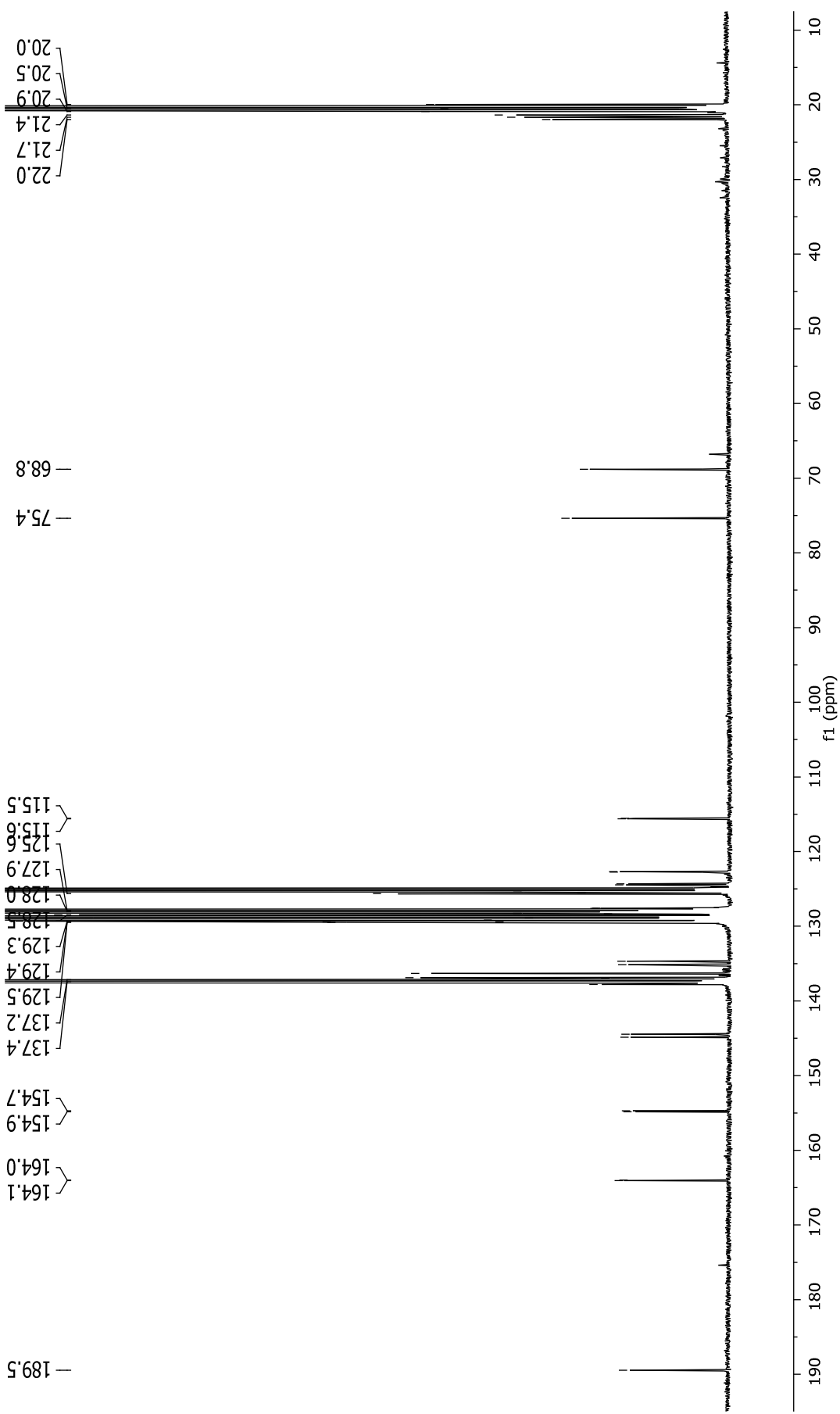


**Figure 15A.**  $^{13}\text{C}\{^1\text{H}\}$  NMR spectrum (125 MHz, toluene- $d_8$ , 298 K) of  $\{\text{ONO}^{\text{SiPh}_3}\}\text{Al}(i\text{Pr}(S))\text{-lactate}$  (**4a**).

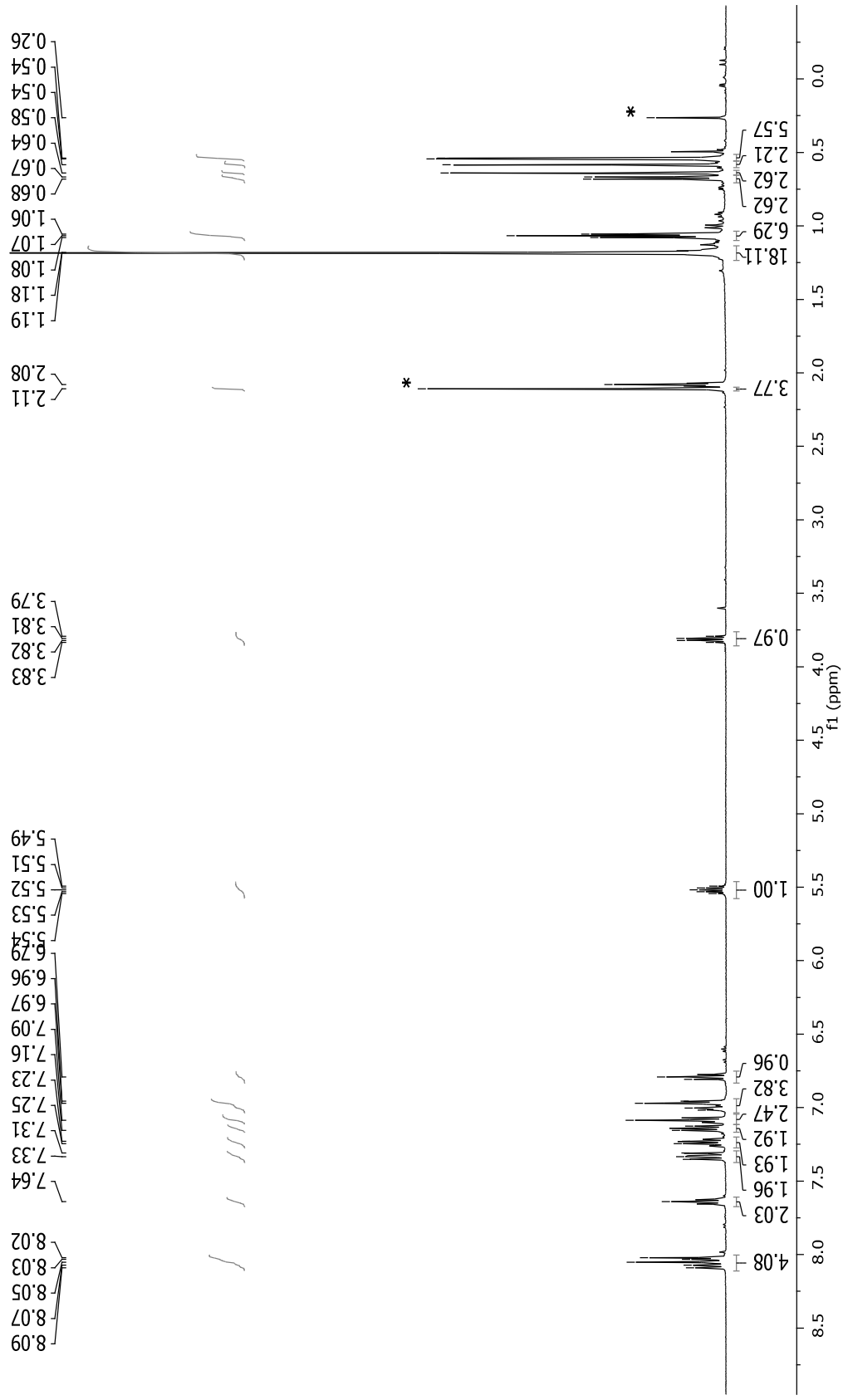


**Figure 16A.**  $^1\text{H}$  NMR spectrum (500 MHz, toluene- $d_8$ , 298 K) of  $\{\text{ONO}^{\text{SiMe}_2\text{tBu}}\}_2\text{Al}(i\text{Pr}(S)\text{-lactate})$  (**4b**) (\*stands for residual toluene and silicon grease resonances).



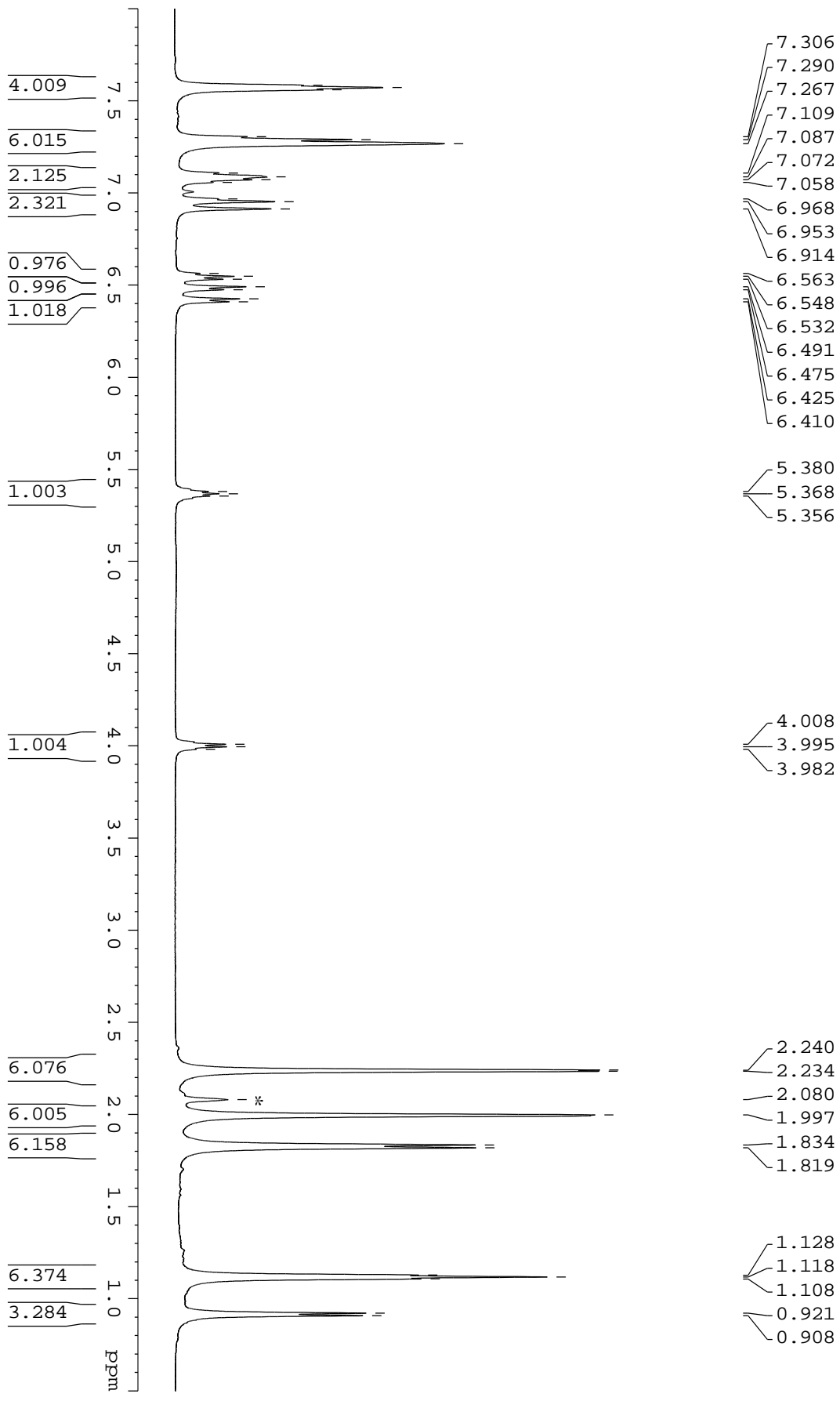
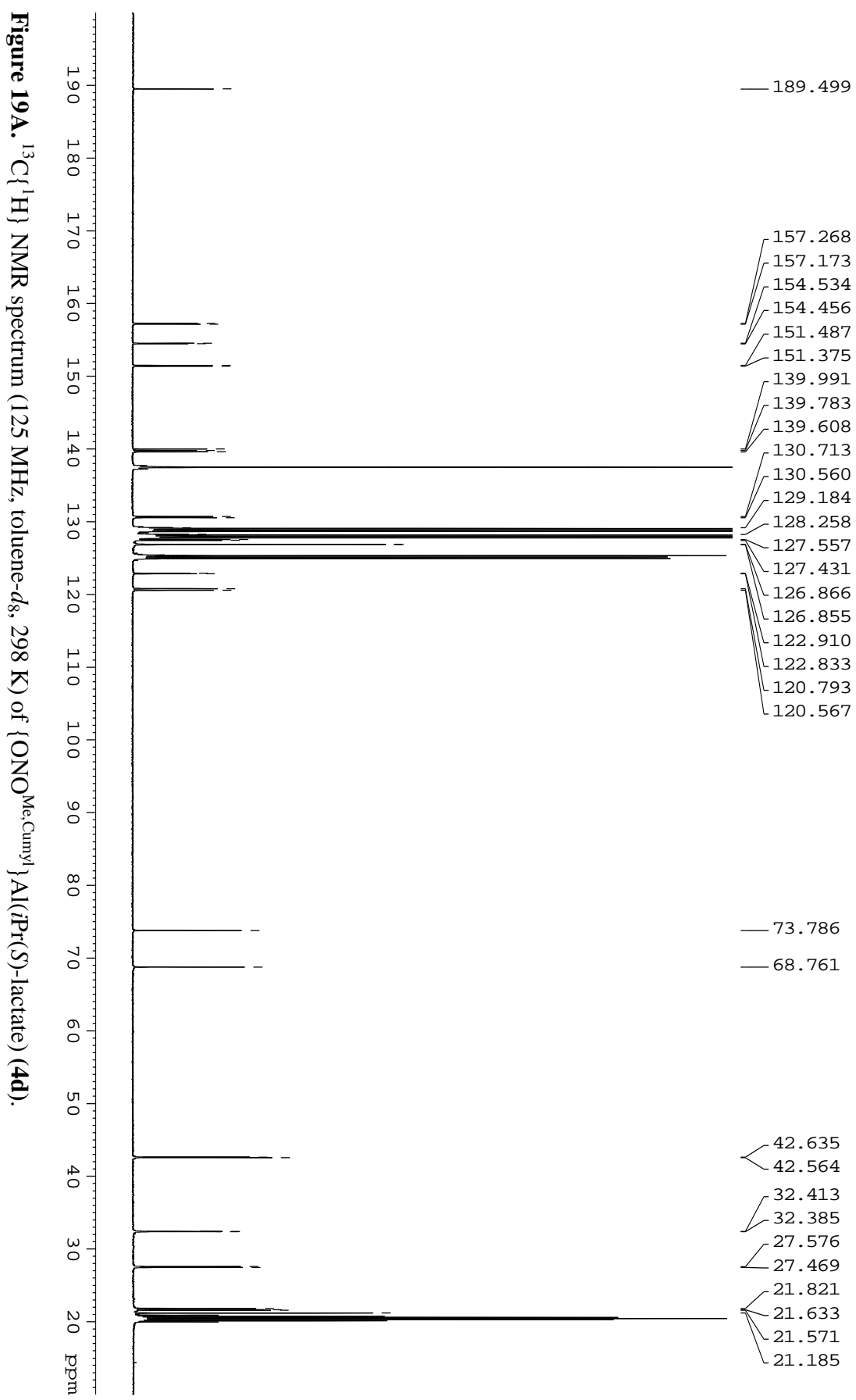
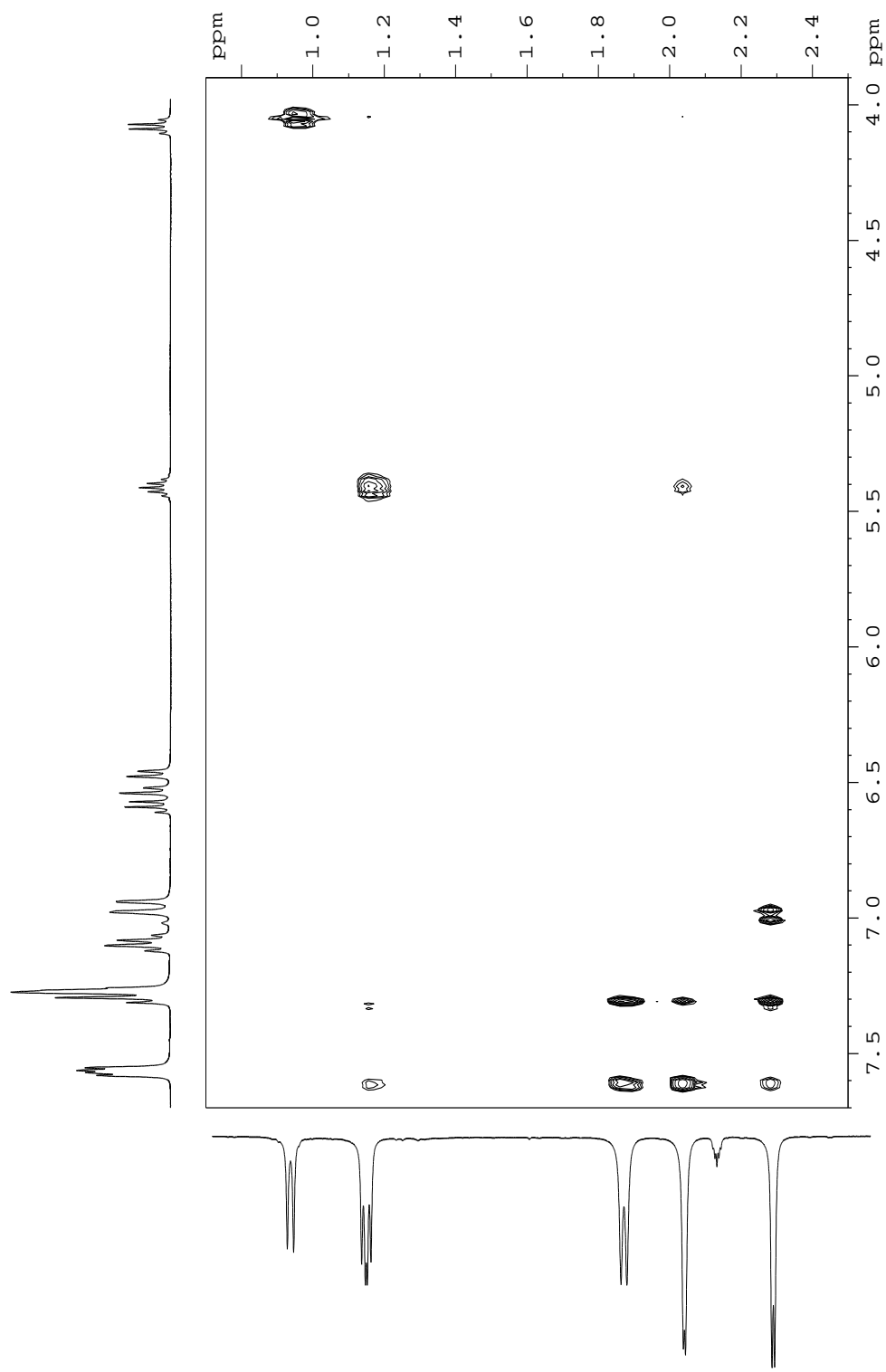
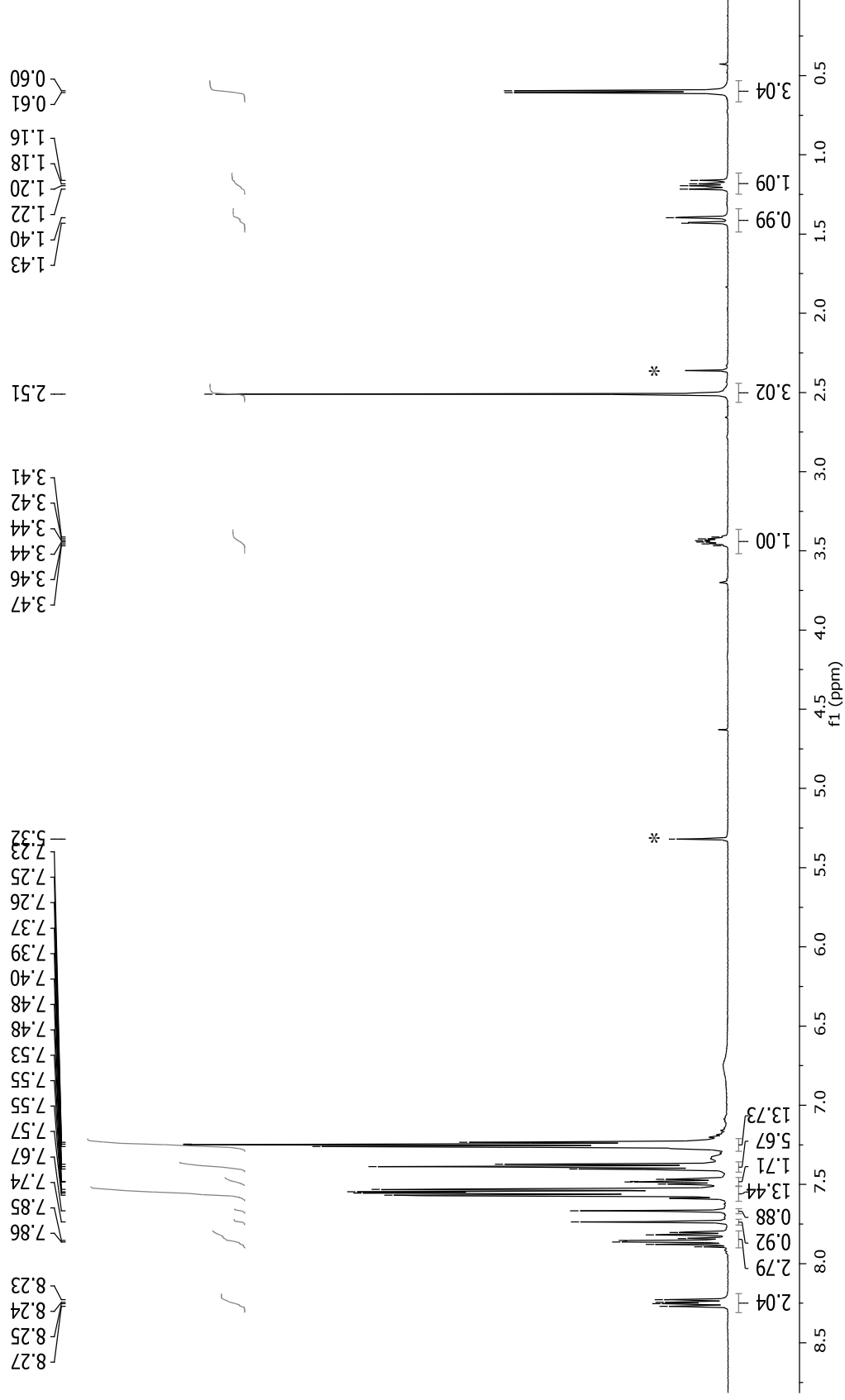


Figure 18A. <sup>1</sup>H NMR spectrum (500 MHz, toluene-*d*<sub>8</sub>, 298 K) of {ONO<sup>Me</sup><sub>2</sub>C<sub>6</sub>H<sub>4</sub>Y<sup>1</sup>}Al(*i*Pr(*S*)-lactate) (**4d**) (\*stands for residual solvent resonances).

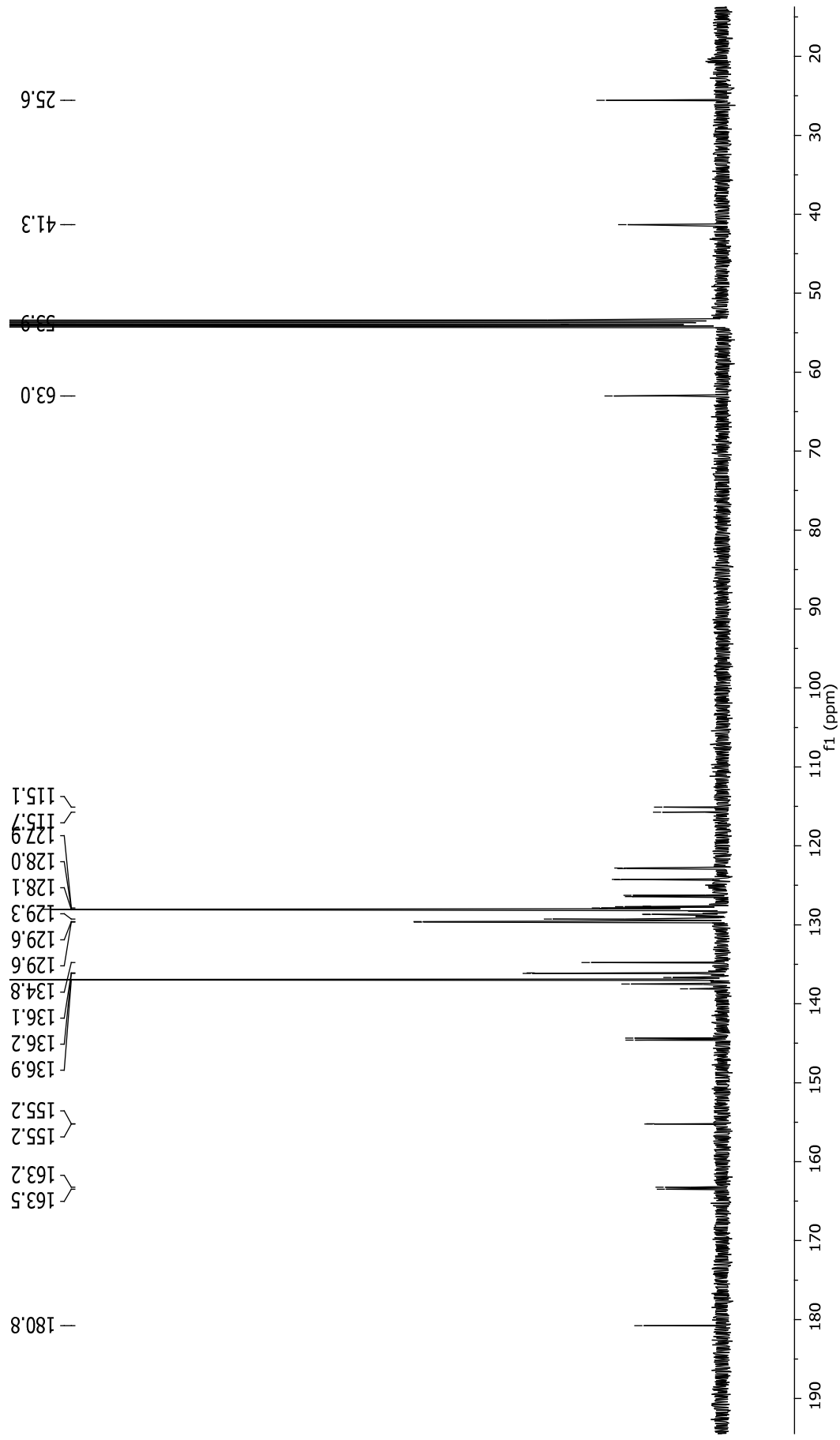




**Figure 20A.**  $^1\text{H}$ - $^1\text{H}$  NOESY NMR spectrum (400 MHz, toluene- $d_8$ , 298 K) of  $\{\text{ONO}^{\text{Me,Cumyl}}\text{Al}(i\text{Pr}(S)\text{-lactate})$  (**4d**).

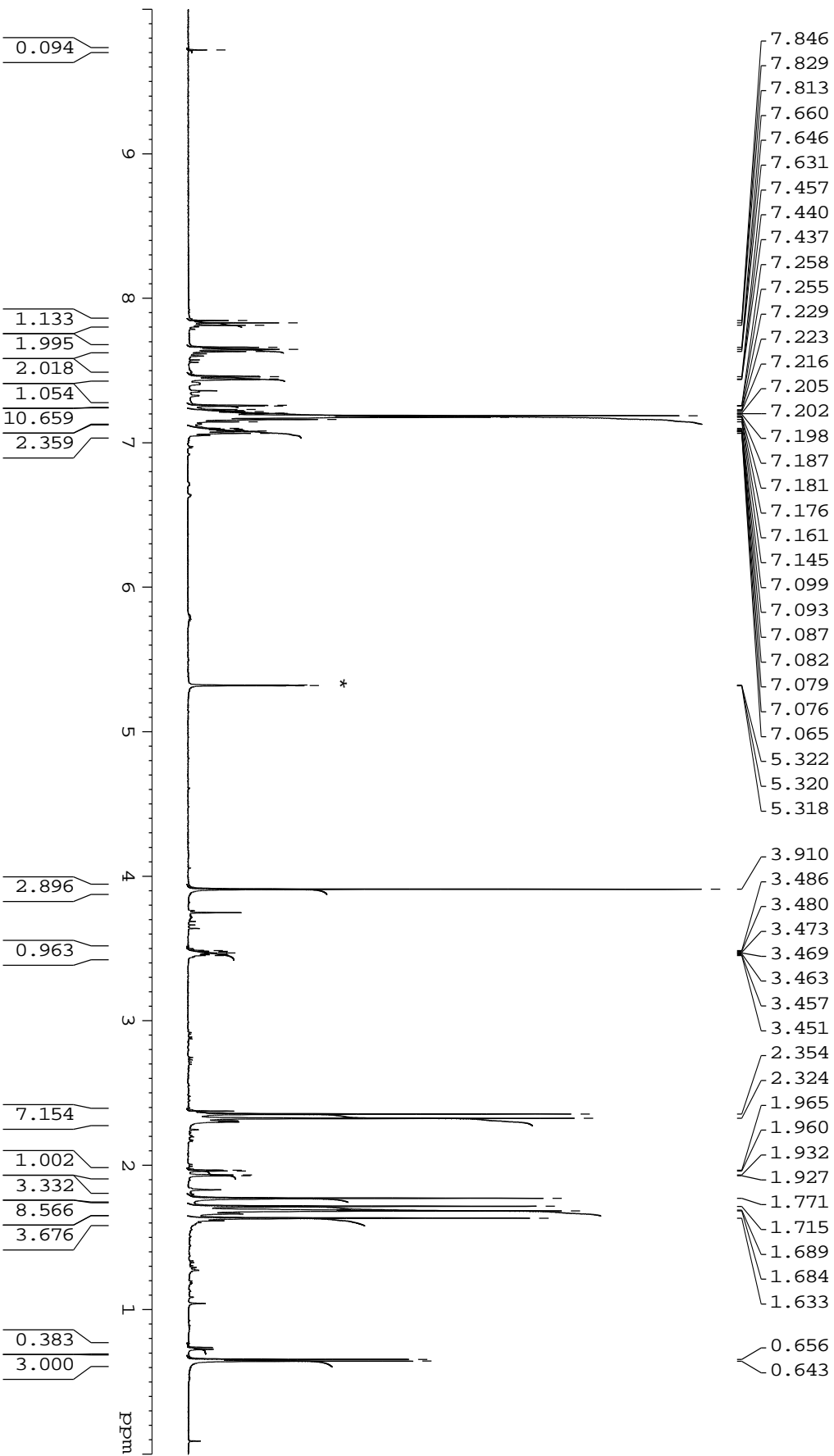


**Figure 21A.**  $^1\text{H}$  NMR spectrum (500 MHz,  $\text{CD}_2\text{Cl}_2$ , 298 K) of  $\{\text{ONO}^{\text{SiPh}_3}\}_3\text{Al}((R)\text{-OCH}(\text{CH}_3)\text{CH}_2\text{COOMe})$  (**5a**) (\*stands for residual solvent resonances).

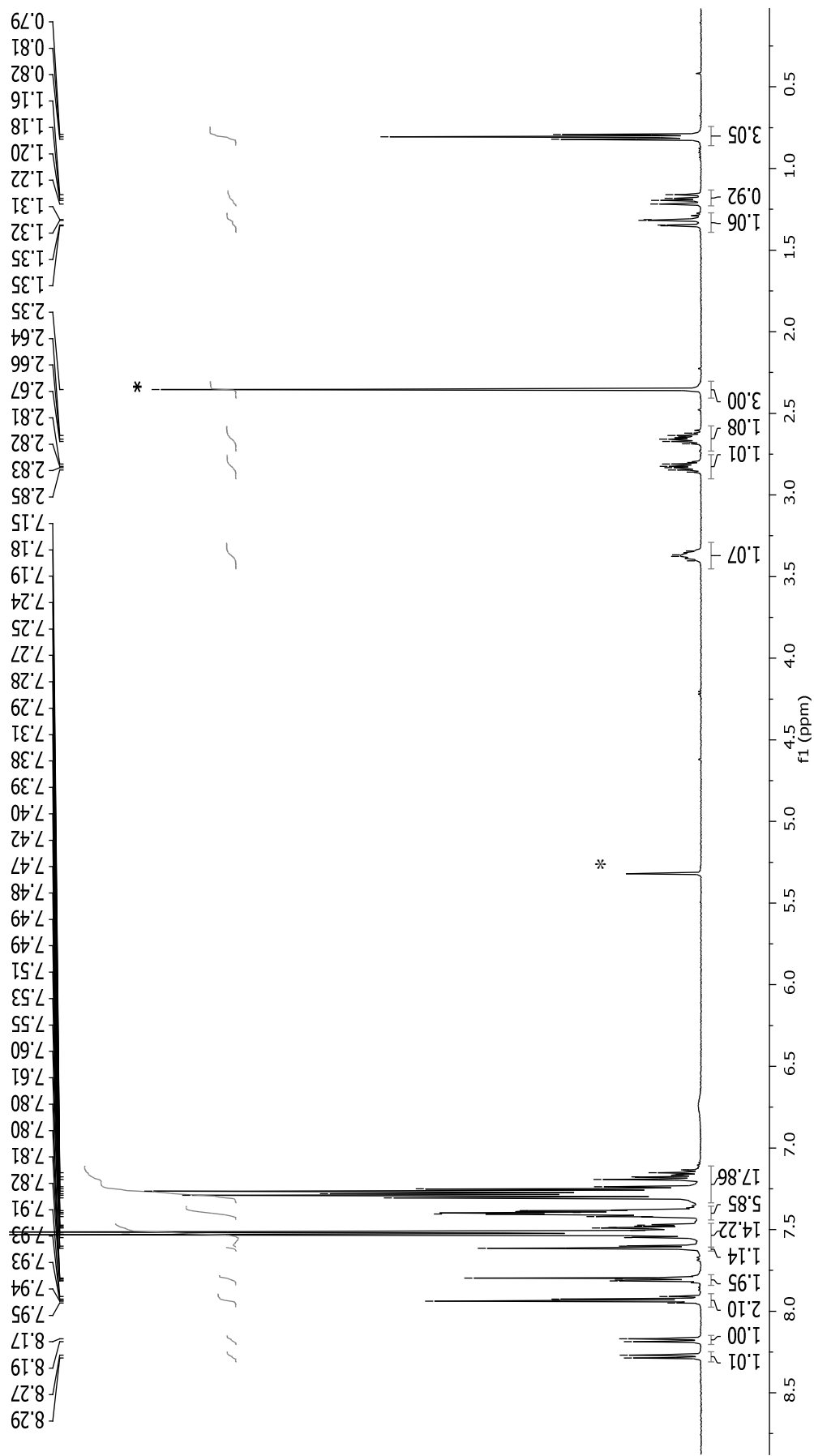


**Figure 22A.**  $^{13}\text{C}\{^1\text{H}\}$  NMR spectrum (125 MHz,  $\text{CD}_2\text{Cl}_2$ , 298 K) of  $\{\text{ONO}^{\text{SiPh}_3}\}\text{Al}((R)\text{-OCH}(\text{CH}_3)\text{CH}_2\text{COOMe})$  (5a).

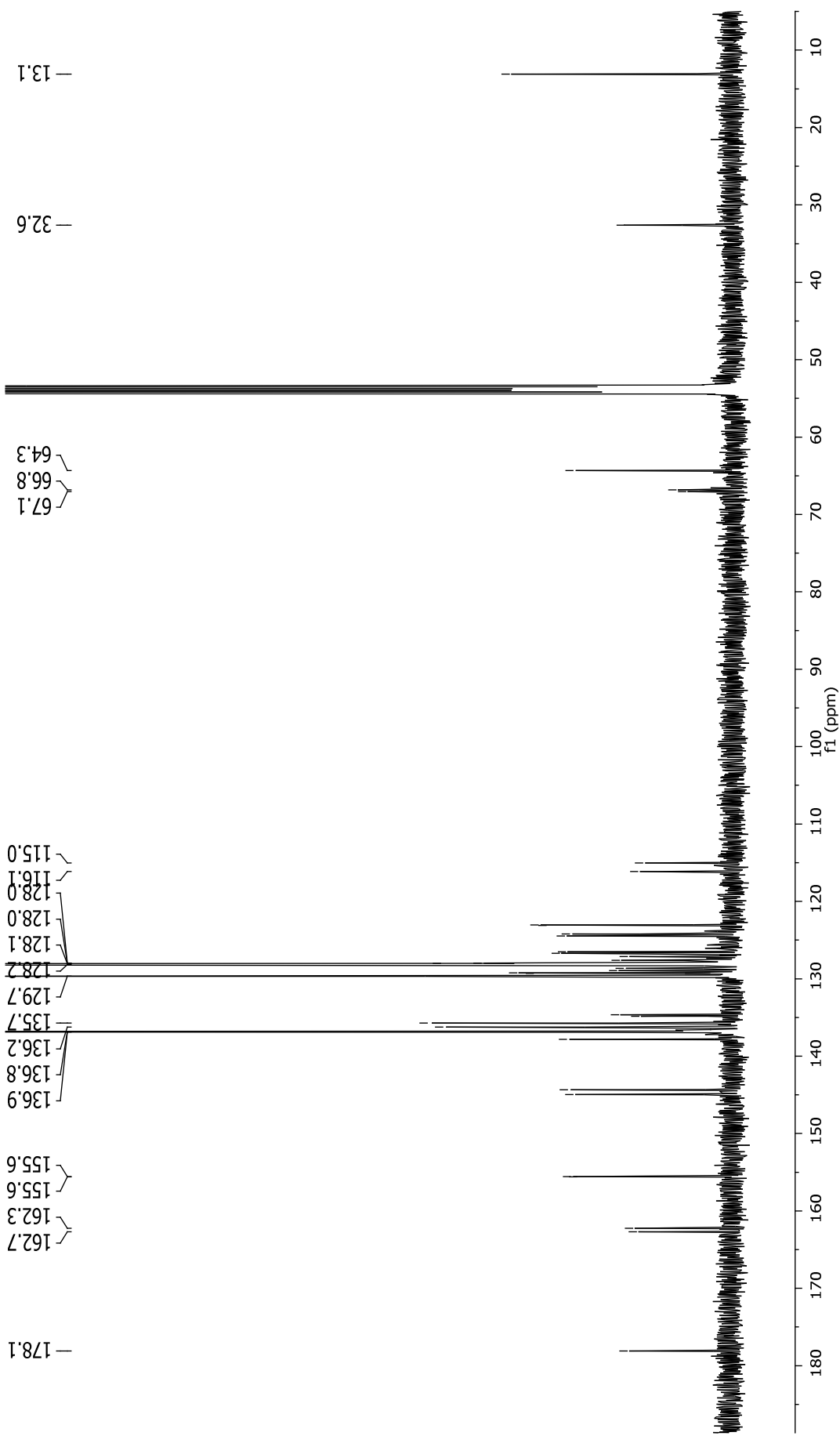




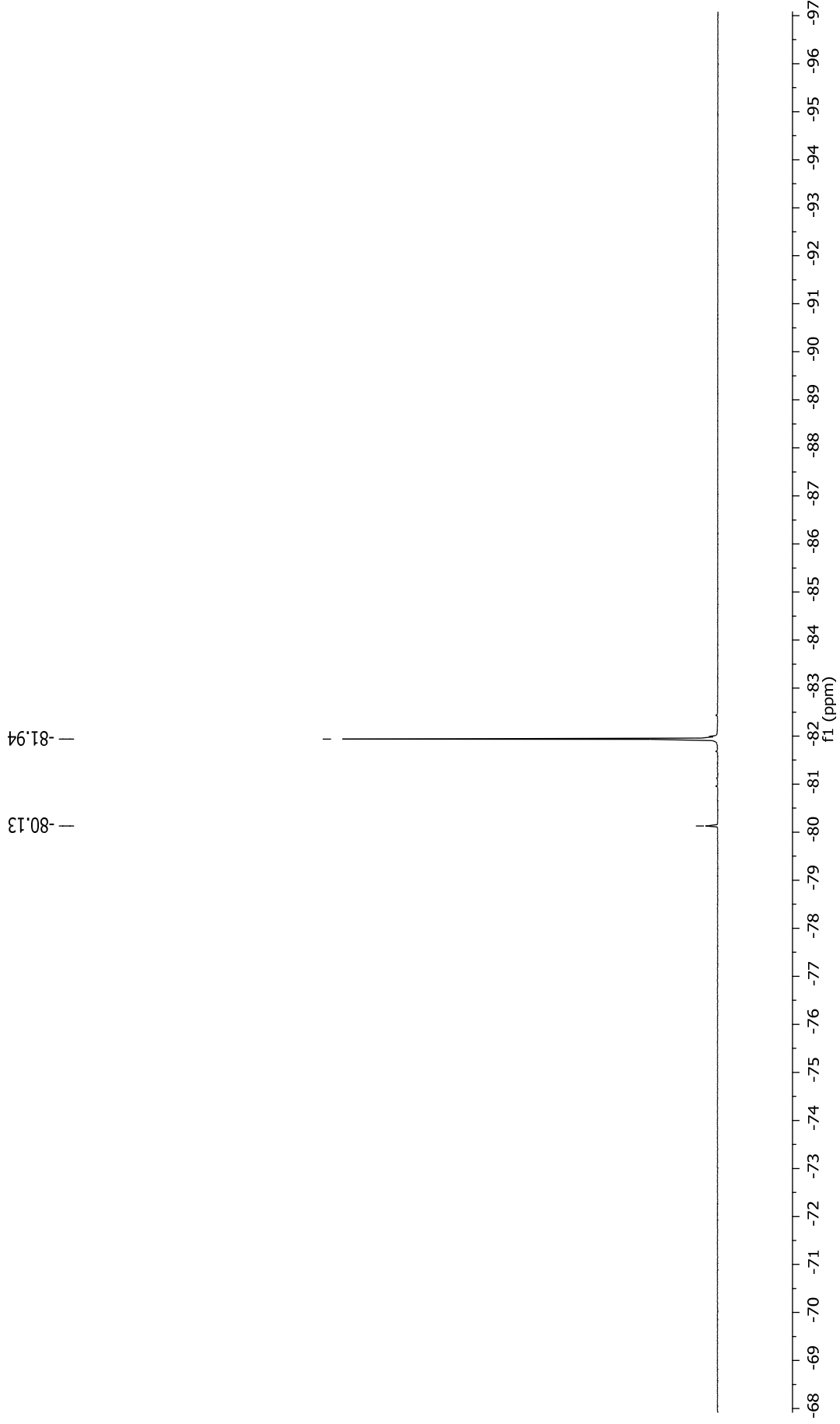
**Figure 23A.**  $^1\text{H}$  NMR spectrum (500 MHz,  $\text{CD}_2\text{Cl}_2$ , 298 K) of  $\{\text{ONO}^{\text{Me,Cunpy}}\}\text{Al}((R)\text{-OCH}(\text{CH}_3)\text{CH}_2\text{COOMe})$  (**5d**). (\*stands for residual solvent resonances). (P.S: we can notice the release of the ligand. We didn't succeed to purify this complex to use it in polymerization)



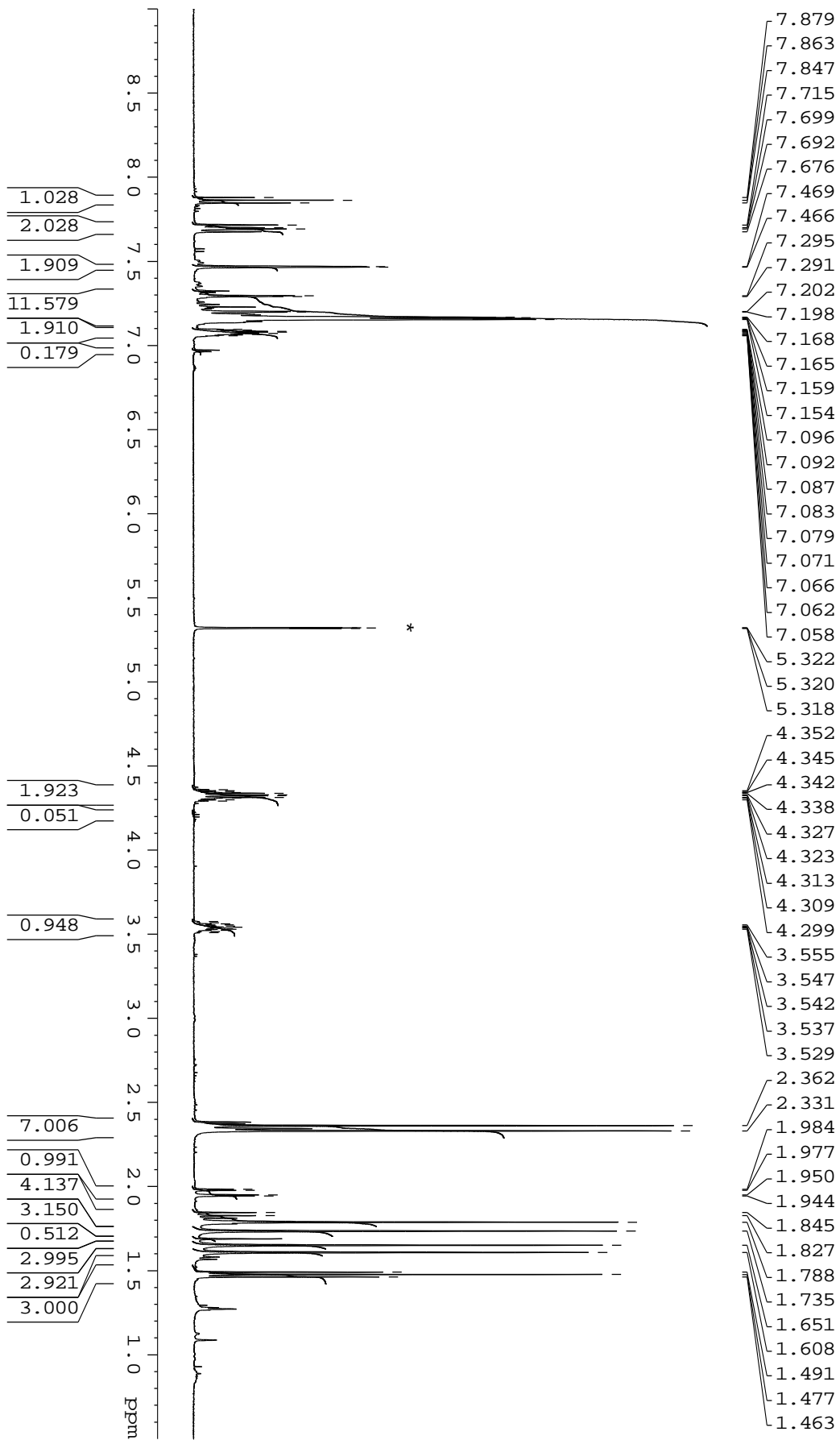
**Figure 24A.**  $^1\text{H}$  NMR spectrum (500 MHz,  $\text{CD}_2\text{Cl}_2$ , 298 K) of  $\{\text{ONO}^{\text{SiPh}_3}\}_3\text{Al}(\text{rac})\text{-OCH}(\text{CF}_3)\text{CH}_2\text{COOEt}$  (**6a**) (\*stands for residual solvent resonances).



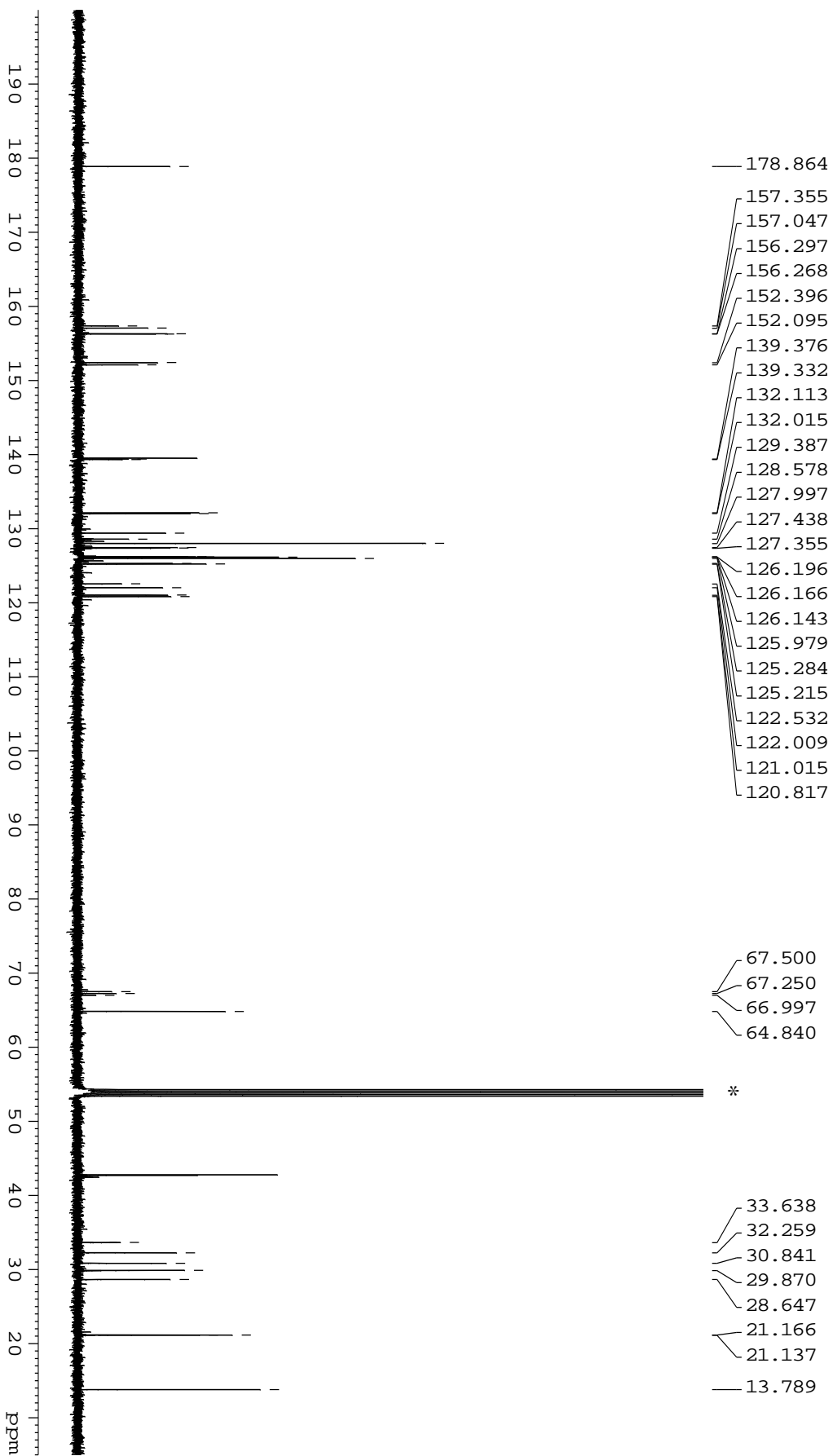
**Figure 25A.**  $^{13}\text{C}\{^1\text{H}\}$  NMR spectrum (125 MHz,  $\text{CD}_2\text{Cl}_2$ , 298 K) of  $\{\text{ONO}^{\text{SiPh}_3}\}_3\text{Al}(\text{rac})\text{-OCH}(\text{CF}_3)\text{CH}_2\text{COOEt}$  (**6a**).



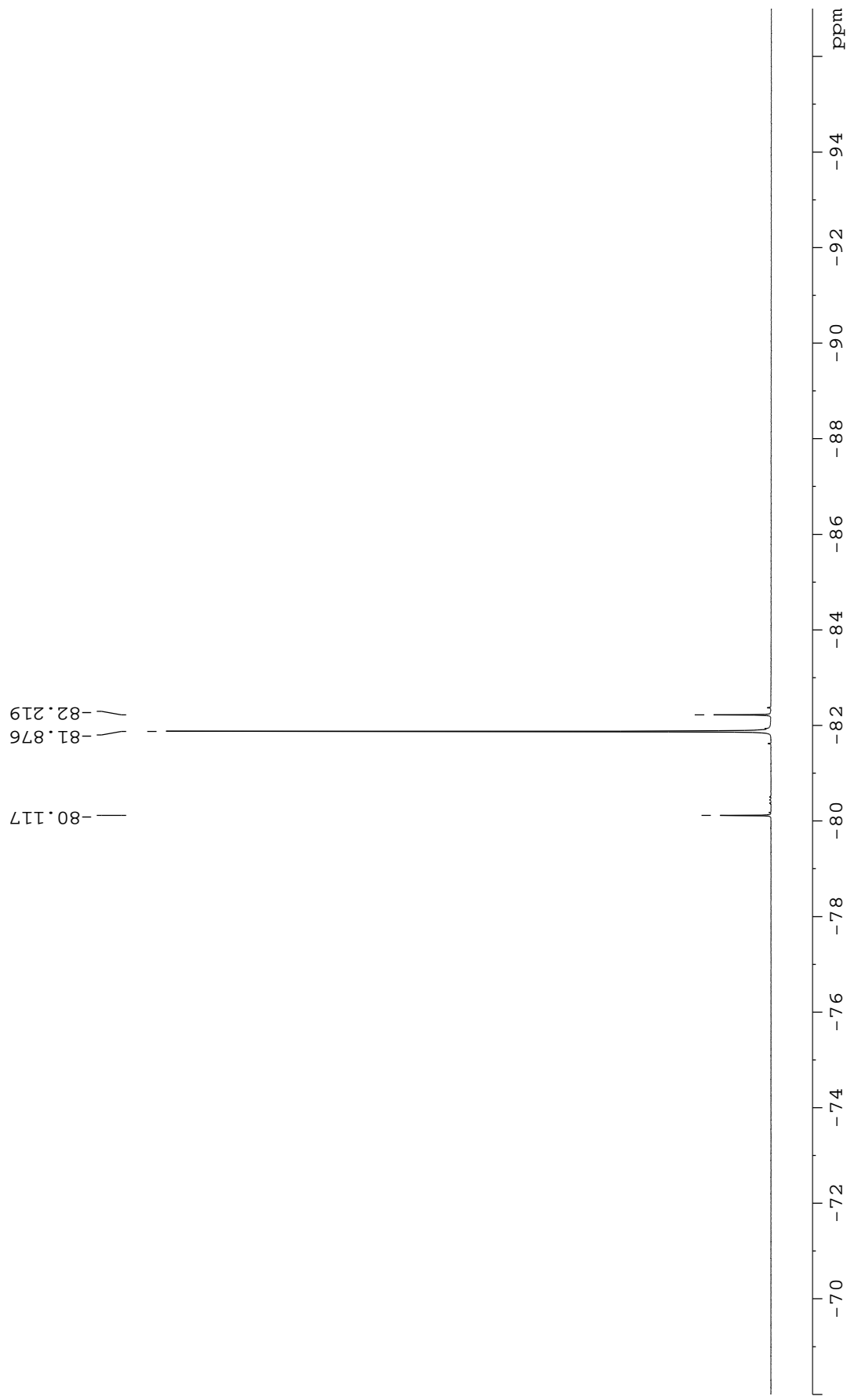
**Figure 26A.**  $^{19}\text{F}\{^1\text{H}\}$ NMR spectrum (185 MHz,  $\text{CD}_2\text{Cl}_2$ , 298 K) of  $\{\text{ONO}^{\text{SiPh}_3}\text{Al}((\text{rac})\text{-OCH}(\text{CF}_3)\text{CH}_2\text{COOEt})\}$  (**6a**).



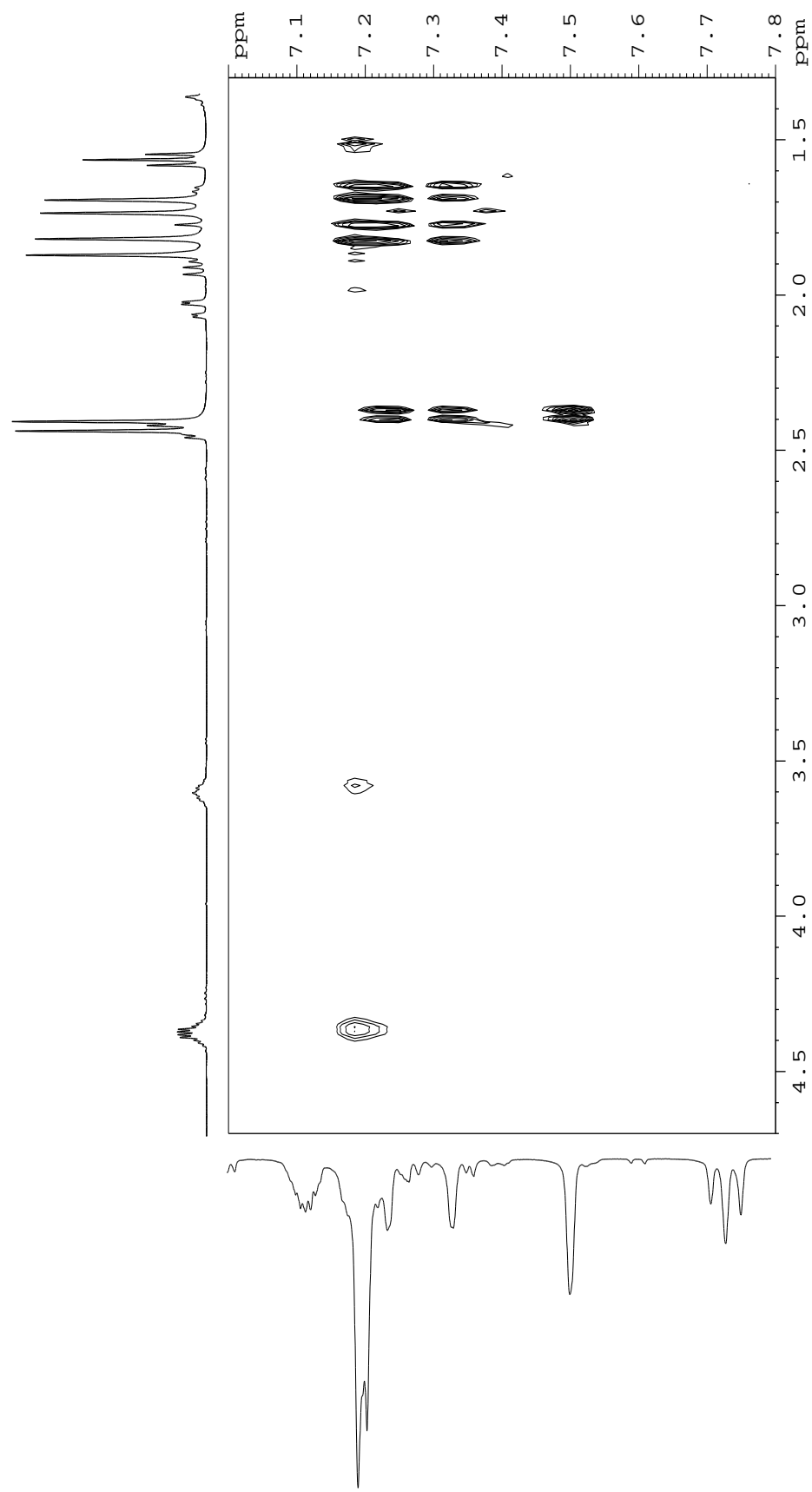
**Figure 27A.**  $^1\text{H}$  NMR spectrum (500 MHz,  $\text{CD}_2\text{Cl}_2$ , 298 K) of  $\{\text{ONO}^{\text{SiPh}_3}\}_2\text{Al}((rac)\text{-OCH}(\text{CF}_3)\text{CH}_2\text{COOEt})$  (**6d**) (\*stands for residual solvent resonances).



**Figure 28A.**  $^{13}\text{C}\{^1\text{H}\}$  NMR spectrum (125 MHz,  $\text{CD}_2\text{Cl}_2$ , 298 K) of  $\{\text{ONO}^{\text{Me,Cumyl}}\}\text{Al}(\text{rac})\text{-OCH}(\text{CF}_3)\text{CH}_2\text{COOEt}$  (**6d**) (\*stands for residual solvent resonances).

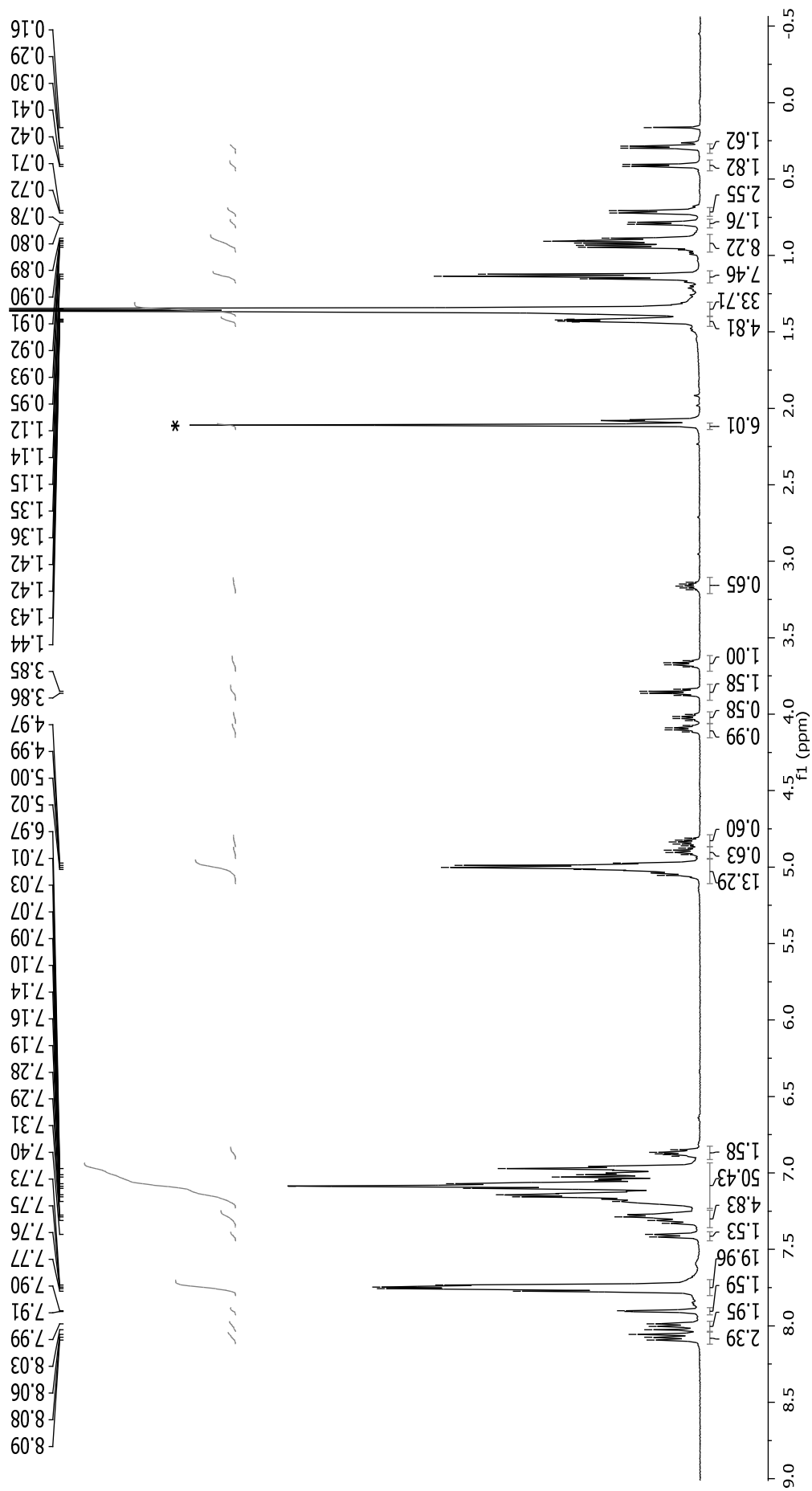


**Figure 29A.**  $^{19}\text{F}\{^1\text{H}\}$ NMR spectrum (185 MHz,  $\text{CD}_2\text{Cl}_2$ , 298 K) of  $\{\text{ONO}^{\text{Me,Cumyl}}\}\text{Al}((\text{rac})\text{-OCH}(\text{CF}_3)\text{CH}_2\text{COOEt})$  (**6d**).

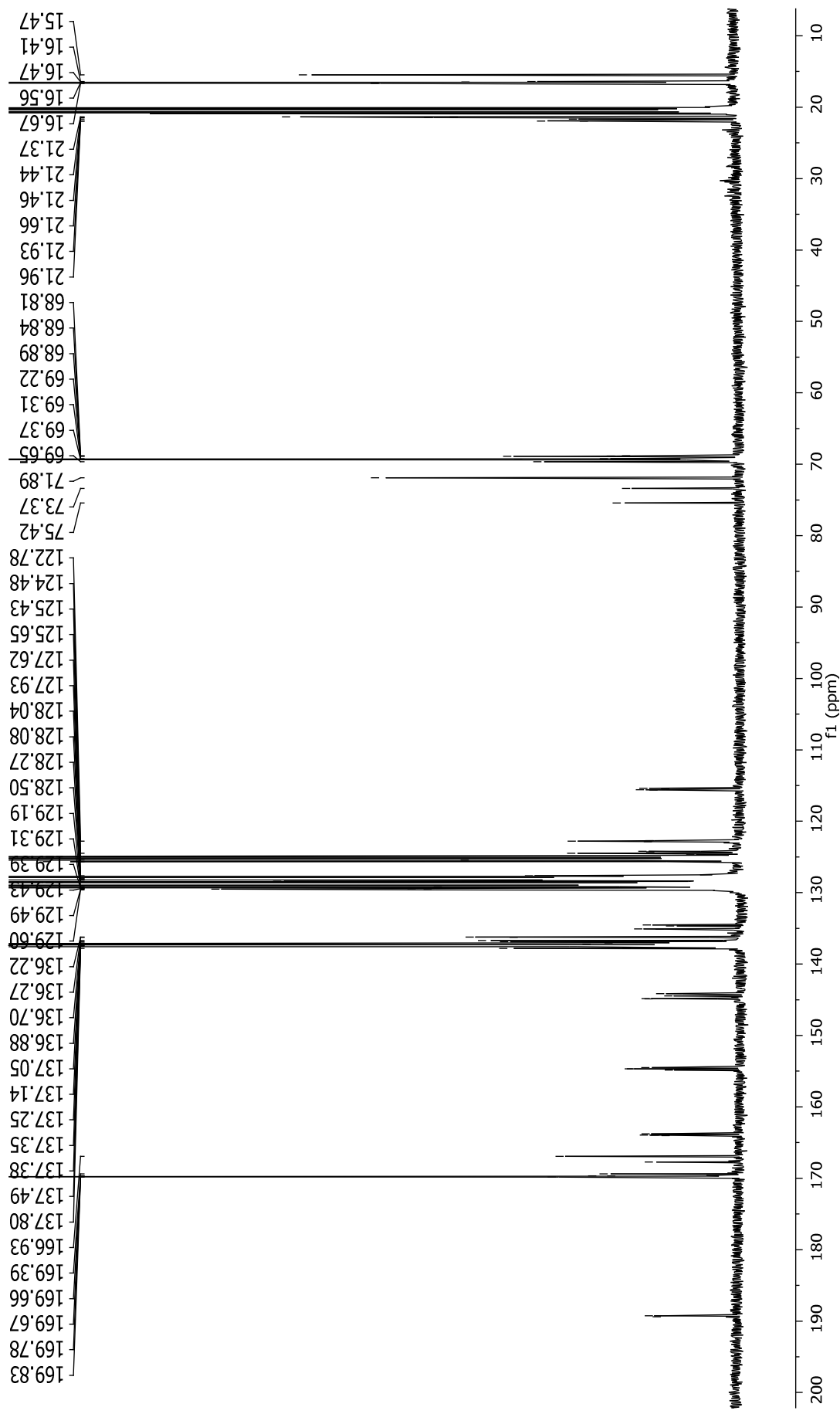


**Figure 30A.** <sup>1</sup>H-<sup>1</sup>H NOESY NMR spectrum (400 MHz, CD<sub>2</sub>Cl<sub>2</sub>, 298 K) of [ONO<sup>Me,Cumyl</sup>Al((*rac*)-OCH(CF<sub>3</sub>)CH<sub>2</sub>COOEt) (6d)].

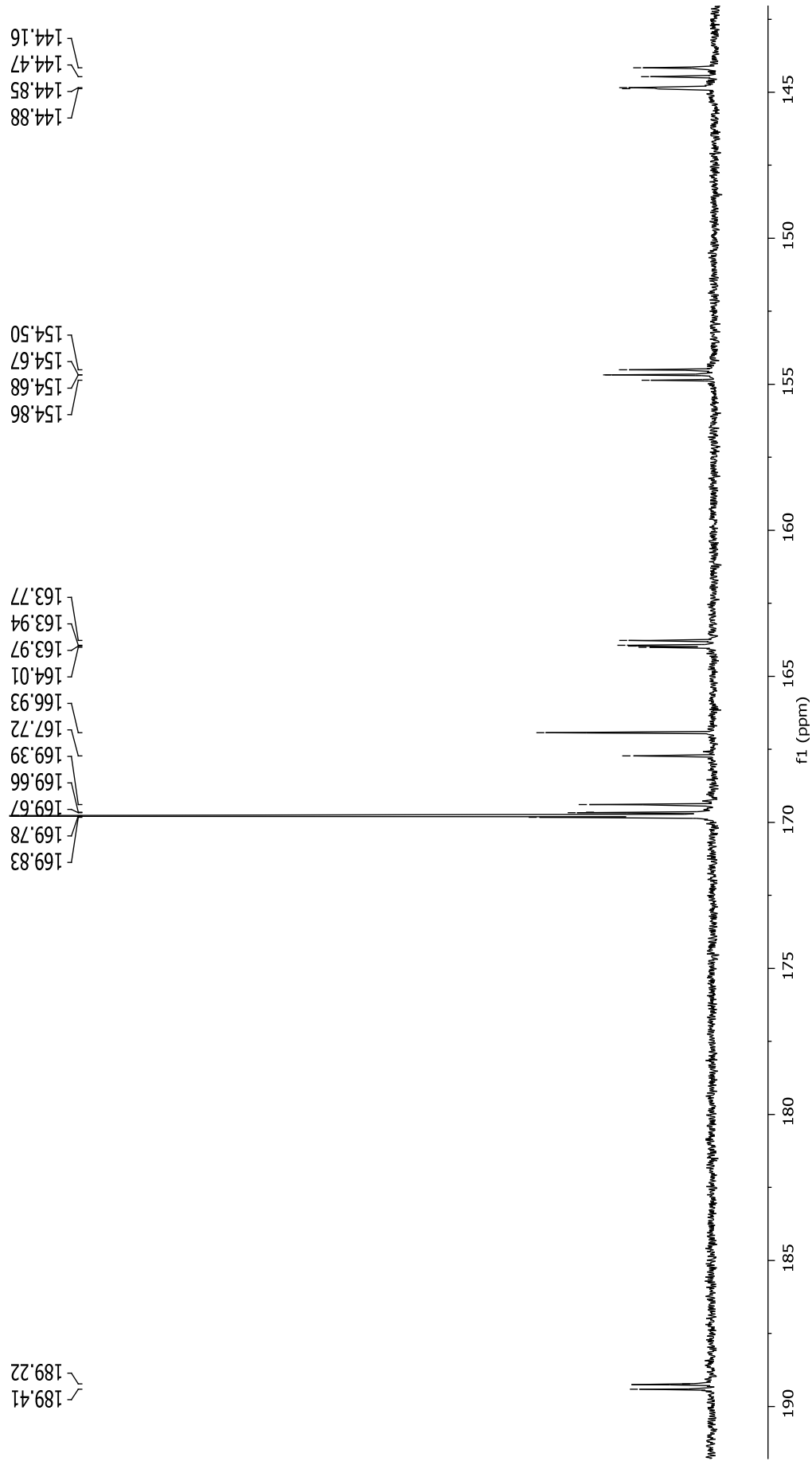




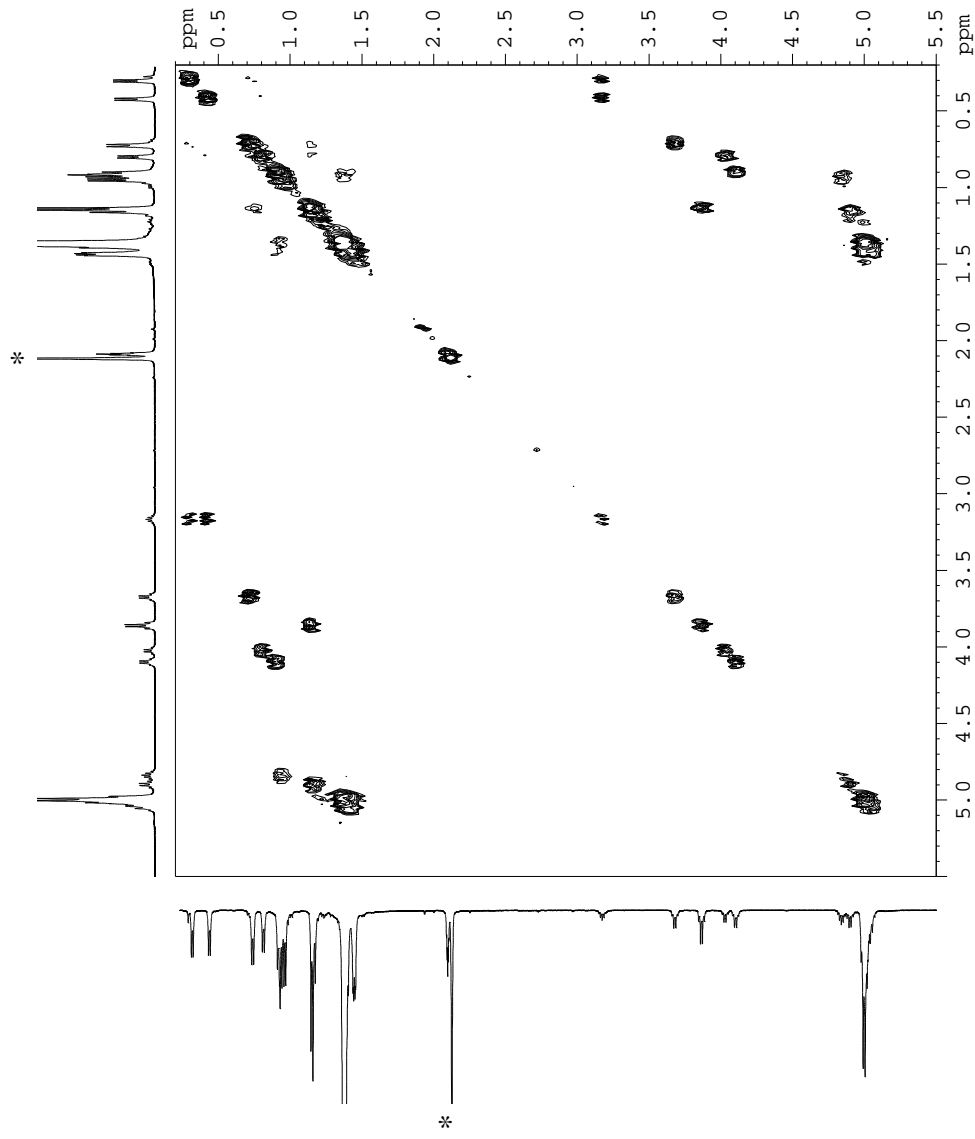
**Figure 31A.** <sup>1</sup>H NMR spectrum (500 MHz, toluene-*d*<sub>8</sub>, 298 K) of the 1:5 reaction of a mixture of (*S*)-**4a** and L-LA after 18 h at 80 °C in toluene-*d*<sub>8</sub> (\*stands for residual toluene resonance).



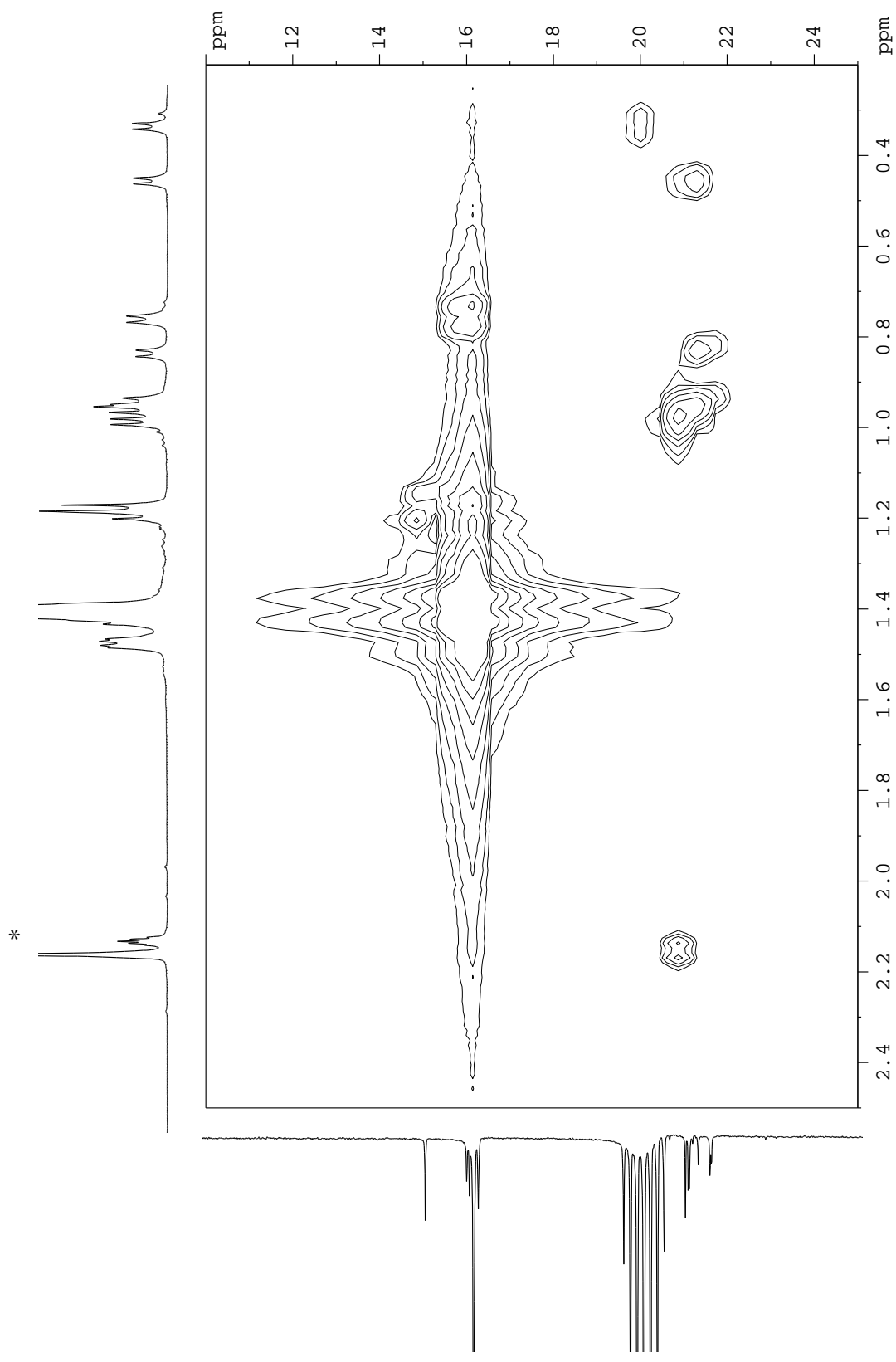
**Figure 32A.**  $^{13}\text{C}\{^1\text{H}\}$  NMR spectrum (125 MHz, toluene- $d_8$ , 298 K) of the 1:5 reaction of a mixture of (S)-4a and L-LA after 18 h at 80 °C.



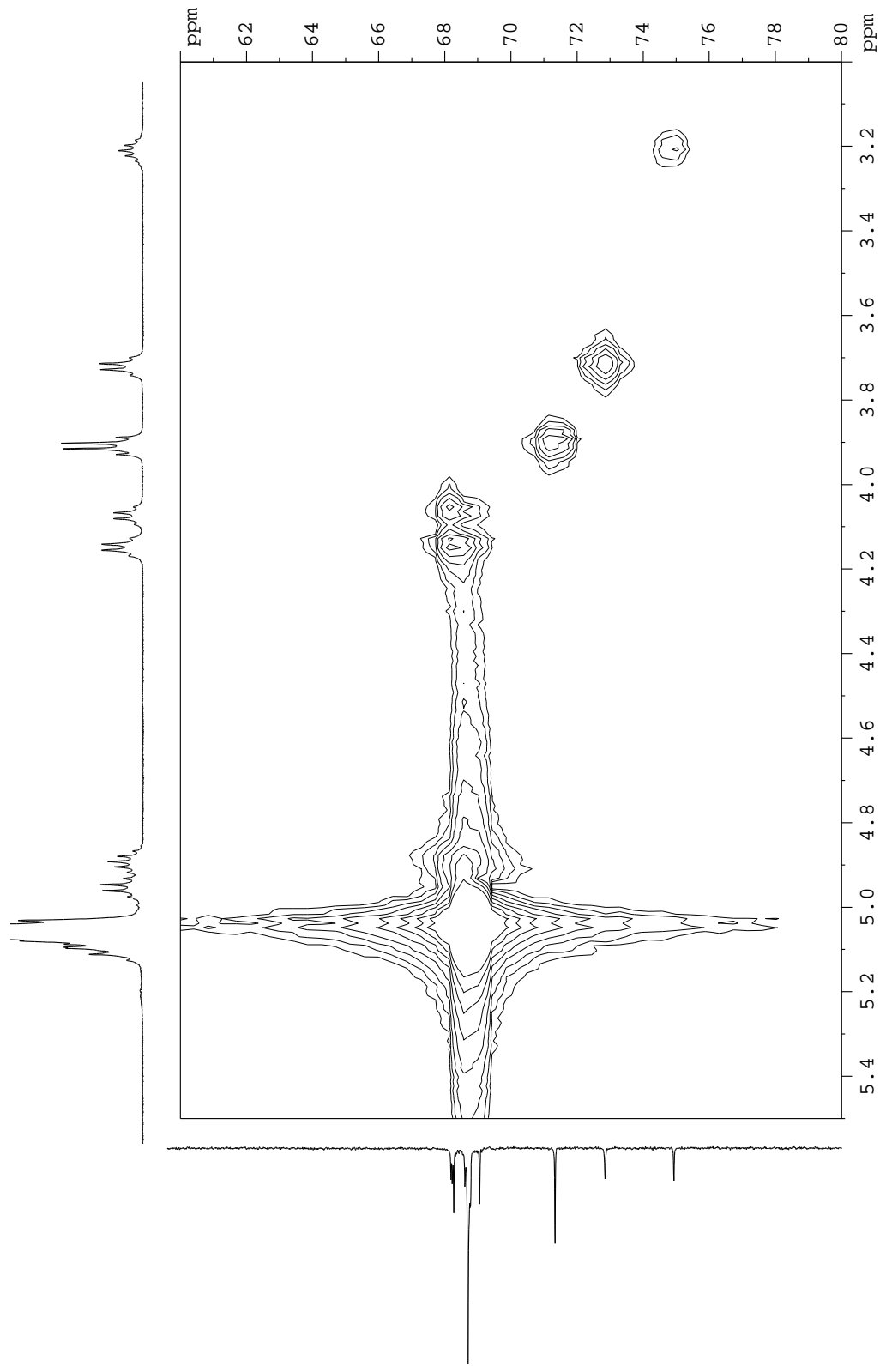
**Figure 33A.** Details of the upfield region [COO, CO, C-N and C<sup>4</sup>] of the <sup>13</sup>C{<sup>1</sup>H} NMR spectrum (125 MHz, toluene-*d*<sub>8</sub>, 298 K) of the 1:5 reaction of a mixture of (*S*)-**4a** and L-LA after 18 h at 80 °C in toluene-*d*<sub>8</sub>.



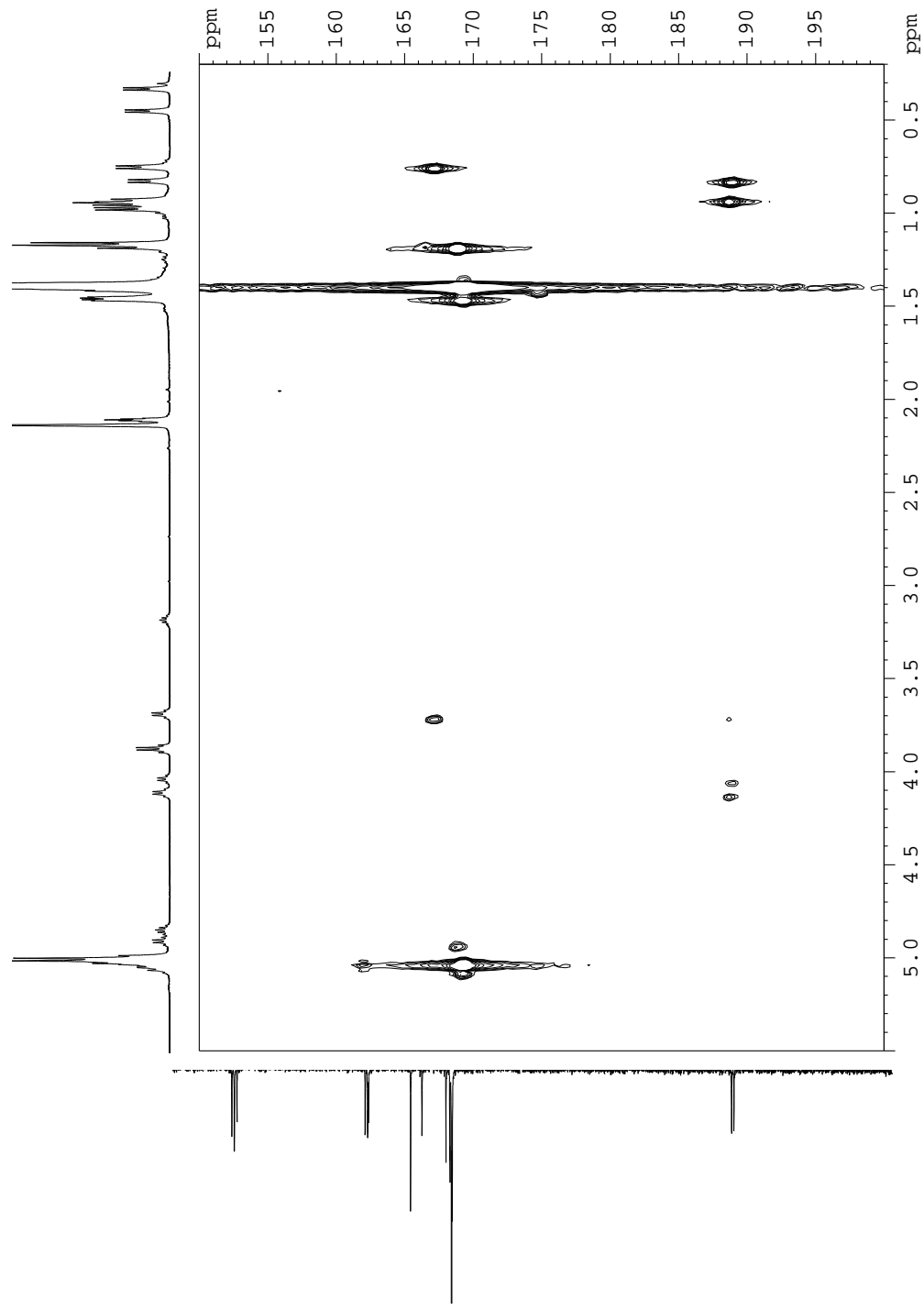
**Figure 34A.**  $^1\text{H}$ - $^1\text{H}$  COSY NMR spectrum (500 MHz, toluene- $d_8$ , 298 K) of the 1:5 reaction of a mixture of (*S*)-**4a** and L-LA after 18 h at 80 °C in toluene- $d_8$  (\*stands for residual toluene resonance).



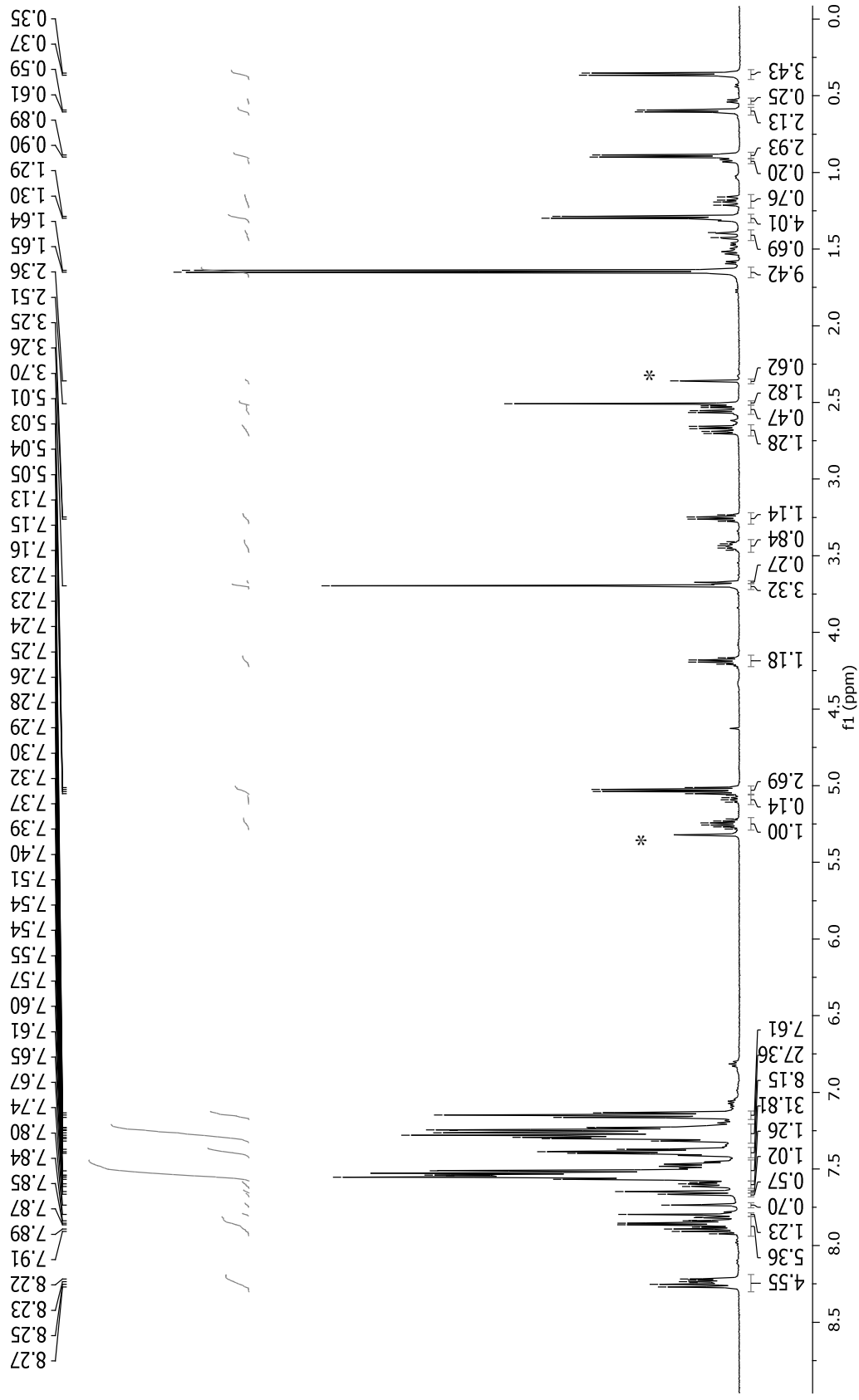
**Figure 35A.**  $^1\text{H}$ - $^1\text{H}$  HMQC NMR spectrum (500 MHz, toluene- $d_8$ , 298 K) of the 1:5 reaction of a mixture of (*S*)-**4a** and L-LA after 18 h at 80 °C in toluene- $d_8$  (\*stands for residual toluene resonance).



**Figure 36A.**  $^1\text{H}$ - $^1\text{H}$  HMQC NMR spectrum (500 MHz, toluene- $d_8$ , 298 K) of the 1:5 reaction of a mixture of (S)-4a and L-LA after 18 h at 80 °C in toluene- $d_8$ .



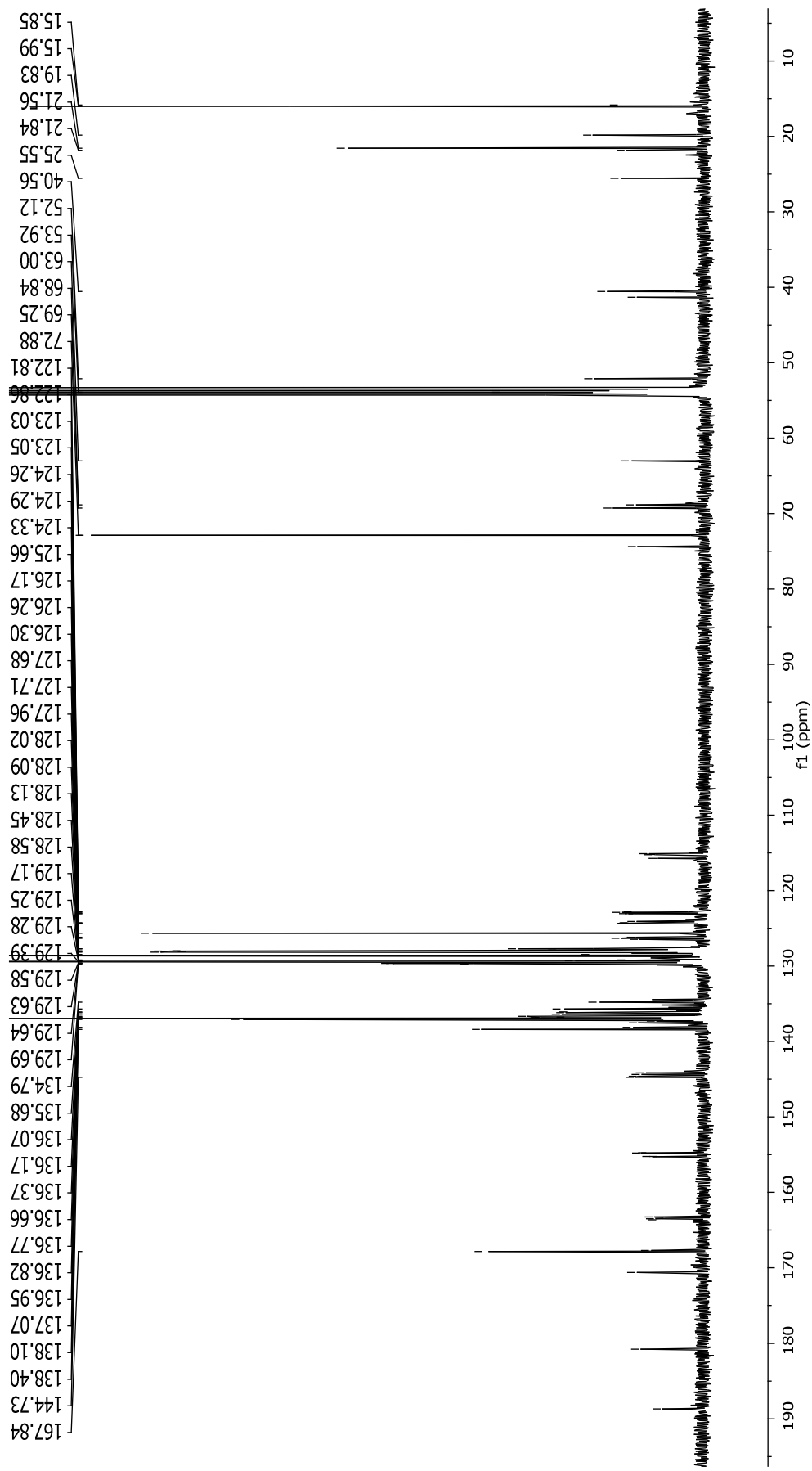
**Figure 37A.**  $^1\text{H}$ - $^1\text{H}$  HMBC NMR spectrum (500 MHz, toluene- $d_8$ , 298 K) of the 1:5 reaction of a mixture of (*S*)-**4a** and L-LA after 18 h at 80 °C in toluene- $d_8$ .



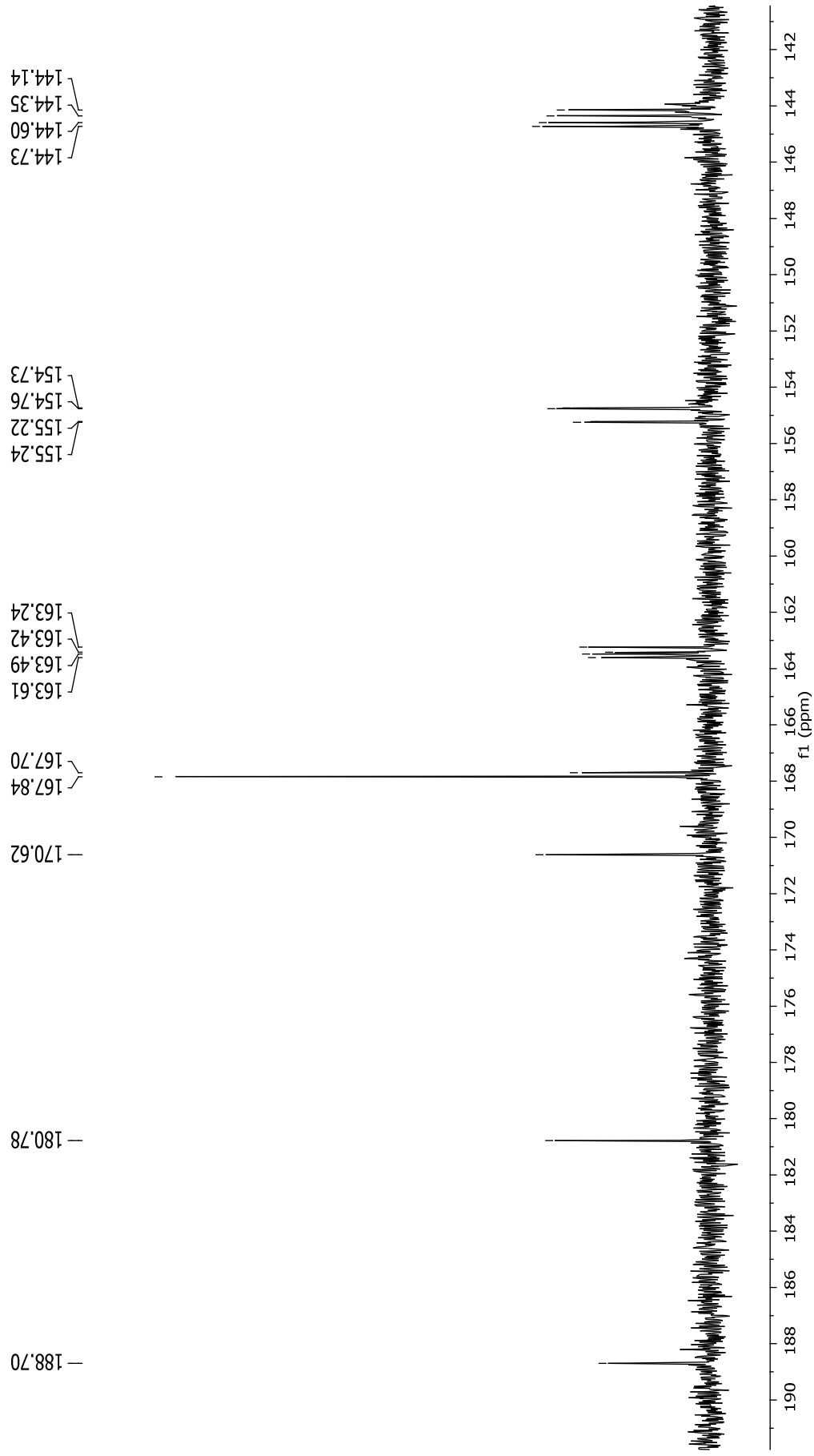
**Figure 38A.**  $^1\text{H}$  NMR spectrum (500 MHz,  $\text{CD}_2\text{Cl}_2$ , 298 K) of the 1:1.35 reaction of a mixture of (R)-5a and L-LA after 23 h at 25 °C in  $\text{CD}_2\text{Cl}_2$ .

(\*stands for residual solvent resonance).

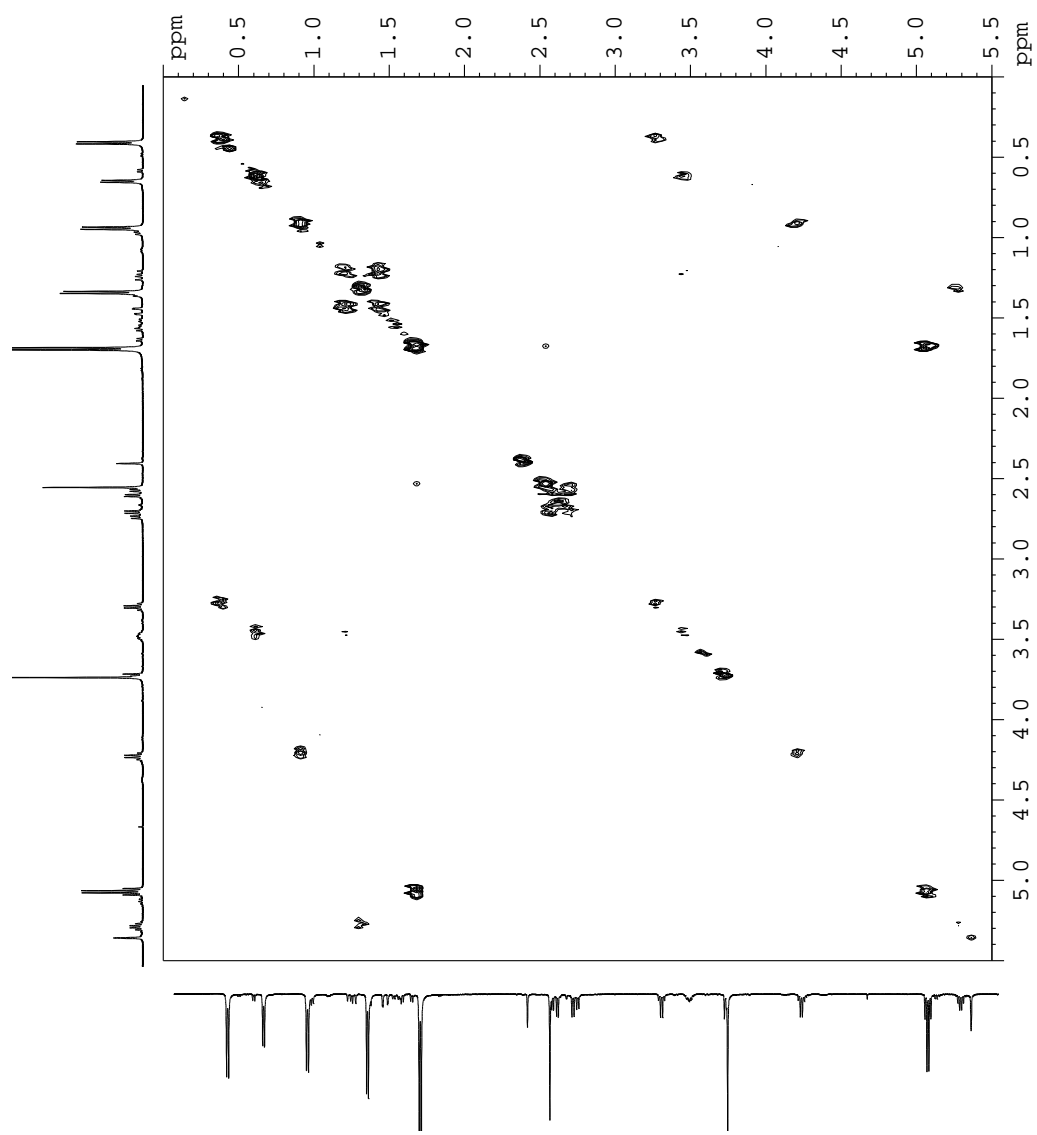




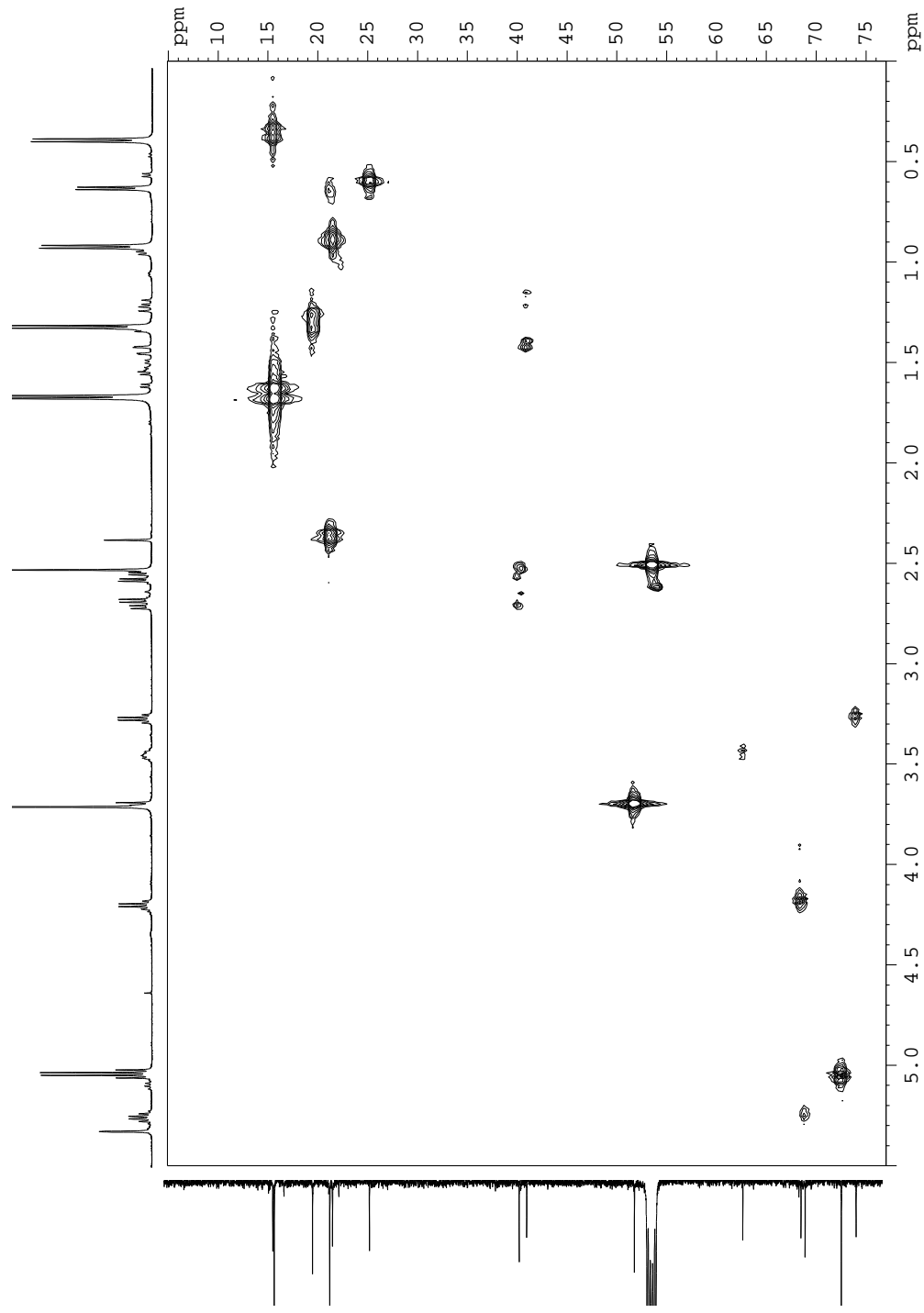
**Figure 39A.**  $^{13}\text{C}\{^1\text{H}\}$  NMR spectrum (125 MHz,  $\text{CD}_2\text{Cl}_2$ , 298 K) of the 1:1.35 reaction of (*R*)-**5a** and L-LA after 23 h at 25 °C in  $\text{CD}_2\text{Cl}_2$ .



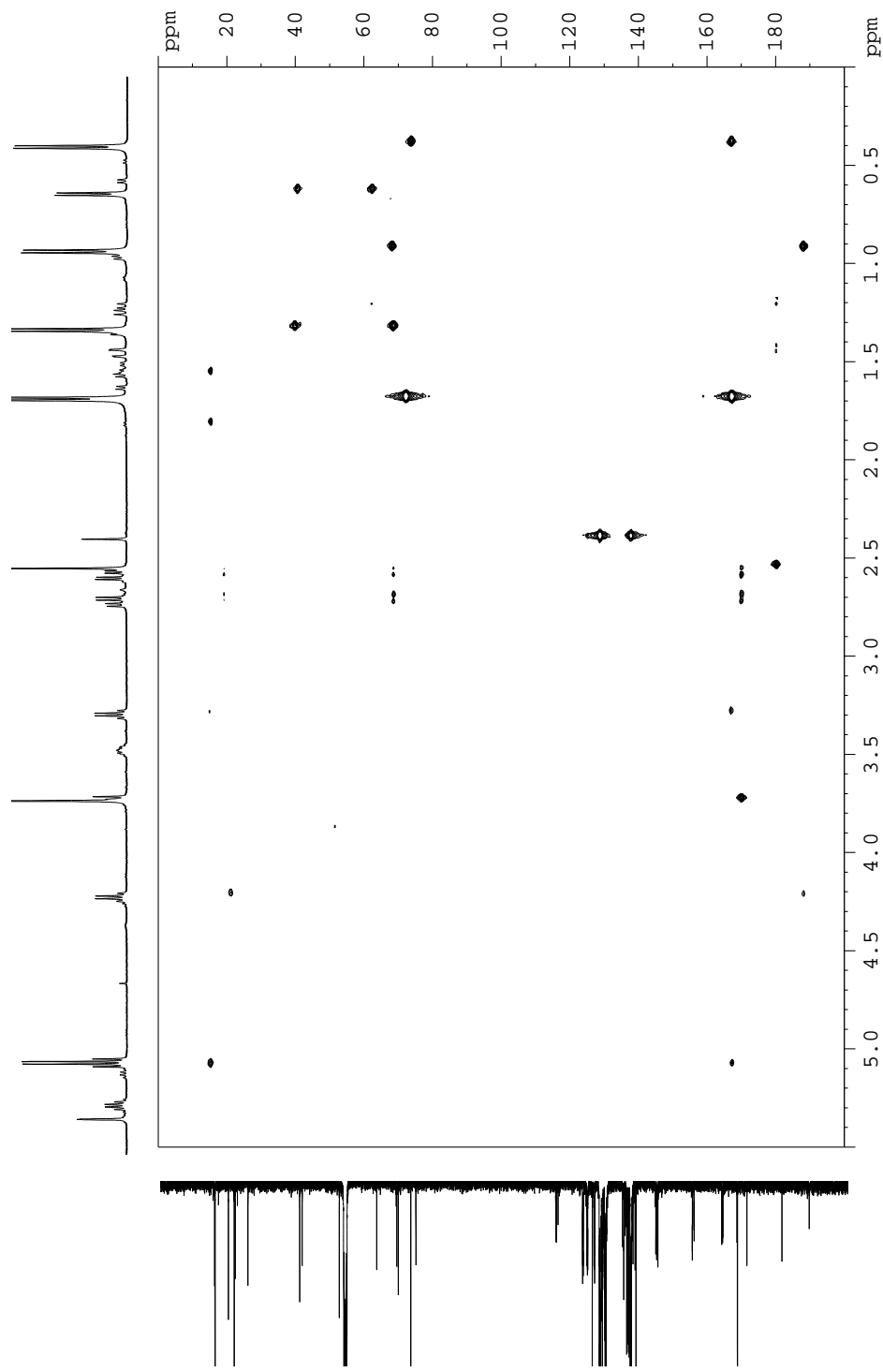
**Figure 40A.** Details of the upfield region [COO, CO, C-N and C<sup>4</sup>] of the <sup>13</sup>C{<sup>1</sup>H} NMR spectrum (125 MHz, CD<sub>2</sub>Cl<sub>2</sub>, 298 K) of the 1:1.35 reaction of a mixture of (*R*)-**5a** and L-LA after 23 h at 25 °C in CD<sub>2</sub>Cl<sub>2</sub>.



**Figure 41A.**  $^1\text{H}$ - $^1\text{H}$  COSY NMR spectrum (500 MHz,  $\text{CD}_2\text{Cl}_2$ , 298 K) of the 1:1.35 reaction of a mixture of (*R*)-**5a** and L-LA after 23 h at 25 °C in  $\text{CD}_2\text{Cl}_2$ .

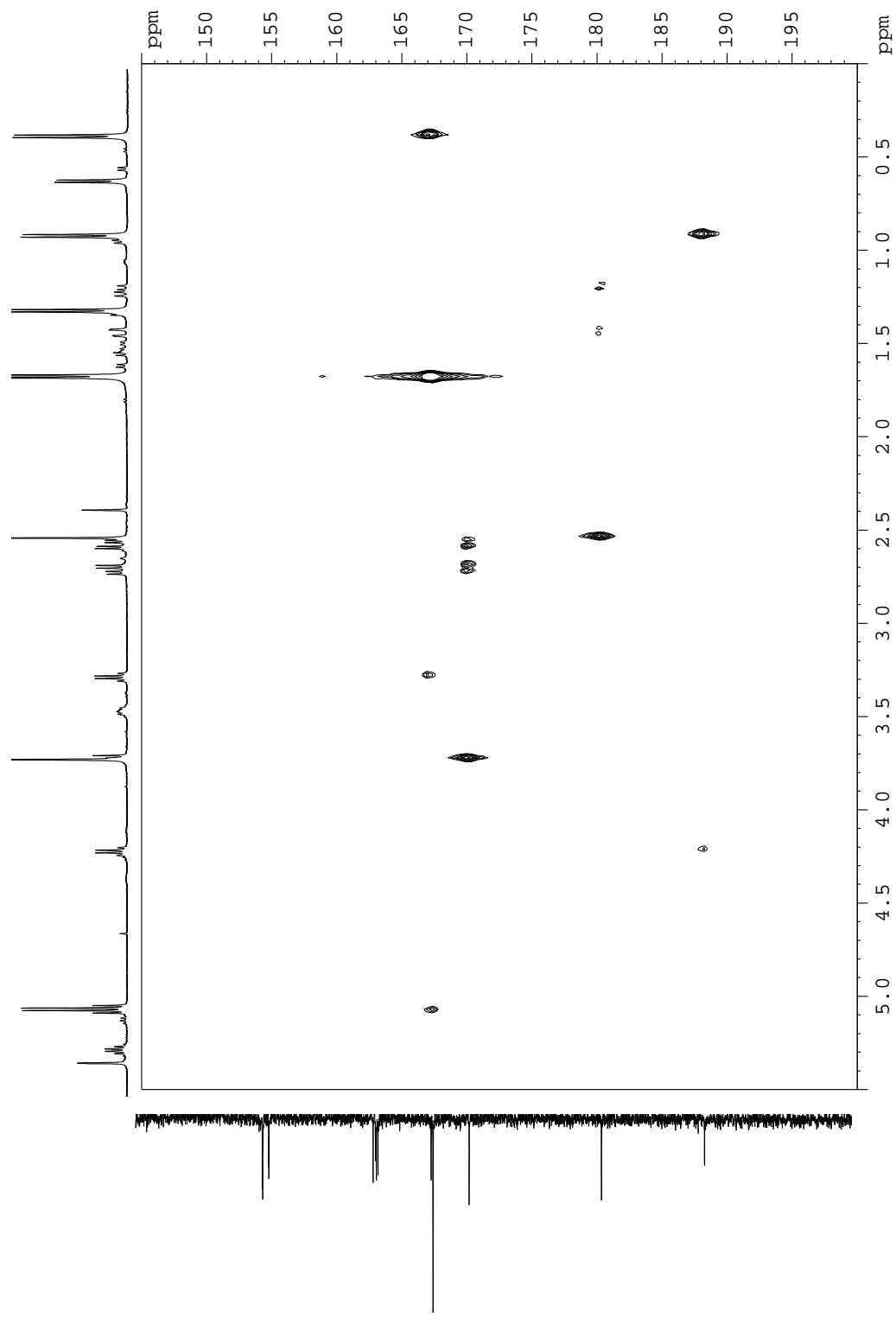


**Figure 42A.**  $^1\text{H}$ - $^1\text{H}$  HMQC NMR spectrum (500 MHz,  $\text{CD}_2\text{Cl}_2$ , 298 K) of the 1:1.35 reaction of a mixture of (*R*)-**5a** and L-LA after 23 h at 25  $^\circ\text{C}$  in  $\text{CD}_2\text{Cl}_2$ .



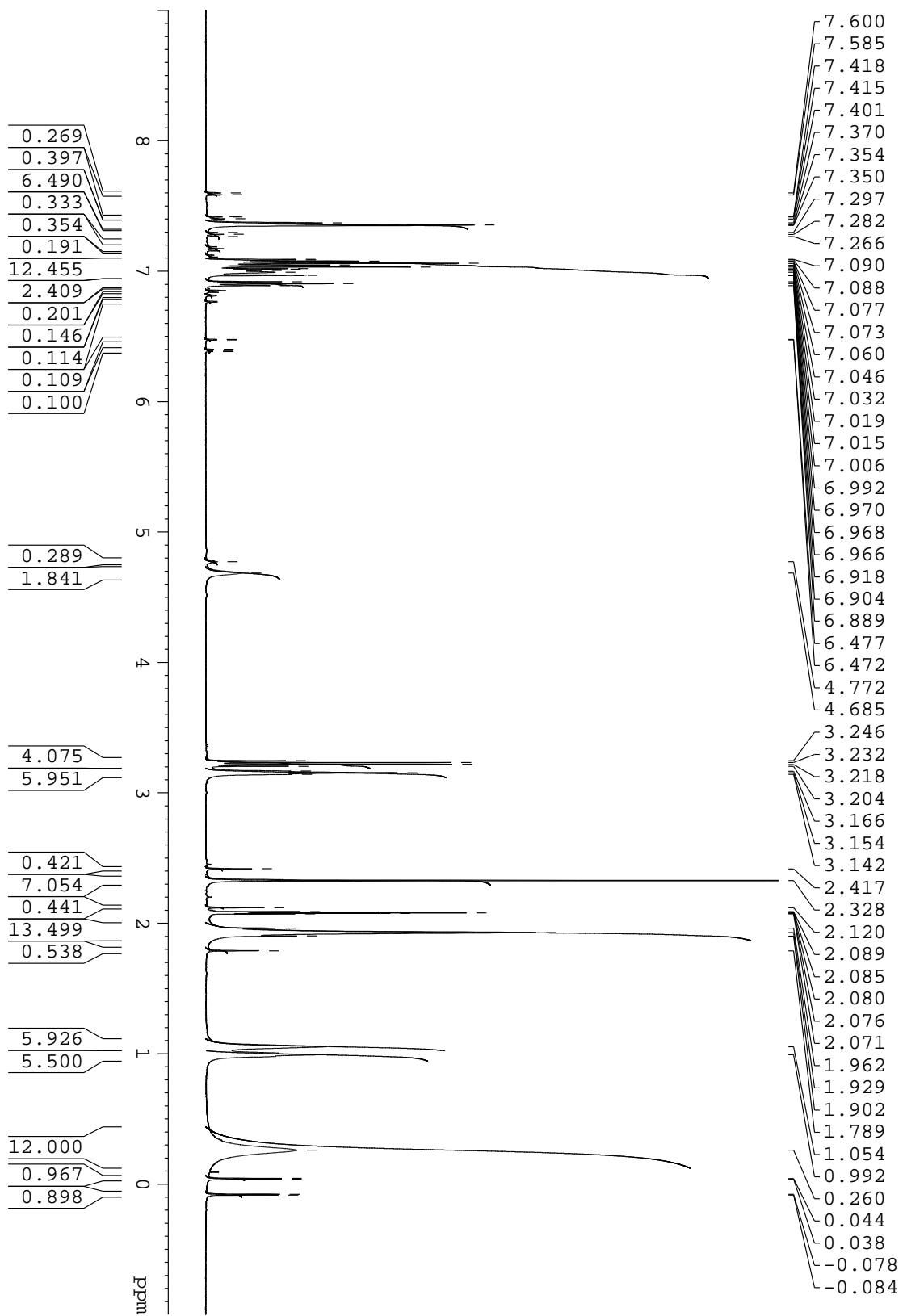
**Figure 43A.**  $^1\text{H}$ - $^1\text{H}$  HMBC NMR spectrum (500 MHz,  $\text{CD}_2\text{Cl}_2$ , 298 K) of the 1:1.35 reaction of a mixture of (*R*)-**5a** and L-LA after 23 h at 25

$^\circ\text{C}$  in  $\text{CD}_2\text{Cl}_2$ .



**Figure 44A.**  $^1\text{H}$ - $^1\text{H}$  HMBC NMR spectrum (500 MHz,  $\text{CD}_2\text{Cl}_2$ , 298 K) of the 1:1.35 reaction of a mixture of (*R*)-**5a** and L-LA after 23 h at 25  $^\circ\text{C}$  in  $\text{CD}_2\text{Cl}_2$ .

Figure 45A.  $^1\text{H}$  NMR spectrum (500 MHz, toluene- $d_8$ , 298 K) of  $\{\text{ONO}^{\text{Me}}_{\text{Cumyl}}\}[\text{Y}(\text{N}(\text{SiHMe}_2)_2)(\text{THF})(\text{Et}_2\text{O})](\mathbf{9})$ .



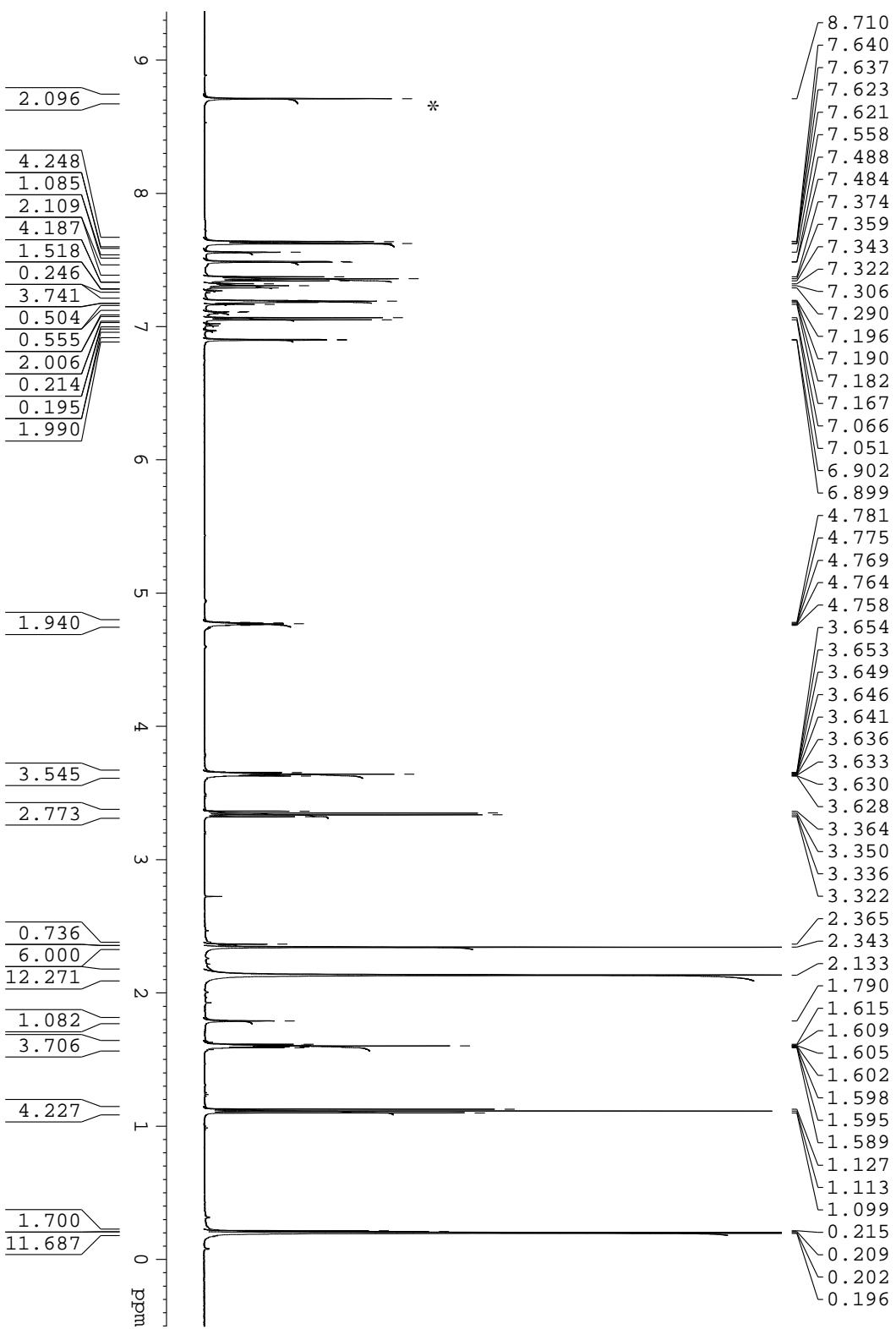


**Figure 46A.**  $^1\text{H}$  NMR spectrum (500 MHz, Pyridine- $d_5$ , 298 K) of  $\{\text{ONO}^{\text{Me,Cumyl}}\} \text{Y}[\text{N}(\text{SiHMe}_2)_2](\text{THF})(\text{Et}_2\text{O})$  (**9**) (\*stands for residual solvent resonance).



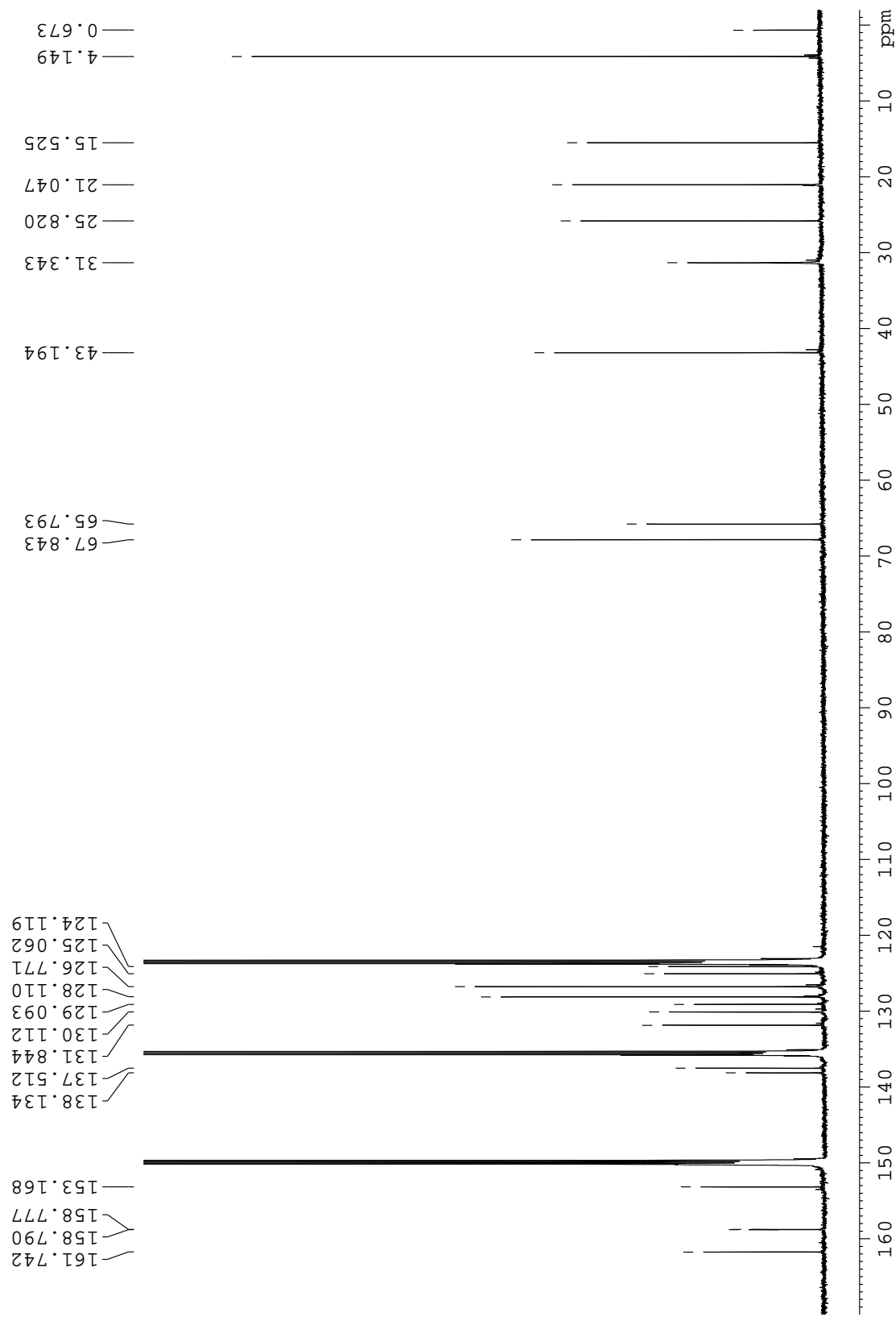


**Figure 47A.**  $^{13}\text{C}$  NMR spectrum (500 MHz, Pyridine- $d_5$ , 298 K) of  $\{\text{ONO}^{\text{Me,Cumyl}^1}\text{Y}[\text{N}(\text{SiHMe}_2)_2](\text{THF})(\text{Et}_2\text{O})$  (**9**).

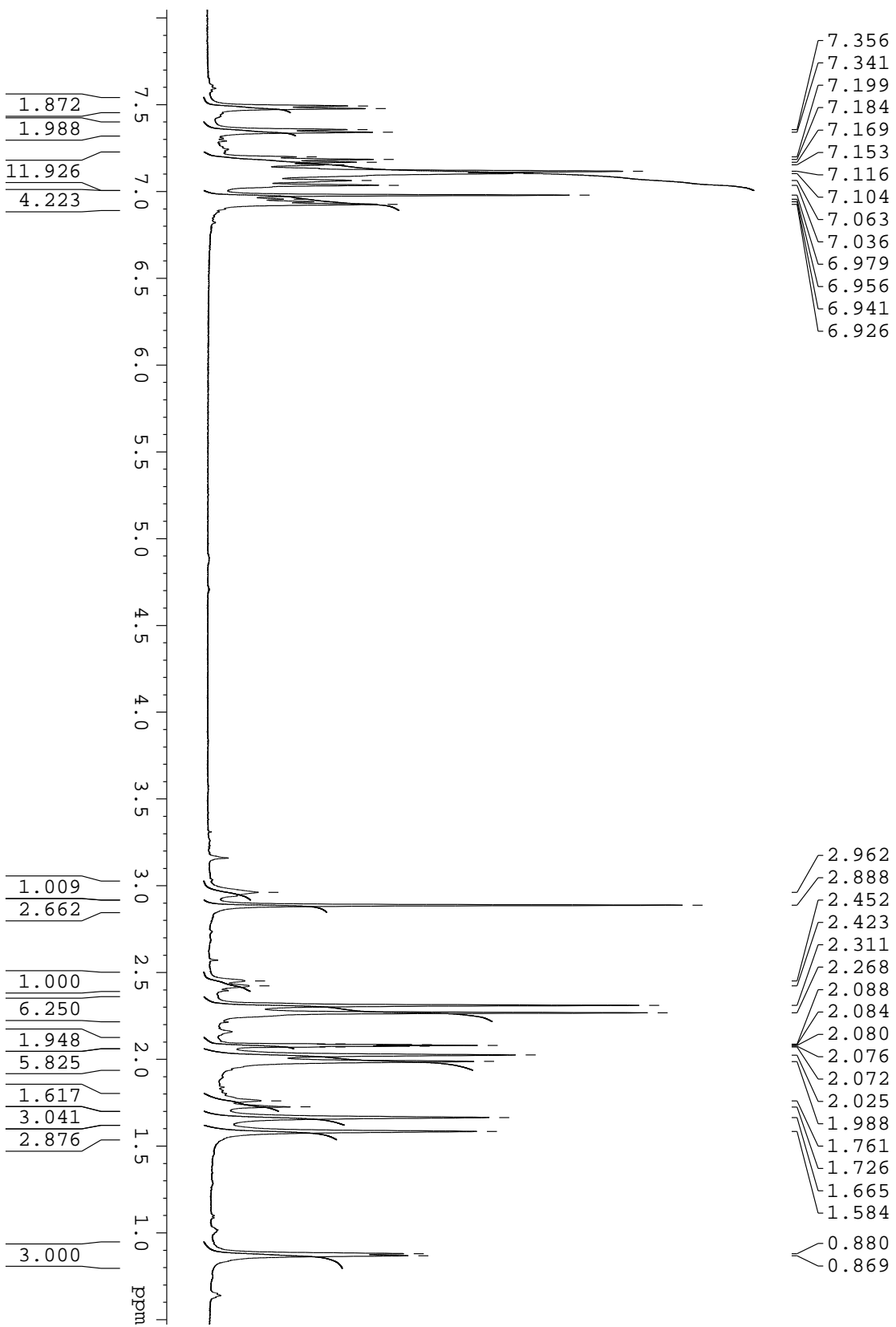
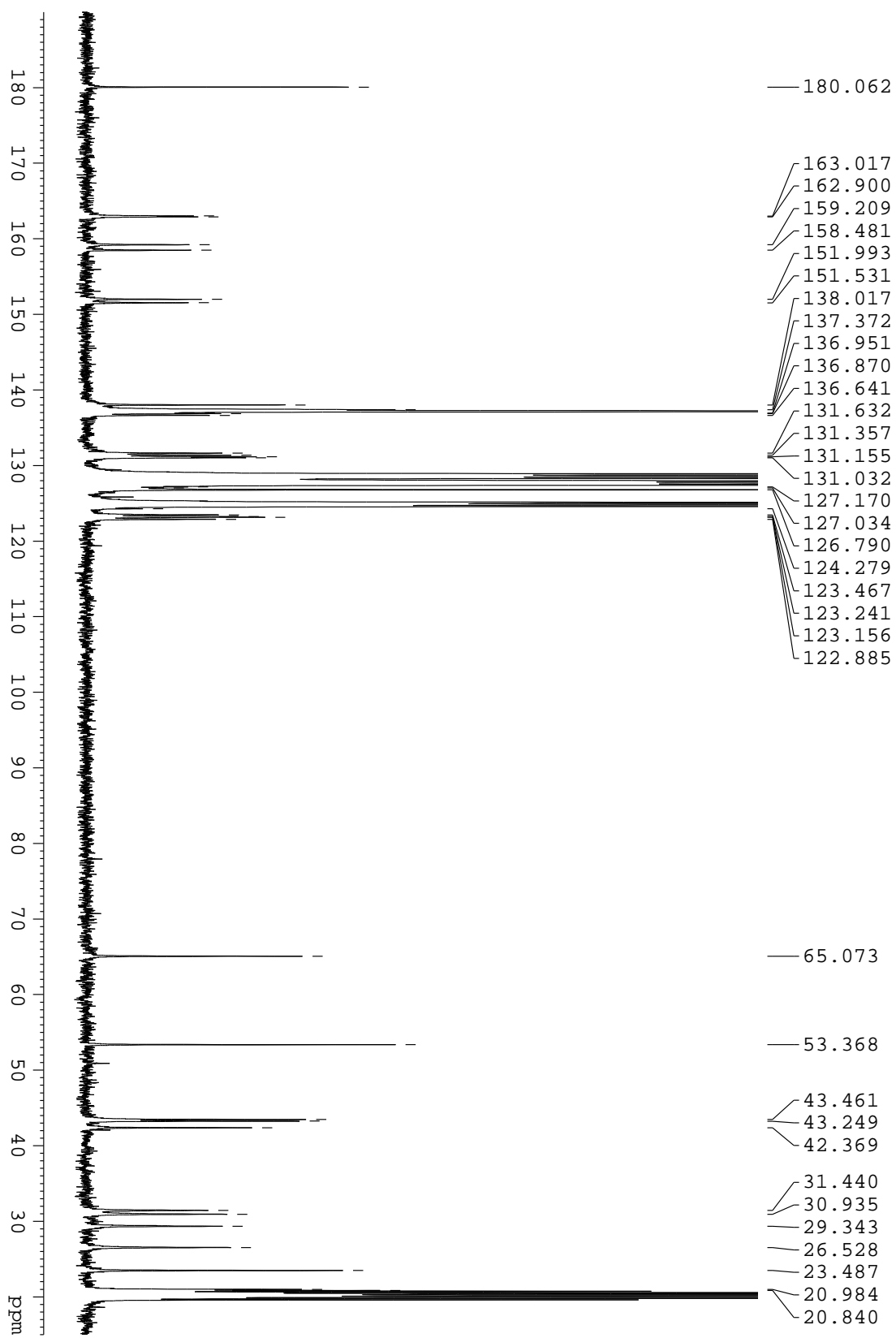
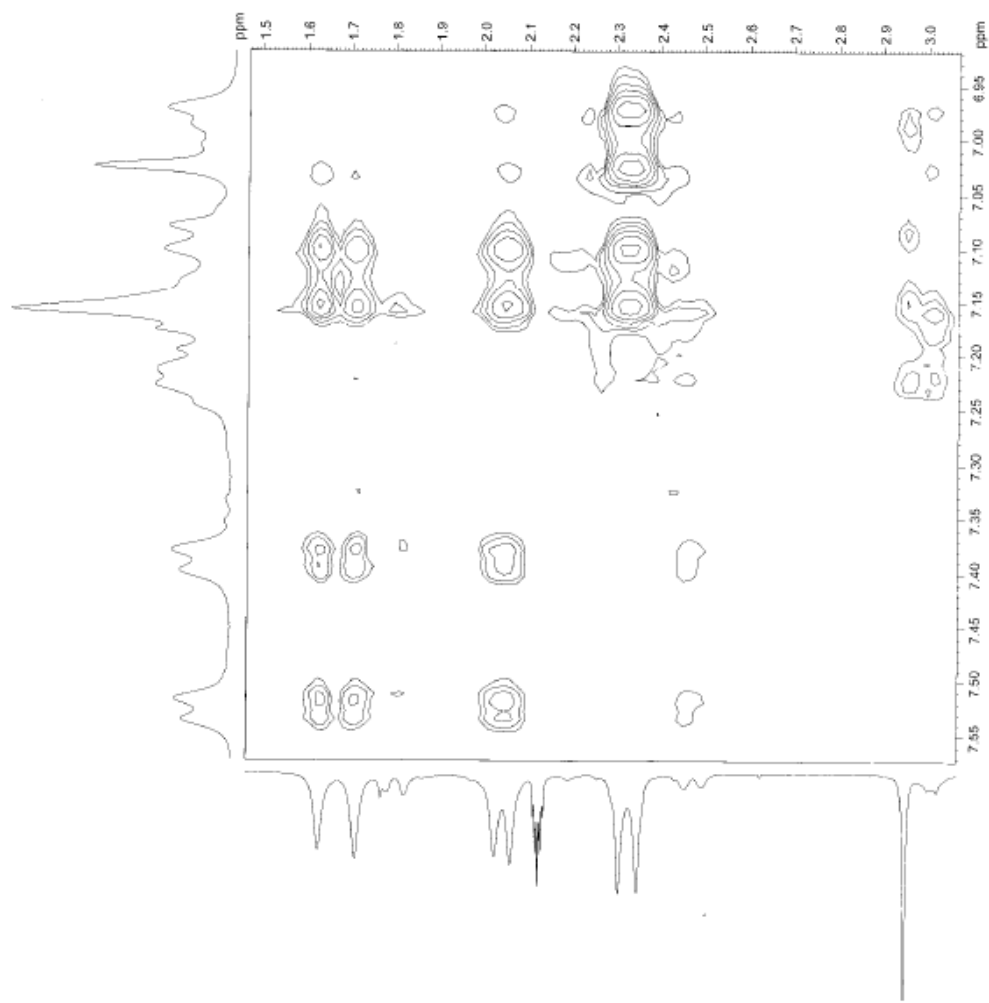


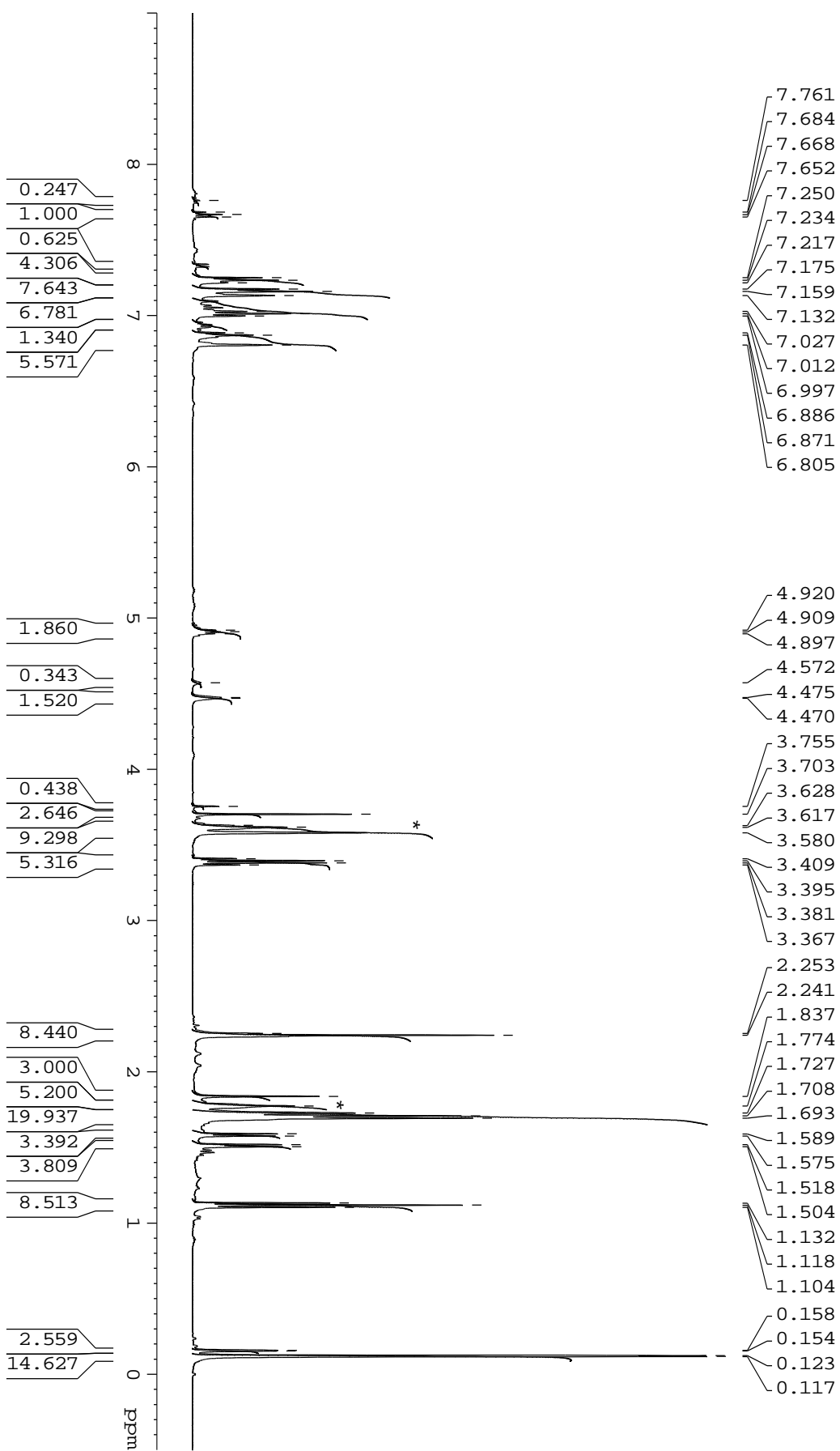
Figure 48A.  $^1\text{H}$  NMR spectrum (500 MHz, toluene- $d_8$ , 258 K) of  $\{\text{ONO}^{\text{Me}}_{\text{Cumyl}}\} \text{Y}((R)\text{-OCH}(\text{CH}_3)\text{CH}_2\text{COOMe})(\mathbf{10})$ .

Figure 49A.  $^{13}\text{C}\{^1\text{H}\}$  NMR (100 MHz, toluene- $d_8$ , 258 K) of  $\{\text{ONO}^{\text{Me,Cunyl}}\}_2\text{Y}((R)\text{-OCH}(\text{CH}_3)\text{CH}_2\text{COOMe})$  (**10**).





**Figure 50A.**  $^1\text{H}$ - $^1\text{H}$  NOESY spectrum (400 MHz, toluene- $d_8$ , 258 K) of  $\{\text{ONO}^{\text{Me,Cumyl}}\}_2\text{Y}((R)\text{-OCH}(\text{CH}_3)\text{CH}_2\text{CO}_2\text{Me})$  (**10**).



**Figure S1A.**  $^1\text{H}$  NMR spectrum (500 MHz,  $\text{THF-}d_8$ , 298 K) of  $\{\text{ONO}^{\text{Me}}_{\text{Cu}}^{\text{Y}}\}_n\{\text{Y}((S,S)\text{-OCH}(\text{CH}_3)\text{OCH}(\text{CH}_3)\text{COOMe})_2(\text{THF})\}_m$  (\*stands for residual solvent resonance).

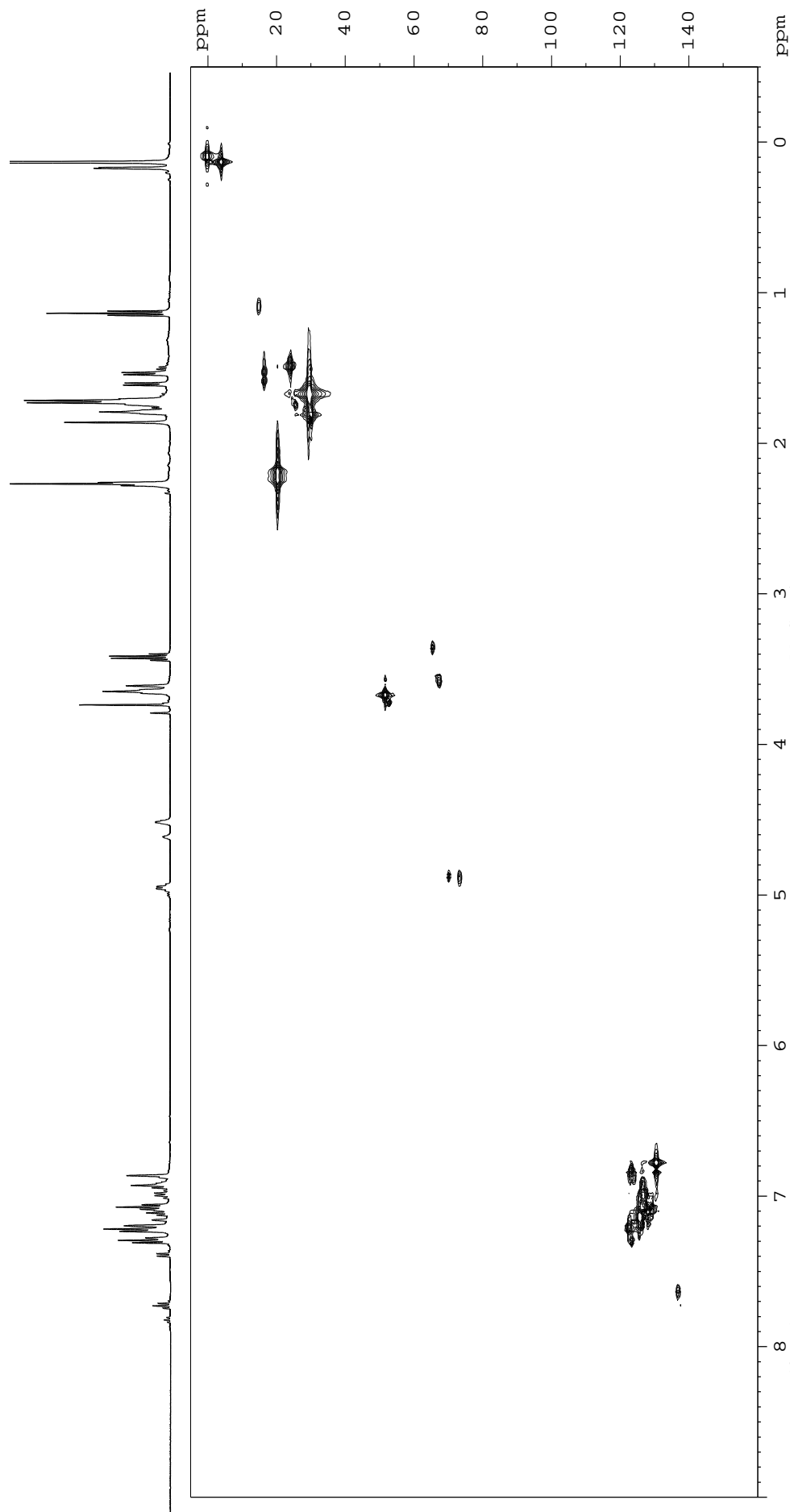


**Figure 52A.**  $^{13}\text{C}$ - $^1\text{H}$  HMQC NMR spectrum (500 MHz, THF- $d_8$ , 298 K) of  $\{\text{ONO}^{\text{Me,Cumyl}}\} \text{Y}((S,S)\text{-OCH}(\text{CH}_3)\text{OCH}(\text{CH}_3)\text{COOMe})(\text{THF})(11)$ .

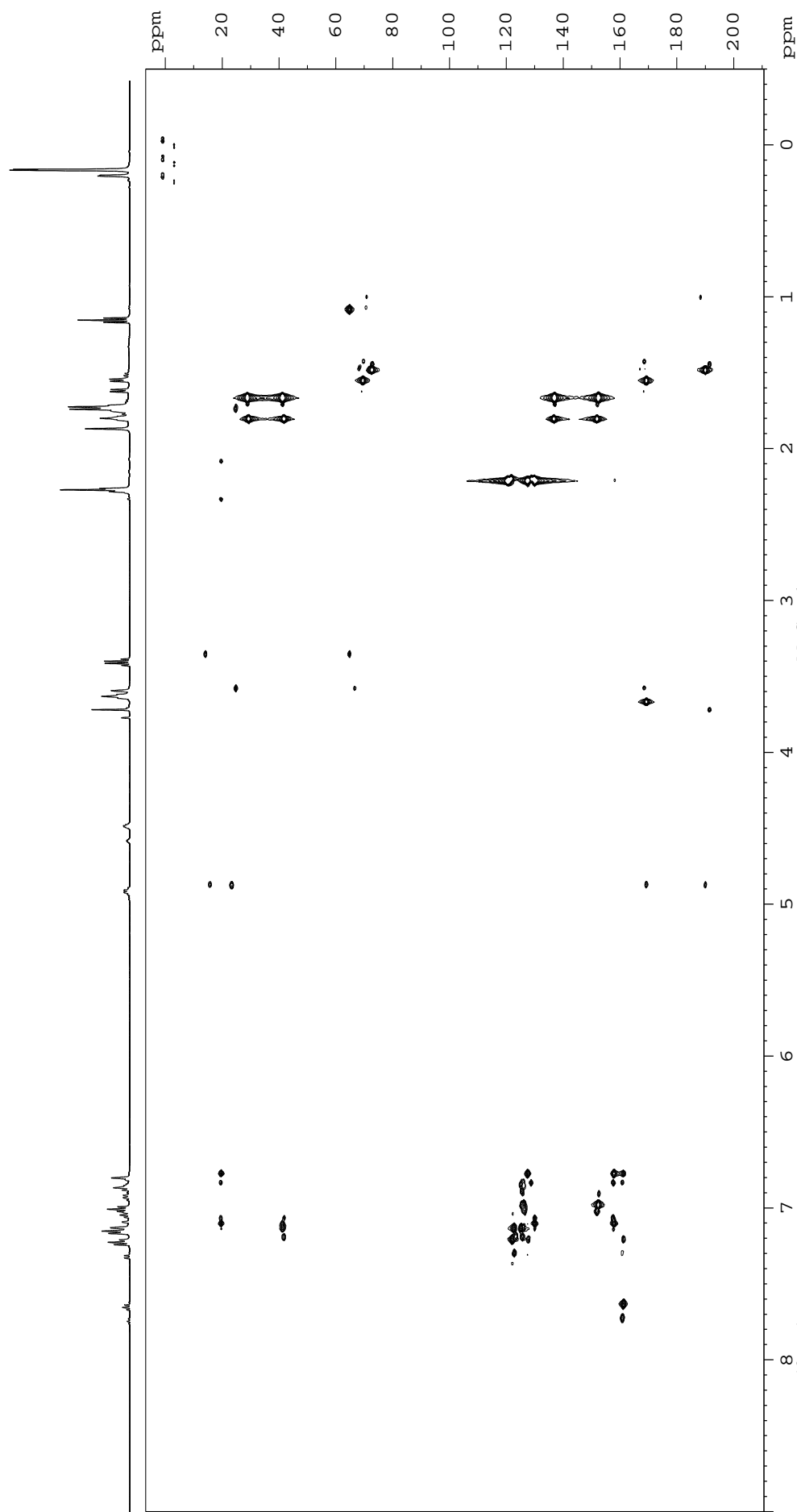


**Figure 53A.**  $^{13}\text{C}$ - $^1\text{H}$  HMBC NMR spectrum (500 MHz, THF- $d_8$ , 298 K) of {ONO<sup>Me,Cumyl</sup>]<sub>3</sub>Y((S,S)-OCH(CH<sub>3</sub>)OCH(CH<sub>3</sub>)COOMe)(THF)(**11**).

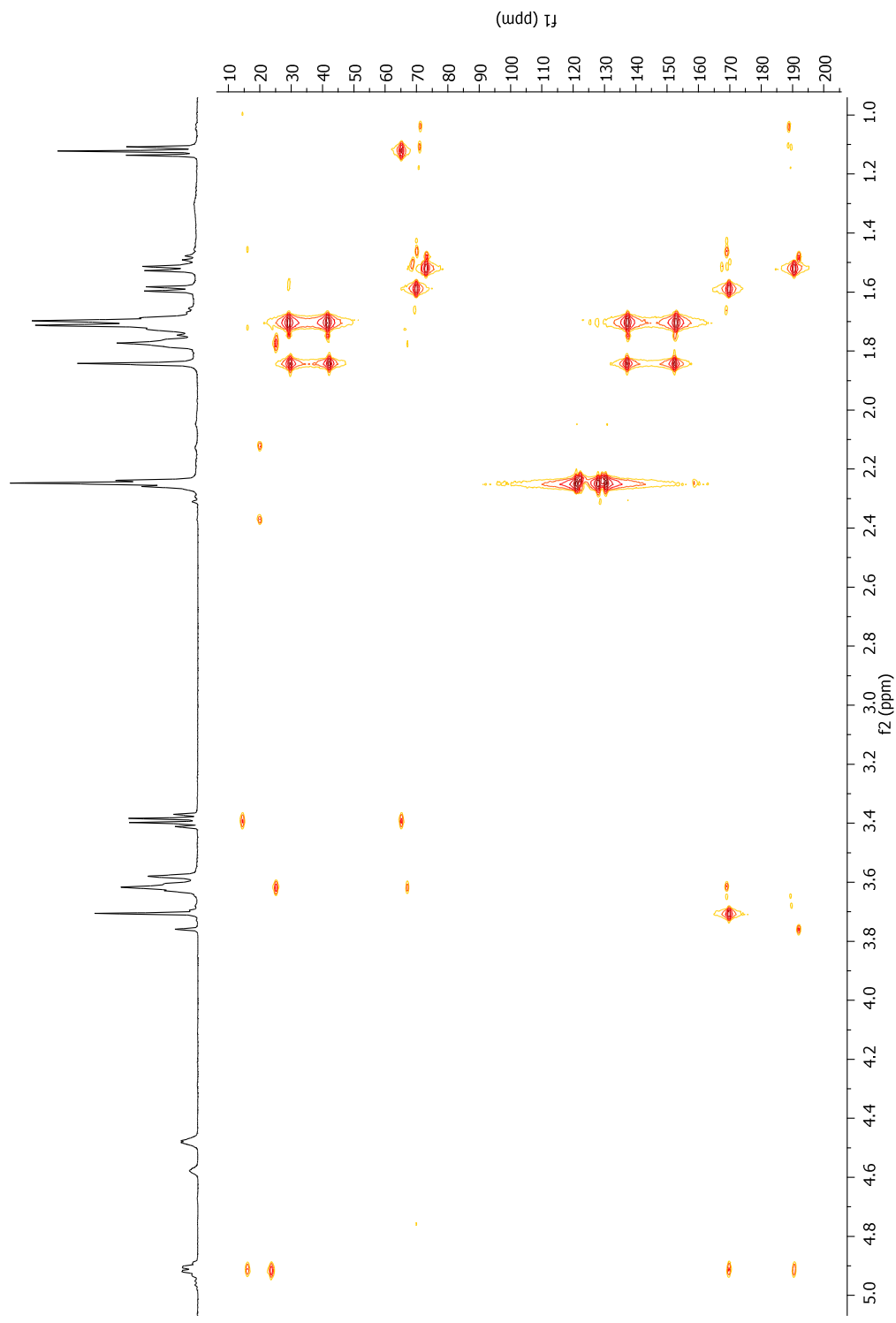


**Figure 54A.** Selected region of  $^{13}\text{C}$ - $^1\text{H}$  HMBC NMR spectrum (500 MHz,  $\text{THF}-d_8$ , 298 K) of  $\{\text{ONO}^{\text{Me,Cumyl}}\text{Y}((\text{S},\text{S})\text{-OCH}(\text{CH}_3)\text{OCH}(\text{CH}_3)\text{COOMe})(\text{THF})(\mathbf{11})\}$ .